LACUSTRINE PALEOECOLOGICAL RECORDS AND MODERN TRAINING SETS FROM LAKE MALAWI: IMPLICATIONS FOR AFRICAN PALEOCLIMATE AND CONNECTIONS TO HUMAN PREHISTORY

by

Margaret Whiting Blome

A Dissertation Submitted to the Faculty of the

DEPARTMENT OF GEOSCIENCES

In Partial Fulfillment of the Requirements
For the Degree of

DOCTOR OF PHILOSOPHY

In the Graduate College

THE UNIVERSITY OF ARIZONA

2012

THE UNIVERSITY OF ARIZONA
GRADUATE COLLEGE

As members of the Dissertation Committee, we certify that we have read the dissertation

prepared by Margaret Whiting Blome

entitled Lacustrine Paleoecological Records and Modern Training Sets from Lake Malawi: Implications for African Paleoclimate and Connections to Human Prehistory

and recommend that it be accepted as fulfilling the dissertation requirement for the

Degree of Doctor of Philosophy

_____ Date: 11/20/12
Dr. Andrew Cohen

_____ Date: 11/20/12
Dr. Julia Cole

_____ Date: 11/20/12
Dr. Owen Davis

_____ Date: 11/20/12
Dr. Vance Holliday

Final approval and acceptance of this dissertation is contingent upon the candidate's submission of the final copies of the dissertation to the Graduate College.

I hereby certify that I have read this dissertation prepared under my direction and recommend that it be accepted as fulfilling the dissertation requirement.

_____ Date:
Dissertation Director: Dr. Andrew Cohen

STATEMENT BY AUTHOR

This dissertation has been submitted in partial fulfillment of requirements for an advanced degree at the University of Arizona and is deposited in the University Library to be made available to borrowers under rules of the Library.

Brief quotations from this dissertation are allowable without special permission, provided that accurate acknowledgment of source is made. Requests for permission for extended quotation from or reproduction of this manuscript in whole or in part may be granted by the head of the major department or the Dean of the Graduate College when in his or her judgment the proposed use of the material is in the interests of scholarship. In all other instances, however, permission must be obtained from the author.

SIGNED: Margaret Whiting Blome

ACKNOWLEDGEMENTS

I would like to thank the U.S. National Science Foundation (NSF) Earth-System History Program (EAR-0602350), the International Continental Scientific Drilling Program, the Smithsonian Institution, DOSECC Inc. (Drilling, Observation and Sampling of the Earth's Continental Crust), the NSF Integrative Graduate Education and Research Traineeship (IGERT) program, the Foreign Language and Area Studies (FLAS) fellowship program, the Southern Arizona Geosciences Union for Academics, Research and Outreach (SAGUARO) program at the University of Arizona, and summer scholarships from Chevron and BP for providing generous funding and support of my research.

Discussions with my advisor, Andrew Cohen, and my committee members Julia Cole, David Dettman, Vance Holliday, and Steven Kuhn, were invaluable and extremely useful for my studies. I am happy to have had several friends and colleagues who helped improve my work and made the effort more enjoyable such as Sarah Ivory, Michael McGlue, Christine Gans, Jessica Conroy, Devon Orme, and Mark Warren.

I would also like to extend my thanks to my family, far and near, for their much appreciated support of my academic efforts.

DEDICATION

I would like to dedicate this dissertation to my parents, Richard and Wendy Blome, for their unwavering belief in me and what I could achieve.

TABLE OF CONTENTS

TABLE OF CONTENTS - *Continued*

TABLE OF CONTENTS - *Continued*

ABSTRACT

African climate changed considerably throughout the Pleistocene (2.588 million (Ma) to 12 thousand years ago (ka)). The timing, rate, and magnitude of past climate change across the continent impacted the evolutionary and migratory history of many mammalian species, including hominins. Investigating paleoclimatic variability through time at local and regional scales allows for an assessment of the extent to which climate change affected hominin evolution in Africa. This dissertation presents three approaches for increasing the understanding of past climate change in Africa. One method is to critically synthesize the existing literature of African climate (n=85) and hominid demography (n=64) over a restricted time frame (150 ka to 30 ka) and specific spatial scale (regional). Results from this study are two-fold: 1) climate change in Africa during this period was variable by region, responding to different climate-forcing mechanisms, and 2) changes in population and climate were asynchronous and likely created alternating opportunities for migration into adjacent regions, including hominin migrations out of Africa (~140-80 ka). The second approach is to evaluate modern ecological relationships between species and their environment to better quantify interpretations of paleoecological records. A modern distribution study of 33 ostracode species from 104 sites in the southwest arm of Lake Malawi suggest that depth-dependent variables likely define species niches. Relationships between ostracodes, fish and the green algae *Botryococcus*, were used to inform the paleoecological interpretations in the third study of this dissertation. Additional results suggest that macrocharcoal is likely delivered to the lake basin via river rather than wind-borne methods. The third approach

involves primary analysis of climatic indicators from the sedimentary record to chronicle paleoecological and paleoenvironmental change at the basin scale through time. Results from a 380.7 meter-long sediment core recovered from Lake Malawi indicate a change of state likely caused by local tectonism, which affected ostracode assemblages, but had little effect on lake level history through time. Furthermore, the local hydroclimate of Lake Malawi alternately covaried with global glacial/interglacial cycles and local insolation maxima over the past 1.25 Ma. The magnitude and frequency of hydroclimatic variability in the watershed will be further assessed in future research.

1. INTRODUCTION

The paleoclimate and paleoenvironmental history of Africa has become an increasingly important issue for many reasons, not the least of which is the current concern over global climate change. One of the most pressing questions is what impact anthropogenic climate change will have on tropical Africa and specifically, what is the sensitivity of this climatically vulnerable region? To answer these questions, (paleo)climatologists are studying the history of climate change in the tropics at various time scales to determine the natural response of climate through time (e.g. Tjallingii et al. 2008, Russell et al. 2003).

In addition to informing models of current climate change, paleoenvironmental history and variability during the Middle and Late Pleistocene may have played a crucial role in shaping the biological diversity, distribution and behavior of *Homo sapiens* populations during this period. A number of studies have focused on providing the environmental context for subsequent hominin dispersals out of Africa (cf. Vaks et al., 2007; Osbourne et al., 2008; Carto et al., 2009; but see Basell, 2008; Cowling et al., 2008; Drake et al., 2008). Recent genetic evidence has also indicated the importance of Pleistocene population dispersal within Africa (e.g., Reed and Tishkoff, 2006; Behar et al., 2008; Verdu et al., 2009). One goal of the first study in this dissertation (Appendix A) is to explore climatic variability within Africa during the Middle and Late Pleistocene (150-30 ka) to better understand both the context of intra-African hominin population dispersal and conditions relevant to out-of-Africa scenarios.

This study focuses on the 150 ka to 30 ka time interval for theoretical and practical reasons. This time period is important as it includes much of the early history of *Homo sapiens*, and from an archaeological perspective, it includes the shift from the Middle Stone Age (MSA) to Later Stone Age (LSA) technologies, an important change that may signal changes in human cognition or demography (cf. Klein, 2009; Powell et al., 2009). Pragmatically, 150 ka marks the beginning of the time interval for which statistically significant numbers of detailed, well-constrained records are available from both the oceanic sites surrounding Africa and for a number of the key lake records such as Lake Malawi. In addition, the paleoclimate records for the past 30 kyr (thousand years) in Africa have long been a focus of earlier reviews (e.g., Street and Grove, 1979; Nicholson and Flohn, 1980).

Different temporal and spatial frameworks are important for interpreting the role of climate change in human evolution. Macro-scale approaches include those that examine continental scale changes across long time intervals (e.g., Potts, 1998; deMenocal, 2004) or use coarse temporal frameworks such as the Marine Isotope Stage boundaries and glacial/interglacial variation (e.g., Lahr and Foley, 1998; Basell, 2008; Crowley and Hyde, 2008). At the other end of the continuum are micro-scale approaches that seek to understand the response of small populations to environmental change over relatively short periods recorded at a single archaeological site or depositional basin (e.g., Potts et al., 1999).

Following other recent efforts (e.g., Fisher et al., 2010; Drake et al., 2011), part of this study uses a ‘meso-scale’ approach in the examination of sub-continental variation in

paleoclimate and the human fossil and archaeological records. Paleoclimate data from diverse datasets of varying temporal and spatial resolution from three broad categories is synthesized. These categories include: (1) cores from offshore marine sites, which provide relatively continuous data sampled over a large area on sea surface temperatures and ocean circulation patterns, changes in terrestrial vegetation patterns, and relative aridity; (2) cores from a number of African lakes, which provide relatively continuous records of watershed and regional environmental change; (3) a number of other terrestrial sedimentary archives, including caves, rockshelters, and open-air archaeological sites, which provide temporally discontinuous, often highly local records of climatic and environmental change. These climatic and environmental data are compared to a database of published, radiometrically dated hominin fossil- or artifact-bearing deposits to test whether these changes are coincident with demographic changes in Pleistocene African hominin populations.

Modern distribution studies of species assemblages in relation to environmental variables are often used to quantify paleoecological studies (e.g. Fritz, 1996, Mischke et al., 2002; Horne, 2007; Smith, 1993). The second study presented in this dissertation (Appendix B) focuses on the modern distribution of ostracodes specifically within the nearshore (1-60m) environment of Lake Malawi to identify the relationship between species and the ecological range of their habitat. The relationships between ostracodes and quantifiable variables not observable in sediment cores (e.g. water chemistry, depth), as well as to variables of physical limnology that are measurable in a sediment core (e.g.

grain size, organic and inorganic carbon content), will inform future interpretations of the paleoenvironment of Lake Malawi (e.g. Appendix C – this dissertation).

Paleoecological reconstruction from lacustrine fossils is a well-tested method that has been used for many years with a variety of indicators. However, this is the first study to quantitatively be applied to ostracodes from Lake Malawi. Their usefulness as paleoecological indicators has long been understood (Delorme, 1969), for the following reasons: First, ostracodes are small, bivalved crustaceans with shells of low-magnesium calcite, which preserves well in most alkaline environments (pH >7.5) (Holmes, 2001, Cohen, 2003). Second, the shape or size of the valve, the presence or absence of nodes, pores and/or reticulations on the outer surface, and internal valve characteristics readily distinguish the species commonly found in East Africa, and in Lake Malawi in particular (e.g. Martens, 2002). Third, the environment in which an ostracode lives is determined by the geology, hydrology and climate of the watershed, and each taxon has a certain ecological tolerance (Delorme 1969). And fourth, previous studies have demonstrated that many ostracode assemblages reflect lake water chemistry variations with strong correlations to total conductivity and alkalinity (Cohen et al., 1983), and solute composition and concentration (Delorme, 1969, Mezquita et al. 2005). The known relationships between ostracodes and their environment increase with each new study. From these, lake level histories and water depth can be quantitatively inferred in paleoecological records.

The third study in this dissertation (Appendix C) seeks to chronicle the paleoecological variability recorded in a suite of biological and mineralogical indicators

from Lake Malawi between 1.25 Ma and 147 ka. Continuous continental sediment records are extremely valuable for reconstructing regional hydrology and climate and as terrestrial records, they have added utility when comparing observed variation to the hominin record. Continuous climate records from offshore marine sites are useful, but may have been recovered far from the area of interest (e.g. Hooghiemstra et al., 1992). On the contrary, continental sediment archives in lakes spanning more than 100,000 years can provide valuable information about long term climate history (Melles et al., 2012; Stone et al., 2011; Cohen et al., 2007). Rift basin lakes such as Lake Malawi are considered especially good candidates for paleoclimatic studies for the following reasons: 1) they are very deep and therefore contain long and rarely interrupted sedimentation records; 2) their sediments often contain abundant fossils and other useful paleoclimate indicators; and 3) when "closed", they are hydrologically sensitive to variations in water balance, i.e. precipitation minus evaporation (P-E), which is in turn coupled to local climate (Nicholson, 1998; Holmes, 1992). Previous studies using sediment drill core records from Lake Malawi have proved extremely important, defining a series of megadrought events during the Middle-Late Pleistocene (135-90 ka) (e.g. Cohen et al., 2007; Scholz et al., 2007; Park and Cohen, 2011; Reinthal et al., 2011; Stone et al., 2011). Here I describe results from a much longer drill core record from the same location in central Lake Malawi.

Lake Malawi, situated between 9-14°S, lies within the East African Rift System (EARS) which comprises a series of aligned tectonic basins, each 100s of kilometers long and 10s of kilometers wide, which individually contain sediment packages thousands of

meters thick (Chorowicz 2005, Rosendahl et al., 1992). The Malawi basin occupies a series of alternating, asymmetric, tilted half-grabens, which are flanked by uplifted shoulders along border faults with offsets of up to seven kilometers (Ebinger et al., 1987, Chorowicz, 2005). The tectonic configuration is responsible for the topographic pattern of high relief "shoulders" next to deep, sediment filled basins (Ebinger et al., 1987). The sedimentation pattern in this region is controlled by the interaction between the underlying geological structure of the basin and the regional climatology (Tiercelin et al. 1988; Chorowicz, 2005) and the position and course of influent rivers within the basin are strongly controlled by the evolution and structural geology of the local rift segments, which may change over time (Flannery and Rosendahl, 1990).

The location for sediment core MAL-05 1B (hereafter Core 1B) was chosen to maximize its potential for recovery of a continuous record of climate change. It is located in Lake Malawi's central basin on the flank of a structural basement high, which should preclude significant accumulation of sediment at the site due to gravity flows (Scholz et al., 2011). This location has the thickest accumulation of sediments in the lake basin (~1.8km) (Ebinger et al., 1987). Further, evidence from seismic data suggest the stratigraphic section at the chosen site lacked any significant unconformities or time-gaps in the record (Scholz et al., 2011).

Lake Malawi is a large (29,500 km^2), deep (706 m), permanently stratified (meromictic) lake that is permanently anoxic below 230-250 meters depth (Eccles, 1974; Eccles; 1988, Patterson and Kachinjika, 1995; Bootsma and Hecky, 1999). Seasonal variations in temperature, wind and precipitation are caused by the migration of the

Intertropical Convergence Zone (ITCZ) (Eccles, 1974). Seasonal mixing occurs from May-August when the ITCZ is sufficiently north of the lake to enhance the SE trade winds at the lake. Due to the morphology and orientation of the lake basin, cooler surface waters and wind combine to decrease the temperature-dependent water density difference, mixing the lake to a depth of 150 meters (Patterson and Kachinjika, 1995; Wüest et al., 1996; Bootsma and Hecky, 1999) which is essential for the redistribution of nutrients serves to increase lake productivity (Eccles, 1974). Additionally, at all times in the past when lake level was over four meters lower than modern, the lake would have been hydrologically closed, and the difference between precipitation and evaporation (P-E) in the watershed would have become the dominant driver of water depth (Holmes, 1992). In the low-latitudes, precipitation amount, intensity, and seasonality is driven primarily by the location of the ITCZ, although there is evidence to suggest that African climate can be affected by both high- and low-latitude forcings, such as global ice cover and regional-global sea surface temperatures (SSTs) (deMenocal et al. 1993; Tierney et al. 2008; Blome et al., 2012 or Appendix A – this dissertation). For these reasons, hydrologic changes in Lake Malawi recorded in the paleoecological variability of a number of biological and mineralogical indicators may be linked to changes in regional and/or global climate.

Overall, the body of work in this dissertation represents individual parts contributing to furthering the understanding of paleoenvironmental variability in Africa and possible implications for human history. In the following section, I summarize the research appearing in each appendix that includes these parts.

2. PRESENT STUDY

I present the methods, results, and conclusions of this study as a combination of three articles appended to this dissertation. These articles are formatted for publication in professional scientific journals. The first article is published (Appendix A), and the final two articles are being prepared for submission to peer-reviewed journals (Appendix B and C). All three articles are multi-authored articles with myself as the lead author. The following is a summary of the most important findings in this document.

The first article synthesizes African paleoclimate from 150 to 30 ka (thousand years ago) using 85 diverse datasets at a regional scale, testing for coherence with North Atlantic glacial/interglacial phases and northern and southern hemisphere insolation cycles (Appendix A). Two major determinants of circum-African climate variability over this time period are supported by principal components analysis: North Atlantic SST variations and local insolation maxima. North Atlantic SSTs correlated with the variability found in most circum-African SST records, whereas the variability of most terrestrial temperature and precipitation records is explained by local insolation maxima, particularly at times when solar radiation was intense and highly variable (e.g. 150-75 ka). We determine that the dominant climate forcing mechanism changes regionally through time suggesting that the tuning of terrestrial records to either global glacial/interglacial cycles or peaks in local insolation maxima is ill-advised. Further, we demonstrate that climates varied with latitude, such that periods of relatively increased aridity or humidity were asynchronous across the northern, eastern, tropical and southern

portions of Africa. Attempts to correlate the archaeological, fossil, or genetic records with generalized patterns of environmental change based solely on northern hemisphere glacial/interglacial cycles are therefore misguided.

Further, we compare our refined climatic framework to a database of 64 radiometrically-dated archaeological and fossil sites to test hypotheses of demographic responses to climatic change among African hominin populations during the 150-30 ka interval. We argue that at a continental scale, population and climate changes were asynchronous and likely occurred under different regimes of climate forcing, creating alternating opportunities for migration into adjacent regions. Our results suggest little relation between large scale demographic and climate change in southern Africa during this time span, but strongly support the hypothesis of hominin occupation of the Sahara during discrete humid intervals ~135-115 ka and 105-75 ka. Hominin populations in equatorial and eastern Africa may have been buffered from the extremes of climate change by locally steep altitudinal and rainfall gradients and the complex and variable effects of increased aridity on human habitat suitability in the tropics. Our data are consistent with hominin migrations out of Africa through varying exit points from ~140-80 ka.

The second article moves from a synthetic approach to a first order data analysis of the modern ecological distribution of ostracodes in Lake Malawi. This modern distribution study from the southwest arm of Lake Malawi quantitatively relates variables of the lake environment (e.g. bottom water temperature, dissolved oxygen content, substrate grain size, organic and inorganic carbon content) to surficial ostracode

assemblages and other taxa from 102 sites, across a gradient of environmental littoral to shallow profundal conditions. Site locations varied by depth (1-60m) and adjacent shoreline environment. The goal of this research is to use the resultant relationships to help quantify paleoecological interpretations of the fossil record from drill cores. Thirty-three ostracode species are identified from 54 sites including four new, previously un-described species of Cypridopsinae (2) and *Limnocythere* (2). Additionally the analysis suggests that two previously separate species, *Limnocythere s.l. sp.9* and *Limnocythere s.l. sp10* are the female and male of a single species, respectively. Ostracodes are extremely abundant between 1 and 25 meters water depth, in all three sub-environments, but are rare to absent between 30 and 60 meters. This disappearance in deeper water is presumed to be taphonomic, with steadily decreasing alkalinity beginning at 25 meters causing shell carbonate dissolution in the death assemblage, because abundant live ostracodes have been found in other parts of the lake at greater than 30 meters depth. A detrended correspondence analysis (DCA) of ostracode species abundance at each site suggests that assemblages are more similar by depth than by sub-environment. This implies that ostracode species niches are determined by ecological factors with specific depth boundaries such as bottom water temperature and dissolved oxygen content.

Many of the distributional relationships observed among taxa in the modern Lake Malawi can be directly applied to interpreting the paleoecological record of Lake Malawi which spans over 1 million years. The final chapter in this dissertation analyses the sand-sized fraction sieved from sediments between 380.7 and 82 meters below lake floor (mblf) recovered from Core MAL05-1B in the central basin of Lake Malawi. This

analysis forms the basis for reconstructing the paleohydrology and paleoecology of Lake Malawi between 1.25 million and 147 thousand years ago. I analyzed the following variables: the absolute abundances of fossil indicators including ostracodes, fish, charred particles, molluscs, green algae and fern spores, the relative abundances of ostracode taxa, taphonomic variables of ostracode preservation, and sand fraction mineralogy. These data are presented, and grouped into biological and lithological facies assemblages of co-occurring indicators. Facies changes throughout the core represent five distinct paleoenvironmental states at the core site. These include a major transition from river to non-river influenced local environments occurring between 230-203 mblf (~800-660 ka), as evidenced by a unidirectional shift in dominant ostracode species assemblages and minerogenic content. This change was likely caused by intra-basinal tectonics cutting off a riverine sediment supply to the core site. In addition, a principal components analysis (PCA) performed on 23 of these variables shows a strong correlation between the first axis of variance (PC1) and depth-dependent indicators, and is thus interpreted as representing relative lake level though time. Ecological variability constrained in the PC1 curve has a clear environmental interpretation as major changes in facies are coincident with shifts in the curve.

3. REFERENCES

Basell, L.S., 2008. Middle Stone Age (MSA) site distributions in eastern Africa and their relationship to Quaternary environmental change, refugia and the evolution of *Homo sapiens*. Quatern. Sci. Rev. 27, 2484-2498.

Behar, D.M., Villems, R., Soodyall, H., Blue-Smith, J., Pereira, L., Metspalu, E., Scozzari, R., Makkan, H., Tzur, S., Comas, D., Bertranpetit, J., Quintana-Murci, L., Tyler-Smith, C., Wells, R.S., Rosset, S., 2008. The dawn of human matrilineal diversity. Am. J. Hum. Genet. 82, 1130-1140.

Blome, M.W., Cohen, A.S., Tryon, C.A., Brooks, A.S., Russell, J., 2012. The environmental context for the origins of modern human diversity: a synthesis of regional variability in African climate 150,000-30,000 years ago. J Hum Evol 62, 563-592.

Bootsma, H.A., Hecky, R.E., 1999. Water Quality Report. Lake Malawi/Nyasa Biodiversity Conservation Project, Senga Bay, Malawi.

Carto, S.L., Weaver, A.J., Hetherington, R., Lam, Y., Wiebe, E.C., 2009. Out of Africa and into an ice age: on the role of global climate change in the late Pleistocene migration of early modern humans out of Africa. J. Hum. Evol. 56, 139-151.

Chorowicz, J., 2005. The East African rift system. Journal of African Earth Sciences 43, 379-410.

Cohen, A.S., Dussinger, R., Richardson, J., 1983. Lacustrine paleochemical interpretations based on eastern and southern African ostracodes. Palaeogeography, Palaeoclimatology, Palaeoecology 43, 129-151.

Cohen, A.S., Stone, J.R., Beuning, K.R.M., Park, L.E., Reinthal, P.N., Dettman, D., Scholz, C.A., Johnsor, T.C., King, J.W., Talbot, M.R., Brown, E.T., Ivory, S.J., 2007. Ecological consequences of early Late Pleistocene megadroughts in tropical Africa. P. Natl. Acad. Sci. USA 104, 16422-16427.

Cohen, A.S., 2003. Paleolimnology: The History and Evolution of Lake Systems. Oxford University Press, Oxford.

Cowling, S.A., Cox, P.M., Jones, C.D., Maslin, M.A., Peros, M., Spall, S.A., 2008. Simulated glacial and interglacial vegetation across Africa: implications for species phylogenies and trans-African migration of plants and animals. Glob. Change Biol. 14, 827-840.

Crowley, T.J., Hyde, W.T., 2008. Transient nature of late Pleistocene climate variability.

Nature 456, 226-230.

Delorme, L.D., 1969. Ostracodes as Quaternary paleoecological indicators. Can J Earth Sci 6: 1471-1476.

deMenocal, P.B., 2004. African climate change and faunal evolution during the Pliocene-Pleistocene. Earth Planet. Sci. Lett. 220, 3-24.

deMenocal, P.B., Ruddiman, W.F., Pokras, E.M., 1993. Influences of high- and low-latitude processes on African terrestrial climate: Pleistocene eolian records from equatorial Atlantic Ocean Drilling Program Site 663. Paleoceanography 8, 209-242.

Drake, N.A., El-Hawat, A.S., Turner, P., Armitage, S.J., Salem, M.J., White, K.H., McLaren, S., 2008. Palaeohydrology of the Fazzan Basin and surrounding regions: the last 7 million years. Paleogeogr. Paleoclimatol. Paleoecol. 263, 131-145.

Drake, N.A., Blench, R.M., Armitage, S.J., Bristow, C.S., White, K.H., 2011. Ancient watercourses and biogeography of the Sahara explain the peopling of the desert. Proc. Natl. Acad. Sci. 108, 458-462.

Ebinger, C., Rosendahl, B., Reynolds, D., 1987. Tectonic model of the Malaŵi rift, Africa. Tectonophysics 141, 215-235.

Eccles, D.H., 1974. An outline of the physical limnology of Lake Malawi (Lake Nyasa). Limnol Oceanogr 19, 730-742.

Eccles, D., 1988. A quarter century of great lakes research in Africa. Journal of the Limnological Society of Southern Africa 14, 41-48.

Fisher, E.C., Bar-Matthews, M., Jerardino, A., Marean, C.W., 2010. Middle and Late Pleistocene paleoscape modeling along the southern coast of South Africa. Quatern. Sci. Rev. 29, 1382-1398.

Flannery, J.W., Rosendahl, B., 1990. The seismic stratigraphy of Lake Malawi, Africa: implications for interpreting geological processes in lacustrine rifts. Journal of African Earth Sciences (and the Middle East) 10, 519-548.

Fritz, S.C., 1996. Paleolimnological records of climatic change in North America. Limnol. Oceanogr. 41, 882-889.

Holmes, J.A., 1992. Nonmarine ostracods as Quaternary palaeoenvironmental indicators. Progress in Physical Geography 16, 405-431

Holmes, J.A., 2001. Ostracoda. In Smol, J.P., Birks, H.J., Last, W.M., (Ed.), Tracking Environmental Change Using Lake Sediments, vol. 4: Zoological Indicators. Kluwer Academic Publishers, Dordrecht, pp. 125-152.

Hooghiemstra, H., Stalling, H., Agwu, C.O.C., Dupont, L., 1992. Vegetational and climatic changes at the northern fringe of the Sahara 250,000-5000 years BP: evidence from 4 marine pollen records located between Portugal and the Canary Islands. Rev. Palaeobot. Palyno. 74, 1-52.

Horne, D.J., 2007. A Mutual Temperature Range method for Quaternary paleoclimatic analysis using European nonmarine Ostracoda. Quaternary Sci Rev 26: 1398-1415.

Klein, R.G., 2009. The Human Career, Third Edition. University of Chicago Press, Chicago.

Lahr, M.M., Foley, R., 1998. Towards a theory of modern human origins: geography, demography, and diversity in recent human evolution. Yearb. Phys. Anthropol. 41, 137-176.

Martens, K., 2002. Task 3: taxonomy of invertebrates, in: Irvine, K. (Ed.), The trophic Ecology of the Demersal Fish Community of Lake Malawi/Niassa, Central Africa, pp. 49-59.

Mezquita, F., Roca, J.R., Reed, J.M., Wansard. G., 2005. Quantifying species-environment relationships in non-marine Ostracoda for ecological and palaeoecological studies: Examples using Iberian data. Palaeogeogr Palaeoclimatol Palaeogeogr 225: 93-117.

Mischke, S., Fuchs, D., Riedel, F., Schudack., 2002. Mid to Late Holocene palaeoenvironment of Lake Eastern Juyanze (north-western China) based on ostracods and stable isotopes. Geobios 35, 99-110.

Nicholson, S.E., Flohn, H., 1980. African environmental and climatic changes and the general atmospheric circulation in Late Pleistocene and Holocene. Clim. Change 2, 313-348.

Nicholson, S.E., 1998. Historical fluctuations of Lake Victoria and other lakes in the northwestern Rift Valley of East Africa. In: Lehman, J.T., (Ed.), Environmental Change and Response in East African Lakes. Kluwer Academic Publishers, Netherlands, pp. 7-35.

Osbourne, A.H., Vance, D., Rohling, E.J., Barton, N., Rogerson, M., Fello, N., 2008. A humid corridor across the Sahara for the migration of early modern humans out of Africa 120,000 years ago. Proc. Natl. Acad. Sci. 105, 16444-16447.

Park, L.E., Cohen, A.S., 2011. Paleoecological response of ostracods to early Late Pleistocene lake-level changes in Lake Malawi, East Africa. Palaeogeography, Palaeoclimatology, Palaeoecology 303, 71-80.

Patterson, G., Kachinjika, O., 1995. Limnology and phytoplankton ecology, in: Menz, A. (Ed.), The fishery potential and productivity of the pelagic zone of Lake Malawi/Niassa. Natural Resource Institute, Chatham, UK, pp. 1-67.

Potts, R., Behrensmeyer, A.K., Ditchfield, P., 1999. Paleolandscape variation and Early Pleistocene hominid activities: Members 1 and 7, Olorgesailie Formation, Kenya. J. Hum. Evol. 37, 747-788.

Potts, R., 1998. Environmental hypotheses of hominin evolution. Yearb. Phys. Anthropol. 41, 93-136.

Powell, A., Shennan, S., Thomas, M.G., 2009. Late Pleistocene demography and the appearance of modern human behavior. Science 324, 1298-1301.

Reed, F.A., Tishkoff, S.A., 2006. African human diversity, origins and migrations, Curr. Opin. Genet. Dev. 16, 597-605.

Reinthal, P.N., Cohen, A.S., Dettman, D.L., 2011. Fish fossils as paleo-indicators of ichthyofauna composition and climatic change in Lake Malawi, Africa. Palaeogeography, Palaeoclimatology, Palaeoecology 303, 126-132.

Rosendahl, B., Kilembe, E., Kaczmarick, K., 1992. Comparison of the Tanganyika, Malawi, Rukwa and Turkana Rift zones from analyses of seismic reflection data. Tectonophysics 213, 235-256.

Russell, J.M., Johnson, T.C., Talbot M.R., 2003. A 725 yr cycle in the climate of central Africa during the late Holocene. Geology 31, 677-680.

Scholz, C.A., Johnson, T.C., Cohen, A.S., King, J.W., Peck, J.A., Overpeck, J.T., Talbot, M.R., Brown, E.T., Kalindekafe, L., Amoako, P.Y.O., Lyons, R.P., Shanahan, T.M., Castañeda, I.S., Heil, C.W., Forman, S.L., McHargue, L.R., Beuning, K.R., Gomez, J., Pierson, J., 2007. East African megadroughts between 135 and 75 thousand years ago and bearing on early-modern human origins. Proc. Natl. Acad. Sci. 104, 16416-16421.

Scholz, C.A., Cohen, A.S., Johnson, T.C., King, J., Talbot, M.R., Brown, E.T., 2011. Scientific drilling in the Great Rift Valley: The 2005 Lake Malawi Scientific Drilling Project — An overview of the past 145,000years of climate variability in Southern Hemisphere East Africa. Palaeogeography, Palaeoclimatology, Palaeoecology 303, 3-19.

Smith, A.J., 1993. Lacustrine ostracodes as hydrochemical indicators in lakes of the north-central United States. J Paleolimnol 8: 121-134.

Street, F.A., Grove, A.T., 1979. Global maps of lake-level fluctuations since 30,000 yr BP. Quatern. Res. 12, 83-118.

Stone, J.R., Westover, K.S., Cohen, A.S., 2011. Late Pleistocene paleohydrography and diatom paleoecology of the central basin of Lake Malawi, Africa. Paleogeogr. Paleoclimatol. Paleoecol. 303, 51-70.

Tiercelin, J.J., Chorowicz, J., Bellon, H., Richert, J.P., Mwanbene, J.T., Walgenwitz, F., 1988. East African rift system: offset, age and tectonic significance of the Tanganyika-Rukwa-Malawi intracontinental transcurrent fault zone. Tectonophysics 148, 241-252.

Tierney, J.E., Russell, J.M., Huang, Y., Damste, J.S., Hopmans, E.C., Cohen, A.S., 2008. Northern hemisphere controls on tropical southeast African climate during the past 60,000 years. Science 322, 252-255.

Tjallingii, R., Claussen, M., Stuut, J.B.W., Fohlmeister, J., Jahn, A., Bickert, T., Lamy, F., Rohl, U., 2008. Coherent high- and low-latitude control of the northwest African hydrological balance. Nat. Geosci. 1, 670-675.

Vaks, A., Bar-Matthews, M., Ayalon, A., Halicz, L., Frumkin, A., 2007. Desert speleothems reveal climatic window for African exodus of early modern humans. Geology 35, 831-834.

Verdu, P., Austerlitz, F., Estoup, A., Vitalis, R., Georges, M., Thery, S., Froment, A., Le Bomin, S., Gessain, A., Hombert, J.M., Van der Veen, L., Quintana-Murci, L., Bahuchet, S., Heyer, E., 2009. Origins and genetic diversity of pygmy hunter-gatherers from western Central Africa. Curr. Biol. 19, 312-318.

Wüest, A., Piepke, G., Halfman, J.D., 1996. Combined effects of dissolved solids and temperature on the density stratification of Lake Malawi, in: Johnson, T.C., Odada, E.O. (Ed.), The limnology, climatology, and paleoclimatology of the East African lakes. Gordon and Breach Publishers, Amsterdam, pp. 183-204.

4. APPENDICES

APPENDIX A: THE ENVIRONMENTAL CONTEXT FOR THE ORIGINS OF MODERN HUMAN DIVERSITY: A SYNTHESIS OF REGIONAL VARIABILITY IN AFRICAN CLIMATE 150,000-30,000 YEARS AGO

Published in the professional journal: *Journal of Human Evolution*, Vol. 62, 563-592

THE ENVIRONMENTAL CONTEXT FOR THE ORIGINS OF MODERN HUMAN DIVERSITY: A SYNTHESIS OF REGIONAL VARIABILITY IN AFRICAN CLIMATE 150,000-30,000 YEARS AGO

Margaret Whiting Blome[a] Andrew S. Cohen[a], Christian A. Tryon[b], Alison S. Brooks[c], Joellen Russell[a]

[a]*Department of Geosciences, University of Arizona, 1040 E 4th St, Tucson, AZ 85712*

[b]*Department of Anthropology, New York University, 25 Waverly Place, NYC, NY 10003*

[c]*Department of Anthropology, George Washington University, 2110 G St., NW, Washington, DC 20052*

Abstract

We synthesize African paleoclimate from 150 to 30 ka (thousand years ago) using 85 diverse datasets at a regional scale, testing for coherence with North Atlantic glacial/interglacial phases and northern and southern hemisphere insolation cycles. Two major determinants of circum-African climate variability over this time period are supported by principal components analysis: North Atlantic sea surface temperature (SST) variations and local insolation maxima. North Atlantic SSTs correlated with the variability found in most circum-African SST records, whereas the variability of the majority of terrestrial temperature and precipitation records is explained by local insolation maxima, particularly at times when solar radiation was intense and highly variable (e.g. 150-75 ka). We demonstrate that climates varied with latitude, such that periods of relatively increased aridity or humidity were asynchronous across the northern, eastern, tropical and southern portions of Africa. Comparisons of the archaeological,

fossil, or genetic records with generalized patterns of environmental change based solely on northern hemisphere glacial/interglacial cycles are therefore imprecise.

We compare our refined climatic framework to a database of 64 radiometrically-dated archaeological and fossil sites to test hypotheses of demographic responses to climatic change among African hominin populations during the 150-30 ka interval. We argue that at a continental scale, population and climate changes were asynchronous and likely occurred under different regimes of climate forcing, creating alternating opportunities for migration into adjacent regions. Our results suggest little relation between large scale demographic and climate change in southern Africa during this time span, but strongly support the hypothesis of hominin occupation of the Sahara during discrete humid intervals ~135-115 ka and 105-75 ka. Hominin populations in equatorial and eastern Africa may have been buffered from the extremes of climate change by locally steep altitudinal and rainfall gradients and the complex and variable effects of increased aridity on human habitat suitability in the tropics. Our data are consistent with hominin migrations out of Africa through varying exit points from ~140-80 ka.

Introduction

Fossil and genetic data are consistent with an African origin of *Homo sapiens* by 195,000 years ago (ka) (Ingman et al., 2000; Clark et al., 2003; White et al., 2003; McDougall et al., 2005; Gonder et al., 2007). Numerous studies have emphasized the diversity in morphology, life history, and genetic signatures likely present among populations of Late and Middle Pleistocene hominins, some of which dispersed from

Africa in the Late Pleistocene, replacing existing hominin populations in parts of Eurasia and eventually colonizing Australia and North and South America. The variability among the source populations within Africa is compounded by local demographic changes and range expansions or contractions, as well as the persistence of ancestral or sister taxa (Lahr and Foley, 1998; Howell, 1999; Excoffier, 2002; Forster, 2004; Harding and McVean, 2004; Eswaran et al., 2005; Prugnolle et al., 2005; Trinkaus, 2005; Garrigan and Hammer, 2006; Garrigan et al., 2007; Smith et al., 2007; Bräuer, 2008; Pearson, 2008; Crevecoeur et al., 2009; Gunz et al., 2009; Hammer et al., 2011, Harvati et al., 2011). Middle Stone Age (MSA) archaeological sites provide the strongest record of the behavior of early African populations of *Homo sapiens*, and these sites record pronounced spatial and temporal variation not seen in earlier periods (McBrearty and Brooks, 2000; Henshilwood and Marean, 2003; Marean and Assefa, 2005; Jacobs et al., 2008a; Shea, 2011).

Paleoenvironmental history and variability during the Middle and Late Pleistocene may have played a crucial role in shaping the biological diversity, distribution and behavior of *Homo sapiens* populations during this period. Environmental change is a causal mechanism for the dispersal and isolation of animal populations, and the accumulation of variation through drift resulting from geographic isolation (allopatry) is a central cause of biological divergence and speciation (e.g., Barraclough and Nee, 2001; Mayr, 2001). Human behavioral change occurs as a result of a range of causal factors and we do not advocate strict environmental determinism. However, recent and ancient human forager subsistence, technology, land use, and some

social behaviors show clear relationships with environment (Kelly, 1995; Binford, 2001; Kuhn and Stiner, 2001; Marlowe, 2005), and archaeological changes at some Middle Stone Age (MSA) sites have been interpreted as behavioral responses to variation in resource structure and availability as a result of environmental shifts (Ambrose and Lorenz, 1990; Marean et al., 2007; McCall, 2007). Our objective here is to synthesize available African Middle and Late Pleistocene paleoclimatic and paleoanthropological records relevant to early populations of *Homo sapiens*. Although a number of studies have focused on providing the environmental context for hominin subsequent dispersals out of Africa (cf. Vaks et al., 2007; Osbourne et al., 2008; Carto et al., 2009; but see Basell, 2008; Cowling et al., 2008; Drake et al., 2008), recent genetic evidence has also indicated the importance of Pleistocene population dispersal within Africa and its importance in shaping modern human genetic diversity (e.g., Reed and Tishkoff, 2006; Behar et al., 2008; Tishkoff et al., 2009; Verdu et al., 2009; see also Hammer et al., 2011). Our goal therefore is to explore climatic variability within Africa during this time period to better understand both the context of intra-African hominin population dispersal and conditions relevant to out-of-Africa scenarios.

We emphasize the importance of considering different temporal and spatial frameworks for interpreting the role of climate change in human evolution, and these can be conceived of as occupying a continuum from macro-scale to micro-scale approaches. Macro-scale approaches include those that examine continental scale changes across long time intervals (e.g., Potts, 1998; deMenocal, 2004) or use coarse temporal frameworks such as the Marine Isotope Stage boundaries and glacial/interglacial variation (e.g., Lahr

and Foley, 1998; Marean and Assefa, 2005; Basell, 2008; Crowley and Hyde, 2008). At the other end of the continuum are micro-scale approaches that seek to understand the response of small populations to environmental change over relatively short periods recorded at a single archaeological site or depositional basin (e.g., Potts et al., 1999). We are not suggesting that either macro-scale or micro-scale approaches are 'better,' but rather that the scale of the available data should match the scale of the questions being asked.

Following other recent efforts (e.g., Fisher et al., 2010; Marean et al., 2010; Drake et al., 2011), we employ what might be termed a 'meso-scale' approach in the examination of sub-continental variation in paleoclimate and the human fossil and archaeological records. To do so, we synthesize paleoclimate data from diverse datasets of varying degrees of temporal and spatial resolution, divided into three broad categories: (1) cores from offshore marine sites, whose age models are largely constrained by the global oxygen isotope time scale. These provide relatively continuous data sampled over a large area, and provide key data on sea surface temperatures and ocean circulation patterns, changes in terrestrial vegetation patterns and relative aridity; (2) cores from a number of African lakes, particularly Lake Malawi and Lake Tanganyika as well as the impact crater lakes Tswaing and Bosumtwi, which provide relatively continuous records of watershed and regional environmental change; (3) a number of other terrestrial sedimentary archives, including caves, rockshelters, and open-air archaeological sites that provide temporally discontinuous, often highly local records of climatic and environmental change. We compare these climatic and environmental data to a database

of published, radiometrically dated hominin fossil- or artifact-bearing deposits to test whether these changes are coincident with demographic changes in Pleistocene African hominin populations.

We focus on the 150 ka to 30 ka time interval for theoretical and practical reasons. This time period is important as it includes much of the early history of *Homo sapiens*, and from an archaeological perspective, it includes the shift from MSA to Later Stone Age (LSA) technologies, an important change that may signal changes in human cognition or demography (cf. Klein, 2009; Powell et al., 2009). Pragmatically, 150 ka marks the beginning of the time interval for which statistically significant numbers of detailed, well-constrained records are available from both the oceanic sites surrounding Africa and for a number of the key lake records such as Lake Malawi. In addition, the paleoclimate records for the past 30 kyr (thousand years) in Africa have long been a focus of earlier reviews (e.g., Street and Grove, 1979; Nicholson and Flohn, 1980). Because we are aggregating datasets of varying degrees of temporal resolution, often particularly poor for the archaeological record, we examine paleoclimate change using 5 kyr intervals and paleoanthropological change using estimated 10 kyr intervals, as detailed below.

Research questions and hypotheses

We synthesize African paleoclimate and paleoanthropological data from 150-30 ka, and use these data to test a number of hypotheses.

1. Pleistocene tropical African precipitation history is coincident with glacial/interglacial history.

Many important recent works have used the Marine Isotope Stage (MIS) boundaries as a framework to explore the relation between Pleistocene African environmental change and human evolution (Lahr and Foley, 1998; Marean and Assefa, 2005; Barham and Mitchell, 2008; Basell, 2008). Such an approach has the potential to provide a common global temporal and environmental framework for exploring variation in Africa and elsewhere, but its utility would be severely compromised if African climates do not vary in phase with recognized MIS boundaries. We therefore test the extent to which changes in African paleoclimates are coincident with changes predicted by MIS boundaries derived from North Atlantic and North Pole data.

2. Pleistocene African climate change is coincident with Northern and Southern Hemisphere insolation cycles on a continent-wide basis.

A number of recent studies (e.g., deMenocal and Rind, 1993; Kingston, 2007; Trauth et al., 2009) have emphasized the importance of monsoon intensity driven by precession-modulated insolation for tropical African climates. This hypothesis predicts that climatic change follows ~19-23 kyr cycles rather than the temporally variable MIS boundaries, and that the impact of this cyclicity is strongly expressed across Africa. We test the extent to which changes in African paleoclimate are coincident with changes predicted by Northern and Southern Hemisphere insolation cycles.

3. Pleistocene tropical African precipitation history is the result of the complex interaction of a number of factors, including atmospheric dynamics.

Neither MIS boundaries nor precessional cycles likely account for all elements of climate change in Africa, and we thus explore other possible mechanisms including the paleo-position of the Westerlies and the Intertropical Convergence Zone (ITCZ). If the location of the Westerlies is a major driver of African climate, then the paleo-humidity records of North and South Africa should co-vary through time. Changes in the average ITCZ position over extended time periods may explain long-term moisture variation between ~20ºN and 15ºS (tropical and/or East Africa) over the 150-30 ka time interval.

4. Climate change is asynchronous across Africa.

Africa is large, spanning more than 70° of latitude. Given its size, it is perhaps unsurprising that a number of recent studies suggest that periods of climate change may be out of phase among different regions of Africa (e.g., Cohen et al., 2007; Scholz et al., 2007). We test this hypothesis by comparing climate change in Africa among four latitudinally-defined regions (North Africa and the Levant, East Africa, tropical Africa, southern Africa). This spatial component is often overlooked or insufficiently stressed in studies combining archaeological and environmental datasets.

5. Changes in climate impacted the distribution of Pleistocene African hominin populations.

Genetic and fossil data suggest demographic changes among Pleistocene African populations of *Homo sapiens*, including fluctuations in size and increases in ancient lineage diversity that may be linked to environmental change (Lahr and Foley, 1998; Excoffier, 2002; Ambrose, 2003; Prugnolle et al., 2005; Mellars, 2006; Basell, 2008; Behar et al., 2008; Carto et al., 2009; Crevecoeur et al., 2009; Gunz et al., 2009; Tishkoff et al., 2009; Marean, 2010). We use the frequency of paleoanthropological sites from across Africa as a crude proxy for changes in relative hominin population size for a given time interval. We expect that climate change and its more local impacts on floral and faunal communities will affect the nature, distribution, and abundance of human forager societies. However, environmental change, particularly increased aridity, likely had different effects on each of our four latitudinally-defined geographic regions. For example, drier intervals in tropical Africa may have made more areas accessible to hominin foragers through the fragmentation of dense forests and consequent creation of new or wider ecotones (e.g., Ambrose, 2001; Cornelissen, 2002). In contrast, some increase in aridity in parts of eastern Africa and the southern African interior could have promoted the expansion of grasslands, where much of the edible biomass is distributed among dispersed migratory game herds, potentially causing hominin foragers to experience resource stress, population dispersal or decline (see discussion in Marean, 1997). Marginal areas, such as deserts, may have been abandoned during periods of heightened aridity. Coastal zones may have been the least affected by increased aridity, although shallow gradient coastal margins would have shifted dramatically with lowered sea levels, exposing new coastal environments (Marean, 2010). We can predict relative

increases and decreases in population density and site visibility from each of these outcomes. Specifically:

(a) The southern African interior (and possibly the coast) was largely depopulated during arid intervals, particularly during the last 60 kyr, as a result of environmental degradation and shoreline shifts. This hypothesis has been most clearly articulated in the work of Deacon and Thackeray (1984), Butzer (1988), and Klein (2009).

(b) Hominin populations in the equatorial portions of the continent show relatively muted responses to climate change. This hypothesis is consistent with Ambrose (1998), Marean and Assefa (2005), and Basell (2008). They suggest that hominin populations in East Africa and, to a lesser extent, tropical Africa may have been buffered from some of the extremes of climate change seen elsewhere as a result of locally steep altitudinal and rainfall gradients. As such, we predict muted demographic responses to environmental change compared to other regions. This hypothesis is also consistent with ecological studies indicating greater endemism among all vertebrate species in more tropical regions with high topographic relief (e.g., Sandel et al., 2011).

(c) The nature and expanse of the Sahara strongly influenced the population history of northern Africa, with occupation of much of the interior of this region limited to periods of increased humidity when the 'green Sahara' was characterized by savanna and lake environments. As a corollary, 'out of Africa' hominin dispersals are similarly constrained to these humid intervals. The impact of environmental change in the Sahara region on local human populations is an idea with a significant intellectual pedigree, but most recently synthesized by Osborne et al. (2008) and Drake et al. (2011).

Methods

To test these hypotheses, we constructed a database from the published literature synthesizing all relevant dated climatic and paleoanthropological data. The geographic locations of these datasets are shown in Figures 1 and 2, with data synthesized in Tables 1 and 2. Note that throughout the paper, paleoclimate data archives are referenced by the numbers presented in Table 1.

Paleoclimate data collection

We collected and examined quantitative and semi-quantitative records of African paleoclimate for the 150-30 ka interval from the published literature from sites across the African continent and the surrounding regions of the Mediterranean, Near East and the adjacent ocean basins. The chosen terrestrial records are radiometrically dated, whereas the marine records are primarily dated through correlation with the marine oxygen isotope record. Data were compiled from published, tabulated information, or, when necessary, digitized from published graphs using DigitizeIt © (www.digitizeit.de). Changes in temperature and moisture availability are the primary indices of terrestrial paleoclimate variation, and we employ a number of different proxy measures of these variables in our analyses. These paleoclimate records from marine, nearshore, and terrestrial settings are summarized in Table 3, with syntheses relying strongly on sea surface temperatures (SSTs) for the marine records, and intervals of 'wet,' 'dry,' 'hot,' or 'cold' relative to the average for a particular site.

African regions

As shown in Figure 1, Africa and its surrounding area are divided into regions for comparisons among the marine and terrestrial data. Marine data archives are classified into one of four regions based on their geographic location: northern Atlantic and Mediterranean, southern Atlantic, Indian Ocean, and Southern Ocean (Figure 1a). The terrestrial data were grouped into regions that show persistent climatic similarities through time, and that are distinct from bounding areas. Regions are divided as follows: North Africa and Levant, East Africa, tropical Africa, southern Africa (Figure 1b). The North Africa region includes those areas north of ~15ºN, East Africa extends northeast from the Eastern Rift Valley towards the Horn of Africa between the North Africa and tropical regions, the tropical region extends southward from ~15ºN in western Africa and ~1ºS in eastern Africa, with the southern boundary at ~19ºS latitude, and southern Africa including areas south of ~19ºS. The exact placement of the northern and southern boundaries for 'tropical Africa' is primarily defined by the location of sites displaying a 'megadrought' signal between 90 and 135 ka (see Scholz et al., 2007). The same terrestrial regions were used to analyze the paleoanthropological data and the data from marine cores housing paleoclimate archives of continental origin, such as windborne pollen records.

Paleoclimate data analysis: regional analyses of temporal trends

Climate histories for the marine SSTs and continental data were summarized based on all data, including discrete and discontinuous datasets. We visually inspected the bivariate plots comparing changes in paleoclimate records and time, to assess the synchrony of aridity/humidity among the different regions of the continent with temperature in local and distant oceanic regions. The relation and timing of changes related to orbital forcing of subtropical summer insolation and high latitude variability and global glacial/interglacial phases was determined using principal components analysis (PCA) using R (http://www.r-project.org/).

Data used in the PCA were taken from each 'usable' dataset every 5 kyr over the period of the analysis, using multiple temperature and precipitation proxies from numerous locations. 'Usable datasets' did not include low-resolution datasets with binary-type information, and had to cover the entire time interval to be included in the analysis. These data were then transformed to satisfy the analytical assumptions of PCA. Specifically, data were normalized to a maximum value of one so that no large value was given more weight than others; rather the polarity of the trends (positive or negative) was highlighted. This normalization also eliminated the potential discrepancies associated with the differing units used in each dataset (e.g., count data may produce values from 0-1000, whereas percentage data may only range from 0-100).

We used PCA to examine all available continuous datasets, however, only 20 (primarily SST or offshore pollen records) covered the entire period from 150-30 ka. Therefore, to maximize the number and types of data included in the total analysis, four sub-intervals of time were selected for separate analyses: 150-100 ka, 140-30 ka, 115-30

ka, and 75-30 ka. These intervals were selected to sample periods of both high and low insolation variability and to maximize the number of datasets included in each discrete analysis. The continuity and length of the record determined which datasets were used for each time interval. More recent intervals are better represented among the published data, so the four sub-intervals included 32-40 datasets, respectively in each analysis.

Paleoanthropological site data collection and analysis

We tabulated known, radiometrically-dated archaeological and hominin fossil sites from Africa with assemblages spanning 150-30 ka, summarized in Figure 2 and Table 2, and used the density for evidence of hominin occupation of a region for a given temporal interval as a measure of demography, with greater site density suggesting larger hominin populations. For more recent periods, others have used the frequency of radiocarbon-dated sites to estimate changes in population density (e.g., Gamble et al., 2005; Surovell et al., 2009). In seeking patterns among the frequency of radiometric dates, where the density of dates is high, a plausible argument can be made that the sheer volume of data removes concerns about error ranges and stratigraphic relations associated with the reported age estimates. This is what is done with most efforts that rely on very large databases ($n \approx 500\text{-}2000$) of radiocarbon age estimates (see discussion in Gamble et al., 2005). When the sample size is low, as it is here, these issues remain serious concerns, and we have opted instead to provide an age range that accounts for instrumental error or uncertainties as well as stratigraphic information, the latter particularly important as most of what is dated at paleoanthropological sites are not the

artifacts or human fossils themselves but rather bounding strata or other materials that provide age minima or maxima.

Our data tabulation and presentation methods consist of six steps. (1) We provide one or more age ranges for each site based on the stratigraphic relations of the published radiometric age estimates (at one standard deviation) to the archaeological strata for a given site. In general, at open-air site complexes, individual sites with overlapping time ranges have been combined to make them more comparable with the more frequently reoccupied, and thus more archaeologically rich, caves and rockshelters. (2) The time span of 30-150 ka is divided into 10 kyr bins (31-40 ka…141-150 ka). Ten thousand years is our arbitrary maximum temporal resolution for the sites considered here. It is estimated on the basis of instrumental error and stratigraphic relations among dated deposits and paleoanthropologically relevant material. (3) A site is given equal probability for the 'true' age to occur within each of the 10 kyr bins in which its range falls. Thus, a site such as Enkapune ya Muto with an estimated age range of 33-55 ka would fall into the 31-40 ka, 41-50, and 51-60 ka bins. The advantage of this approach is that it requires the fewest analytical assumptions and accounts for the fact that we typically lack the basis to reliably assess the likelihood of site dating to a particular year within that range. The disadvantage is that dates with large error ranges that span numerous bins have the potential to mute variation within the total dataset. (4) For each region, we sum the total number of occurrences in each 10 kyr bin, and normalize this value to the total number of age bin occurrences in that region, expressed as a percentage. As a result, proportional change in one region is numerically independent of change in

another region. (5) These data are then expressed as line diagrams to explore temporal changes in the frequency of sites relative to climate change for the each of the North, East, tropical, and southern African regions. (6) To offset the potentially confounding effect of locally increased moisture availability, we separate interior and 'coastal' sites for southern and northern Africa (coastal sites in our time range are largely lacking for East and tropical Africa), and consider Nile Valley separately in this analysis as it represents a highly localized area of available water in otherwise often dry environments. Because the changing position of the South African shoreline is now well-understood, sites from this region are variably attributed to 'coastal' and 'interior' depending on contemporaneous coast location as per data from Van Andel (1989) and Fisher et al. (2010).

As emphasized by Bailey (2007), the temporal resolution of the dataset determines the scale of the questions to be asked, and a 10 kyr time span is too broad an interval to examine in detail the relation between environmental and human behavioral change. This can be seen particularly well in southern Africa, where a comprehensive program of single-grain optically stimulated luminescence dating has demonstrated that distinctive MSA archaeological entities and behavioral traditions such as those seen at Howiesons Poort and Still Bay sites in southern Africa appear, spread, and disappear within ~5 kyr (Jacobs et al., 2008a, b). This is less than the ~10 kyr resolution of our aggregate dataset, and in this particular case, site-specific paleoenvironmental reconstructions are still poorly defined and the relation between environmental and archaeological change is controversial (cf. Ambrose and Lorenz, 1990; McCall, 2007;

Jacobs et al., 2008a; Chase, 2010). Rather than exploring the nature of environmental and behavioral change, the scale of our dataset is more appropriate to larger scale questions about the demographic or biogeographic structure of the archaeological or paleontological record.

Population density or size is notoriously difficult to demonstrate from fossil or archaeological data (but see recent efforts for Late Pleistocene western Europe by Mellars and French, 2011). While a number of site-specific approaches have shown that human impacts on various animal taxa can be a reliable measure of population pressure (Klein, 1980; Stiner et al., 1999; Faith et al., 2011), these sorts of data are not available or reliable for many African sites. Although problematic, our use of site density as a measure of Pleistocene hominin demography for a given time interval remains the best measure available for our pan-African approach. We use bivariate plots to assess temporal changes in paleoanthropological site frequency for each of the four regions relative to the timing of inferred paleoclimate changes.

Interpretive frameworks for African paleoclimates

Modern African climates provide the basic interpretive framework for interpreting Pleistocene climate and environment. The climate of a given location describes the average annual as well as seasonal variation in temperature and precipitation over a long period of time. Climate dynamics refers to the physical mechanisms that create a particular climate in one location, and a different climate in another.

Oceanic currents and surface temperatures

There are four main surface ocean currents that encircle Africa: the Canary, Benguela, Agulhas, and the Antarctic Circumpolar Current (ACC) (Figure 3). The strength and extent of these currents often dictates rainfall patterns along the coast by affecting mean air mass boundaries and moisture availability and transport. The colder currents inhibit regional precipitation, whereas warm currents tend to promote increased rainfall in nearby areas. Global patterns of sea surface temperatures (SSTs) can have a significant effect on the precipitation patterns over the African continent. Two such patterns affecting rainfall in Africa are the El Niño Southern Oscillation (ENSO) and the Indian Ocean Dipole (IOD). 'Normal' ENSO years in the Indian Ocean are characterized by warmer waters in the eastern Indian Ocean (near Australia), colder SSTs in the western Indian Ocean, and 'normal' (limited) rainfall occurs over the Horn of Africa. During El Niño years, the SST patterns and associated rainfall patterns are reversed, bringing extreme drought to Australia and flooding to parts of East Africa. The IOD, once viewed as noise when analyzing ENSO, is increasingly being accepted as its own phenomenon (Marchant et al., 2007). The dipole refers to SST variation across the Indian Ocean associated with the strength of the winter monsoon winds and a cold tongue in the Arabian Sea (Saji et al., 1999; Prasad and McClean, 2004). A positive IOD event produces a pattern similar to El Niño with colder waters near Australia and anomalously warm SSTs in the northwestern Indian Ocean, and the ENSO and IOD may modulate each other when they co-occur (Bowden and Semazzi, 2007; Yuan et al., 2008). Although ENSO and IOD may have far reaching atmospheric teleconnections, the IOD is

defined strictly by temperature variation in the Indian Ocean whereas ENSO is defined by atmospheric pressure patterns over the Pacific Ocean. It is however these atmosphere-ocean teleconnections that may play a large role in local and regional SST to terrestrial precipitation relationships through time.

Air masses

African climate is affected primarily by tropical (continental and marine) and equatorial air masses. Precipitation patterns are driven by the mid-latitude Westerlies in the extreme northern and southern regions of Africa and the location of the Intertropical Convergence Zone, or ITCZ, in the middle portion (Figure 3). The Westerlies are high altitude winds that blow from the west and define areas where cool dry air from the poles collides with warm, moist air from the tropics causing instability and convection (Rohli and Vega, 2008). These are 'frontal boundaries' and are often associated with rising moist air, cloud formation and precipitation. The position of the Westerlies, particularly around Antarctica has recently been shown to vary with global temperature (Toggweiler and Russell, 2008) with the Westerlies strengthening while contracting pole-ward during warm periods and weakening while expanding equator-ward during colder periods. If the location of the Westerlies is the dominant driver of African climate, then northern and southern Africa should be wet when the Westerlies are weak (equator-ward) because they then bring rainfall and weather systems to the region. However, when the Westerlies are strong, northern and southern Africa should be dry, without atmospheric circulation bringing moisture off the ocean.

The ITCZ approximates the zone of maximum insolation (solar energy) received by the atmosphere and the Earth's surface. Insolation duration and intensity is orbitally forced by eccentricity-modulated precession at low-latitudes with a periodicity of 19-23 kyr. The ITCZ moves between the Tropics of Cancer (June) and Capricorn (December), crossing the equator at the equinoxes. It is a 'convergence' zone because: (1) the sun's energy is converted to heat at the surface and in the atmosphere, and (2) air that is warmer than its surroundings will rise forming an area of surface low pressure. This draws in surface winds flowing equator-ward from the east (trade winds, Figure 3) causing the trade winds from the Northern and Southern Hemispheres to converge at the ITCZ. Direct insolation effects on areas within the ITCZ include a 1°C SST increase over the oceans leading to more evaporation, and on land a region of increased convection, and consequently rainfall (Liu et al., 2004).

Monsoons

Monsoon systems are "a seasonal reversal of wind caused by [large]-scale [atmospheric] pressure changes, often accompanied by seasonal changes in moisture" (Rohli and Vega, 2008: 416). The well-known South Asian monsoon, for example, brings torrential rainfall and flooding to the Indian continent. The West African monsoon and the East African monsoon are both caused by differential heating between the land and the neighboring ocean (e.g., enhanced land-ocean temperature contrasts) during the summer (Kutzbach and Liu, 1997). Terrestrial surfaces heat more quickly than the ocean surface as a result of the high specific heat capacity of water. When a coastal region

warms, the land will heat more quickly than the neighboring ocean. Therefore, the air mass over the land will rise (low pressure), drawing moist air landward from the ocean. This convection in the presence of a moisture source produces rainfall. During an off-monsoon season, the land surface will also lose heat more quickly than the ocean, and the winds and pressures will reverse, with a high-pressure system situated over the land, stabilizing the air.

As discussed previously, the ITCZ follows the area of most intense insolation, which occurs when the sun is directly overhead (during the summer), and the position of the ITCZ drives the East and West African monsoons. However, because the monsoonal circulation system (associated with atmospheric pressure changes) is dependent on land-ocean temperature contrasts, an external perturbation (e.g., changes in land-surface albedo, variations in ocean circulation patterns and therefore temperature) in the system can cause monsoon rainfall to be weak or to not arrive at all. In addition, monsoons will be intensified when incoming insolation is high and vice versa.

Monsoons are dynamic systems in two ways: thermally and hydrologically, meaning monsoon systems respond to land/ocean temperature contrasts, and are also dependent on SSTs, evaporation from oceans, and water vapor transport to land (Kutzbach et al., 2008). The differential heating of land and ocean near and below the average location of the ITCZ can upset both oceanic and atmospheric dynamics, ultimately affecting the extent and position of tropical monsoons globally. As a consequence of its effect on monsoon systems, the average position of the ITCZ over time may also greatly affect the climate in regions on the extreme edge of the ITCZ

range, as small shifts one way or another will have a greater impact there (Brown et al., 2007).

Major drivers of climate variability on millennial and longer time scales

Over the time period of interest in this synthesis, there are a number of important drivers of global and regional climate variability. These vary in scale, regional impact, and periodicity. Orbital (large) scale climate drivers include glacial-interglacial periods, greenhouse gas (GHG) concentrations, position of the Westerlies, and insolation intensity, the latter affecting the position of the ITCZ and monsoon strength. Orbital variations in insolation at both high- (obliquity) and low-latitudes (precession) are both potentially important drivers of the climate dynamics of the African continent. These variations affect ice volume at the poles, monsoon intensity, and global SSTs. Millennial scale climate drivers include changes in oceanic circulation patterns, which can change ice sheet stability triggering Heinrich and Dansgaard/Oeschger (D/O) events which have local, regional and global effects.

The periodicity of orbital scale events is determined by the relative position of the Earth in its orbit around the sun at the equinox (precession), the angle of axial tilt relative to the plane of the ecliptic (obliquity), and the shape of the Earth's orbit (eccentricity). These have calculated periodicities of ~23 kyr, ~41 kyr and ~100 kyr, respectively. Additionally, each affects different regions of the globe more than others. Precession is a low-latitude (equatorial) forcing mechanism and is largely responsible for regulating the intensity of the monsoons (Kutzbach, 1981) with greater low-latitude insolation

producing higher intensity monsoons (Rossignol-Strick, 1985; Kutzbach et al., 2008). Obliquity regulates high-latitude insolation receipt and it, in combination with eccentricity, is responsible for the 100 kyr periodicity of glacial/ interglacial cycles (Imbrie and Imbrie, 1980). Eccentricity also has an amplifying effect on the precession cycle, so much so that they are often combined when discussing low latitude forcing, 'eccentricity modulated precession.' It is responsible for variations in tropical African monsoon intensity and timing (deMenocal and Rind, 1993; Trauth et al., 2009). Greenhouse gas concentrations, specifically CO_2, have been shown to vary in concert with global ice volume and thus glacial cycles, at a 100 kyr periodicity (Petit et al., 1999).

Millennial scale events, such as Heinrich and D/O events, are smaller in scale in both time and space, often lasting only a few thousand years or less. Heinrich events are times when numerous icebergs broke off from Arctic glaciers and melted, delivering significant quantities of cold, fresh water to the North Atlantic thereby altering global thermohaline circulation (Bond et al., 1992). D/O events are intervals of rapid warming followed by a gradual cooling (Dansgaard et al., 1993), whereas Heinrich events are characterized by rapid and sudden cooling in the Northern Hemisphere. Both of these events were originally thought to have only high latitude effects, but subsequent research has shown the existence of global teleconnections between presumed high latitude drivers and low latitude climate changes at these time scales, including in Africa (e.g., Tierney et al., 2008; Moernaut et al., 2010; Stager et al., 2011).

Paleoclimate results: sea surface temperatures and paleoceanographic conditions

Sea surface temperatures (SSTs) typically reflect changes in mean global temperature because they are global in extent, and water has a high heat capacity. The various measures of SST are summarized in Table 3. Figure 4 summarizes various measures of sea surface temperatures for the northern Atlantic, Mediterranean, southern Atlantic, Indian Ocean, and Southern Ocean regions.

Northern Atlantic records

As shown in Figure 4, Atlantic SSTs recorded off the NW coast of Africa (>35°N) from 150-30 ka are consistent with the North Atlantic-defined glacial/interglacial MIS pattern, with maximum temperatures around 125 ka and decreasing temperatures towards 50 ka. North Atlantic SSTs show a consistent saw-tooth glacial/interglacial pattern that mirrors the $\delta^{18}O$ record of ice volume recorded in the Greenland ice cores (GRIP and GISP2). At times of lower ice volume and warmer global temperatures, the North Atlantic reflects this change quickly with increased SSTs. This suggests that high latitude forcing affects the SSTs of the subtropical Atlantic Ocean off NW Africa.

Southern Atlantic records

The SST records from the equatorial and southern regions of the Atlantic Ocean (5°N to 25°S latitude) also display the characteristic North Atlantic saw-tooth pattern

(Figure 4). Between 50-45 ka the records diverge as the most northerly record (7°S) and the most southerly record (26°S) inexplicably begin to increase in temperature.

Minor variations in each record may be explained by regional rather than global causes. These could include variations in dominant local wind patterns and/or upwelling activity. For example, a number of studies interpreted the circulation pattern of the Angola-Benguela Front (ABF – 4°N-20°S) through time (see Figure 1) and all conclude that the trade wind belt over Angola has not shifted spatially over time with glacial/interglacial variation in climate. Instead of an increased alongshore flow of the Benguela current during glacial times, there was a shift to more offshore flow coincident with increased trade wind zonality and reduced monsoon intensity (see Table 1: 38a, b, c) (Schneider et al., 1995; Little et al., 1997). Other researchers using data from sites further south (33a) (e.g., Pichevin et al., 2005; Martinez-Mendez et al., 2010) found a negative correlation of SSTs and grain size. During periods of colder SSTs, the sediments being deposited were statistically coarser. As colder waters in this region may indicate upwelling activity and more energy is needed to move sediments of a larger size, it is reasonable to conclude that colder SSTs in the record signal periods of increased wind strength as well as upwelling activity. The different interpretations by Schneider et al. (1995) and Pichevin et al. (2005) of the dynamics in the southern Atlantic may be region-specific, with colder periods further north the result of increased trade wind zonality and further south resulting from stronger overall winds. There is also a 23 kyr periodicity observed in the SSTs off Angola, which Schneider et al. (1995) argue is produced by

changes in low latitude insolation and monsoon intensity, and not by high latitude climate forcing, despite the apparent similarity to North Atlantic records.

These exceptions notwithstanding, the southern Atlantic SST curves are similar to the global marine $\delta^{18}O$ curve used to define the MIS boundaries.

Indian Ocean records

Like the Atlantic Ocean records, the time interval with the warmest SSTs in the Indian Ocean is 130-120 ka (Figure 4). However, the similarity between the Atlantic and (Northern Hemisphere) Indian Oceans decreases through time, and with increased distance from the African coast. Closest to the African coast, the SST records from 3°N, 0°N, and 14°N (1a, 1b, 55a) are the most similar to the North Atlantic record, showing last interglacial peak temperatures (at ~125 ka) and the distinct saw-tooth pattern of temperature variation and decrease overall through time.

Some of the differences between the Atlantic Ocean and Indian Ocean records may again be attributed to changes in deep water upwelling patterns and variation in local to regional monsoonal winds, the latter correlated with Northern Hemisphere glacial/interglacial cycles and strengthened with insolation intensity. Pollen records suggest high frequencies of taxa from the Mediterranean steppe in the Arabian Sea during glacial periods, indicating stronger NE trade winds and increased regional aridity (Van Campo et al., 1982). Additionally, low $CaCO_3$ content in the Arabian Sea during colder periods reflect reduced upwelling due to decreased strength in the SW monsoon airflow (23a) (Leusschner and Sirocko, 2000). Similarly, SSTs determined from two cores off

Oman and southwest of India (37a, b) contribute information about the timing of the NE and SW monsoons (Rostek et al., 1997). At these locations there is a correlation between increased productivity on precessional time scales and glacial periods, with concomitant decreases in productivity during interglacial periods. Like Van Campo et al. (1982) the authors interpret a stronger NE monsoon during glacial times as producing greater wind-induced surface mixing and therefore increased nutrient supply. However, the record off the coast of Oman is more complicated and does not show a precessional signal. The SST records from both sites indicate warmer temperatures during interglacials and interstadials and colder temperatures during glacials and stadials as expected. While the warmest period recorded in the sediments is at ~125 ka during the peak of the last interglacial, the coldest period occurs at ~45 ka, prior to the LGM. As discussed earlier, this may be the result of reduced upwelling during full glacial times, causing an apparent local increase in SST.

The three Indian Ocean SST records closest to the continent (55a, 1a, b) are similar to the global marine $\delta^{18}O$ curve used to define the MIS boundaries, although the 1a and 1b records show a muted response, likely due to their proximity to the equator. The remaining two records show more of a response to local wind and upwelling activity (23a, 37b). The one outlying record is from closer to the central Indian Ocean basin, and may be responding to something different altogether (37a).

Southern Ocean records

For the most part, SST records from the region that is the interface between the southern Atlantic Ocean and the Southern Ocean, which surrounds Antarctica, are extremely similar to the records from the rest of the Atlantic Ocean (Figure 4**)**. They have a characteristic saw-tooth pattern, with maximum SSTs between 120 ka and 130 ka, and gradually decrease in temperature towards 30ka. However, the most southerly record (6a at 49°) lacks the saw-tooth pattern, with temperatures fluctuating around a mid-point of ~3°C with no observable trend. It appears that this region is being affected more by the cold waters of the Antarctic Circumpolar Current (ACC) than the North Atlantic.

Sea surface temperature summary

The SSTs surrounding the African continent are generally consistent with the global marine isotope stage (MIS) record, although the causes for this may be different. Around the continent, the warmest SSTs occurred between 130-120 ka, during the peak of the last interglacial (MIS 5e). The Atlantic records display the characteristic saw-tooth pattern when not interfered with by regional monsoonal effects or local upwelling activity (e.g., Little et al., 1997; Weldeab et al., 2007; Martinez-Mendez et al., 2010) and generally decrease in temperature from ~125 ka to 30 ka. The Indian Ocean records are the least similar to the North Atlantic, with this region likely much more heavily influenced by the East African and Asian monsoons (Rostek et al., 1997; Leuschner and Sirocko, 2000).

Paleoclimate results: terrestrial and marine records of continental temperature and precipitation variability

SSTs are an important measure of global temperature and have an important impact on continental moisture availability, but the relationship between oceanic and continental records is complex. The continental records, although often providing less continuous data than the oceanic records, are more directly relevant for understanding the climatic and environmental context of Pleistocene human evolution. Areal coverage and the types of paleoclimate proxies and indicators available are more varied relative to those used to infer SSTs, summarized in Table 3. Figures 5-8 summarize paleoclimate data by proxy type for each of the African sub-regions, showing the temporal relations of inferred regional wet/dry regimes relative to established MIS boundaries.

North Africa and the Levant (Figure 5)

The types of paleoclimate indicators for North Africa (>18°N) are the most varied of the dataset, and provide the most abundant data. Unlike some of the other sub-regions, many of the datasets from North Africa have good chronological control because of multiple U/Th dated lacustrine (16a, 26a, 47a, 10a), spring-fed (40a, 42a), groundwater (31a), or speleothem carbonates (28a, 3a, b, 54a, 43a), all interpreted as reflecting more humid intervals. Additionally there are numerous datasets with terrestrial climatic indicators collected from marine cores; e.g., pollen (21a-c), freshwater diatoms (34a) and siliciclastic grain size (52a).

$\delta^{18}O$ values in Soreq (3a) and Peqiin (3b) caves in the eastern Mediterranean and speleothem frequencies from a number of other caves in the Dead Sea region of Israel (43a, 54a) have been used to interpret paleo-rainfall and humidity. The Levantine $\delta^{18}O$ records are internally consistent with a considerable wet period extending from 135 ka to 120 ka followed by a drier period from 120 ka to 90 ka. This is followed by a resurgence of humidity from 90-80 ka, after which these records show gradual aridification. In fact, the $\delta^{18}O$ records from Soreq and Peqiin caves record a pattern very similar to the North Atlantic and Mediterranean SST records, suggesting that the $\delta^{18}O$ values in the speleothems may be responding more to $\delta^{18}O$ values in the source water than to regional humidity (McDermott, 2004). Speleothem age frequencies are also used to infer periods of rapid speleothem growth and thus humidity (Vaks et al., 2007; Sorin et al., 2010). Speleothem frequencies from the Dead Sea region support the inference of humidity from 135-120 ka (54a), and record additional humid periods in the more recent record coincident with some seen throughout the rest of North Africa (43a).

Most of the records from carbonates in the Egyptian Sahara and across North Africa indicate wet conditions between 135 ka and 115 ka, similar to the Levantine records (24a-e, 31a, 42a). Like the records further east, there is then a short period of relative aridity followed by a return to humid conditions. Across North Africa this wet period lasted from 100 ka to 75 ka, with humid conditions beginning earlier and lasting longer than in the Levant. The majority of records from North Africa again display more arid conditions from 75 ka to ~45 ka when humid conditions return until 35 ka (24a-e, 30a, 16a, 10a), similar to the Dead Sea speleothems (44a).

Pollen records from three marine cores off the coast of Morocco (21a-c) allow for the reconstruction of the northern and southern boundaries of the NW Sahara. The north to south range of the cores allows for the demarcation of latitudinal differences in the pollen being swept to sea off the African continent and thus changes in the vegetation belts. Changes in the pollen regime from one site to the other allows for interpretation of the expansion and contraction of the NW Sahara through time. The extent of the Sahara fluctuates on glacial/interglacial cycles with an enlarged steppe-like transition zone north of the desert vegetation during glacial periods. Additionally, the northern boundary of the Sahara expanded further northward during glacial times. During interglacials this transition zone was narrow, with Mediterranean vegetation expanding towards the Sahara from the north and Sahelian (or tropical) woodland from the south. The pollen data from this region show a correlation with Northern Hemisphere ice volume.

Aeolian-derived freshwater diatoms of the genus *Melosira* (Pokras and Mix, 1985) from four sites off the coast of West Africa (34a-d) are indicators of extreme continental aridity. The most northerly record (34a) shows periods of aridity that closely follow times when the Saharan desert expands, and vice versa (Hooghiemstra et al., 1992). Generally, this record is similar to the northern records discussed above with a slight lag as this proxy records the extreme aridity that follows lake desiccation, deflation, and windblown transport. The more southerly diatom records (35b-d) reflect aridity in the tropical region and will be discussed further in that section.

A humidity index generated using the ratio of aeolian dust to fluvial mud (52a), has a comparatively fine scale resolution, so while following a similar long-term pattern

as the Sahel/Sahara boundary observed from the offshore pollen record from sites 21a-c, it does not correspond well to the higher frequency freshwater diatom record (34a). In fact, for the period of time it covers (120-30 ka), the record is extremely similar to the oxygen isotope record from Peqiin Cave in Israel (3a). As mentioned earlier, the Israeli cave sites appear to strongly co-vary with changes in the SSTs of the Mediterranean and by extension, the Atlantic Ocean, suggesting that the underlying driver of this 'humidity index' may be marine SSTs, whether through atmospheric teleconnection, or a misinterpretation of the grain size indicator.

In summary, North Africa to the Levant experienced generally humid conditions beginning between 135-130 ka and lasting until 120-115 ka, and again from 100-95 ka until 75 ka. Additionally, a few records across the continent and Levant (44a, 24a-e, 10a, 30a) indicate a more recent wet period from 45-35 ka. These wet periods are dated by speleothem $\delta^{18}O$ measurements and frequencies, the deposition of lacustrine, spring-fed, groundwater and cave carbonates. Conversely, the region was drier between ~115-100 ka and from ~75-45 ka, based upon a paucity of dates for carbonate deposition during these periods and from pollen in offshore marine cores that illustrate the fluctuating limit of the Sahara. Additionally the majority of Levantine cave records and the offshore diatom records are quite variable prior to 75 ka, at which point the climatic variability in NW Africa and the Levant dampens considerably through 30 ka. Overall the regional variations in climate do not appear to fluctuate in response to changing MIS.

East Africa

The records from this region (Figure 6) are derived from a variety of indicators and were recovered from both terrestrial and marine localities. This region is small and in many respects it represents a paleoclimatic transitional zone between the North African records and the tropical records discussed next. On the continent, two discrete records of lake level highstands are interpreted from U/Th dating of lacustrine carbonates (17a, 56a), whereas a continuous record of lake level change was reconstructed using sediment characteristics and diatom assemblages (53a). The paleoclimatic interpretations of this region are relatively consistent with one another despite the variety of indicators used and time periods covered by the individual datasets.

The lake level records presented here are from the Ol Njorowa Gorge area (paleolake deposits close to modern Lake Naivasha) (53a), and Lake Magadi in Kenya, Lake Natron (17a) in Tanzania, and lakes in the Horn of Africa in Somalia (56a). These records show some similarities, with high lake levels indicating extremely wet periods occurring between ~145-120 ka, ~110-95 ka, and ~80-65 ka. The periods of increased humidity have been inferred to be times when the SW monsoon is most active, during interglacials and interstadials (Hillaire-Marcel et al., 1986; Voight et al., 1990). This interpretation is consistent with the offshore pollen record recovered (Van Campo et al., 1982) that demonstrates that interglacials were the most humid, likely due to the dominance of the SW monsoon over the NE monsoon that prevailed during glacial/stadial periods. The NE monsoon brought Mediterranean pollen to the Arabian Sea illustrating the dominant wind patterns at that time. These inferences are further supported by an upwelling record in the Arabian Sea (23a) that shows an increased abundance of $CaCO_3$

during interglacials, implying increased rates of primary production, and increased rates of aeolian deposition from the continent during glacial times, suggesting increased aridity. Increased productivity is an indication of increased upwelling, which brings nutrients to the surface, and it is expected when the SW monsoon is strongest. Likewise, decreased upwelling and aeolian deposition from the NE is expected when the NE monsoon is dominant. However the continuous record from Ol Njorowa Gorge demonstrates the importance of peaks in equatorial (local) insolation, rather than high-latitude forcing (Trauth et al., 2003). Unlike insolation intensity further from the equator that is highly variable for a time, and then dampens after 75 ka, the insolation at the equator maintains a constant variability in intensity throughout the period of interest (150-35 ka). This local forcing is evident in the constant, cyclic nature of this record (Trauth et al., 2003). Further, the records from East Africa share similar wet/dry interval patterns with the southern extent of the Saharan desert (21a-c). This suggests that the northern boundary of the region may be more transitional, whereas the East African records lack the characteristic 'megadrought' signal found at locations just to the south in the tropical region, suggesting its southern boundary is more abrupt.

In summary, based on lake level and vegetation reconstructions and upwelling histories, we infer that the East African region was wet ~145-120 ka, ~110-95 ka, ~80-65 ka and 50-55 ka. These variations were likely caused by or related to the changing influences of the NE and SW monsoon regimes forced by changes in local insolation at the equator with increasing influence of high latitude/glacial forcing moving away from the equator.

Tropical Africa (Figure 7)

The terrestrial data for tropical Africa are derived from a mix of offshore pollen and diatom records (12a, 13a-d, 34b-d), lacustrine records (48a, b, 45a, 27a) and aeolian dune sediments (2a, 44a, 49a). The northern part of the region contains both continuous and discrete records from a number of the East African Rift lakes, e.g., Tanganyika and Malawi, and meteorite/volcanic crater lakes, e.g., Bosumtwi (Ghana) and Challa (Tanzania). The southern area of the region extends to the northern Kalahari and yields a climate signal from dune migration.

The unifying climatic similarity of the records in this region is that they all show evidence of intense 'megadroughts' between 90 ka and 115 ka (Cohen et al., 2007; Scholz et al., 2007) that are not seen at locations both north and south of the region (53a and 7a respectively; Figure 7). At Lake Tanganyika, the maximum low-stand occurred at ~106 ka (25a) (McGlue et al., 2008). An earlier arid excursion is recorded at Lake Malawi (45a) and one offshore diatom record (34b) from 135 ka and 130 ka, but is not seen in the northern Kalahari records (44a), or the other two offshore diatom records (34c, d). Perhaps this was a very localized event that happened to be captured by one of three distant marine records. After 90 ka, the entire region gradually, though irregularly, becomes more humid until ~50 ka when the southern dune records are no longer synchronous with the northern lake records. Between 50 ka and 40 ka, the southern portion of the region (44a, 48b) becomes more arid while the northern lakes (45a, 27a) indicate greater or similar humidity (Figure 7). The entire tropical region is wet between

35 ka and 30 ka. Off the coast of West Africa, three equatorial pollen records support the regional patterns of aridity and humidity primarily during MIS5, with a short time lag observed similar to the offshore diatom records (34b-d).

Compared to the dune records, some of the lake records provide climate data at a higher resolution over the entire period of interest (Stone et al., 2011) and during the more recent portion of that time period (Tierney et al., 2008; Woltering et al., 2011). Scholz et al. (2007) argued for high amplitude lake level variability at Lake Malawi prior to ~70 ka, with approximately 20 kyr periodicities, followed by lowered variability (but with overall high lake levels), consistent with a general pattern of insolation forcing (an eccentricity-modulated precessional pattern). A similar pattern appears to hold at Lakes Tanganyika and perhaps Lake Bosumtwi. There is, for example, evidence at Lakes Malawi and Bosumtwi for a short-lived arid event around 75 ka (39a, 45a). Additionally, at Lake Challa in the north there was a minor low-stand, inferred to have occurred at ~60 ka (27a), while at the same time, Lake Malawi LSTs dropped to their lowest temperature recorded between 65 and 55 ka (60a). Based on LSTs, diatoms, and sedimentology, Heinrich events 4, 5, and 6 have been recognized in Lakes Tanganyika (Tierney et al., 2008), Malawi (Stone et al., 2011; Woltering et al., 2011), and Challa (Moernaut et al., 2010). Lake level and temperature data together indicate that this region may have been cold and dry for brief periods of time between 60 ka and 35 ka. The evidence for Heinrich events in the climate signal of tropical Africa suggests a relationship between the Northern Hemisphere climate and the equatorial interior of Africa.

Over the past 60 kyr, LST values for Lake Tanganyika suggest tropical African terrestrial precipitation is more closely linked to Indian Ocean SSTs, as opposed to local LSTs. Even during periods of colder local LST values, warmer Indian Ocean temperatures appear to provide sufficient moisture to induce rainfall in the region, whereas the location of the ITCZ (often considered the primary driver of tropical precipitation) appears to have primarily controlled wind direction at Lake Tanganyika (Tierney et al., 2008). Thus, Indian Ocean SSTs and the extent of the ITCZ need to be working in concert for extreme humid periods in tropical Africa. This apparent collaboration between Indian Ocean SSTs and the ITCZ/local insolation maxima between 60 ka and 30 ka adds to the mystery of the early Late Pleistocene African megadroughts. Between 115 ka and 90 ka, insolation variability was extreme and local Indian Ocean SSTs were relatively warm, suggesting that Lake Malawi (for example) should have been very dry, then very wet, as opposed to extremely dry for over 20 kyr. This suggested link between regional terrestrial precipitation and Indian Ocean SSTs also does not explain the widespread geographic extent of the extended megadrought period. The Indian Ocean records in this synthesis indicate a weakened SW monsoon with lower $CaCO_3$ and decreased upwelling off the coast of Oman (23a), suggesting a decreased contrast between land surface temperature and neighboring SSTs, but not substantially reduced SSTs; only 0.5-1°C decrease, in the three records available (1a, b, 37b). Something must be different between the time of the megadrought event and the more recent record. Given these data, it is likely that the Indian Ocean SST effect is only evident in tropical Africa when the insolation swings are not as strong as they were prior to 70 ka.

The pollen data from off the west coast of tropical Africa are difficult to interpret over the entire time interval in terms of a regional signal because they are dominated by local pollen from mountainous refugia along the western coast of Africa, from Guinea to Angola (Dupont and Weinelt, 1996; Dupont et al., 2000). However, the patterns appear to indicate responses to North Atlantic SSTs with ubiquitous rainforest expansion during OIS substages 5a, 5c, and 5e, and dry woodland expansion during MIS substages 5b and 5d.

In summary, this region of tropical Africa extends from Lakes Bosumtwi and Challa in the north to the northern Kalahari Desert in the south. A significant difference between it and the neighboring regions is the presence of a regional 'megadrought' signal from ~115-90 ka. Additionally, these records indicate a gradual, though at times erratic, trend toward a more humid climate from 90 ka to 35 ka. While not applicable over the entire period of interest, there appears to be a tenuous relationship between the tropical lakes and MIS, particularly after insolation variability dampens ~75 ka, at the beginning of MIS 4.

Southern Africa (Figure 8)

Unlike the records of tropical Africa, the climate of southern Africa is much more punctuated with no clear trends of either increasing or decreasing humidity through time across the region. The Mababe Depression (Figure 7, 44a at 19°S, 27°E) borders the region to the north and shows a punctuated megadrought-like signal from 110-95 ka. However, sites just to the west at Drotsky's Cave (8a at 20°S, 23°E) and to the south at

Lobatse Caves (48a at 25°S, 25°E) demonstrate a clearly humid climate throughout this same time period. It is possible then that the southwest extent of the 'megadrought belt' lies between ~19°-25°S latitude, and ~23°-27°E longitude. The orientation of this border between the 'megadrought belt' and southern Africa may mirror the angled track of the ITCZ across the continent, suggesting that the extent of the ITCZ may be an important factor in the millennia-long megadrought events (see 'causal mechanisms').

The records that extend through the entire time period of interest do show a precessional signal (23 kyr cycle) of wet/dry periods (5a, 32a, 8a, b) (Brook et al., 1996; Partridge, 1999; Burrough et al., 2007) with humid periods coinciding with Southern Hemisphere insolation maxima. The record from Tswaing crater (32a), one of the two records that shows a variable humidity signal (not just a discrete signal of wet or not), does indicate a trend of decreasing variability from 90-35 ka as expected with eccentricity-modulated precession. However, the offshore humidity record (site 46a) does not correlate with the inferred rainfall record from the Tswaing Crater (cf. Figure 8). The offshore record shows a slight trend towards increasing humidity from 115-35 ka, whereas Tswaing Crater shows a slight trend towards decreasing humidity over the same time interval. Although the tuning of the Tswaing Crater grain size record has been called into question in the past, the precessional cyclicity has been seen in the data using other proxies as well (Kristen et al., 2007). All records except the most southern dune record (5a at 27°S) depict a coherent, increasingly humid signal from ~60-45 ka. A possible explanation for this discrepancy is its relative proximity to both the eastern and southern coasts of the continent compared with the other dune records. Recent research

suggests coastal or barrier dunes are primarily affected by distance to shore and thus sediment availability for dune migration, rather than the classic interpretation that dunes migrate during arid times and are stable during humid times (Carr et al., 2006, 2007; Bateman et al., 2011). Despite this site's relative proximity to the coasts, compared with the other dune sites discussed in this synthesis, it is hardly a 'coastal dune' location. In addition, it is bordered to the west and east by mountain barriers to coastal influence and thus OSL dates from this site should be responding to an aridity signal unlike true 'coastal' dunes. Thus the reason for this discrepancy must be a more local effect.

The isotope record from Pinnacle Point on the tip of South Africa displays trends coherent with the Southern Ocean SST records that follow a North Atlantic SST pattern (4a) (Bar-Matthews et al., 2010). During MIS 4 (glacial), the speleothem carbonates are isotopically enriched (higher $\delta^{18}O$). This is expected because during ice ages, oxygen isotopes in ocean water will be preferentially heavier than during interglacial periods (lighter isotopes of oxygen locked in polar and mountain ice), causing the rain-water, and thus cave-water to begin its hydrologic journey more enriched during glacial periods.

In summary, the northern boundary of this region exhibits a modified/punctuated 'megadrought' signal, whereas the rest of the region does not. There is a clear eccentricity-modulated precessional cyclicity to the wet/dry climate of southern Africa, although no clear trend toward increasing or decreasing humidity through the time interval of interest. In addition, there appears to be no clear regional climatic relationship to the MIS boundaries.

Regional coherence of temporal trends in African climate change

The evidence presented above indicates that SSTs often co-vary with climate changes predicted by δ^{18}O-derived MIS boundaries, with terrestrial data often out of phase although varying by sub-region. Principal components analysis (PCA) provides a more formal means of comparing aggregate data from both marine and terrestrial sources. On a PCA plot, datasets with similar patterns of variability will plot together. The PCA results are presented in Figures 9-11**.** For the purposes of clarifying regional trends, the data are presented with their site number plotted on the PC ordination plot for each time period, and the PC axis values are mapped spatially by data type, identified by a single letter prefix for SSTs (S), terrestrial temperature (T), or precipitation (P). In addition to circum-Africa datasets, maximum summer insolation values at 15ºN and 15ºS were also included in each analysis, as well as a typical North Atlantic SST dataset (35a) (Raymo et al., 2004), to determine the correlation of the individual African paleoclimate datasets to possible regional/global influences on local paleoclimate records. We present here the results of comparisons for 140-30 ka, 115-30 ka and 75-30 ka, as patterns (or lack thereof) in the data are clearest for these time intervals. The analysis for the 150-100 ka interval is presented as online supplemental data. In all analyses, the first principal component (PC1) is statistically significant, and is interpreted as the response to variability due to North Atlantic SST forcing, whereas the second principal component (PC2) (with differing degrees of significance) is interpreted as the response to insolation variability.

140-30 ka (Figure 9, Table 4)

This time period was chosen because it maximizes the number of datasets used (32) over the greatest percentage of the time period of interest (92%). Over this interval, only the first two principal components were statistically significant: PC1 (SST) explains 42% of the variance and PC2 (insolation variability) explains 16% of variance. Most of the SST records cluster together and are particularly constrained along the PC1 axis with values ranging from -1.07 to -0.79 (Figure 9). One SST record falls somewhat outside the tightly constrained PC1 range, 34a (26°S), and another SST record, 6a (49°S, nearly in the Southern Ocean), differs significantly from the other SST records. This may be a reflection of the circum-Antarctica SST trends as opposed to circum-Africa SSTs (Figure 9).

The terrestrial records (both precipitation and temperature) plot away from the 'SST cluster' along the PC1 axis, and most have similar trends to the maximum Northern Hemisphere summer insolation (N. Insol). Notable exceptions to this are four precipitation records: two off the northwest coast of Africa (21c, 34a), one in sub-tropical East Africa (45a), and another in the Levant (43a). The lake level record from Lake Malawi (45a) surprisingly shows almost no correlation with PC2 axis, perhaps indicating another factor contributing strongly to PC2 in this interval. In contrast to the $\delta^{18}O$ records at Peqiin and Soreq caves (3a, b), which again vary in concert with the SST records, the climatic trends observed in the record of speleothem growth frequency in the Levant (43a) are surprisingly similar to those over this period at Lake Malawi (45a), and yet they differ greatly from the other records in the North African region (see Figure 9:

34a, 21c). Offshore records of tropical African climate are strongly correlated with 15°N insolation, and both the tuned and un-tuned records of the Pretoria Salt Pan in southern Africa (32a, b) are more similar to the maximum southern summer insolation, and again show some relationship to the climatic trends of SST records (Figure 9).

115-30 ka (Figure 10, Table 5)

This interval was chosen to increase the number of datasets used (38) over a significant percentage of the time period of interest (71%). This period also covered an interval of decreasing insolation variability in the latter part of this time period. In spite of this, there are still very clear, significant patterns in the climatic trends of SSTs (PC1, 44% of variance) and northern versus southern maximum summer insolation (PC2, 15% of variance). There is a very tight cluster of PC1 values for the majority of SST records (-0.99 to -0.69). The southern Atlantic site (33a) at 26°S latitude, which for the 140-30 ka interval analysis was significantly offset from the remaining SST cluster, is more closely linked to this cluster for the 115-30 ka analysis (Figure 10). In contrast, two SST records vary considerably from the other SST records (Figure 10): one again from the Southern Ocean (6a at 49°S), the other in an upwelling zone off the Arabian Peninsula (23a at 18°N). As observed in the previous time intervals, the Levantine cave records plot within the SST cluster (3a, b), as does another precipitation record, (52a**)** the offshore grain-size humidity index. This confirms the similarity through time of these two records noted earlier.

The majority of terrestrial precipitation and temperature records plot away from the SST group along the PC1 axis and there is a very coherent grouping along the PC2 axis as well with values ranging from -0.72 to -0.57, still trending over time similar to 15°N maximum summer insolation. Exceptions for this time period once again include the Tswaing crater records (32a, b), plotting half way between the SST grouping and the 15°S maximum summer insolation pattern. However, both the tuned and un-tuned grain size records plot similarly, reaffirming that the tuning quality of the records is unlikely to explain the pattern seen in the dataset (e.g., Kristen et al., 2007). Instead, the Tswaing crater data suggests that insolation plays a much smaller role in the response of this record over the 115-30 ka interval than for 140-30 ka. The Lake Malawi (45a) and Levantine speleothem frequency (43a) records once again plot towards the origin of the PC2 axis, and the terrestrial temperature record that is furthest south (13d) at 12°S plots near the middle of PC2 (Figure 10). Off the coast of northwest Africa, both a precipitation record at 18°N (34a) and temperature record at 4°N (13a) appear to be anti-correlated with trends in both types of records just to the south (Figure 10). Perhaps ~4°N is an important climatic boundary over this time period.

75-30 ka (Figure 11, Table 6)

This interval was chosen to investigate possible spatial patterns during a period of dampened insolation variability. This interval also had the highest number of usable datasets (40). For this interval, only one axis was significant (PC1), which explains 39% of the variance, and Northern and Southern Hemisphere insolation no longer shows

significant loadings relative to the entire dataset (Figure 11a). Although the majority of SST records versus terrestrial records are still strongly contrasted along the PC1 axis (with no strong relationship to latitude), they are considerably more scattered than the previous time periods analyzed. The tropical terrestrial precipitation records continue to have values similar to that of 15°N maximum summer insolation (Figure 11b), or 15°S for the Tswaing Crater (33a, 33b), whereas the terrestrial temperature records show little to no spatial correlation pattern in PC1 values (Figure 11c). As anticipated, there is a decreased effect of insolation maxima on terrestrial records during this interval of dampened eccentricity-modulated precession.

The PCA results support a generally clear separation between SST data and those from terrestrial sources, the latter often associated with maximum insolation. This separation is only apparent during periods of lower insolation variability (e.g., 75-30 ka). These results suggest that different climate mechanisms are affecting the marine and terrestrial environments in Africa during much of the 150-30 ka period.

An evaluation of causal mechanisms

Throughout the discussion of the SST records, there was a recurring theme: all records seem to follow global MIS boundaries, except where they do not. In other words, circum-Africa SSTs record both the global temperature variability, as well as perturbations in that overall signal by local or regional effects such as changing wind zonality and/or upwelling activity. As illustrated in the previous section, terrestrial temperature and precipitation across Africa do not seem to be responding to North

Atlantic SST forcing (MIS boundaries, PC1 on Figures 9-11). This does not imply that SST and other marine data have no useful information for continental climate variability. Rather, those perturbations in the global marine temperature signal may be the key to discrete periods of continental climate variability. In this section, we examine two potential drivers of local or regional climate variability: the changing position of the Westerlies and the ITCZ through time. We consider how these regional variations would be represented in the paleo-record, and whether we see evidence for changes in the location of either the Westerlies or the ITCZ between 150 ka and 30 ka.

Position of the Westerlies

Strengthening or weakening of the Westerlies may help explain moisture variation in the northern and southern extremes of Africa. This strengthening was modeled by Toggweiler and Russell (2008) to occur when there is a significant contrast between temperatures at the equator and at the poles, similar to the modern climate. When the Westerlies are strong, they are pulled closer to the poles and divert the rain elsewhere. Alternatively, during glacial or stadial periods there is less of a temperature contrast between the equator and poles, the Westerlies are weaker, and they are positioned closer to the equator, bringing precipitation to both extreme regions of Africa (Figure 12a). This interpretation is consistent with recent research on the southern African coast where colder periods (such as MIS4) were also wetter (Chase, 2010). Grain size analysis of ocean sediment from a marine core taken from just south of the South African shore (36°19.2′S; 19°28.2′E) suggests a northward movement of the Antarctic Circumpolar

Current (ACC) during glacial periods as well (Martinez-Mendez et al., 2008), perhaps following the equator-ward movement of the Westerlies.

Multiple indicators can be examined to infer the paleo-location of the Westerlies. In the Southern Hemisphere, when the Westerlies are strong and pulled tighter around the poles they leave a gap between the tip of Africa and their circulation pattern. When this happens, warm water from the Indian Ocean (the Agulhas Current) is able to round the tip of Africa making the SSTs off of the western tip of South Africa warm. Colder SSTs in the same region would therefore indicate weakened Westerlies that cross the southern tip of Africa and prevent Indian Ocean leakage into the South Atlantic. If the location of the Westerlies is the dominant driver of African climate, then North and South Africa should be wet when the Westerlies are weak (equator-ward), and the SSTs in the Benguela current should be cold. However, when the Westerlies are strong, northern and southern Africa should be dry, and the SSTs in the Benguela current will be warm (Figure 12b). From 130-115 ka, the SSTs in the Benguela region are warm and many paleo-precipitation records in the north and south indicate dry conditions (strengthened, pole-shifted Westerlies). However, Egyptian records (37a, 48a, 32a) indicate very wet conditions for this time. In contrast, from 50-35 ka when SSTs are cold, northern and southern Africa are wet, again with the exception of the Egyptian records, which are dry (weak, equator shifted Westerlies).

These data suggest the strength and position of the Westerlies likely had a significant impact on regional precipitation patterns throughout the 150-30 ka interval. However, they also demonstrate that eastern North Africa and the Levant are out of phase

with the rest of the northern and southern portions of the continent. For the earlier period (130-115 ka), perhaps the pole-ward shift of the Westerlies allowed the SE trade winds to bring moisture from a different source to eastern North Africa (e.g., the Indian Ocean), meanwhile NW Africa remained dry in response to colder North Atlantic SSTs. For the later period (50-35 ka), perhaps the moisture-laden Westerly winds were rained-out crossing the expansive, dry Sahara prior to reaching Egypt and the Levant.

Influence of ITCZ location

Changes in the average ITCZ position over extended time periods may explain long-term moisture variation between ~20ºN and 15ºS over the 150-30 ka time interval. As shown in our PCA, precipitation across tropical Africa fluctuated similarly with changes in tropical insolation, particularly over periods of maximum NH insolation variability and intensity.

Monsoons are dynamic systems in two ways: thermal and hydrologic, meaning monsoon systems respond to land/ocean temperature contrasts, and are also dependent on SSTs, evaporation from oceans, and water vapor transport to land (Kutzbach et al., 2008). The differential heating of land and ocean near and below the average location of the ITCZ can upset both oceanic and atmospheric dynamics, ultimately affecting the extent and position of tropical monsoons globally. As a consequence of its effect on monsoon systems, the average position of the ITCZ over time may also greatly affect the climate in regions on the extreme edge of the ITCZ range, as small shifts one way or another will have a greater impact there (Brown et al., 2007). For example, during periods of extreme

insolation variability, when Asian monsoonal circulation is intensified, the average position of the ITCZ may in fact be further north over those time periods, and consequently areas at the edge of the southern range of the ITCZ may not receive much rainfall at all.

This idea can be tested by comparing the hydrologic record of Lake Malawi (currently at the edge of the southern range of the ITCZ) with Northern Hemisphere tropical insolation. If the Asian monsoon has such an extreme effect on the southern extent of the ITCZ, in years when the Asian monsoon is strong, and the ITCZ is further north, Lake Malawi (and other areas in the extreme southern tropics of Africa) will be drier (Figure 13a). The reverse is also true. The tropical region will likely be wet during times when the Asian monsoon (and Northern Hemisphere insolation) is weak. It has been observed in climate models that the stronger Asian monsoons occur during times of Northern Hemisphere insolation maxima (or ice volume minima, e.g., interglacials) and vice versa (Clemens et al., 2008). This idea appears to be valid in the tropical region until ~75 ka when the variability, or the range of extreme values, in insolation declines (Figure 13b). This is exactly what is seen in the PCA of terrestrial precipitation patterns. The majority of the tropical datasets vary in concert with tropical insolation (PC2), until the 75-30 ka analysis. From 75 ka to 30 ka, insolation variability is weakening and there is no clear relationship between insolation and precipitation (Figure 13c). This weakening may allow other factors to become relatively more significant at this time, and may help explain why some lakes outside the ‘megadrought belt’ stabilize at low levels

after 70 ka, whereas Lakes Malawi, Tanganyika and Bosumtwi all stabilize at high levels after this time.

Synthesis: African climate from 150-30 ka

African paleoclimates from 150-30 ka are spatially and temporally complex, with variation in the outcome of multiple related processes. We summarize these here before considering their implications for human evolution, determining the degree to which our hypotheses are supported or rejected.

Hypothesis 1. Pleistocene African climate change is coincident with North Atlantic glacial/interglacial periods.

Figure 14 demonstrates that although SSTs do tend to vary with glacial/interglacial cycles and MIS boundaries, this pattern does not hold for much of the African continent over the 150-30 ka interval. There do appear to be instances after 75 ka in three of the four regions (North, tropical, and southern Africa) when terrestrial precipitation and temperature change is coincident with MIS boundaries (cf. Figure 14, MIS 4 interval).

Hypothesis 2. Pleistocene African climate change is coincident with Northern and Southern Hemisphere insolation cycles.

Our PCA results (Figures 9-11) support this hypothesis, showing that precipitation across tropical Africa fluctuated similarly with changes in tropical insolation. However, more

detailed comparison of continuous datasets indicate that this hypothesis is supported only for ~150-75 ka, a period of high Northern Hemisphere insolation variability and intensity, and is not well supported for the ~75-30 ka interval of dampened insolation variability and intensity (see also Supplemental Online Information).

Hypothesis 3. Pleistocene African climate change is the result of the complex interaction of a number of factors, including atmospheric dynamics.

Our results support this hypothesis (Figures 12-13). The position of the Westerlies and the ITCZ through time appear to have affected terrestrial climate variability at discrete times, and also may be the underlying cause of region/site specific temperature excursions in circum-Africa SSTs between 150 and 30 ka.

Hypothesis 4. Climate change is asynchronous across Africa.

As shown in Figure 14, there is strong support for this hypothesis for terrestrial climates. This suggests that continental-scale examinations of climate, environment, and human evolution must account for these temporal offsets between regions, with inter-regional differences in the timing of shifts to humid or arid conditions often on the order of 10 kyr.

Paleoanthropological implications

The results of our regional comparisons of paleoanthropological site density and inferred climate for each of the four sub-regions are summarized in Figure 15. The

results are used to test each of our three hypotheses linking climate change to Pleistocene African hominin demography, followed by suggestions for further testing at similar and finer analytical scales. Overall, there is a general increase in the relative frequency of sites over time in most regions (Figure 15). This pattern is consistent with the taphonomic bias modeled by Surovell et al. (2009), in which younger sites are more likely to be found and thus skew inferences of demographic change from these data. As the models of Surovell et al. (2009) extend only to ~40 ka, the extent to which our dataset spanning ~150-30 ka is affected by taphonomic bias is unknown. Examining differences between or within regions for particular time intervals partially offsets this, as there is no evidence at the moment to suggest that the taphonomic bias against site recovery affects one region or area more than another for any given time interval.

Hypothesis 5a. The southern African interior (and possibly the coast) was largely depopulated during arid intervals, particularly within the last 60 kyr.

This hypothesis predicts strong evidence for a decrease in site abundance in the 60-30 ka interval. For inland sites, there is no evidence for a decline in site numbers <60 ka and thus no support for the hypothesis, with inland site numbers showing a slight increase during this interval (Figure 15), nor is there support for inland population decline during prior arid intervals. In particular, our data actually suggest relatively humid conditions at coastal and near-coastal sites during MIS 4 (~72-60ka), as also reported by Chase (2010). This is in contrast with earlier models that suggest that Still Bay and Howiesons Poort industries appear during arid or more open conditions previously

inferred for MIS 4 in southern Africa (e.g., Ambrose and Lorenz, 1990; McCall, 2007), demonstrating the complex relation between marine isostope stages and terrestrial African climates.

The number of coastal sites in southern Africa does show a decline from ~75-65 ka, followed by a sharp decline consistent with the hypothesis of population decline or regional abandonment (Figure 15). However, the decline in coastal site numbers is likely due to the seaward movement of the coast during arid/glacial intervals and the loss of these habitation sites and associated rich coastal plain resources during subsequent sea level rise, e.g., during MIS 3 (see Van Andel, 1989; Fisher et al., 2010). Our data provide no support for population declines in southern Africa that cannot be explained as a function of sea level fluctuation.

Hypothesis 5b. Hominin populations in the tropical and eastern portions of the continent show relatively muted responses to climate change.

This hypothesis predicts little change in hominin site abundances relative to changes in relative humidity. The data summarized in Figure 15 support this hypothesis. Despite extreme changes in climate, fluctuations in relative site density in East Africa and tropical Africa are relatively minor. Comparisons between the two regions indicate that eastern and tropical Africa show inversely related abundances throughout much of the time span considered here, particularly between ~130-60 ka. During much of this interval, when relative site frequency increases in the tropical region, it decreases in East Africa. As noted above, site proportions are calculated independently for each region,

such that change in one need not cause a change in the other. Relative site abundances in tropical Africa increase during one period of aridity (~115-90 ka), and in East Africa decline during the comparable interval of humidity (~110-95 ka). As such, the data suggest that the mid-latitudinal portions of the continent may be linked in interesting ways in terms of population and environmental histories during parts of the Late Pleistocene. Neither the patterning in inversely related site abundance between regions nor climatic change within regions holds after ~65 ka.

The scale of our analysis does not permit direct identification of the reasons for little change in the hominin demographic signal for eastern and tropical Africa. The consequences of absolute changes in long-term water availability may be less dramatic for these regions compared with northern or southern Africa. For example, following Ambrose (1998), Mercader et al. (2000), Marean and Assefa (2005), and Basell (2008), the periods of increased aridity in these regions may be offset by relatively steep gradients in altitudinal relief and rainfall that may have allowed localized movement to higher, cooler, and wetter altitudes, as well as the expansion of forest populations when the canopy was more open and fragmented.

Although increased aridity is often associated with a decrease in habitat suitability for hominin populations (cf. northern Africa discussed below), the opposite may hold true for heavily forested regions such as those found in much of the tropical African region. Tropical rainforests are difficult environments for human foragers, and forest fragmentation increases ecotone extent, potentially making the region more attractive to hominin populations (cf. Ambrose, 2001; Cornelissen, 2002). Our meso-scale results

shown in Figure 15 provide some support for this, with increased site abundances in tropical Africa during shifts to aridity, particularly during the ~115-90 ka interval. This pattern is also supported at the smaller scale of individual archaeological sites. The sites of Katanda (36), dated to 120-60 ka, and Matupi Cave (37), dated to 32-41 ka are both found in what are today ecotones on the margins of heavily forested regions of the Democratic Republic of the Congo. Several lines of evidence suggest that Pleistocene hominin occupation of these sites favored drier intervals when more open grassland habitats occurred in their vicinities. Site Kt9 at Katanda preserves fossils of zebra (*Equus* cf. *E. burchelli*) and wildebeest (*Connochaetes taurinus*), indicative of open savanna grasslands and not found in the area today (Brooks et al., 1995). At Matupi Cave, grass (*Gramineae*) pollen and spores, isotopic analyses of speleothem, and a fossil fauna that includes ostrich (*Struthio camelus*) and warthog (*Phacochoerus aethiopicus*) all suggest a cooler, drier, and more open habitat than at present (Van Noten, 1977; Van Neer, 1989; Brook et al., 1990). These data suggest Stone Age occupation of forest ecotones during drier, more open conditions and emphasize that arid (and conversely humid) intervals may have had different impacts on human populations in each of the four African sub-regions.

Another consequence of forest fragmentation is the creation of a mosaic of local refugia that were intermittently connected as a result of environmental change. Genetic evidence provides some support that these processes may have led to the accumulation of biological differences in various animal populations, in particular multiple species of bovid (Lorenzen et al., 2010). Among humans, mtDNA, Y-chromosome, and non-coding

regions of the human nuclear genome suggest that the ancestors of central African forest ('pygmy') hunter-gatherers and ancestors of Bantu-speaking agricultural populations in tropical Africa likely diverged ca. 71 (50-106) ka (Batini et al., 2007, 2011; Quintana-Murci et al., 2008; Patin et al., 2009), with mtDNA evidence suggesting that asymmetric gene flow from pygmy maternal lineages to eventual farming populations was reinitiated sometime after 40 ka and followed by multiple gene flow events involving other African populations during the terminal Pleistocene and Holocene. The work of Tishkoff et al. (2009) implies similar complex relationships between the ancestors of various present-day forest hunter-gatherer groups and those of surrounding populations. Offshore terrestrial temperature (12a, 13a-d) and precipitation/aridification records (34b-d) suggest a significant cold period just prior to the suggested divergence interval. Regional precipitation records indicate a significant dry spell just before or concurrent with the beginning of the 73-60 ka divergence interval and a return to humid conditions <60 ka (Figure 15). These results are consistent with models suggesting that forest fragmentation during arid conditions are periods when population fragmentation, isolation, and differentiation are most likely (e.g., Cowling et al., 2008). The archaeological data for this region are sparse and as yet lack the sort of chronological control to offer support for this model (Cornelissen, 2002; Mercader and Martí, 2003), but these results do suggest the power of integrating genetic, demographic, and meso-scale environmental data.

Hypothesis 5c. The nature and expanse of the Sahara strongly influenced the population history of northern Africa, with occupation of much of the interior of this region limited to periods of increased humidity when the 'green Sahara' was characterized by savanna environments. As a corollary, 'out of Africa' hominin dispersals are similarly constrained to these humid intervals.

This hypothesis predicts that hominin site density should co-vary with climate change, with decreased site abundance during periods of increased aridity. This hypothesis is variably supported according to site location along the coast or in the interior (Figure 15). Coastal sites show a very gradual increase in numbers over time, with little evidence for any linkage between hominin demography and climate change. The absence of a noticeable recent decline in coastal site numbers is likely due to the relatively steep gradient of the northwest African Mediterranean coast relative to that in South Africa; sea level change had a minimal impact on site-to-shore distance in northwest Africa.

Sites in the interior of northern Africa reveal a more complex pattern. Because the Nile River provides a narrow zone of available water in otherwise often dry environments, the Nile Valley sites of Nazlet Khater 4, Nazlet Safaha, and Taramsa 1 are plotted separately on Figure 15. Among our dataset, radiometrically dated sites from the Nile Valley are first documented at ~100 ka, with a progressive increase through time. This increase may simply reflect taphonomic bias, and further interpretation is hampered by a particularly small sample size.

The remaining sites from the interior of northern Africa show a very different pattern, with multiple periods marked by substantial increases or decreases in relative site abundance. Site numbers show a sharp increase ~130-120 ka, reach their maximum ~100-70 ka, and show a sharp decline <70 ka (Figure 15). The periods of site increase or maximum density broadly coincide with humid intervals in northern Africa, whereas the rapid decline in site density in the interior from ~70-30 ka starts shortly after the return to arid conditions (Figure 15). These findings support the 'green Sahara' hypothesis of Drake et al. (2011), which suggest the repeated reoccupation of the Sahara by animal communities (including humans) during humid intervals. These data suggest that much of the occupation of the northern African interior by Aterian MSA hominin populations was largely limited to humid intervals when savanna environments may have dominated the region. This is supported by the limited available faunal data from undated Aterian sites from the Sahara, including equids (*Equus* sp.) and alcelaphine bovids (*Alcelaphus buselaphus*, reported as *Bubalis boselaphus*) from the Aterian type-site of Bir-el-Ater in Algeria (Morel, 1974), and more strikingly, cut-marked hippopotamus (*Hippopotamus amphibius*) remains from Adrar Bous, in the Aïr Mountains of Niger (Gifford-Gonzalez and Parham, 2008).

Hominin dispersals to Eurasia via northern Africa have also been linked to humid intervals (Osbourne et al., 2008; Drake et al., 2011). From ~30-75 ka, northern Africa experienced arid climate regimes. The Sahara expanded 65-50 ka and the demographic data imply abandonment of the interior of northern Africa during this time (Figure 15), suggesting that dispersals from northern Africa occurred prior to 75 ka. This finding is at

odds with hypotheses that posit a dispersal timing of ca. 60 ka (Mellars, 2006), or a dispersal origin in the South African Howiesons Poort industry at 65-60 ka. (Marean, 2010), although a ca. 65-60 ka dispersal could well have occurred from eastern Africa over the Bab el-Mendeb, as humid conditions dominated the latter region between 80 and 65 ka. The timing of the humid intervals in northern Africa (~135-115 ka and ~105-75 ka) corresponds with those in the Levant (54a) (Vaks et al., 2007), providing multiple opportunities for one or more earlier hominin dispersals out of Africa via the Sahara, or an early exodus from East Africa to Arabia over the Bab el Mendeb (e.g., Rose et al., 2011). This pattern does not rule out possible migrations from this region during either the earlier or the later interval through the Nile Valley. However, during the ~105-75 ka humid interval in northern Africa, East Africa (where the sources of the Nile occur) was largely under an arid climate regime, except for a narrow window ~80 ka when both northern and eastern Africa were experiencing humid climates (Figure 15), placing a more restricted temporal window on dispersal via the Nile Valley. We note that although only one out of Africa event is recorded in the modern human genome (e.g., Prugnolle et al., 2005), this fact is not inconsistent with earlier multiple migration and extinction events using any of these routes, with only a single lineage surviving to the present.

Conclusions

In this paper. we synthesized African paleoclimate from 150 ka to 30 ka using diverse datasets at a regional scale, testing for coherence with North Atlantic glacial/interglacial phases, Northern and Southern Hemisphere insolation cycles, and the

atmospheric dynamics responsible for the observed regional climates. We have examined the temporal and spatial components of paleoenvironmental change across the continent, in order to further investigate the relationship between the varying regional climates and the evidence of human occupation in those regions.

Between 150 and 30 ka, the SSTs from the northern Atlantic and the Mediterranean Sea are consistent with the North Atlantic glacial/interglacial SST pattern observed further north, as are the SSTs recorded in the southern Atlantic. This suggests the importance of high latitude forcing for all Atlantic SSTs off the western coast of Africa. Southern Ocean records close to the African continent also show a strong coherence with North Atlantic SSTs, suggesting that the influence of the North Atlantic extends all the way down the African coast until the Antarctic Circumpolar Current takes over dominance north of 49°S latitude. The Indian Ocean records are the least similar to the North Atlantic, suggesting that this region is much more heavily influenced by the East African and Asian monsoons over this time interval. However, it is likely that glacial boundary conditions and insolation intensity together modulate the strength of the monsoons on either side of the continent. This is evident from the 'SST clusters' observed in the PCA, which includes all regional SSTs. There is a very tight 'cluster' during periods of high insolation variability and strength, and a diffuse, scattered relationship between 75 and 35 ka when insolation variability and strength is low.

North Africa experienced humid conditions beginning between 135-130 ka and lasting until 120-115 ka, and again from 100-95 ka until 75 ka. Many North African records are also quite variable prior to 75 ka, after which time the climatic variability in

the region dampens considerably through 30 ka, suggesting a link between insolation strength and variability and North African climate. There is also evidence suggesting that North African precipitation is affected by the expansion and contraction of the Westerlies, diverting moisture towards the continent when they are weak (equator-ward), and away when they are strong (pole-ward). This is particularly evident between 100 ka and 70 ka.

The East African region was wet ~145-120 ka, ~110-95 ka, ~80-65 ka, and 55-50 ka. These variations were likely caused by or related to the changing influences of the NE and SW monsoon regimes, forced by changes in local insolation at the equator with increasing influence of high latitude/glacial forcing moving away from the equator.

The regional climate from 150-30 ka in tropical Africa differs from its neighboring regions primarily due to the presence of a region-wide series of 'megadroughts' from ~115-90 ka. Based on the spatial distribution of sites displaying a megadrought signal, it is likely that the southwest extent of the 'megadrought belt' lies between ~19°S and 25°S latitude, and ~23°E and 27°E longitude. The northern boundary lies at approximately 18°N from the Atlantic Ocean in the west to ~37°E longitude where the northern boundary shifts to 3°S latitude. The cause of these megadroughts may lie in a northward shift of the ITCZ, resulting from extremely strong Northern Hemisphere insolation and thus intensification of the Asian monsoon. Although there is evidence of insolation-driven control of regional precipitation in tropical Africa (specifically prior to 70 ka), the more recent record (60-30 ka) suggests that Indian Ocean SSTs also control precipitation in tropical Africa; i.e., the oceanic teleconnections to tropical Africa

precipitation patterns are more evident when not swamped by a strong insolation signal. This SST-regional precipitation relationship is also observed in modern data.

The climate in the South African region differs from north to south. The northern boundary of this region exhibits a modified/punctuated 'megadrought' signal, whereas the rest of the region does not. There is a clear eccentricity-modulated precessional cyclicity to the wet/dry climate of southern Africa, although no clear trend toward increasing or decreasing humidity through the time interval of interest. As in North Africa, there is evidence that regional precipitation in South Africa is affected by the expansion and contraction of the Westerlies between 100 and 70 ka.

Four sub-intervals of time were further analyzed for temporal trends in the data using a PCA: 150-100 ka, 140-30 ka, 115-30 ka, and 75-30 ka. The analyses suggest that North Atlantic SSTs are a consistent determinant of variability through the entire time interval. This is evident especially in the earlier three sub-intervals when the majority of SST records surrounding the continent plot in a tight 'cluster' particularly along the main axis of variability. However, even in the latter sub-interval the majority of SST datasets are loosely correlated with one another and none are anti-correlated. It is evident that variability in terrestrial climate from 150-30 ka is strongly correlated with the local hemisphere insolation maxima, except during periods of time when insolation variability and intensity is negligible (e.g., 75-30 ka), at which times other factors, such as regional SSTs can become dominant drivers of climate variability at 1-10 kyr time scales.

This climate synthesis provides a framework to test hypotheses regarding regional climate influences on the demographic structure of African hominins from ~150-30 ka.

A dataset of 64 sites demonstrates multiple temporal changes in the frequency of sites relative to climate change for the each of the North, East, tropical, and southern African regions. Southern African sites do not show any decline in relative frequency that is not explicable by changes in sea level, which is inconsistent with hypotheses that suggest periodic depopulation of that region within the last 60 kyr. Sites in the 90-60 ka period increase in number during a humid interval, but this may be an artifact of recent research programs.

The degree of temporal change in site density in East and tropical Africa is low compared with North and southern Africa, and consistent with hypotheses that steep altitudinal gradients or other local changes in environment may have buffered populations in these regions from the extremes of climate change. East and tropical Africa also show inversely related abundances throughout much of the time span considered here, particularly between ~130-60 ka. This suggests that the history of early populations of *Homo sapiens* in the generally wetter mid-latitudinal portions of the continent may be linked in different ways than at the more arid north and south ends of the continent. During arid intervals between ~120-80 ka, relative site abundances in tropical Africa increase, whereas those of eastern Africa decrease, perhaps tracking the local effects of forest fragmentation and grassland expansion. Processes of forest fragmentation and grassland expansion may also explain population isolation and contact suggested by genetic data from the region, which indicate a complex intertwining of climate and human population movement between these two interior continental regions.

Site densities in the interior of northern Africa record changes that appear to track climatic changes, with relative increases during humid intervals and declines with shifts to aridity, consistent with hypotheses linking human occupation of the Sahara to wetter conditions when the region supported a number of lakes and savanna habitats. Figure 16 summarizes contrasting paleoenvironmental syntheses for two humid time intervals during which hominin populations may have dispersed out of Africa through either northern Africa (Osborne et al., 2008; Drake et al., 2011) or via the Horn of Africa (Armitage et al., 2011). Figure 16 serves to further emphasize synchronous climate variability across Africa for a given time interval, as well as the complex relation between changes in terrestrial and oceanic conditions.

Our comparisons are constrained by the ~10 kyr resolution of our dataset, but our results demonstrate the following: (1) There is often a poor fit between the timing and nature of environmental change on continental Africa and oceanic records; (2) the timing of relative changes in moisture availability varied with latitude, such that different climate regimes characterized different regions of Africa at any given time; and (3) coarse measures of Pleistocene hominin demographic change can be used to test hypotheses that relate human population history to climate change. We look forward to exploring new avenues of research into demography/climate change connections in Africa at the local to regional scale as the density of the archaeological record improves, measures of population diversification are refined, and age estimates for archaeological and fossil sites as well as intervals of genetic changes are increasingly resolved.

Acknowledgements

Many thanks to the NSF Integrative Graduate Education and Research Traineeship (IGERT) program and the Foreign Language and Area Studies (FLAS) fellowship program for providing financial support during the research and writing of this manuscript. In addition, many thanks to colleagues who provided comments, advice, and support throughout the process, especially Michael McGlue, Christine Gans, Jessica Conroy, Sarah Ivory, Mark Warren, Daniel Peppe, and Tyler Faith. Sarah Pilliard and Ryan Higgins assisted with some of the archaeological data collection. The initial Smithsonian Human Origins Data Base was developed as part of an NSF-HOMINID grant to Potts and co-PIs (BCS - 0218511). This grant also funded a conference on the importance of climate change in human evolution, which sparked this collaborative effort. Tryon was supported by the Human Origins Program at the Smithsonian Institution's National Museum of Natural History and Cohen by a Senior Fellowship and the Paleobiology Department of the NMNH and NSF EAR-0602350 during the early phases of this project, and both would like to particularly acknowledge the support of Rick Potts and Kay Behrensmeyer.

References

Ambrose, S.H., 1998. Late Pleistocene human population bottlenecks, volcanic winter and differentiation of modern humans. J. Hum. Evol. 34, 623–651.

Ambrose, S.H., 2001. Middle and Later Stone Age settlement patterns in the Central Rift Valley, Kenya: comparisons and contrasts. In: Conard, N.J. (Ed.), Settlement Dynamics in the Middle Paleolithic and Middle Stone Age. Kerns-Verlag, Tübingen, pp. 21–44.

Ambrose, S.H., 2003. Population bottleneck. In: Robinson, R. (Ed.), Genetics. Volume 3. MacMillan Reference USA, New York, pp. 167–171.

Ambrose, S.H., Lorenz, K.G., 1990. Social and ecological models for the Middle Stone Age in southern Africa. In: Mellars, P. (Ed.), The Emergence of Modern Humans: An Archaeological Perspective. Edinburgh University Press, Edinburgh, pp. 3–33.

Armitage, S.J., Jasim, S.A., Marks, A.E., Parker, A.G., Usik, V.I., Uerpmann, H.P., 2011. The Southern Route "Out of Africa": Evidence for an early expansion of Modern Humans into Arabia. Science 331, 453–456.

Assefa, Z., Lam, Y.M., Mienis, H.K., 2008. Symbolic use of terrestrial gastropod opercula during the Middle Stone Age at Porc-Epic Cave, Ethiopia. Curr. Anthropol. 49, 746–756.

Bailey, G., 2007. Time perspectives, palimpsests and the archaeology of time. J. Anthropol. Archaeol. 26, 198–223.

Bard, E., Rostek, F., Sonzogoni, C., 1997. Interhemispheric synchrony of the last deglaciation inferred from alkenone paleothermometry. Nature 385, 707–710.

Barham, L.H., 2000. The Middle Stone Age of Zambia, South Central Africa. Western Academic and Specialist Press Limited, Bristol.

Barham, L.H., Mitchell, P., 2008. The First Africans: African Archaeology from the Earliest Tool Makers to Most Recent Foragers. Cambridge University Press, Cambridge.

Barich, B.E., Garcea, E.A.A., Giraudi, C., 2005. Between the Mediterranean and the Sahara: geoarchaeological reconnaissance in the Jebel Gharbi, Libya. Antiquity 80, 567–582.

Barker, P., Williamson, D., Gasse, F., Gibert, E., 2003. Climatic and volcanic forcing revealed in a 50,000-year diatom record from Lake Massoko, Tanzania. Quatern. Res. 60, 368–376.

Bar-Matthews, M., Ayalon, A., Gilmour, M., Matthews, A., Hawkesworth, C.J., 2003. Sea-land oxygen isotopic relationships from planktonic foraminifera and speleothems in the Eastern Mediterranean region and their implications for paleo-rainfall during interglacial intervals. Geochim. Cosmochim. Ac. 67, 3181–3199.

Bar-Matthews, M., Marean, C.W., Jacobs, Z., Karkanas, P., Fisher, E.C., Herries, A.I.R., Brown, K., Williams, H.M., Bernatchez, J., Ayalon, A., Nilssen, P.J., 2010. A

high resolution and continuous isotopic speleothem record of paleoclimate and paleoenvironment from 90-53 ka from Pinnacle Point on the south coast of South Africa. Quatern. Sci. Rev. 29, 2131–2145.

Barraclough, T.G., Nee, S., 2001. Phylogenetics and speciation. Trends Ecol. Evol. 16, 391–399.

Barton, R.N.E., Bouzouggar, A., Collcutt, S.N., Schwenninger, J.-L., Clark-Balzan, L., 2009. OSL dating of the Aterian levels at Dar es-Soltan I (Rabat, Morocco) and implications for the dispersal of modern *Homo sapiens*. Quatern. Sci. Rev. 28, 1914–1931.

Basell, L.S., 2008. Middle Stone Age (MSA) site distributions in eastern Africa and their relationship to Quaternary environmental change, refugia and the evolution of *Homo sapiens*. Quatern. Sci. Rev. 27, 2484–2498.

Bateman, M.D., Carr, A.S., Dunajko, A.C., Holmes, P.J., Roberts, D.L., McLaren, S.J., Bryant, R.G., Marker, M.E., Murray-Wallace, C.V., 2011. The evolution of coastal barrier systems: a case study of the Middle-Late Pleistocene wilderness barriers, South Africa. Quatern.Sci. Rev. 30, 63–81.

Bateman, M.D., Thomas, D.S.G., Singhvi, A.K., 2003. Extending the aridity record of the southwest Kalahari: current problems and future perspectives. Quatern. Int. 111, 37–49.

Batini, C., Coia, V., Battaggia, C., Rocha, J., Pilkington, M.M., Spedini, G., Comas, D., Destro-Bisol, G., Calafell, F., 2007. Phylogeography of the human mitochondrial L1c haplogroup: genetic signatures of the prehistory of Central Africa. Mol. Phylogenet. Evol. 43, 635–644.

Batini, C., Lopes, J., Behar, D.M., Calafell, F., Jorde, L.B., van der Veen, L., Quintana-Murci, L., Spedini, G., Destro-Bisol, G., Comas, D., 2011. Insights into the demographic history of African Pygmies from complete mitochondrial genomes. Mol. Biol. Evol. 28, 1099–1110.

Beaumont, P.B., Vogel, J.C., 2006. On a timescale for the past million years of human history in central South Africa. S. Afr. J. Sci. 102, 217–228.

Behar, D.M., Villems, R., Soodyall, H., Blue-Smith, J., Pereira, L., Metspalu, E., Scozzari, R., Makkan, H., Tzur, S., Comas, D., Bertranpetit, J., Quintana-Murci, L., Tyler-Smith, C., Wells, R.S., Rosset, S., 2008. The dawn of human matrilineal diversity. Am. J. Hum. Genet. 82, 1130–1140.

Binford, L.R., 2001. Constructing Frames of Reference: An Analytical Method for

Archaeological Theory Building Using Ethnographic and Environmental Data Sets. University of California Press, Berkeley.

Bird, M.I., Fifield, L.K., Santos, G.M., Beaumont, P.B., Zhou, Y., di Tada, M.L., Hausladen, P.A., 2003. Radiocarbon dating from 40 to 60 ka BP at Border Cave, South Africa. Quatern. Sci. Rev. 22, 943–947.

Bond, G., Heinrich, H., Broecker, W., Labeyrie, L., Mcmanus, J., Andrews, J., Huon, S., Jantschik, R., Clasen, S., Simet, C., Tedesco, K., Klas, M., Bonani, G., Ivy, S., 1992. Evidence for massive discharges of icebergs into the North-Atlantic Ocean during the last glacial period. Nature 360, 245–249.

Bouzouggar, A., Barton, N., Vanhaeren, M., d'Errico, F., Collcutt, S., Higham, T., Hodge, E., Parfitt, S., Rhodes, E., Schwenninger, J.-L., Stringer, C., Turner, E., Ward, S., Moutmir, A., Stambouli, A., 2007. 82,000-year-old shell beads from North Africa and implications for the origins of modern human behavior. Proc. Natl. Acad. Sci. 104, 9964–9969.

Bowden, J.H., Semazzi, F.H.M., 2007. Empirical analysis of intraseasonal climate variability over the Greater Horn of Africa. J. Climate 20, 5715–5731.

Brandt, S.A., Gresham, T.H., 1989. L'âge de la pierre en Somalie. L'Anthropologie 94, 459–482.

Brathauer, U., Abelmann, A., 1999. Late Quaternary variations in sea surface temperatures and their relationship to orbital forcing recorded in the Southern Ocean (Atlantic sector). Paleoceanography 14, 135–148.

Bräuer, G., 2008. The origin of modern anatomy: by speciation or intraspecific evolution. Evol. Anthropol. 17, 22–37.

Brook, G.A., Burney, D.A., Cowart, J.B., 1990. Paleoenvironmental data for Ituri, Zaire, from sediments in Matupi Cave, Mt. Hoyo. In: Boaz, N.T. (Ed.), Evolution of Environments and Hominidae in the African Western Rift Valley. Virginia Museum of Natural History Memoir 1, Martinsville, pp. 49–70.

Brook, G.A., Cowart, J.B., Marais, E., 1996. Wet and dry periods in the southern African summer rainfall zone during the last 300 kyr from speleothem, tufa and sand dune age data. Palaeoecology of Africa and the Surrounding Islands and Antarctica 24, 147–158.

Brooks, A.S., Hare, P.E., Kokis, J.E., Miller, G.H., Ernst, R.D., Wendorf, F., 1990. Dating Pleistocene archaeological sites by protein diagenesis in ostrich eggshell. Science 248, 60–64.

Brooks, A.S., Helgren, D.M., Cramer, J.M., Franklin, A., Hornyak, W., Keating, J.M., Klein, R.G., Rink, W.J., Schwarcz, H.P., Smith, J.N.L., Stewart, K., Todd, N.E., Verniers, J., Yellen, J.E., 1995. Dating and context of three Middle Stone Age sites with bone points in the upper Semliki Valley, Zaire. Science 268, 548–553.

Brown, E.T., Johnson, T.C., Scholz, C.A., Cohen, A.S., King, J.W., 2007. Abrupt change in tropical African climate linked to the bipolar seesaw over the past 55,000 years. Geophys. Res. Lett. 34, L20702, DOI:10.1029/2007GL031240.

Burrough, S.L., Thomas, D.S.G., Shaw, P.A., Bailey, R.M., 2007. Multiphase Quaternary highstands at Lake Ngami, Kalahari, northern Botswana. Palaeogeogr. Palaeoclimatol. Palaeoecol. 253, 280–299.

Burrough, S.L., Thomas, D.S.G., Singarayer, J.S., 2009. Late Quaternary hydrological dynamics in the Middle Kalahari: forcing and feedbacks. Earth-Sci. Rev. 96, 313–326.

Butzer, K.W., 1988. A 'marginality' model to explain major spatial and temporal gaps in the Old and New World Pleistocene settlement records. Geoarchaeology 3, 193–203.

Butzer, K.W., Beaumont, P.B., Vogel, J.C., 1978. Lithostratigraphy of Border Cave, Kwazulu, South-Africa: a Middle Stone-Age sequence beginning c. 195,000 b.p. J. Archaeol. Sci. 5, 317–341.

Carr, A.S., Bateman, M.D., Holmes, P.J., 2007. Developing a 150 ka luminescence chronology for the barrier dunes of the southern Cape, South Africa. Quatern. Geochronol. 2, 110–116.

Carr, A.S., Thomas, D.S.G., Bateman, M.D., 2006. Climatic and sea level controls on Late Quaternary eolian activity on the Agulhas Plain, South Africa. Quatern. Res. 65, 252–263.

Carto, S.L., Weaver, A.J., Hetherington, R., Lam, Y., Wiebe, E.C., 2009. Out of Africa and into an ice age: on the role of global climate change in the late Pleistocene migration of early modern humans out of Africa. J. Hum. Evol. 56, 139–151.

Causse, C., Ghaleb, B., Chkir, N., Zouari, K., Ouezodou, H.B., Mamou, A., 2003. Humidity changes in southern Tunisia during the late Pleistocene inferred from U-Th dating of mollusc shells. Appl. Geochem. 18, 1691–1703.

Chase, B.M., 2010. South African palaeoenvironments during marine oxygen isotope stage 4: a context for the Howiesons Poort and Still Bay industries. J. Archaeol.

Sci. 37, 1359–1366.

Clark, J.D., Beyene, Y., WoldeGabriel, G., Hart, W.K., Renne, P., Gilbert, H., Defleur, A., Suwa, G., Katoh, S., Ludwig, K.R., Boisserie, J.-R., Asfaw, B., White, T.D., 2003. Stratigraphic, chronological and behavioural contexts of Pleistocene *Homo sapiens* from Middle Awash, Ethiopia. Nature 423, 747–752.

Clark, J.D., Williams, K.D., Michels, J.W., Marean, C.A., 1984. A Middle Stone Age occupation site at Porc Epic Cave, Dire Dawa (east-central Ethiopia). Afr. Archaeol. Rev. 2, 37–72.

Clemens, S.C., Prell, W.L., Sun, Y., Liu, Z., Chen, G., 2008. Southern Hemisphere forcing of Pliocene $\delta^{18}O$ and the evolution of Indo-Asian monsoons. Paleoceanography 23, 1–15.

Cohen, A.S., Stone, J.R., Beuning, K.R.M., Park, L.E., Reinthal, P.N., Dettman, D., Scholz, C.A., Johnson, T.C., King, J.W., Talbot, M.R., Brown, E.T., Ivory, S.J., 2007. Ecological consequences of early Late Pleistocene megadroughts in tropical Africa. Proc. Natl. Acad. Sci. 104, 16422–16427.

Cornelissen, E., 2002. Human responses to changing environments in central Africa between 40,000 and 12,000 B.P. J. World Prehist. 16, 197–235.

Cowling, S.A., Cox, P.M., Jones, C.D., Maslin, M.A., Peros, M., Spall, S.A., 2008. Simulated glacial and interglacial vegetation across Africa: implications for species phylogenies and trans-African migration of plants and animals. Glob. Change Biol. 14, 827–840.

Cremaschi, M., Di Lernia, S., 1999. Wadi Teshuinat: Palaeoenvironment and Prehistory in South-Western Fezzan (Libyan Sahara). Edizioni All'Insegna del Giglio, Firenze.

Cremaschi, M., Di Lernia, S., Garcea, E.A.A., 1998. Some insights on the Aterian in the Libyan Sahara: chronology, environment, and archaeology. Afr. Archaeol. Rev. 15, 261–286.

Crevecoeur, I., Rougier, H., Grine, F., Froment, A., 2009. Modern human cranial diversity in the Late Pleistocene of Africa and Eurasia: evidence from Nazlet Khater, Peştera cu Oase, and Hofmeyr. Am. J. Phys. Anthropol. 140, 347–358.

Crombie, M.K., Arvidson, R.E., Sturchio, N.C., El Alfy, Z., Abu Zeid, K., 1997. Age and isotopic constraints on Pleistocene pluvial episodes in the Western Desert, Egypt. Palaeogeogr. Palaeoclimatol. Palaeoecol. 130, 337–355.

Crowley, T.J., Hyde, W.T., 2008. Transient nature of late Pleistocene climate variability. Nature 456, 226–230.

Dansgaard, W., Johnsen, S.J., Clausen, H.B., Dahljensen, D., Gundestrup, N.S., Hammer, C.U., Hvidberg, C.S., Steffensen, J.P., Sveinbjornsdottir, A.E., Jouzel, J., Bond, G., 1993. Evidence for general instability of past climate from a 250-kyr ice-core record. Nature 364, 218–220.

Deacon, H.J., Thackeray, J.F., 1984. Late Pleistocene environmental changes and implications for the archaeological record in southern Africa. In: Vogel, J.C. (Ed.), Late Cainozoic Palaeoclimates of the Southern Hemisphere. A.A. Balkema, Rotterdam, pp. 375–390.

Debénath, A., Raynal, J.-P., Roche, J., Texier, J.-P., Ferembach, D., 1986. Stratigraphie, habitat, typologie et devenir de l'Atérien Marocain: données récentes. L'Anthropologie 90, 233–246.

deMenocal, P.B., 2004. African climate change and faunal evolution during the Pliocene-Pleistocene. Earth Planet. Sci. Lett. 220, 3–24.

deMenocal, P.B., Rind, D., 1993. Sensitivity of Asian and African climate to variations in seasonal insolation, glacial ice cover, sea surface temperature, and Asian orography. J. Geophys. Res. 98, 7265–7287.

deMenocal, P.B., Ruddiman, W.F., Pokras, E.M., 1993. Influences of high- and low-latitude processes on African terrestrial climate: Pleistocene eolian records from equatorial Atlantic Ocean Drilling Program Site 663. Paleoceanography 8, 209–242.

Di Lernia, S., 1999. The Uan Afuda Cave: hunter-gatherer societies of Central Sahara. Arid Zone Archaeology, Monographs 1. Edizioni All'Insegna del Giglio, Firenze, pp. 223–237.

Domínguez-Rodrigo, M., Mabulla, A., Luque, L., Thompson, J.W., Rink, J., Bushozi, P., Díez-Martin, F., Alcala, L., 2008. A new archaic *Homo sapiens* fossil from Lake Eyasi, Tanzania. J. Hum. Evol. 54, 899–903.

Donahue, R.E., Murphy, M.L., Robbins, L.H., 2004. Lithic microwear analysis of Middle Stone Age artifacts from White Paintings Rock Shelter, Botswana. J. Field Archaeol. 29, 155–163.

Drake, N.A., Blench, R.M., Armitage, S.J., Bristow, C.S., White, K.H., 2011. Ancient watercourses and biogeography of the Sahara explain the peopling of the desert. Proc. Natl. Acad. Sci. 108, 458–462.

Drake, N.A., El-Hawat, A.S., Turner, P., Armitage, S.J., Salem, M.J., White, K.H., McLaren, S., 2008. Palaeohydrology of the Fazzan Basin and surrounding regions: the last 7 million years. Paleogeogr. Paleoclimatol. Paleoecol. 263, 131–145.

Dupont, L.M., Jahns, S., Marret, F., Ning, S., 2000. Vegetation change in equatorial West Africa: time slices for the last 150 ka. Palaeogeogr. Palaeoclimatol. Palaeoecol. 155, 95–122.

Dupont, L., Weinelt, M., 1996. Vegetation history of the Savanna corridor between the Guniean and the Congolian rain forest during the last 150,000 years. Veg. Hist. Archaeobot. 5, 273–292.

Emeis, K.C., Schulz, H., Struck, U., Rossignol-Strick, M., Erelnkeuser, H., Howell, M.W., Kroon, D., Mackensen, A., Ishizuka, S., Oba, T., Sakamoto, T., Koizumi, I., 2003. Eastern Mediterranean surface water temperatures and $\delta^{18}O$ composition during deposition of sapropels in the late Quaternary. Paleoceanography 18, 1005, DOI:10.1029/2000PA000617.

Eswaran, V., Harpending, H., Rogers, A.R., 2005. Genomics refutes an exclusively African origin of humans. J. Hum. Evol. 49, 1–18.

Excoffier, L., 2002. Human demographic history: refining the recent African origin model. Curr. Opin. Genet. Dev. 12, 675–682.

Faith, J.T., Choiniere, J.N., Tryon, C.A., Peppe, D.J., Fox, D.L., 2011. Taxonomic status and paleoecology of *Rusingoryx atopocranion* (Mammalia, Artiodactyla), an extinct Pleistocene bovid from Rusinga Island, Kenya. Quatern. Res. 75, 697–707.

Feathers, J.K., 2002. Luminescence dating in less than ideal conditions: case studies from Klasies River main site and Duinefontein, South Africa. J. Archaeol. Sci. 29, 177–194.

Feathers, J.K., Bush, D.A., 2000. Luminescence dating of Middle Stone Age deposits at Die Kelders. J. Hum. Evol. 38, 91–119.

Feathers, J.K., Migliorini, E., 2001. Luminescence dating at Katanda: a reassessment. Quatern. Sci. Rev. 20, 961–966.

Fisher, E.C., Bar-Matthews, M., Jerardino, A., Marean, C.W., 2010. Middle and Late Pleistocene paleoscape modeling along the southern coast of South Africa. Quatern. Sci. Rev. 29, 1382–1398.

Fontes, J.C., Gasse, F., 1991. Palhydaf (paleohydrology in Africa) program: objectives, methods, major results. Palaeogeogr. Palaeoclimatol. Palaeoecol. 84, 191–215.

Forster, P., 2004. Ice Ages and the mitochondrial DNA chronology of human dispersals: a review. Phil. Trans. R. Soc. B 359, 255–264.

Gamble, C., Davies, W., Pettitt, P., Hazelwood, L., Richards, M., 2005. The archaeological and genetic foundations of the European population during the late glacial: implications for 'agricultural thinking'. Cambridge Archaeol. J. 15, 193–223.

Garrigan, D., Hammer, M.F., 2006. Reconstructing human origins in the genomic era. Nat. Rev. Genet. 7, 669–680.

Garrigan, D., Kingan, S.B., Pilkington, M.M., Wilder, J.A., Cox, M.P., Soodyall, H., Strassmann, B., Destro-Bisol, G., de Knijff, P., Novelletto, A., Friedlaender, J., Hammer, M.F., 2007. Inferring human population sizes, divergence times and rates of gene flow from mitochondrial, X and Y chromosome resequencing data. Genetics 177, 2195–2207.

Gaven, C., Hillaire-Marcel, C., Petit-Maire, N., 1981. A Pleistocene lacustrine episode in southeastern Libya. Nature 290, 131–133.

Gifford-Gonzalez, D., Parham, J.F., 2008. Fauna from Adrar Bous and surrounding areas. In: Gifford-Gonzalez, D. (Ed.), Adrar Bous: Archaeology of a Central Saharan Granitic Ring Complex in Niger. Royal Museum for Central Africa Studies in Human Sciences 170, Tervuren, pp. 313–353.

Gonder, M.K., Mortensen, H.M., Reed, F.A., de Sousa, A., Tishkoff, S.A., 2007. Whole mtDNA genome sequence analysis of ancient African lineages. Mol. Biol. Evol. 24, 757–768.

Grine, F.E., Bailey, R.M., Harvarti, K., Nathan, R.P., Morris, A.G., Henderson, G.M., Ribot, I., Pike, A.W.G., 2007. Late Pleistocene human skull from Hofmeyr, South Africa, and modern human origins. Science 315, 226–229.

Grün, R., Beaumont, P.B., Tobias, P.V., Eggins, S., 2003. On the age of Border Cave 5 human mandible. J. Hum. Evol. 45, 155–167.

Grün, R., Brink, J.S., Spooner, N.A., Taylor, L., Stringer, C.B., Franciscus, R.G., Murray, A.S., 1996. Direct dating of Florisbad hominid. Nature 382, 500–501.

Grün, R., Shackleton, N.J., Deacon, H.J., 1990. Electron-spin-resonance dating of tooth

enamel from Klasies River Mouth Cave. Curr. Anthropol. 31, 427–432.

Grün, R., Stringer, C., 1991. Electron spin resonance dating and the evolution of modern humans. Archaeometry 33, 153–199.

Gunz, P., Bookstein, F.L., Mitteroecker, P., Stadlmayr, A., Seidler, H., Weber, G.W., 2009. Early modern human diversity suggests subdivided population structure and a complex out-of-Africa scenario. Proc. Natl. Acad. Sci. 106, 6094–6098.

Hammer, M.F., Woerner, A.E., Mendez, F.L., Watkins, J.C., Wall, J.D., 2011. Genetic evidence for archaic admixture in Africa. Proc. Natl. Acad. Sci. 108, 15123–15128.

Harding, R.M., McVean, G., 2004. A structured ancestral population for the evolution of modern humans. Curr. Opin. Genet. Dev. 14, 667–674.

Harvati, K., Stringer, C., Grün, R., Aubert, M., Allsworth-Jones, P., Folorunso, C.A., 2011. The Later Stone Age calvaria from Iwo Eleru, Nigeria: morphology and chronology. Plos One 6, e24024.

Henshilwood, C., d'Errico, F., Yates, R., Jacobs, Z., Tribolo, C., Duller, G.A.T., Mercier, N., Sealy, J., Valladas, H., Watts, I., Wintle, A., 2002. Emergence of modern human behaviour: Middle Stone Age engravings from South Africa. Science 295, 1278–1280.

Henshilwood, C.S., Marean, C.W., 2003. The origin of modern human behavior: a review and critique of models and test implications. Curr. Anthropol. 44, 627–651.

Hillaire-Marcel, C., Carro, O., Casanova, J., 1986. 14C and Th/U dating of Pleistocene and Holocene stromatolites from East Africa paleolakes. Quatern. Res. 25, 312–329.

Hodell, D.A., Venz, K.A., Charles, C.D., Ninnemann, U.S., 2003. Pleistocene vertical carbon isotope and carbonate gradients in the South Atlantic sector of the Southern Ocean. Geochem. Geophy. Geosy. 4, 1–19.

Holmgren, K., Karlen, W., Shaw, P., 1995. Paleoclimatic significance of the stable isotope composition and petrology of a Late Pleistocene stalagmite from Botswana. Quatern. Res. 43, 320–328.

Holzkamper, S., Holmgren, K., Lee-Thorp, J., Talma, S., Mangini, A., Partridge, T., 2009. Late Pleistocene stalagmite growth in Wolkberg Cave, South Africa. Earth Planet. Sci. Lett. 282, 212–221.

Hooghiemstra, H., Stalling, H., Agwu, C.O.C., Dupont, L., 1992. Vegetational and climatic changes at the northern fringe of the Sahara 250,000-5000 years BP: evidence from 4 marine pollen records located between Portugal and the Canary Islands. Rev. Palaeobot. Palyno. 74, 1–52.

Howell, F.C., 1999. Paleo-demes, species clades, and extinctions in the Pleistocene hominin record. J. Anthropol. Res. 55, 191–243.

Imbrie, J., Imbrie, J.Z., 1980. Modeling the climatic response to orbital variations. Science 207, 943–953.

Ingman, M., Kaessmann, H., Pääbo, S., Gyllensten, U., 2000. Mitochondrial genome variation and the origin of modern humans. Nature 408, 708–713.

Jacobs, Z., Duller, G.A.T., Wintle, A.G., Henshilwood, C.S., 2006. Extending the chronology of deposits at Blombos Cave, South Africa, back to 140 ka using optical dating of single and multiple grains of quartz. J. Hum. Evol. 51, 255–273.

Jacobs, Z., Roberts, R.G., Galbraith, R.F., Deacon, H.J., Grün, R., Mackay, A., Mitchell, P., Vogelsang, R., Wadley, L., 2008a. Ages for the Middle Stone Age of southern Africa: implications for human behavior and dispersal. Science 322, 733–735.

Jacobs, Z., Wintle, A.G., Duller, G.A.T., Roberts, R.G., Wadley, L., 2008b. New ages for the post-Howiesons Poort, late and final Middle Stone Age at Sibudu, South Africa. J. Archaeol. Sci. 35, 1790–1807.

Kelly, R.L., 1995. The Foraging Spectrum. Smithsonian Institution Press, Washington.

Kiberd, P., 2006. Bundu farm: a report on archaeological and palaeoenvironmental assemblages from a pan site in Bushmanland, Northern Cape, South Africa. S. Afr. Archaeol. Bull. 61, 189–201.

Kingston, J.D., 2007. Shifting adaptive landscapes: progress and challenges in reconstructing early hominid environments. Yearb. Phys. Anthropol. 50, 20–58.

Klein, R.G., 1980. Environmental and ecological implications of large mammals from Upper Pleistocene and Holocene sites in southern Africa. Annals of the South African Museum 81, 223–283.

Klein, R.G., 2009. The Human Career, Third Edition. University of Chicago Press, Chicago.

Klein, R.G., Cruz-Uribe, K., Beaumont, P.B., 1991. Environmental, ecological, and paleoanthropological implications of the Late Pleistocene mammalian fauna from

Equus Cave, Northern Cape Province, South Africa. Quatern. Res. 36, 94–119.

Kristen, I., Fuhrmann, A., Thorpe, J., Röhl, U., Wilkes, H., Oberhänsli, H., 2007. Hydrological changes in southern Africa over the last 200 ka as recorded in lake sediments from the Tswaing impact crater. S. Afr. J. Geol. 110, 311–326.

Kuehn, D.D., Dickson, B.D., 1999. Stratigraphy and noncultural site formation at the Shurmai Rockshelter (GnJm1) in the Mukugodo Hills of north-central Kenya. Geoarchaeology 14, 63–85.

Kuhn, S.L., Stiner, M.C., 2001. The antiquity of hunter-gatherers. In: Panter-Brick, C., Layton, R.H., Rowley-Conwy, P. (Eds.), Hunter-Gatherers: An Interdisciplinary Perspective. Cambridge University Press, Cambridge, pp. 99–142.

Kutzbach, J.E., 1981. Monsoon climate of the Early Holocene: climate experiment with the Earth's orbital parameters for 9000 years ago. Science 214, 59–61.

Kutzbach, J.E., Liu, Z., 1997. Response of the African monsoon to orbital forcing and ocean feedbacks in the Middle Holocene. Science 278, 440–443.

Kutzbach, J.E., Liu, X., Liu, Z., 2008. Simulation of the evolutionary response of global summer monsoons to orbital forcing over the past 280,000 years. Clim. Dynam. 30, 567–579.

Lahr, M.M., Foley, R., 1998. Towards a theory of modern human origins: geography, demography, and diversity in recent human evolution. Yearb. Phys. Anthropol. 41, 137–176.

Laskar, J., Robutel, P., Joutel, F., Gastineau, M., Correia, A.C.M., Levrard, B., 2004. A long-term numerical solution for the insolation quantities of the Earth. Astron. Astrophys. 428, 261–265.

Lea, D.W., Mashiotta, T.A., Spero, H.J., 1999. Controls on magnesium and strontium uptake in planktonic foraminifera determined by live culturing. Geochim. Cosmochim. Ac. 63, 2369–2379.

Lee-Thorp, J.A., Beaumont, P.B., 1995. Vegetation and seasonality shifts during the late Quaternary deduced from $^{13}C/^{12}C$ ratios of grazers at Equus Cave, South Africa. Quatern. Res. 43, 426–432.

Leuschner, D.C., Sirocko, F., 2000. The low-latitude monsoon climate during Dansgaard-Oeschger cycles and Heinrich Events. Quatern. Sci. Rev. 19, 243–254.

Lezzine, A., Casanova, J., 1991. Correlated oceanic and continental records demonstrate past climate and hydrology of North Africa (0-140 ka). Geology 19, 307–310.

Little, M.G., Schneider, R.R., Kroon, D., Price, B., Bickert, T., Wefer, G., 1997. Rapid palaeoceanographic changes in the Benguela Upwelling System for the last 160,000 years as indicated by abundances of planktonic foraminifera. Palaeogeogr. Palaeoclimatol. Palaeoecol. 130, 135–161.

Liu, X., Liu, Z., Kutzbach, J.E., Clemens, S.C., Prell, W.L., 2006. Hemispheric insolation forcing of the Indian Ocean and Asian monsoon: local versus remote impacts. J. Climate 19, 6195–6208.

Liu, Z., Harrison, S.P., Kutzbach, J., Otto-Bliesner, B., 2004. Global monsoons in the mid-Holocene and oceanic feedback. Clim. Dynam. 22, 157–182.

Lombard, M., Wadley, L., Jacobs, Z., Mohapi, M., Roberts, R.G., 2010. Still Bay and serrated points from Umhlatuzana Rock Shelter, Kwazulu-Natal, South Africa. J. Archaeol. Sci. 37, 1773–1784.

Lorenzen, E.D., Masembe, C., Actander, P., Siegismund, H.R., 2010. A long-standing Pleistocene refugium in southern Africa and a mosaic of refugia in East Africa: insights from mtDNA and the common eland antelope. J. Biogeogr. 37, 571–581.

Manega, P.C., 1993. Geochronology, geochemistry and isotopic study of the Plio-Pleistocene hominid sites and the Ngorongoro Volcanic Highlands in northernTanzania. Ph.D. Dissertation, University of Colorado.

Marchant, R., Mumbi, C., Behera, S., Yamagata, T., 2007. The Indian Ocean dipole – the unsung driver of climatic variability in East Africa. Afr. J. Ecol. 45, 4–16.

Marean, C.W., 1997. Hunter-gatherer foraging strategies in tropical grasslands: model-building and testing in the East African Middle and Later Stone Age. J. Anthropol. Archaeol. 16, 189–225.

Marean, C.W., 2010. Pinnacle Point Cave 13B (Western Cape Province, South Africa) in context: the Cape Floral kingdom, shellfish, and modern human origins. J. Hum. Evol. 59, 425–443.

Marean, C.W., Assefa, Z., 2005. The Middle and Upper Pleistocene African record for the biological and behavioral origins of modern humans. In: Stahl, A.B. (Ed.), African Archaeology. Blackwell Publishing, Malden, pp. 93–129.

Marean, C.W., Bar-Matthews, M., Bernatchez, J., Fisher, E., Goldberg, P., Herries, A.I.R., Jacobs, Z., Jerardino, A., Karkanas, P., Minichillo, T., Nilssen, P.J.,

Thompson, E., Watts, I., Williams, H.M., 2007. Early human use of marine resources and pigment in South Africa during the Middle Pleistocene. Nature 449, 905–908.

Marean, C.W., Bar-Matthews, M., Fisher, E., Goldberg, P., Herries, A., Karkanas, P., Nilssen, P.J., Thompson, E., 2010. The stratigraphy of the Middle Stone Age sediments at Pinnacle Point Cave 13B (Mossel Bay, Western Cape Province, South Africa). J. Hum. Evol. 59, 234–255.

Marlowe, F.W., 2005. Hunter-gatherers and human evolution. Evol. Anthopol. 14, 54–67.

Martinez-Méndez, G., Zahn, R., Hall, I.R., Frank, J.C., Peeters, L.D., Cacho, I., Negre, C., 2010. Contrasting multiproxy reconstructions of surface ocean hydrography in the Agulhas Corridor and implications for the Agulhas Leakage during the last 345,000 years. Paleoceanography 25, PA4227, DOI: 10.1029/2009PA001879.

Martinez-Méndez, G., Zahn, R., Hall, I.R., Pena, L.D., Cacho, I., 2008. 345,000-year-long multi-proxy records off South Africa document variable contributions of Northern versus Southern Component Water to the Deep South Atlantic. Earth Planet. Sci. Lett. 267, 309–321.

Mayr, E., 2001. What Evolution Is. Basic Books, New York.

McBrearty, S., 1992. Sangoan technology and habitat at Simbi, Kenya. Nyame Akuma 38, 29–33.

McBrearty, S., Brooks, A., 2000. The revolution that wasn't: a new interpretation of the origin of modern human behavior. J. Hum. Evol. 39, 453–563.

McCall, G.S., 2007. Behavioral ecological models of lithic technological change during the later Middle Stone Age of South Africa. J. Archaeol. Sci. 34, 1738–1751.

McDermott, F., 2004. Palaeo-climate reconstruction from stable isotope variations in speleothems: a review. Quatern. Sci. Rev. 23, 901–918.

McDermott, F., Stringer, C., Grün, R., Williams, C.T., Din, V. K., Hawkesworth, C. J., 1996. New Late-Pleistocene uranium-thorium and ESR dates for the Singa hominid (Sudan). J. Hum. Evol. 31, 507–516.

McDougall, I., Brown, F.H., Fleagle, J.G., 2005. Stratigraphic placement and age of modern humans from Kibish, Ethiopia. Nature 433, 733–736.

McGlue, M.M., Lezzar, K.E., Cohen, A.S., Russell, J.M., Tiercelin, J.J., Felton, A.A., Mbede, E., Nkotagu, H.H., 2008. Seismic records of late Pleistocene aridity in Lake Tanganyika, tropical East Africa. J. Paleolimnol. 40, 635–653.

McKenzie, J.A., 1993. Pluvial conditions in the eastern Sahara following the penultimate deglaciation: implications for changes in atmospheric circulation patterns with global warming. Palaeogeogr. Palaeoclimatol. Palaeoecol. 103, 95–105.

Mehlman, M.J., 1991. Context for the emergence of modern man in eastern Africa: some new Tanzanian evidence. In: Clark, J.D. (Ed.), Cultural Beginnings: Approaches to Understanding Early Hominid Life-Ways in the African Savanna. Dr. Rudolph Habelt GMBH, Bonn, pp. 177–196.

Mellars, P., 2006. Why did modern human populations disperse from Africa ca. 60,000 years ago? A new model. Proc. Natl. Acad. Sci. 103, 9381–9386.

Mellars, P., French, J.C., 2011. Tenfold population increase in Western Europe at the Neanderthal-to-modern human transition. Science 333, 623–627.

Mercader, J., Asmerom, Y., Bennett, T., Raja, M., Skinner, A., 2009. Initial excavation and dating of Ngalue Cave: a Middle Stone Age site along the Niassa Rift, Mozambique. J. Hum. Evol. 57, 63–74.

Mercader, J., Martí, R., 2003. The Middle Stone Age occupation of Atlantic Central Africa: new evidence from equatorial Guinea and Cameroon. In: Mercader, J. (Ed.), Under the Canopy: The Archaeology of Tropical Rain Forests. Rutgers University Press, London, pp. 64–92.

Mercader, J., Runge, F., Vrydaghs, L., Doutrelepont, H., Ewango, C.E.N., Juan-Tresseras, J., 2000. Phytoliths from archaeological sites in the tropical forest of Ituri, Democratic Republic of Congo. Quatern. Res. 54, 102–112.

Mercier, N., Valladas, H., Froget, L., Joron, J.-L., Vermeersch, P.M., Van Peer, P., Moeyersons, J., 1999. Thermoluminescence dating of a Middle Paleolithic occupation at Sodmein Cave, Red Sea Mountains (Egypt). J. Archaeol. Sci. 26, 1339–1345.

Mercier, N., Wengler, L., Valladas, H., Joron, J.-L., Froget, L., Reyss, J.-L., 2007. The Rhafas Cave (Morocco): chronology of the Mousterian and Aterian archaeological occupations and their implications for Quaternary geochronology based on luminescence (TL/OSL) age determinations. Quatern. Geochronol. 2, 309–313.

Miller, G.H., Beaumont, P.B., Deacon, H.J., Brooks, A.S., Hare, P.E., Jull, A.J.T., 1999.

Earliest modern humans in southern Africa dated by isoleucine epimerization in ostrich eggshell. Quatern. Sci. Rev. 18, 1537–1548.

Moernaut, J., Verschuren, D., Charlet, F., Kristen, I., Fagot, M., De Batist, M., 2010. The seismic-stratigraphic record of lake-level fluctuations in Lake Challa: hydrological stability and change in equatorial East Africa over the last 140 kyr. Earth Planet. Sci. Lett. 290, 241–223.

Moeyersons, J., Vermeersch, P.M., Van Peer, P., 2002. Dry cave deposits and their paleoenvironmental significance during the last 115 ka, Sodmein Cave, Red Sea Mountains, Egypt. Quatern. Sci. Rev. 21, 837–851.

Morel, J., 1974. La station eponyme de l'Oued Djebbana a Bir-el-Ater (Est Algérien): contribution a la connaissance de son industrie et de sa fauna. L'Anthropologie 78, 53–80.

Morel, A., Tillet, Th., Poupeau, G., 1991. Le bassin de Taoudenni. In: Tillet, G. (Ed.), Paleoenvironments and Prehistoric Populations of the Sahara in the Upper Pleistocene. Abstracts Colloque de Solignac, PICG 252.

Nespoulet, R., El Hajraoui, M.A., Amani, F., Ben Ncer, A., Debénath, A., El Idrissi, A., Lacombe, J.-P., Michel, P., Oujaa, A., Stoetzel, E., 2008. Paleolithic and Neolithic occupations in the Témara region (Rabat, Morocco): recent data on hominin contexts and behavior. Afr. Archaeol. Rev. 25, 21–39.

Nicholson, S.E., Flohn, H., 1980. African environmental and climatic changes and the general atmospheric circulation in Late Pleistocene and Holocene. Clim. Change 2, 313–348.

Nürnberg, D., Groeneveld, J., 2006. Pleistocene variability of the subtropical convergence at East Tasman Plateau: evidence from (ODP Site 1172A). Geochem. Geophys. Geosy. 7, Q04P11.

Osbourne, A.H., Vance, D., Rohling, E.J., Barton, N., Rogerson, M., Fello, N., 2008. A humid corridor across the Sahara for the migration of early modern humans out of Africa 120,000 years ago. Proc. Natl. Acad. Sci. 105, 16444–16447.

Osmond, J.K., Dabous, A.A., 2004. Timing and intensity of groundwater movement during Egyptian Sahara pluvial periods by U-series analysis of secondary U in ores and carbonates. Quatern. Res. 61, 85–94.

Partridge, T.C., 1999. Tswaing: Investigations into the Origin, Age and Palaeoenvironments of the Pretoria Saltpan. Council for Geoscience, S. Africa Memoir 85.

Patin, E., Laval, G., Barreiro, L.B., Salas, A., Semino, O., Santachiara-Benerecetti, S., Kidd, K.K., Kidd, J. R., van der Veen, L., Hombert, J. M., Gessain, A., Froment, A., Bahuchet, S., Heyer, E., Quintana-Murci, L., 2009. Inferring the demographic history of African farmers and Pygmy hunter-gatherers using a multilocus resequencing data set. Plos Genet. 5, 1–7.

Pearson, O.M., 2008. Statistical and biological definitions of 'anatomically modern' humans: suggestions for a unified approach to modern morphology. Evol. Anthopol. 17, 38–48.

Petit, J.R., Jouzel, J., Raynaud, D., Barkov, N.I., Barnola, J.M., Basile, I., Bender, M., Chappellaz, J., Davis, M., Delaygue, G., Delmotte, M., Kotlyakov, V.M., Legrand, M., Lipenkov, V.Y., Lorius, C., Pepin, L., Ritz, C., Saltzman, E., Stievenard, M., 1999. Climate and atmospheric history of the past 420,000 years from the Vostok ice core, Antarctica. Nature 399, 429-436.

Pichevin L., Cremer, M., Giraudeau, J., Bertrand, P., 2005. A 190 kyr record of lithogenic grain-size on the Namibian slope: forging a tight link between past wind-strength and coastal upwelling dynamics. Mar. Geol. 218, 81–96.

Pienaar, M., Woodborne, S., Wadley, L., 2008. Optically stimulated luminescence dating at Rose Cottage Cave. S. Afr. J. Sci. 104, 65–70.

Pokras, E.M., Mix, A.C., 1985. Eolian evidence for spatial variability of late Quaternary climates in tropical Africa. Quatern. Res. 24, 137–149.

Potts, R., 1998. Environmental hypotheses of hominin evolution. Yearb. Phys. Anthropol. 41, 93–136.

Potts, R., Behrensmeyer, A.K., Ditchfield, P., 1999. Paleolandscape variation and Early Pleistocene hominid activities: Members 1 and 7, Olorgesailie Formation, Kenya. J. Hum. Evol. 37, 747–788.

Powell, A., Shennan, S., Thomas, M.G., 2009. Late Pleistocene demography and the appearance of modern human behavior. Science 324, 1298–1301.

Prahl, F.G., Muehlhausen, L.A., Zahnle, D.L., 1988. Further evaluation of long-chain alkenones as indicators of paleoceanographic conditions. Geochim. Cosmochim. Ac. 52,
2303–2310.

Prasad, T.G., McClean, J.L., 2004. Mechanisms for anomalous warming in the western Indian Ocean during dipole mode events. J. Geophys. Res. Oceans 109, CO2019,

DOI: 10.1029/2003JC001872.

Prugnolle, F., Manica, A., Balloux, F., 2005. Geography predicts neutral genetic diversity of human populations. Curr. Biol. 15, 159–160.

Quickert, N.A., Godfrey-Smtih, D.I., Casey, J.L., 2003. Optical and thermoluminescence dating of Middle Stone Age and Kintampo bearing sediments at Birimi, a multi-component archaeological site in Ghana. Quatern. Sci. Rev. 22, 1291–1297.

Quintana-Murci, L., Quach, H., Harmant, C., Luca, F., Massonnet, B., Patin, E., Sica, L., Mouguiama-Daouda, P., Comas, D., Tzur, S., Balanovsky, O., Kidd, K.K., Kidd, J.R., van der Veen, L., Hombert, J.M., Gessain, A., Verdu, P., Froment, A., Bahuchet, S., Heyer, E., Dausset, J., Salas, A., Behar, D.M., 2008. Maternal traces of deep common ancestry and asymmetric gene flow between Pygmy hunter-gathereres and Bantu-speaking farmers. Proc. Natl. Acad. Sci. 105, 1596–1601.

Rasse, M., Soriano, S., Tribolo, C., Stokes, S., Huysecom, E., 2004. La séquence Pléistocène supérieur d'Ounjougou (Pays dogon, Mali, Afrique de l'Ouest): évolution géomorphologique, enregisterements sédimentaires et changements culturels. Quaternaire 15, 329–341.

Raymo, M.E., Oppo, D.W., Flower, B.P., Hodell, D.A., McManus, J.F., Venz, K.A., Kleiven, K. F., McIntyre, K., 2004. Stability of North Atlantic water masses in face of pronounced climate variability during the Pleistocene. Paleoceanography 19, PA2008, DOI: 10.1029/2003PA000921.

Reed, F.A., Tishkoff, S.A., 2006. African human diversity, origins and migrations, Curr. Opin. Genet. Dev. 16, 597–605.

Reynolds, S.C., Clarke, R.J., Kuman, K.A., 2007. The view from the Lincoln Cave: mid- to late Pleistocene fossil deposits from Sterkfontein hominid site, South Africa. J. Hum. Evol. 53, 260–271.

Richter, D., Moser, J., Nami, M., Eiwanger, J., Mikdad, A., 2010. New chronometric data from Ifri n'Ammar (Morocco) and the chronostratigraphy of the Middle Paleolithic in the western Maghreb. J. Hum. Evol. 59, 672–679.

Robbins, L.H., Murphy, M.L., Brook, G.A., Ivester, A.H., Campbell, A.C., Klein, R.G., Milo, R.G., Stewart, K.M., Downey, W.S., Stevens, N.J., 2000. Archaeology, palaeoenvironment, and chronology of the Tsodilo Hills White Paintings Rock Shelter, northwest Kalahari Desert, Botswana. J. Archaeol. Sci. 27, 1085–1113.

Robert, A., Soriano, S., Rasse, M., Stokes, S., Huysecom, E., 2003. First chrono-cultural reference framework for the West African Paleolithic: new data from Ounjougou,

Dogon Country, Mali. J. Afr. Archaeol. 1, 151–169.

Rohli, R.V., Vega, A.J., 2008. Climatology. Jones and Bartlett Publishers, Sudbury.

Rose, J.I., Usik, V.I., Marks, A.E., Hilbert, Y.H., Galletti, C.S., Parton, A., Geiling, J.M., Cerny, V., Morley, M.W., Roberts, R.G., 2011. The Nubian complex of Dhofar, Oman: an African Middle Stone Age industry in southern Arabia. Plos One 6, 1–22.

Rossignol-Strick, M., 1985. Mediterraniean Quaternary sapropels, an immediate response of the African monsoon to variation of insolation. Palaeogeogr. Palaeoclimatol. Palaeoecol. 49, 237–263.

Rostek, F., Bard, E., Beaufort, L., Sonzogni, C., Ganssen, G., 1997. Sea surface temperature and productivity records for the past 240 ka in the Arabian Sea. Deep-Sea Res. 44, 1461–1480.

Saji, N.H., Goswami, B.N., Vinayachandran, P.N., Yamagata, T., 1999. A dipole mode in the tropical Indian Ocean. Nature 401, 360–363.

Sandel, B., Arge, L., Dansgaard, B., Davies, R.G., Gaston, K.J., Sutherland, W.J., Svenning, J.-C., 2011. The influence of late Quaternary climate change velocity on species endemism. Science 334, 660–664.

Schneider, R.R., Muller, P.J., Ruhland, G, Meinecke, G., Schmidt, H., Wefer, G., 1995. Late Quaternary surface temperatures and productivity in the east equatorial South Atlantic: response to changes in trade/monsoon wind forcing and surface water advection. In: Wefer, G., Berger, W.H., Siedler, G., Webb, D.J. (Eds.), The South Atlantic: Present and Past Circulation. Springer Verlag, Berlin, pp. 527–551.

Scholz, C.A., Johnson, T.C., Cohen, A.S., King, J.W., Peck, J.A., Overpeck, J.T., Talbot, M.R., Brown, E.T., Kalindekafe, L., Amoako, P.Y.O., Lyons, R.P., Shanahan, T.M., Castañeda, I.S., Heil, C.W., Forman, S.L., McHargue, L.R., Beuning, K.R., Gomez, J., Pierson, J., 2007. East African megadroughts between 135 and 75 thousand years ago and bearing on early-modern human origins. Proc. Natl. Acad. Sci. 104, 16416–16421.

Schwarcz, H.P., Blackwell, B., Goldberg, P., Marks, A.E., 1993. Uranium series dating of carbonates from Bir Tarfawi and Bir Sahara East. In: Wendorf, F., Schild, R., Close, A.E. (Eds.), Egypt During the Last Interglacial: The Middle Paleolithic of Bir Tarfawi and Bir Sahara East. Plenum Press, New York, pp. 205–217.

Schwarcz, H.P., Rink, W.J., 2000. ESR dating of the Die Kelders Cave 1 site, South

Africa. J. Hum. Evol. 38, 121–128.

Shea, J.J., 2008. The Middle Stone Age archaeology of the Lower Omo Valley Kibish Formation: excavations, lithic assemblages, and inferred patterns of early *Homo sapiens* behavior. J. Hum. Evol. 55, 448–485.

Shea, J.J., 2011. *Homo sapiens* is as *Homo sapiens* was? Curr. Anthropol. 52, 1–35.

Sicre, M.A., Ternois, Y., Paterne, M., Boireau, A., Beaufort, L., Martinez, P., Bertrand, P., 2000. Biomarker stratigraphic records over the last 150 kyears off the NW African coast at 25˚N. Org. Geochem. 31, 577–588.

Skinner, A.R., Hay, R.L., Masao, F., Blackwell, B.A.B., 2003. Dating the Naisiusiu Beds, Olduvai Gorge, by electron spin resonance. Quatern. Sci. Rev. 22, 1361–1366.

Smith, J.R., Hawkins, A.L., Asmerom, Y., Polyak, V., Giegengack, R., 2007. New age constraints on the Middle Stone Age occupations of Kharga Oasis, Western Desert, Egypt. J. Hum. Evol. 52, 690–701.

Sorin, L., Vaks, A., Bar-Matthews, M., Porat, R., Frumkin, A., 2010. Late Pleistocene paleoclimatic and paleoenvironmental reconstruction of the Dead Sea area (Israel), based on speleothems and cave stromatolites. Quatern. Sci. Rev. 29, 1201–1211.

Stager, J.C., Ryves, D.B., Chase, B.M., Pausata, F.S., 2011. Catastrophic drought in the Afro-Asian monsoon region during Heinrich event 1. Science 331, 1299–1302.

Stiner, M.C., Munro, N.D., Surovell, T.A., Tchernov, E., Bar-Yosef, O., 1999. Paleolithic population growth pulses evidenced by small animal exploitation. Science 283, 190–194.

Stokes, S., Haynes, G., Thomas, D.S.G., Horrocks, J.L., Higginson, M., Malifa, M., 1998. Punctuated aridity in southern Africa during the last glacial cycle: the chronology of linear dune construction in the northeast Kalahari. Palaeogeogr. Palaeoclimatol. Palaeoecol. 137, 305–322.

Stone, J.R., Westover, K.S., Cohen, A.S., 2011. Late Pleistocene paleohydrography and diatom paleoecology of the central basin of Lake Malawi, Africa. Palaeogeogr. Palaeoclimatol. Palaeoecol. 303, 51–70.

Street, F.A., Grove, A.T., 1979. Global maps of lake-level fluctuations since 30,000 yr BP. Quatern. Res. 12, 83–118.

Stuut, J.B.W., Lamy, F., 2004. Climate variability at the southern boundaries of the Namib (southwestern Africa) and Atacama (northern Chile) coastal deserts during the last 120,000 yr. Quatern. Res. 62, 301–309.

Surovell, T.A., Finley, J.B., Smith, G.M., Brantingham, P.J., Kelly, R., 2009. Correcting temporal frequency distributions for taphonomic bias. J. Archaeol. Sci. 36, 1715–1724.

Szabo, B.J., Haynes, C.V., Maxwell, T.A., 1995. Ages of Quaternary pluvial episodes determined by uranium series and radiocarbon dating of lacustrine deposits of eastern Sahara. Palaeogeogr. Palaeoclimatol. Palaeoecol. 113, 227–242.

Thomas, D.S.G., Bailey, R., Shaw, P.A., Durcan, J.A., Singarayer, J.S., 2009. Late Quaternary highstands at Lake Chilwa, Malawi: frequency, timing and possible forcing mechanisms in the last 44 ka. Quatern. Sci. Rev. 28, 526–539.

Thomas, D.S.G., Shaw, P.A., 2003. Late Quaternary environmental change in central southern Africa: new data, synthesis, issues and prospects. Quatern. Sci. Rev. 21, 783–797.

Tierney, J.E., Russell, J.M., Huang, Y., Sinninghe Damsté, J.S., Hopmans, E.C., Cohen, A.S., 2008. Northern Hemisphere controls on tropical southeast African climate during the past 60,000 years. Science 322, 252–255.

Tishkoff, S.A., Reed, F.A., Friedlaender, F.R., Ehret, C., Ranciaro, A., Froment, A., Hirbo, J.B., Awomoyi, A.A., Bodo, J.M., Doumbo, O., Ibrahim, M., Juma, A.T., Kotze, M.J., Lema, G., Moore, J.H., Mortensen, H., Nyambo, T.B., Omar, S.A., Powell, K., Pretorius, G.S., Smith, M.W., Thera, M.A., Wambebe, C., Weber, J.L., Williams, S.M., 2009. The genetic structure and history of Africans and African Americans. Science 324, 1035–1044.

Tisserand, A., Malaizé, B., Jullien, E., Zaragosi, S., Charlier, K., Grousset, F., 2009. African monsoon enhancement during the penultimate glacial period (MIS 6.5 ~ 170 ka) and its atmospheric impact. Paleoceanography 24, PA2220, DOI: 10.1029/2008PA001630.

Tjallingii, R., Claussen, M., Stuut, J.B.W., Fohlmeister, J., Jahn, A., Bickert, T., Lamy, F., Röhl, U., 2008. Coherent high- and low-latitude control of the northwest African hydrological balance. Nat. Geosci. 1, 670–675.

Toggweiler, J.R., Russell, J., 2008. Ocean circulation in a warming climate. Nature 451, 286–288.

Trauth, M.H., Deino, A.L., Bergner, A.G.N., Strecker, M.R., 2003. East African climate change and orbital forcing during the last 175 kyr BP. Earth Planet. Sci. Lett. 206, 297–313.

Trauth, M.H., Larrasoaña, J.C., Mudelsee, M., 2009. Trends, rhythms, and events in Plio-Pleistocene African climate. Quatern. Sci. Rev. 28, 399–411.

Tribolo, C., Mercier, N., Selo, M., Valladas, H., Joron, J.L., Reyss, J.L., Henshilwood, C., Sealy, J., Yates, R., 2006. TL dating of burnt lithics from Blombos Cave (South Africa): further evidence for the antiquity of modern human behaviour. Archaeometry 48, 341–357.

Tribolo, C., Mercier, N., Valladas, H., 2005. Chronologie des technofaciès Howiesons Poort et Still Bay (Middle Stone Age, Afrique du Sud): bilan et nouvelles données de la luminescnece. Bull. Soc. Préhist. Fr. 102, 855–866.

Trinkaus, E., 2005. Early modern humans. A. Rev. Anthropol. 34, 207–230.

Tryon, C.A., Faith, J.T., Peppe, D.J., Fox, D.L., McNulty, K.P., Jenkins, K., Dunsworth, H., Harcourt-Smith, W., 2010. The Pleistocene archaeology and environments of the Wasiriya Beds, Rusinga Island, Kenya. J. Hum. Evol. 59, 657–671.

Tryon, C.A., Roach, N.T., Logan, M.A.V., 2008. The Middle Stone Age of the northern Kenyan Rift: age and context of new archaeological sites from the Kapedo Tuffs. J. Hum. Evol. 55, 652–664.

Vaks, A., Bar-Matthews, M., Ayalon, A., Halicz, L., Frumkin, A., 2007. Desert speleothems reveal climatic window for African exodus of early modern humans. Geology 35, 831–834.

Valladas, H., Wadley, L., Mercier, N., Froget, L., Tribolo, C., Reyss, J.L., Joron, J.L., 2005. Thermoluminescence dating on burnt lithics from Middle Stone Age layers at Rose Cottage Cave. S. Afr. J. Sci. 101, 169–174.

Van Andel, T.H., 1989. Late Pleistocene sea levels and the human exploitation of the shore and shelf of southern South Africa. J. Field Archaeol. 16, 133–155.

Van Campo, E., Duplessy, J.C., Rossignol-Strick, M., 1982. Climatic conditions deduced from a 150 kyr oxygen isotope-pollen record from the Arabian Sea. Nature 296, 56–59.

Van Neer, W., 1989. Contribution to the Archaeozoology of Central Africa. Musee Royal de l'Afrique Centrale, Annales Sciences Zoologiques Vol. 259, Tervuren.

Van Noten, F., 1977. Excavations at Matupi Cave. Antiquity 51, 35–40.

Van Peer, P., Fullagar, R., Stokes, S., Bailey, R.M., Moeyersons, J., Steenhoudt, F., Geerts, A., Vanderbeken, T., De Dapper, M., Geus, F., 2003. The Early to Middle Stone Age transition and the emergence of modern human behaviour at site 8-B-11, Sai Island, Sudan. J. Hum. Evol. 45, 187–193.

Verdu, P., Austerlitz, F., Estoup, A., Vitalis, R., Georges, M., Thery, S., Froment, A., Le Bomin, S., Gessain, A., Hombert, J.M., Van der Veen, L., Quintana-Murci, L., Bahuchet, S., Heyer, E., 2009. Origins and genetic diversity of pygmy hunter-gatherers from western Central Africa. Curr. Biol. 19, 312–318.

Vermeersch, P.M., 2002. Palaeolithic Quarrying Sites in Upper and Middle Egypt. Leuven University Press, Leuven.

Vermeersch, P.M., Paulissen, E., Stokes, S., Charlier, C., Van Peer, P., Stringer, C.B., Lindsay, W., 1998. A Middle Paleolithic burial of a modern human at Taramsa Hill, Egypt. Antiquity 72, 475–484.

Vogel, J.C., 2001. Radiometric dates for the Middle Stone Age in South Africa. In: Tobias, P.V., Raath, M., Maggi-Cecchi, J., Doyle, G. (Ed.), Humanity from African Naissance to Coming Millenia: Colloquia in Human Biology and Paleoanthropology. Florence University Press, Florence, pp. 261–268.

Vogel, J.C., Fuls, A., Visser, E., 1986. Pretoria radiocarbon dates III. Radiocarbon 28, 1133–1172.

Vogel, J.C., Partridge, T.C., 1984. Preliminary radiometric ages for the Taung tufas. In: Vogel, J.C. (Ed.), Late Cainozoic Palaeoclimates of the Southern Hemisphere. A.A. Balkema, Rotterdam, pp. 507–514.

Vogelsang, R., 1998. Middle Stone Age Fündstellen in Sudwest-Namibia. Heinrich Barth Institut, Köln.

Voight, B., Gabriel, B., Lassonczy, K., Ghod, M., 1990. Quaternary events at the Horn of Africa. Berliner geowissenschaftliche Abhandlungen 120, 679–694.

Walter, R., Buffler, R.T., Bruggemann, J.H., Guillaume, M.M.M., Berhe, S.M., Negassi, B., Libeskal, Y., Cheng, H., Edwards, R.L., Von Cosel, R., Néraudeau, D., Gagnon, M., 2000. Early human occupation of the Red Sea coast of Eritrea during the last interglacial. Nature 405, 65–69.

Wang, Q., Tobias, P.V., Roberts, D.L., Jacobs, Z., 2008. A re-examination of a human femur found at the Blind River Site, East London, South Africa: its age,

morphology, and breakage pattern. Anthropol. Rev. 71, 43–61.

Wefer, G., Berger, W.H., 1991. Isotope paleontology: growth and composition of extant calcareous species. Mar. Geol. 100, 207–248.

Weisrock, A., Wengler, L., Mathieu, J., Ouammou, A., Fontugne, M., Mercier, N., Reyss, J.-L.,
Valladas, H., Guery, P., 2006. Upper Pleistocene comparative OSL, U/Th, and ^{14}C datings of sedimentary sequences and correlative morphodynamical implications in the south-western Anti-Atlas (Oued Noun, 29° N, Morocco). Quaternaire 17, 45–59.

Weldeab, S., Lea, D.W., Schneider, R.R., Andersen, N., 2007. 155,000 years of West African Monsoon and Ocean Thermal Evolution. Science 316, 1303–1307.

Wendorf, F., Close, A., Schild, R., 1987. Middle Paleolithic occupations at Bir Tarfawi, Egypt. Afr. Archaeol. Rev. 5, 4963.

Wendorf, F., Schild, R., Close, A.E., 1989. The Prehistory of Wadi Kubbaniya, Vol 2. Stratigraphy, Paleoeconomy and Environment. Southern Methodist University Press, Dallas.

Wendorf, F., Schild, R., Close, A.E., 1993. Middle Palaeolithic occupations at Bir Tarfawi and Bir Sahara East, Western Desert of Egypt. In: Krzyzaniak, L., Kobusiewicz, M., Alexander, J. (Ed.), Environmental Change and Human Culture in the Nile Basin and Northern Africa until the Second Millennium B.C. Museum Archeologiczne W. Poznianu, Poznan, pp. 103–112.

White, T.D., Asfaw, B., DeGusta, D., Gilbert, H., Richards, G.D., Suwa, G., Howell, F.C., 2003. Pleistocene *Homo sapiens* from Middle Awash, Ethiopia. Nature 423, 742–747.

Woltering, M., Johnson, T.C., Werne, J.P., Schouten, S., Sinninghe Damsté, J.S., 2011. Late Pleistocene temperature history of southeast Africa: a TEX_{86} temperature record from Lake Malawi. Palaeogeogr. Palaeoclimatol. Palaeoecol. 303, 93–102.

Wrinn, P.J., Rink, W.J., 2003. ESR dating of tooth enamel from Aterian levels at Mugharet el 'Aliya (Tangier, Morocco). J. Archaeol. Sci. 30, 123–133.

Yellen, J.E., Brooks, A.S., Helgren, D.M., Tappen, M., Ambrose, S.H., Bonnefille, R., Feathers, J.K., G., G., Ludwig, K., Renne, P., Stewart, K., 2005. The archaeology of Aduma Middle Stone Age Sites in the Awash Valley, Ethiopia. Paleoanthropology 10, 25–100.

Yuan, Y., Zhou, W., Yang, H., Li, C., 2008. Warming in the northwestern Indian Ocean associated with the El Niño event. Adv. Atmos. Sci. 25, 246–252.

Zhao, M., Beveridge, N.A.S., Shackleton, N.J., Sarnthein, M., Eglinton, G., 1995. Molecular stratigraphy of cores off northwest Afica; sea surface temperature history over the last 80 ka. Paleoceanography 10, 661–675.

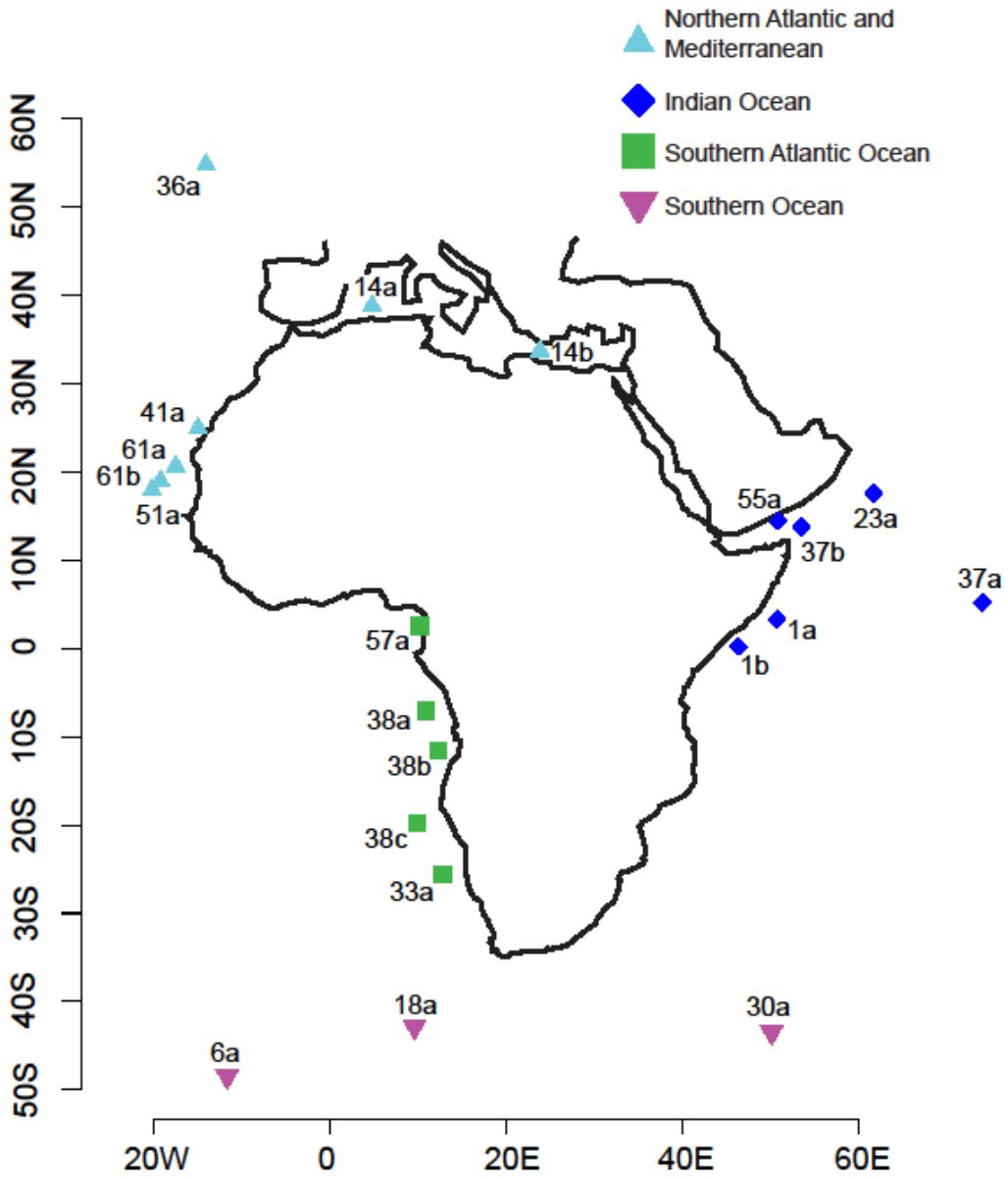

Figure A-1. A) Regional distribution of marine climate sites.

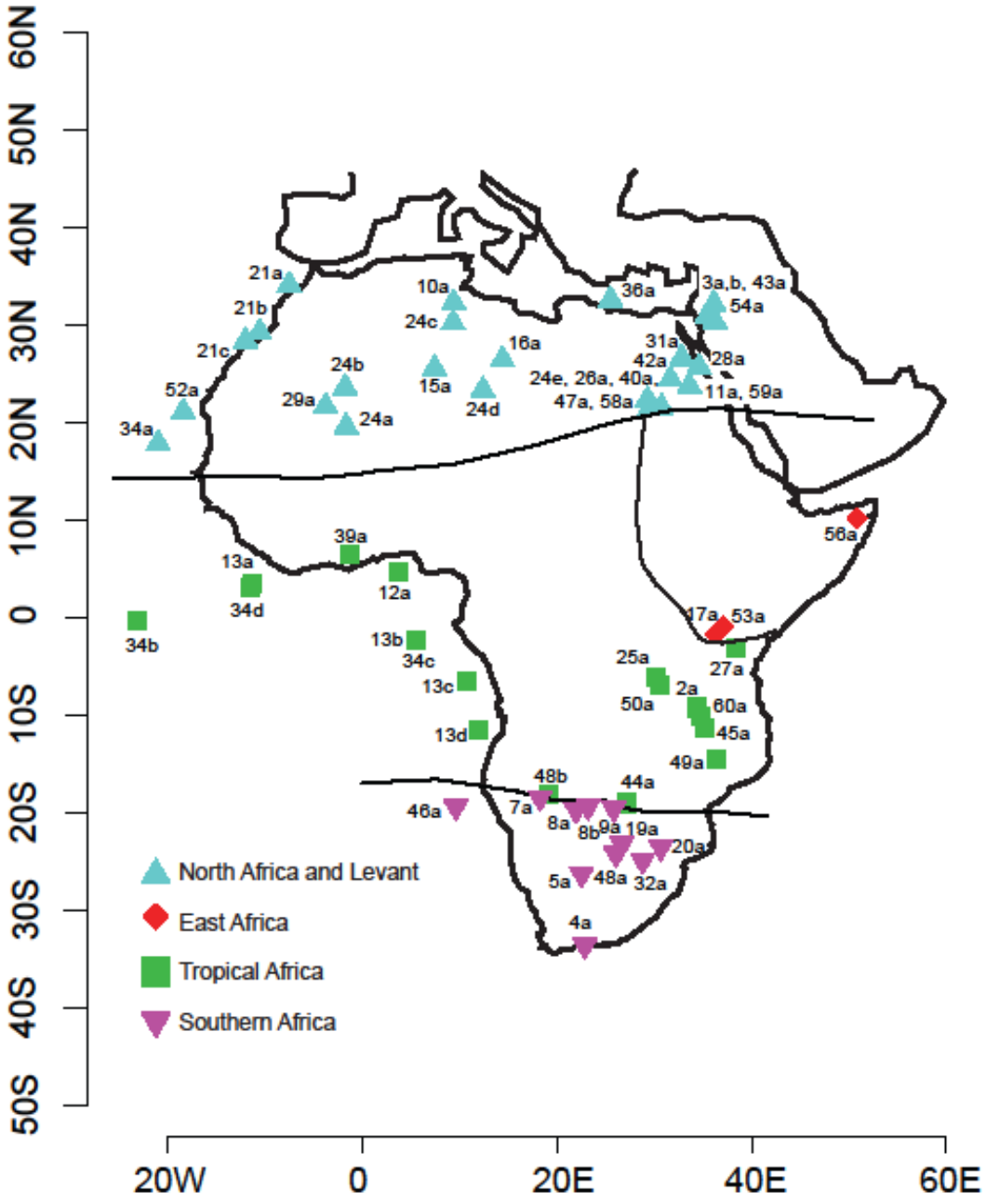

Figure A-1. B) Regional distribution of continental climate sites.

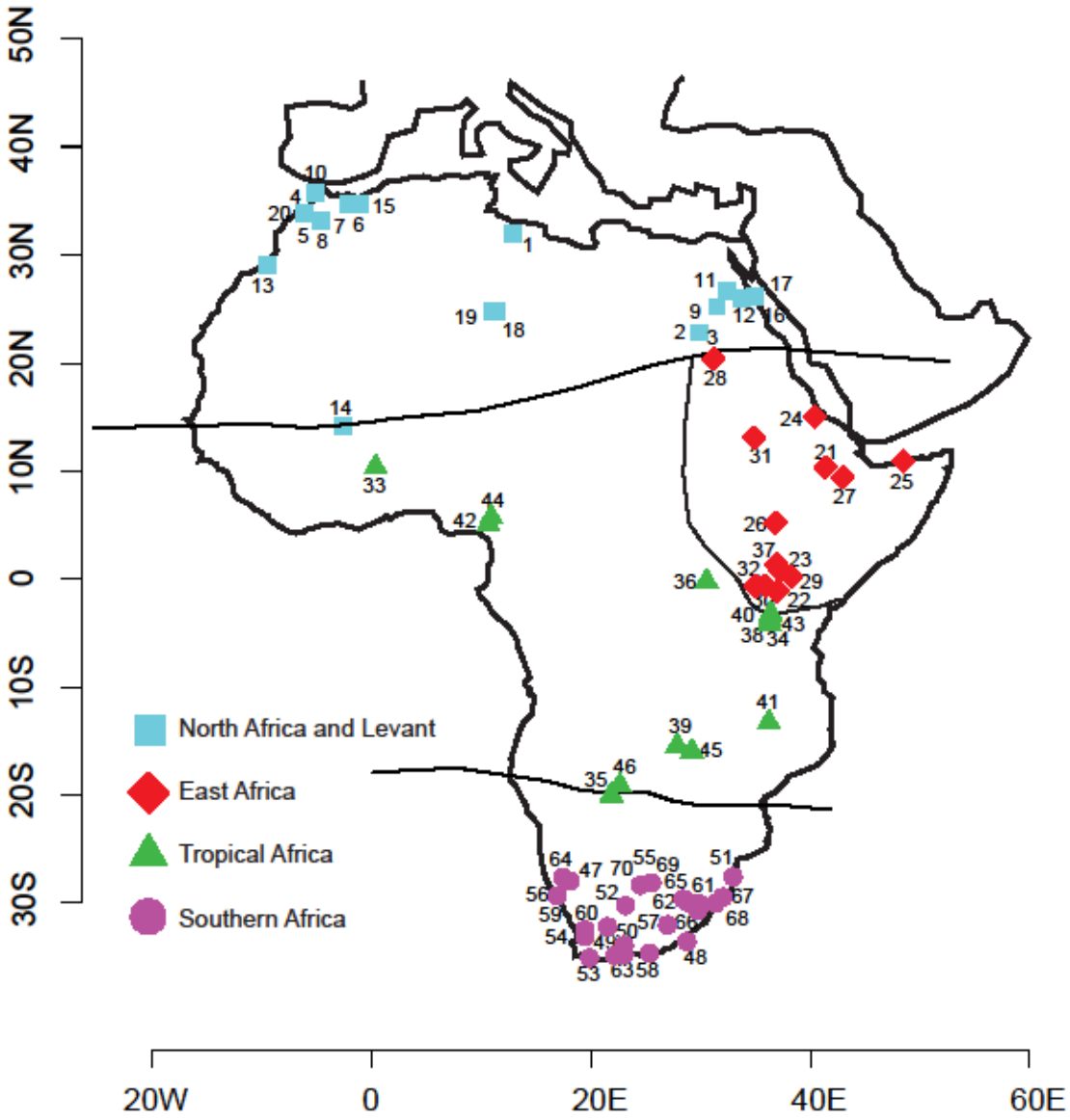

Figure A-2. Regional distribution of paleoanthropological sites used in this synthesis.

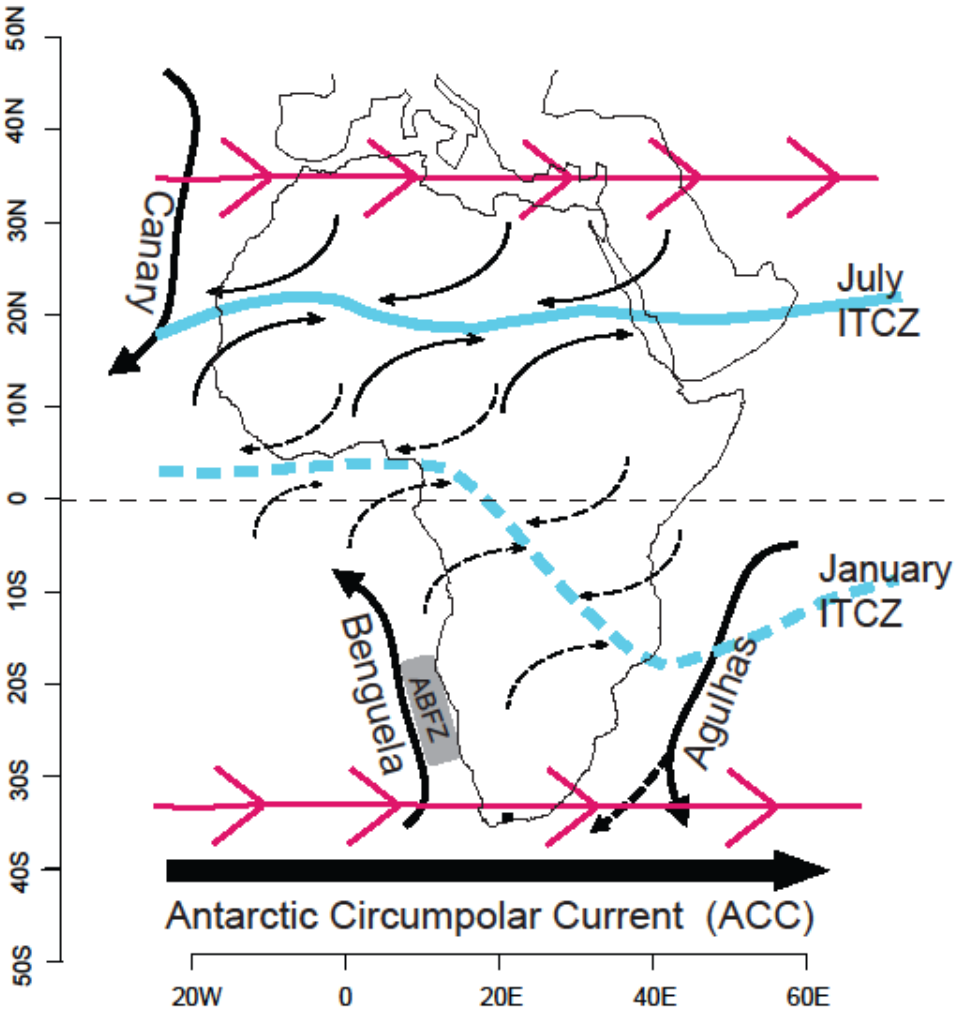

Figure A-3. Idealized position of the Intertropical Convergence Zone (ITCZ) in January and July (blue lines), and the associated trade winds. Average position of mid-latitude Westerlies (red arrows). Major surface ocean currents and the Angola-Benguela Frontal Zone (ABFZ) are also labeled.

Figures 4-8: Site numbers are closely associated with their respective datasets. Marine Isotope Stages (MIS) 6-3 and the overall inferred regional climate conditions through time are noted at the bottom for all dataset figures. Additionally, increasing warmth and humidity is toward the top of the graph, increasing cold and dryness toward the bottom.

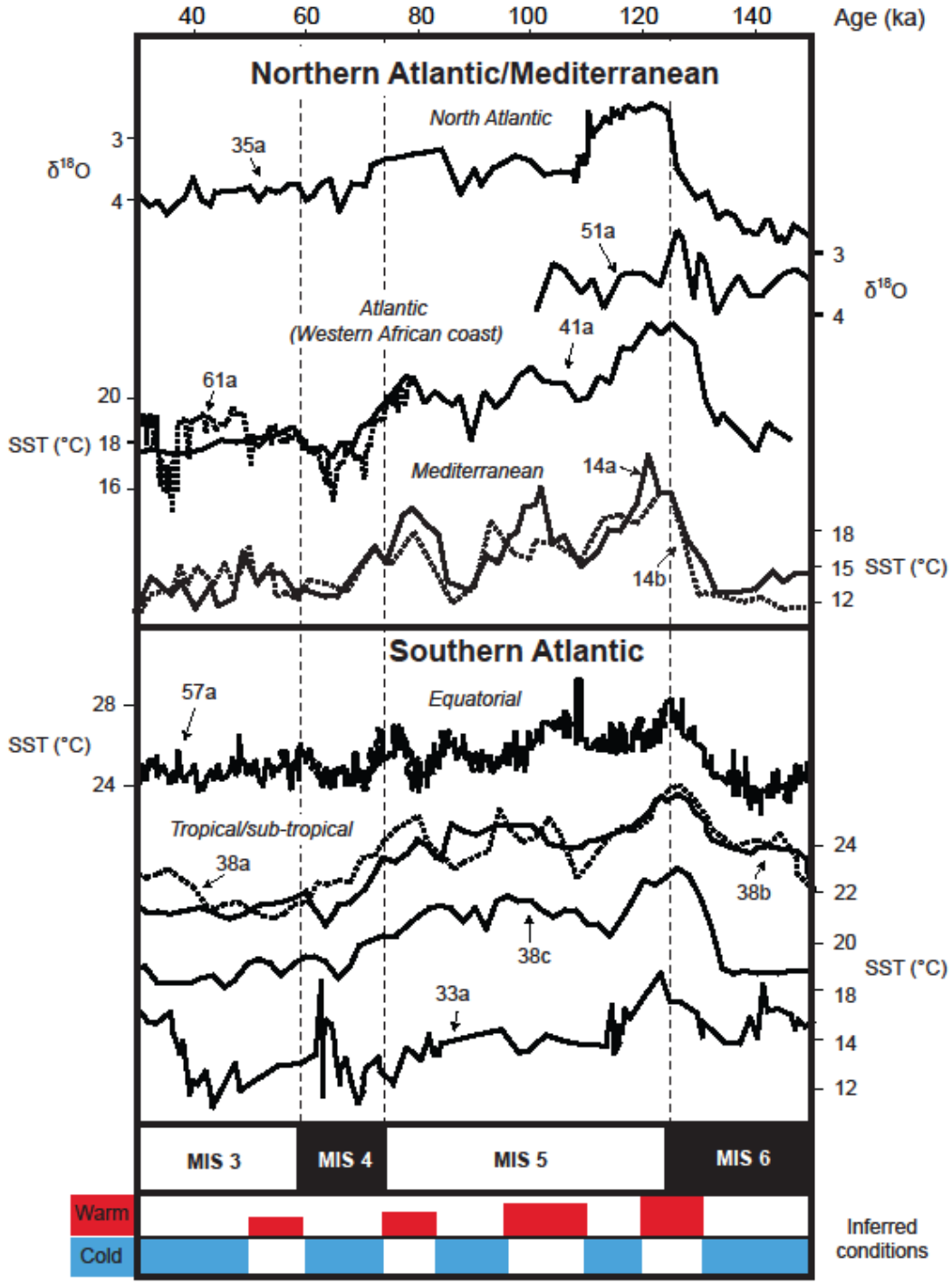

Figure A-4. Sea surface temperature (SST) data by region. These data are ordered from north to south on the vertical axis within each region. A) Atlantic Ocean

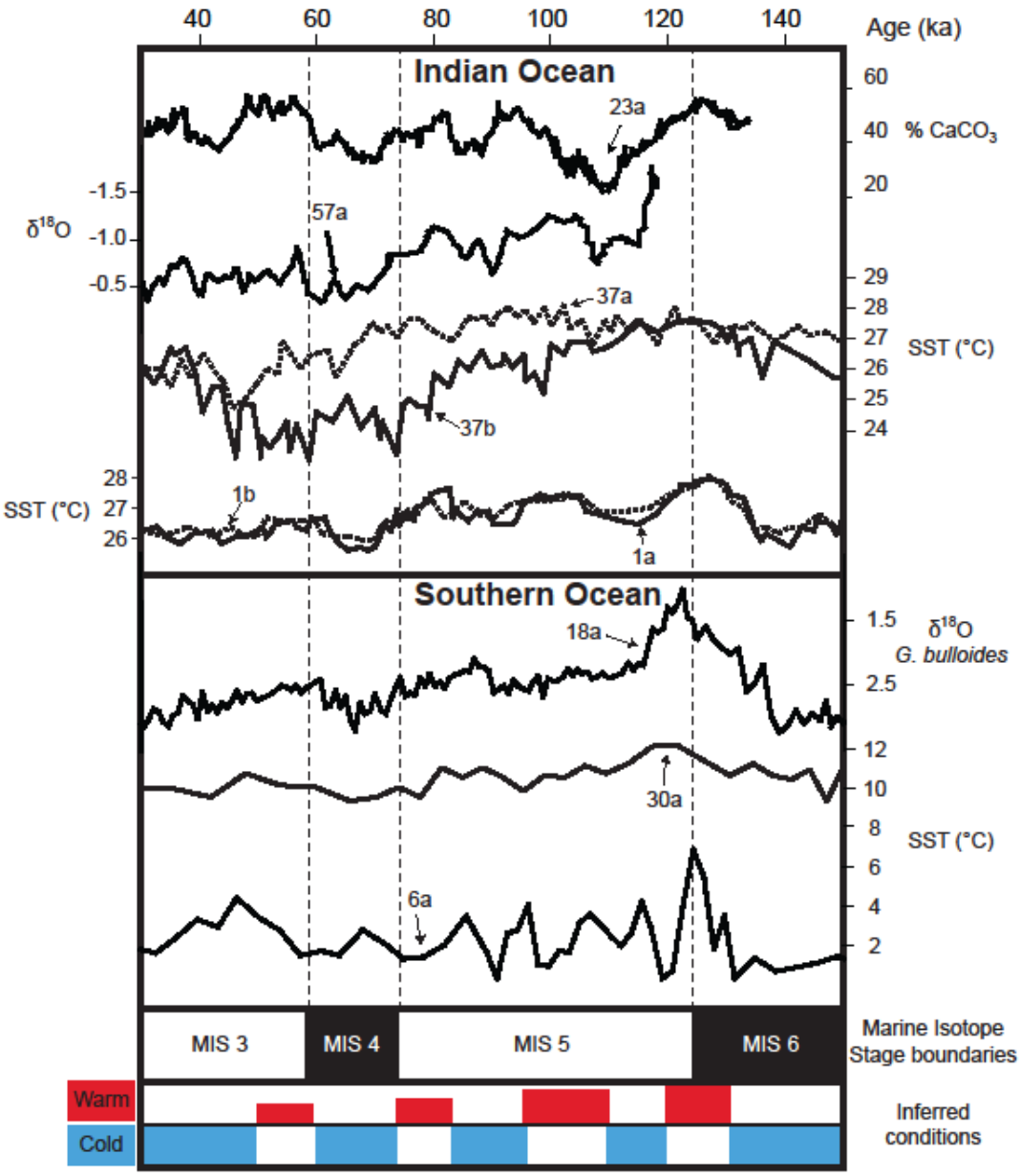

Figure A-4. B) Indian and Southern Ocean

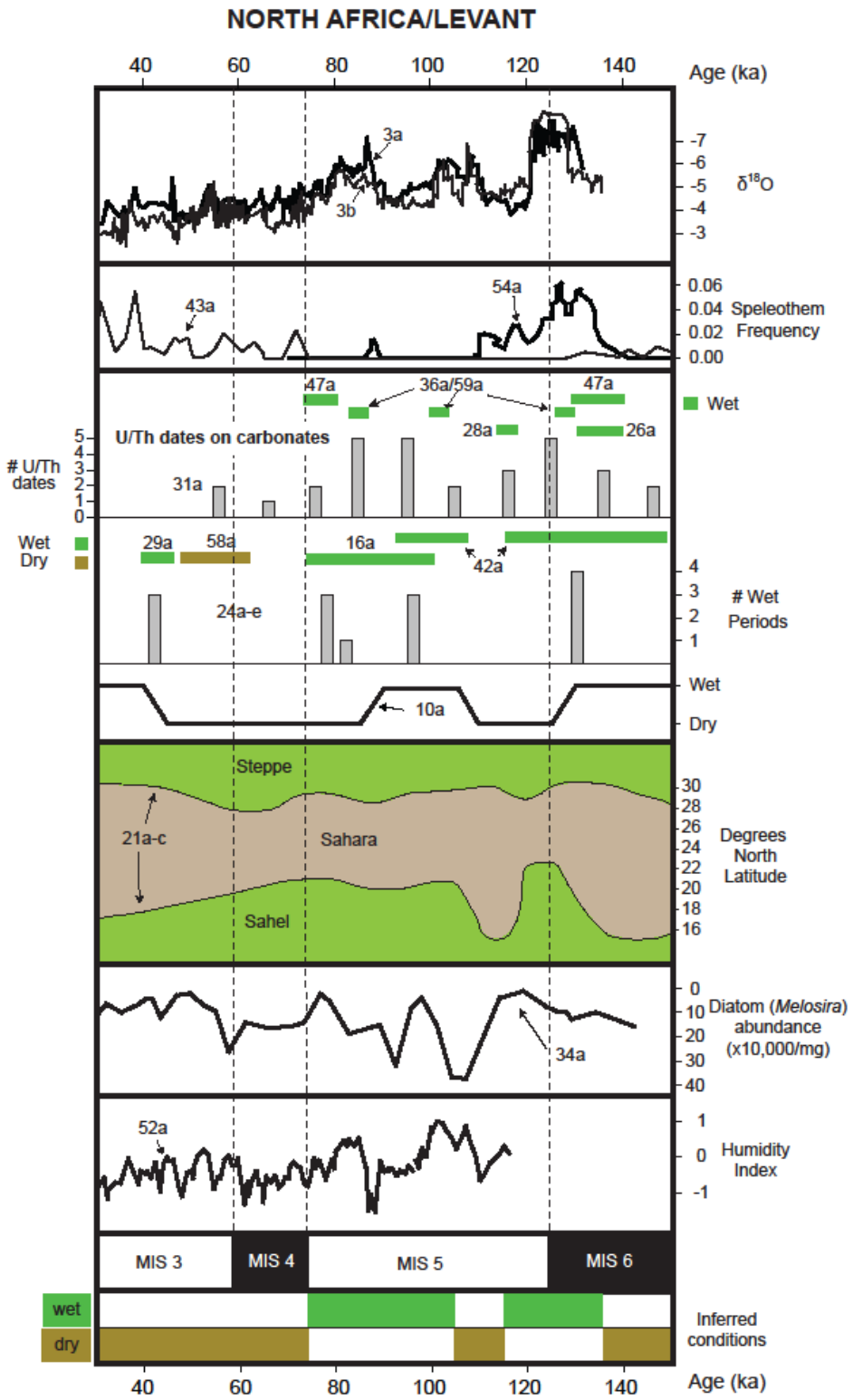

Figure A-5. North Africa/Levant datasets. Records are arranged in the order they are discussed in the text and grouped by indicator type.

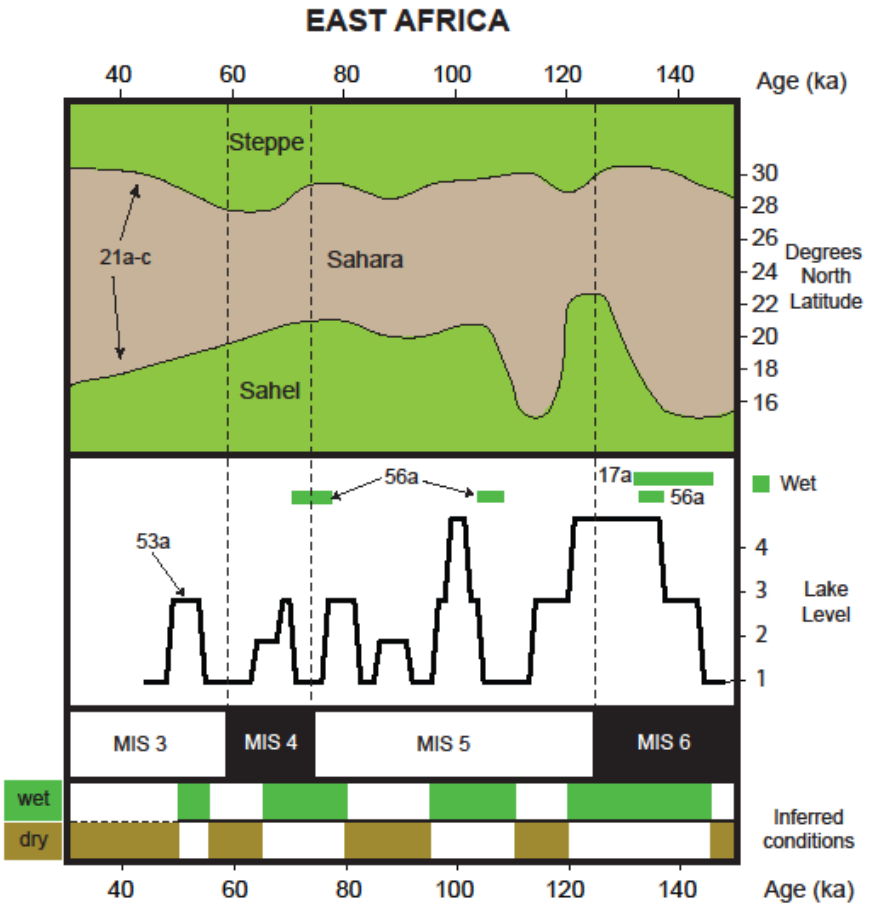

Figure A-6. East African terrestrial datasets. Records are arranged in the order they are discussed in the text and grouped by indicator type.

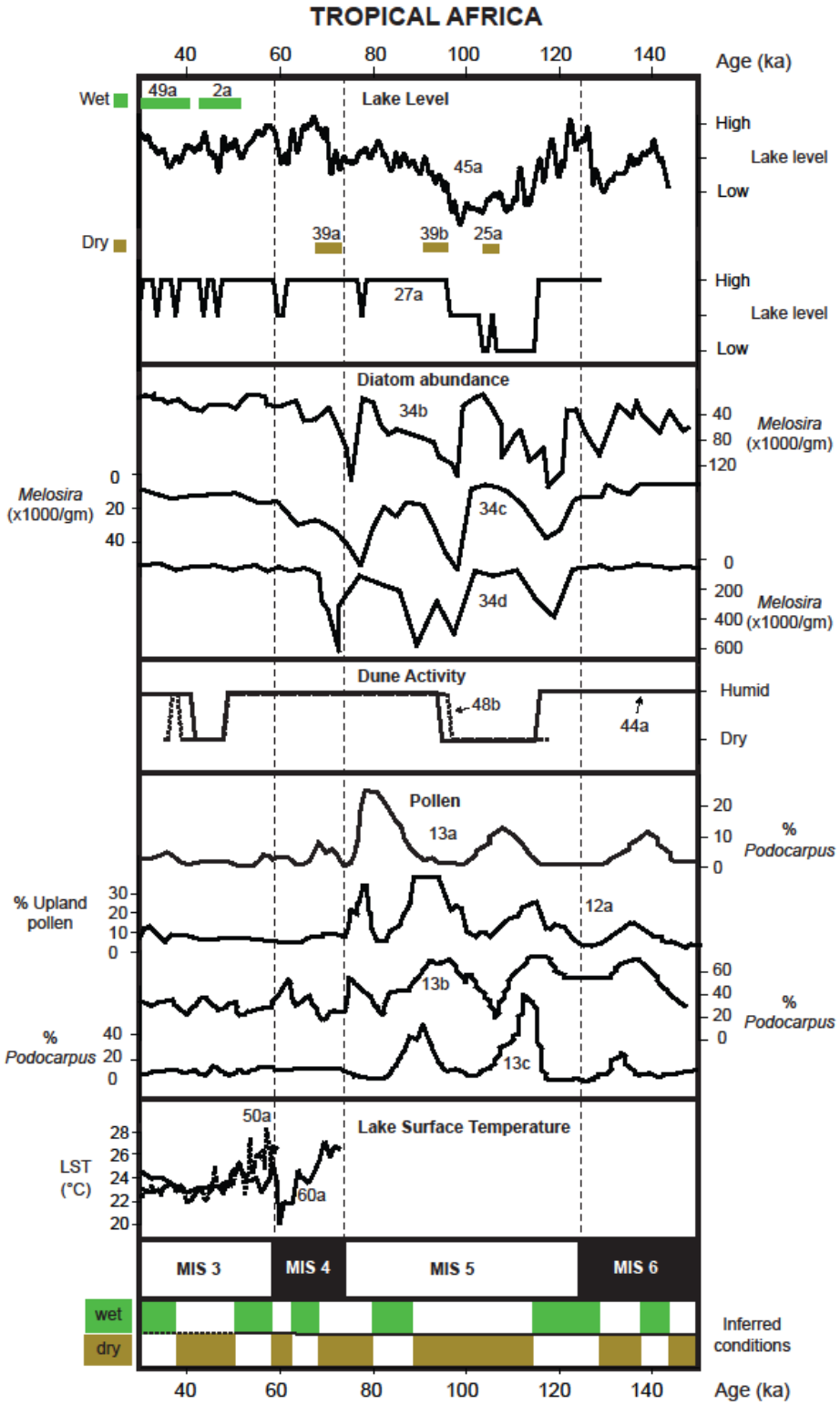

Figure A-7. Terrestrial datasets from tropical Africa. Records are arranged in the order they are discussed in the text and grouped by indicator type.

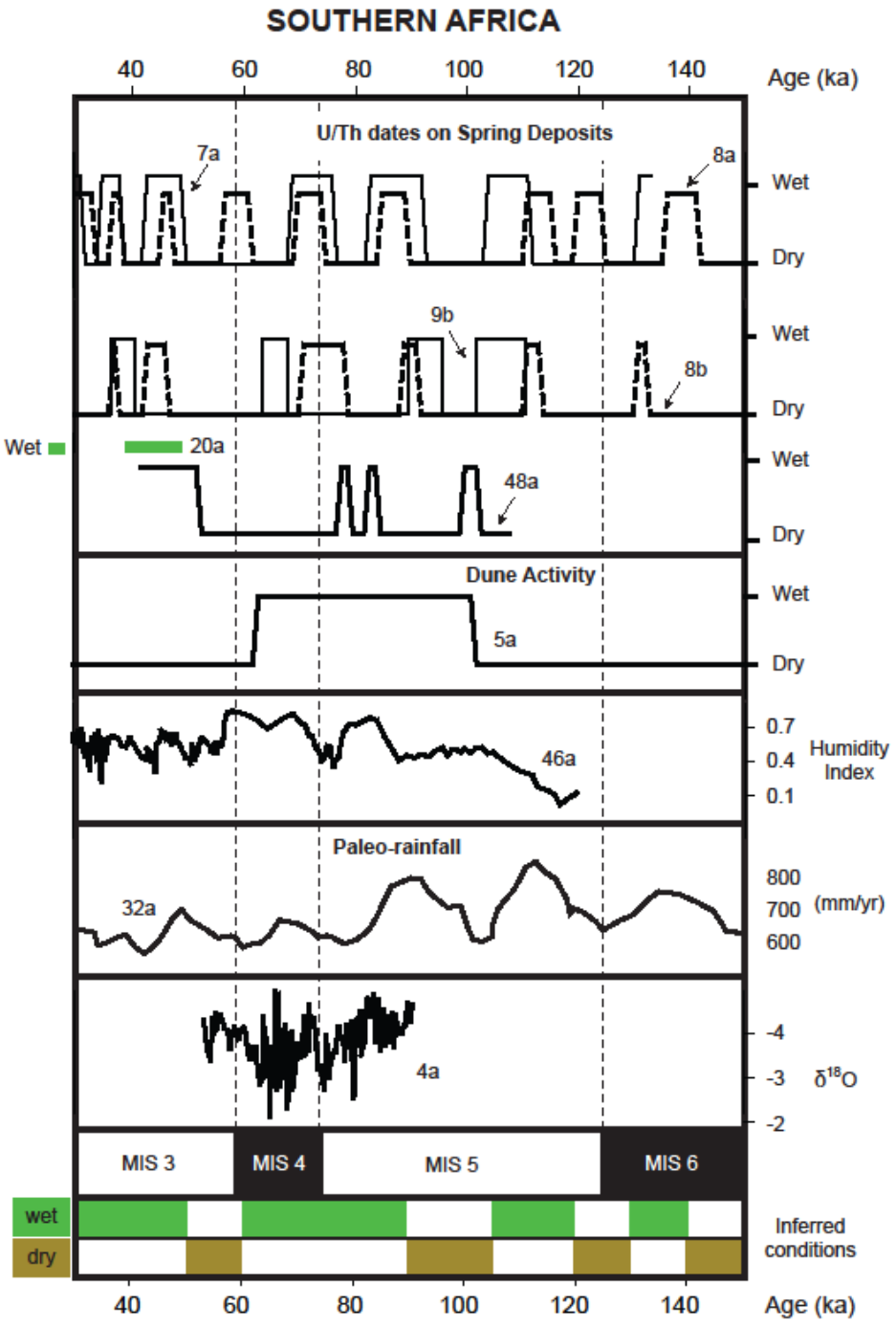

Figure A-8. South African terrestrial datasets. Records are arranged in the order they are discussed in the text and grouped by indicator type.

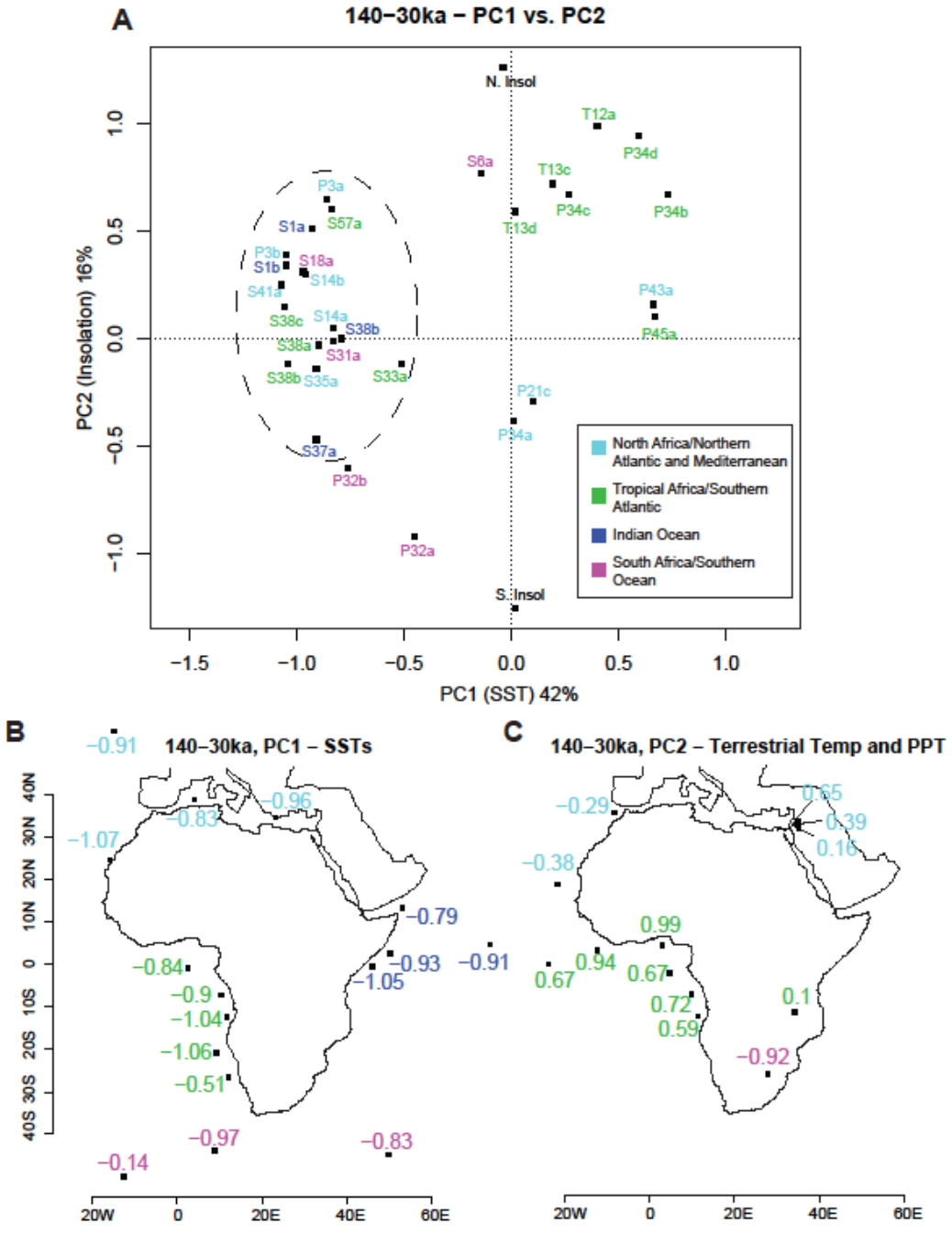

Figure A-9. Principal component (PC) analysis of all available continuous data over the 140-30 ka time interval. Regional color key applicable to entire figure. A) Ordination plot. B) Spatial distribution of PC1 scores from circum-Africa SST datasets. C) Spatial distribution of PC2 scores from terrestrial precipitation and temperature datasets.

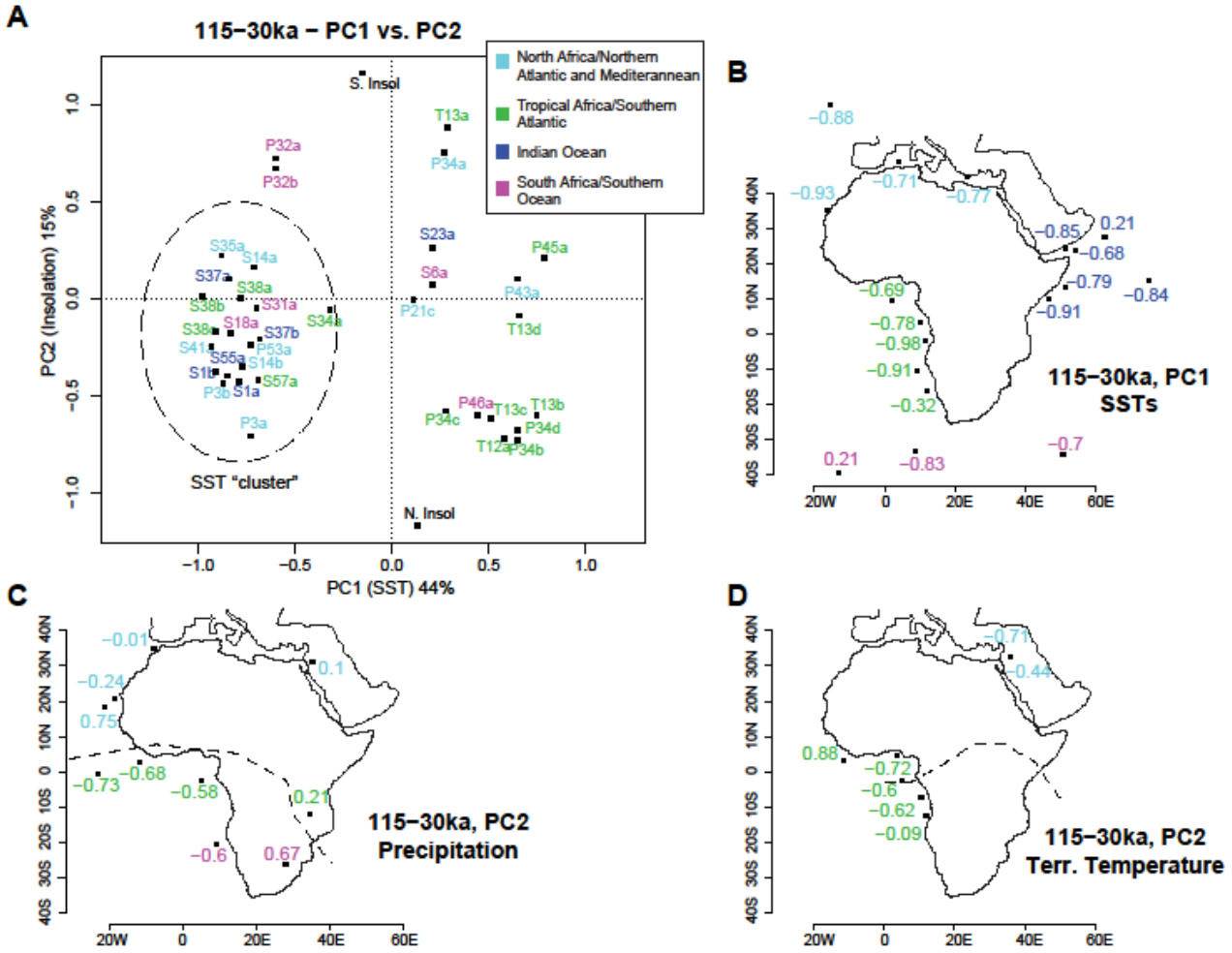

Figure A-10. Principal component (PC) analysis of all available continuous data over the 115-30 ka time interval. Regional color key applicable to entire figure. A) Ordination plot - note sea surface temperature (SST) 'cluster' labeled. B) Spatial distribution of PC1 scores on SST datasets. C) Spatial distribution of PC2 scores from terrestrial precipitation, and D) temperature datasets. Dashed line represents interpreted location of a division in climate trends over this time period.

Figure A-11. Principal component (PC) analysis for time interval 75-30 ka. Regional color key applicable to entire figure. A) Ordination plot, only PC1 is significant. Notice how the variation due to insolation appears to be more muted during this time interval whereas the SST variability still shows a coherent trend along the PC1 axis, the only significant axis. B) Spatial distribution of PC1 scores from circum-Africa SST datasets. C) Spatial distribution of PC1 scores from terrestrial precipitation and temperature datasets.

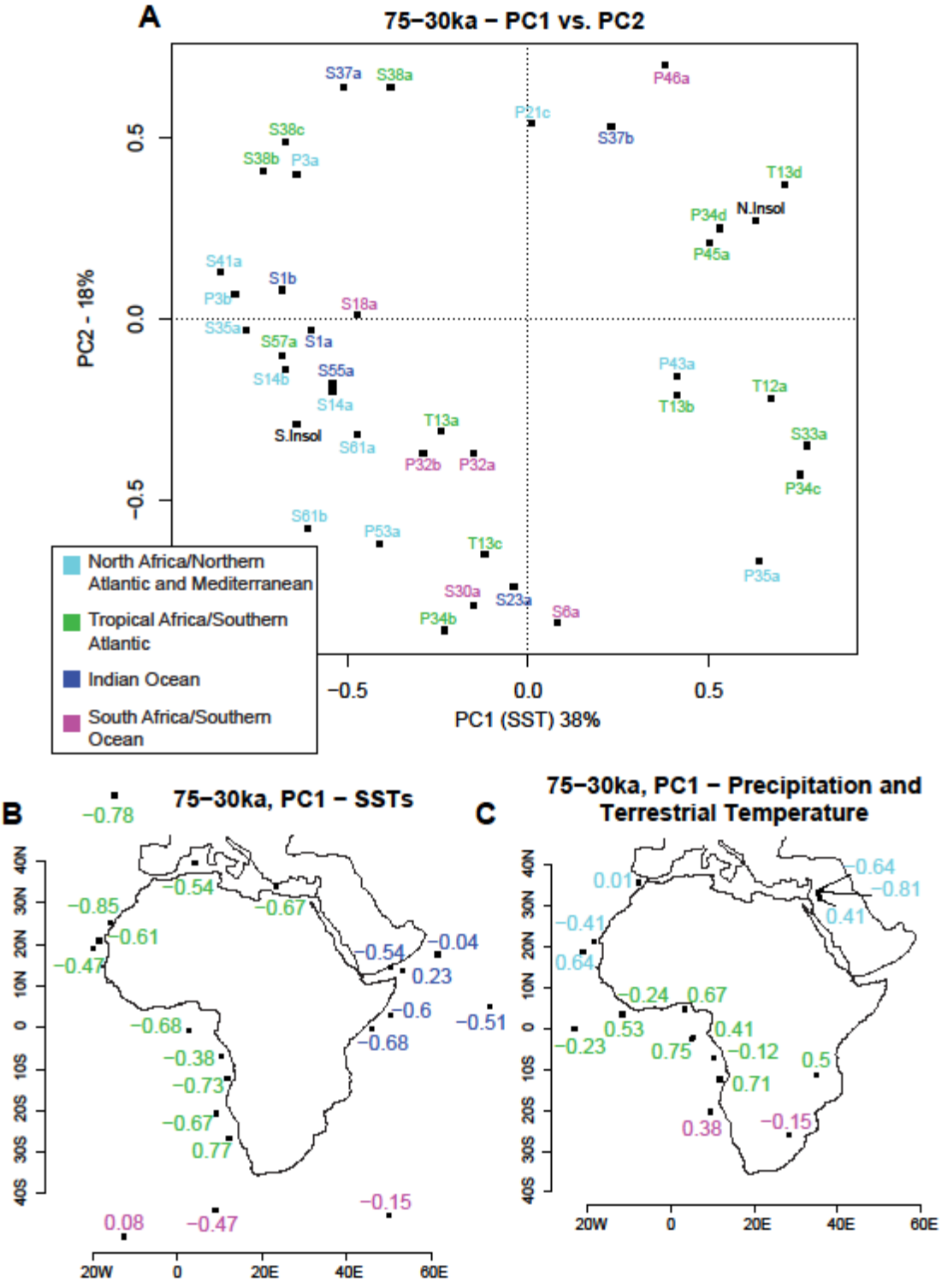
A
75−30ka − PC1 vs. PC2
PC2 - 18%
PC1 (SST) 38%
North Africa/Northern Atlantic and Mediterranean
Tropical Africa/Southern Atlantic
Indian Ocean
South Africa/Southern Ocean
B
75−30ka, PC1 − SSTs
C
75−30ka, PC1 − Precipitation and Terrestrial Temperature

Figure A-12. A) Diagram illustrating the possible consequences of the Westerlies shifting over time. Situation 1 places the Westerlies more equator-ward bringing precipitation to North and South Africa, and cutting off Agulhas current 'leakage' around the tip of the continent. Situation 2 shows the Westerlies more pole-ward, with the opposite effect. B) Paleo-data showing that the two scenarios are observed in the record for North and South Africa. Also illustrates how the records from Egypt may be responding to another dynamic mechanism as they are out of phase with either situation over the 150-30 ka period.

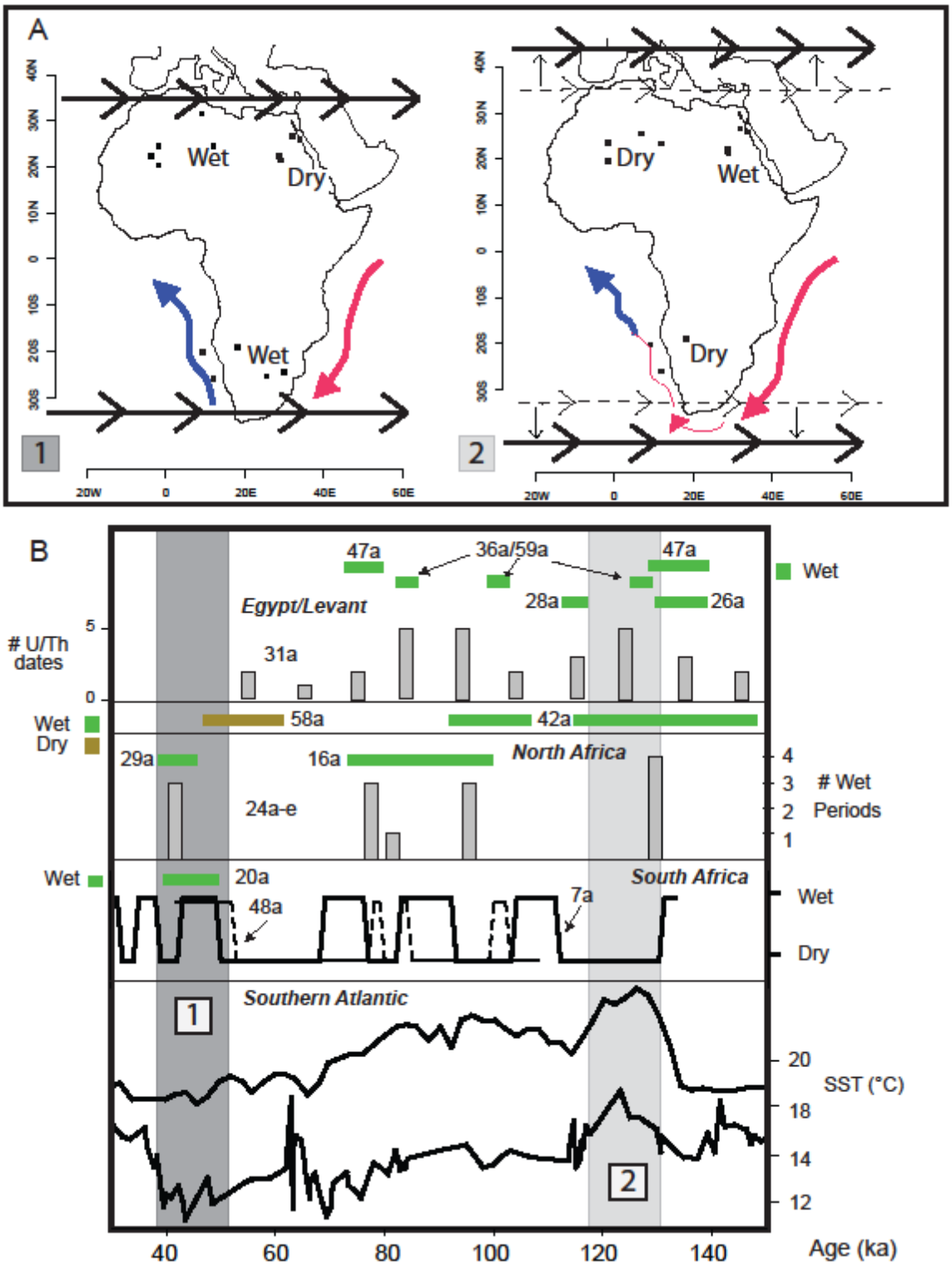
A
Wet
Dry
Wet
1
Dry
Wet
Dry
2
40N
30N
20N
10N
0
10S
20S
30S
20W
0
20E
40E
60E
B
47a
36a/59a
47a
Wet
Egypt/Levant
28a
26a
U/Th dates
5
0
31a
Wet
Dry
58a
42a
29a
16a
North Africa
24a-e
4
3
2
1
Wet Periods
Wet
20a
48a
7a
South Africa
Wet
Dry
1
Southern Atlantic
20
18
14
12
SST (°C)
2
40
60
80
100
120
140
Age (ka)

Figure A-13. A) Diagram showing possible northward movement of the Intertropical Convergence Zone (ITCZ) during periods of strong Northern Hemisphere insolation. B) Paleo-data supporting the hypothesis from 98-117 ka with extremely strong Northern Hemisphere insolation during the peak of the 'megadrought,' as well as a gradual wettening and subsequent decrease in variability at Lake Malawi (45a) as Northern Hemisphere insolation weakens and becomes less variable (70-30ka). C) Principal component (PC) analysis plot from 75-30 ka supports this observation, showing the decreased control insolation has on climate variability during this interval.

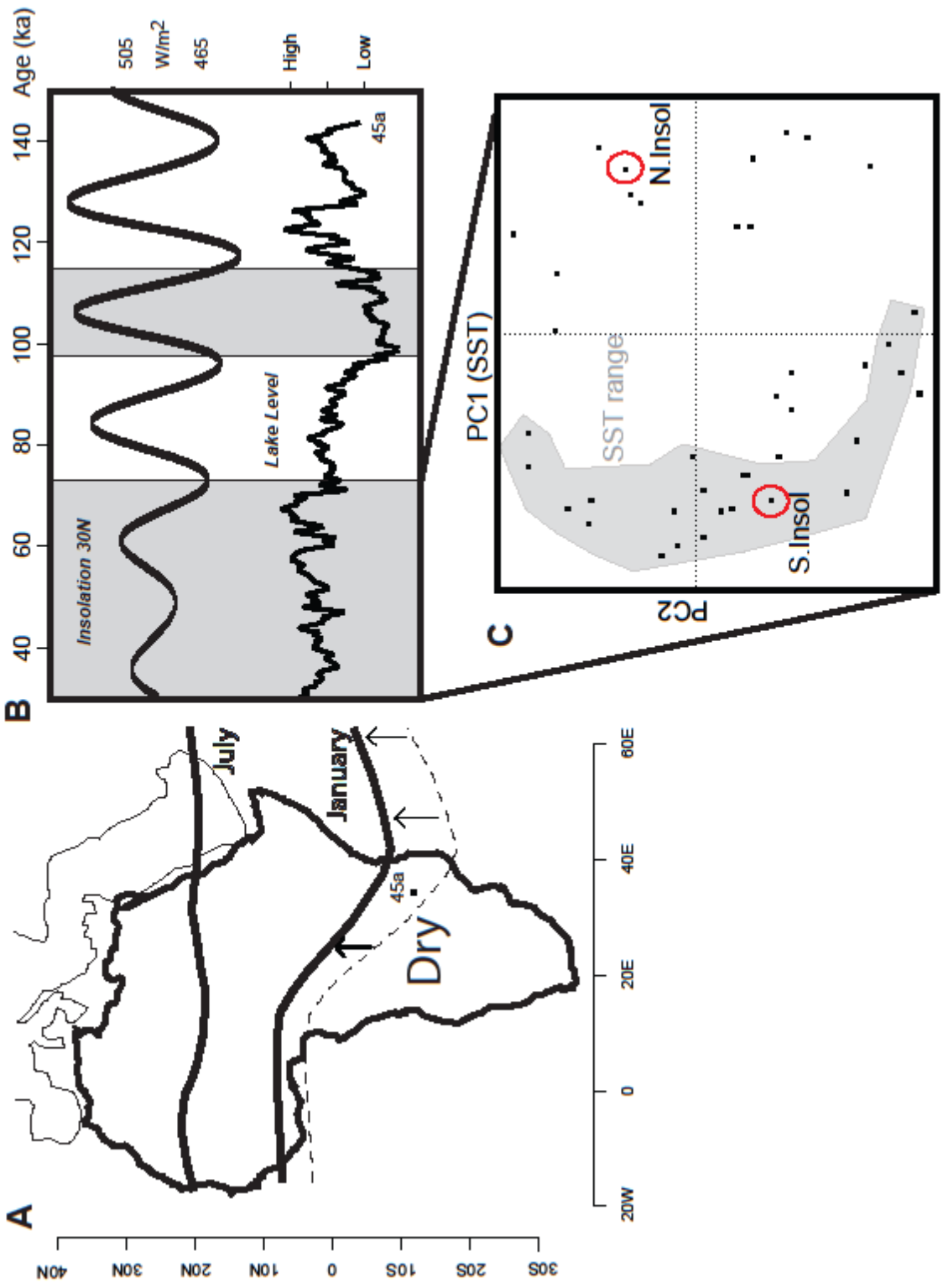
A
B
C
July
January
Dry
45a
20W
0
20E
40E
60E
30S
20S
10S
0
10N
20N
30N
40N
Age (ka)
40
60
80
100
120
140
505
W/m2
465
High
Low
Insolation 30N
Lake Level
45a
PC1 (SST)
PC2
SST range
N.Insol
S.Insol

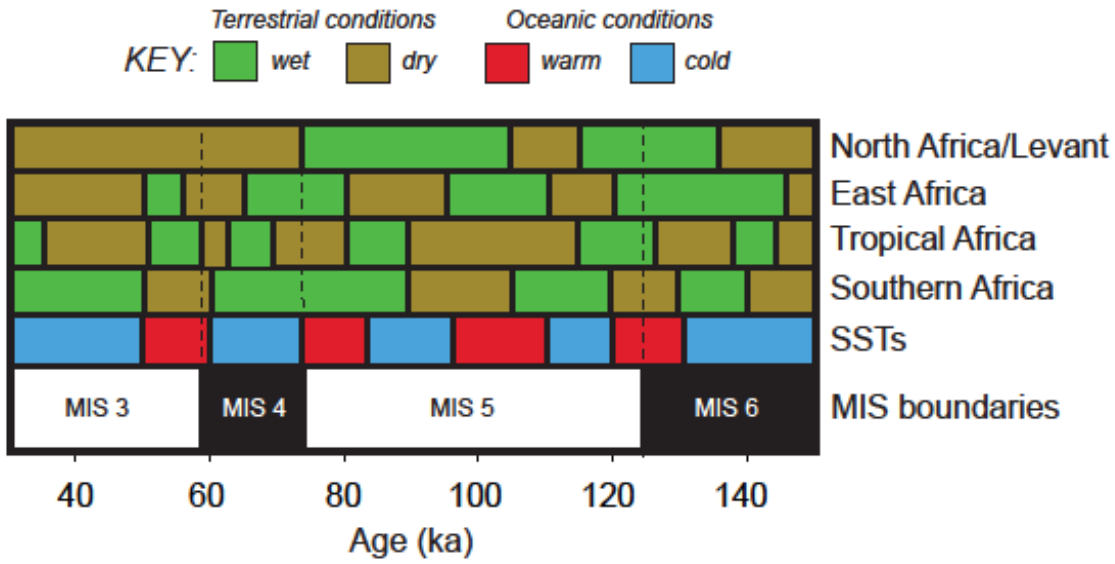

Figure A-14. Summary of the circum-Africa climate data from 150-30 ka including sea surface temperatures (SSTs) and each region from north to south on the continent. The terrestrial data across the continent do not vary in concert with the Marine Isotope Stages, whereas the SSTs appear to be following this more global signal.

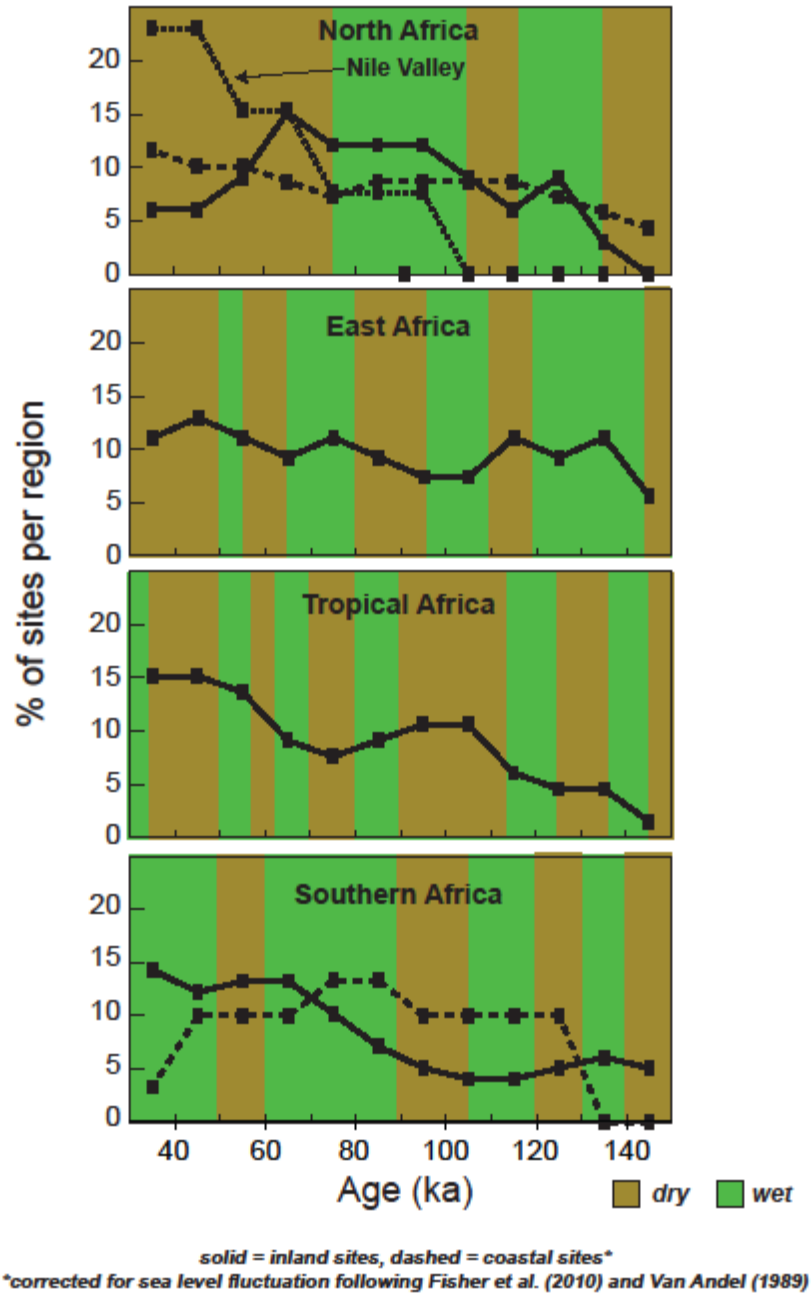

Figure A-15. Line graphs summarizing the relative density of archaeological sites in 10 kyr bins for the North, East, tropical, and southern African regions. Data from Table 2. Juxtaposed with the archaeological data are the regional climate histories for a first-order summary of climate-demography interaction from 150-30 ka. See text for further discussion.

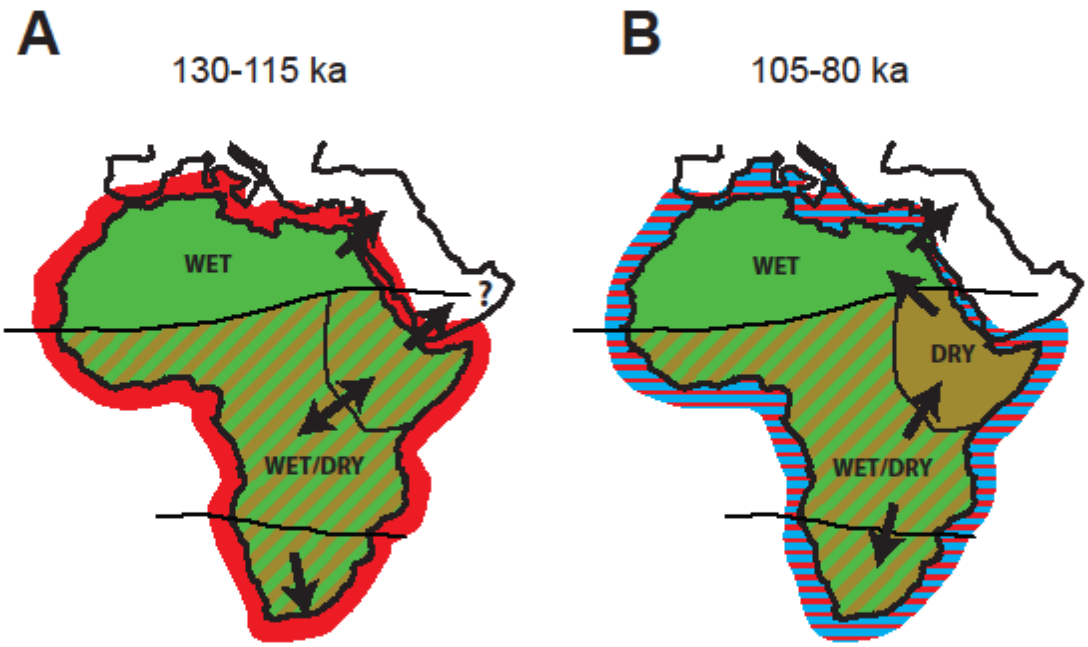

Figure A-16. Synthesis of variability in African terrestrial and oceanic conditions during A) 130-115 ka, and B) 105-80 ka (see Figure 14), with arrows indicating possible hominin population movements based on demographic changes among regions.

Supplemental Figure 1. Principal component (PC) analysis of all available continuous data over the 150-100 ka time interval. A) Ordination plot. Letter before site number indicates type of record: S - SST, T - Terrestrial Temperature, P - Precipitation. B) Spatial distribution of PC2 scores from terrestrial precipitation datasets. C) Spatial distribution of PC1 scores from circum-Africa SST datasets.

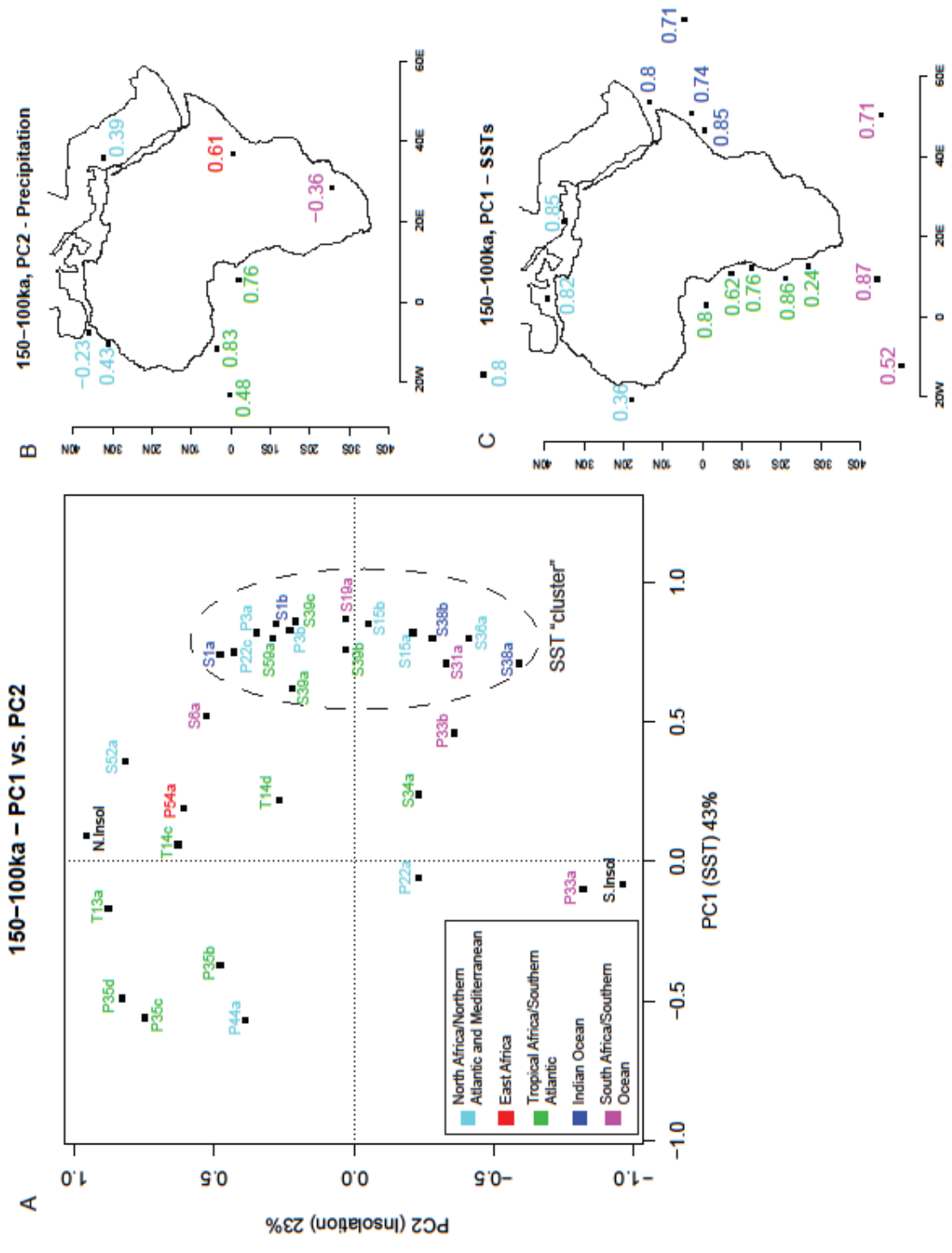
A
150–100ka – PC1 vs. PC2
PC2 (Insolation) 23%
PC1 (SST) 43%
SST "cluster"
N.Insol
S.Insol
North Africa/Northern Atlantic and Mediterranean
East Africa
Tropical Africa/Southern Atlantic
Indian Ocean
South Africa/Southern Ocean
B
150–100ka, PC2 - Precipitation
C
150–100ka, PC1 – SSTs

Labels	Authors	Lat	Long	Region	TerrSST	STP?
1a	Bard et al. 1997	3.18	50.43	Indian	SST	S
1b	Bard et al. 1997	0.02	46.03	Indian	SST	S
2a	Barker et al. 2003	-9.35	33.75	Tropical	Terr	
3a	Bar-Matthews et al. 2003	32.58	35.19	North	Terr	P
3b	Bar-Matthews et al. 2003	31.50	35.00	North	Terr	P
4a	Bar-Matthews et al. 2010	-34.21	22.09	South	Terr	
5a	Bateman et al. 2003	-27.00	22.00	South	Terr	
6a	Brathauer and Abelmann 1999	-49.01	-12.70	South	SST	S
7a	Brook et al. 1996	-19.00	18.00	South	Terr	
8a	Burrough et al. 2007	-20.00	22.50	South	Terr	
8b	Burrough et al. 2007	-20.02	21.35	South	Terr	
9a	Burrough et al. 2009	-19.99	25.21	South	Terr	
10a	Causse et al. 2003	33.00	9.00	North	Terr	
11a	Crombie et al. 1997	24.00	32.30	North	Terr	
12a	Dupont and Weinelt 1996	4.80	3.40	Tropical	Terr	T
13d	Dupont et al. 2000	-11.75	11.70	Tropical	Terr	T
13c	Dupont et al. 2000	-6.60	10.30	Tropical	Terr	T
13b	Dupont et al. 2000	-2.20	5.10	Tropical	Terr	T
13a	Dupont et al. 2000	3.75	-11.40	Tropical	Terr	T
14a	Emeis et al. 2003	38.99	4.02	North	SST	S
14b	Emeis et al. 2003	34.81	23.19	North	SST	S
15a	Fontes and Gasse 1991	26.00	7.00	North	Terr	
16a	Gaven et al. 1981	27.00	14.00	North	Terr	
17a	Hillaire-Marcel et al. 1986	-2.00	36.00	East	Terr	
18a	Hodell et al. 2003	-42.92	8.90	South	SST	S
19a	Holmgren et al. 1995	-23.70	26.00	South	Terr	
20a	Holzkamper et al. 2009	-24.10	29.88	South	Terr	
21c	Hooghiemstra et al. 1992	29.05	-12.10	North	Terr	P
21b	Hooghiemstra et al. 1992	30.00	-10.65	North	Terr	
21a	Hooghiemstra et al. 1992	34.90	-7.80	North	Terr	P
22a	Laskar et al. 2004	15.00	N/A		Insol	INSOL
22b	Laskar et al. 2004	-15.00	N/A		Insol	INSOL

Labels	Authors	Lat	Long	Region	TerrSST	STP?
23a	Leuschner and Sirocko 2000	17.50	61.50	Indian	SST	S
24a	Lezzine and Cassanova 1991	20.00	-2.00	North	Terr	
24e	Lezzine and Cassanova 1991	22.00	30.00	North	Terr	
24b	Lezzine and Cassanova 1991	24.00	-2.00	North	Terr	
24d	Lezzine and Cassanova 1991	24.00	12.00	North	Terr	
24c	Lezzine and Cassanova 1991	31.00	9.00	North	Terr	
25a	McGlue et al. 2008	-6.70	29.80	Tropical	Terr	
26a	McKenzie 1993	23.00	29.00	North	Terr	
27a	Moernot et al. 2010	-3.30	37.70	Tropical	Terr	
28a	Moeyersons et al. 2002	26.25	33.98	North	Terr	
29a	Morel et al. 1991	22.00	-4.00	North	Terr	
30a	Nuernberg and Groeneveld 2006	-43.96	49.93	South	SST	S
31a	Osmond and Dabous 2004	27.00	32.00	North	Terr	
32a	Partridge 1999, tuned	-25.60	28.08	South	Terr	P
32b	Partridge 1999, untuned	-25.60	28.08	South	Terr	P
33a	Pichevin et al. 2005	-25.81	12.13	Tropical	SST	S
34c	Pokras and Mix 1985	-2.28	5.18	Tropical	Terr	P
34b	Pokras and Mix 1985	-0.20	-23.15	Tropical	Terr	P
34d	Pokras and Mix 1985	3.05	-11.82	Tropical	Terr	P
34a	Pokras and Mix 1985	18.26	-21.10	North	Terr	P
35a	Raymo et al. 2004	55.00	-15.00	North	SST	S
36a	Rossignol-Strick 1985	33.42	25.00	North	Terr	
37a	Rostek et al. 1997	5.07	73.88	Indian	SST	S
37b	Rostek et al. 1997	13.70	53.25	Indian	SST	S
38c	Schneider et al. 1995	-6.58	10.32	Tropical	SST	S
38b	Schneider et al. 1995	6.50	-1.40	Tropical	SST	S
38a	Schneider et al. 1995	-6.00	29.60	Tropical	SST	S
39a	Scholz et al. 2007	-20.10	9.18	Tropical	Terr	
39b	Scholz et al. 2007	-11.76	11.68	Tropical	Terr	
40a	Schwarcz et al. 1993	22.90	28.75	North	Terr	
41a	Sicre et al. 2000	25.00	-16.00	North	SST	S
42a	Smith et al. 2007	25.00	31.00	North	Terr	

Labels	Authors	Lat	Long	Region	TerrSST	STP?
43a	Sorin et al. 2010	31.30	35.30	North	Terr	P
44a	Stokes et al. 1998	-19.20	26.65	Tropical	Terr	
45a	Stone et al. 2011	-11.30	34.45	Tropical	Terr	P
46a	Stuut and Lamy 2004	-20.00	9.26	South	Terr	P
47a	Szabo et al. 1995	22.00	29.00	North	Terr	
48a	Thomas and Shaw 2003	-25.00	25.35	South	Terr	
48b	Thomas and Shaw 2003	-18.80	18.40	Tropical	Terr	
49a	Thomas et al. 2009	-14.98	35.66	Tropical	Terr	
50a	Tierney et al. 2008	-6.70	29.83	Tropical	Terr	
51a	Tisserand et al. 2009	18.10	-21.15	North	SST	S
52a	Tjallingii et al. 2008	20.75	-18.57	North	Terr	
53a	Trauth et al. 2003	-0.90	36.33	East	Terr	P
54a	Vaks et al. 2007	31.60	35.10	North	Terr	
55a	Van Campo et al. 1982	14.40	50.50	Indian	SST	S
56a	Voight et al. 1990	10.50	49.90	East	Terr	
57a	Weldeab et al. 2007	2.50	9.40	Tropical	SST	S
58a	Wendorf et al. 1987	22.90	28.75	North	Terr	
59a	Wendorf et al. 1989	24.20	32.85	North	Terr	
60a	Woltering et al. 2010	-10.02	34.18	Tropical	Terr	
61b	Zhao et al. 1995	19.00	-20.17	North	SST	S
61a	Zhao et al. 1995	20.75	-18.58	North	SST	S

Table A-1. Climate sites used in the synthesis. Those used for the PCA analysis have S, T, or P under the heading "STP?" to designate the type of record: sea surface temperature (S), terrestrial temperature (T), or terrestrial precipitation (P).

Site	Name	Age Range	Region	Coast/Inland	Lat	Long	Reference
1	Ain Shakshuk	31-46	North	Inland	32.00	11.95	Barich et al., 2005
2	Bir Sahara East	70-110, 125-135	North	Inland	22.90	28.75	Wendorf et al., 1993
3	Bir Tarfawi	60-130	North	Inland	22.92	28.83	Wendorf et al., 1993
4	Dar-es-Soltan 1	31-145	North	Coast	33.97	-6.88	Barto et al., 2009
5	El Mnasra	<30-40	North	Coast	33.92	-6.95	Nespoulet et al., 2008
6	Grotte des Pigeons	20-113	North	Coast	34.81	-2.41	Bouzouggar et al., 2007
7	Ifri n'Ammar	38-183	North	Coast	34.78	-3.05	Richter et al., 2010
8	Jebel Irhoud	90-190	North	Coast	33.25	-5.50	Grün and Stringer, 1991; Smith et al., 2007
9	Kharga Oasis	89-126	North	Inland	25.30	30.47	Smith et al., 2007
10	Mugharet el 'Aliya	27-61	North	Coast	35.75	-5.93	Wrinn & Rink, 2003
11	Nazlet Khater 4	28-50	North	Nile Valley	26.78	31.38	Vermeersch, 2002
12	Nazlet Safaha	36-65	North	Nile Valley	26.1	32.57	Vermeersch, 2002
13	Oued Noun	25-53	North	Coast	29.10	-10.34	Weisrock et al., 2006
14	Ounjougou	25-69	North	Inland	14.4	-3.52	Robert et al., 2003; Rasse et al., 2004
15	Rhafas Cave	60-127	North	Coast	34.80	-1.88	Mercier et al., 2007
16	Sodmein Cave	25-137	North	Coast	26.24	33.97	Mercier et al., 1999; Moeyersons et al., 2002

Site	Name	Age Range	Region	Coast/Inland	Lat	Long	Reference
17	Taramsa 1	50-80	North	Nile Valley	26.10	32.70	Vermeersch et al, 1998
18	Uan Afuda	61-100	North	Inland	24.87	10.50	Cremaschi et al., 1998; Cremaschi and Di Lernia, 1999; Di Lernia, 1999
19	Uan Tabu	51-71	North	Inland	24.86	10.11	Cremaschi et al., 1998; Cremaschi and Di Lernia, 1999
20	Zouhrah a El Harhoura	26-45	North	Coast	33.92	-6.92	Debénath et al., 1986
21	Aduma	80-120	East	N/A	10.42	40.52	Yellen et al., 2005
22	Enkapune ya Muto	33-55	East	N/A	-0.83	36.15	Ambrose, 1998
23	Kapedo Tuffs	123-135	East	N/A	1.07	36.08	Tryon et al., 2008
24	Massawa/Abdur	118-136	East	N/A	15.15	39.42	Walter et al., 2000
25	Midhishi 2	40-90	East	N/A	10.95	47.37	Brandt and Gresham, 1989
26	Omo Kibish (BNS)	103-198	East	N/A	5.41	35.90	Shea, 2008
27	Porc Epic	33-79	East	N/A	9.63	41.87	Clark et al., 1984; Assefa, 2008
28	Sai Island	30-160	East	N/A	20.57	30.25	Van Peer et al., 2003
29	Shurmai Rockshelter	20-46	East	N/A	0.50	37.20	Kuehn and Dickson, 1999
30	Simbi	50-200	East	N/A	-0.35	35.00	McBrearty, 1992
31	Singa	131-135	East	N/A	13.17	33.95	McDermott et al., 1996
32	Wasiriya Beds	33-100	East	N/A	-0.42	34.17	Tryon et al., 2010
33	Birimi	24-51	Tropical	N/A	10.54	-0.38	Quickert et al., 2003

Site	Name	Age Range	Region	Coast/Inland	Lat	Long	Reference
34	Eyasi Beds	88-132	Tropical	N/A	-3.52	35.17	Dominguez-Rodrigo et al., 2008
35	Gi	33-65	Tropical	N/A	-19.62	21.02	Brooks et al., 1990
36	Katanda	60-120	Tropical	N/A	0.10	29.62	Brooks et al., 1995; Feathers & Migliorini, 2001
37	Matupi Cave	32-41	Tropical	N/A	1.50	36.00	Van Noten, 1977
38	Mumba	25-137	Tropical	N/A	-3.53	35.32	Mehlman, 1991
39	Mumbwa	32-46, 96-194	Tropical	N/A	-15.02	26.98	Barham, 2000
40	Nasera	23-57	Tropical	N/A	-2.74	35.36	Mehlman, 1991
41	Ngalue	42-105	Tropical	N/A	-12.85	35.18	Mercader et al., 2009
42	Njuinje	18-35	Tropical	N/A	5.25	9.73	Mercader and Marti, 2003
43	Olduvai Gorge Naisiusiu Beds	42-60	Tropical	N/A	-2.93	35.42	Manega, 1993; Skinner et al., 2003
44	Shum Laka[a]	13-37	Tropical	N/A	5.85	10.07	Cornelissen, 2002
45	Twin Rivers	11-102	Tropical	N/A	-15.52	28.18	Barham, 2000
46	White Paintings	31-105	Tropical	N/A	-18.77	21.75	Robbins et al., 2000; Donahue et al., 2004
47	Apollo 11	30-83	South	Inland	-27.75	17.10	Miller et al., 1999
48	Blind River	122-127	South	Coast	-33.02	27.9	Wang et al., 2008
49	Blombos	60-140	South	Coast	-34.42	21.22	Henshilwood et al., 2002; Jacobs et al., 2006; Tribolo et al., 2006

Site	Name	Age Range	Region	Coast/Inland	Lat	Long	Reference
50	Boomplaas	31-62	South	Inland	-33.38	22.18	Miller et al., 1999; Vogel, 2001
51	Border Cave	32-238	South	Inland	-27.02	31.99	Miller et al., 1999; Grun et al., 2003; Bird et al., 2003
52	Bundu Farm	129-370	South	Inland	-29.75	22.20	Kiberd, 2006
53	Die Kelders	50-80	South	Coast	-34.53	19.03	Feathers and Bush, 2000; Schwarcz and Rink, 2000
54	Diepkloof	46-75	South	Coast	-32.67	18.50	Tribolo et al., 2006; Jacobs et al., 2008a
55	Equus Cave	27-103	South	Inland	-27.62	24.63	Klein et al., 1991; Lee-Thorp and Beaumont, 1995
56	Florisbad	115-178	South	Inland	-28.77	16.07	Grun et al., 1996
57	Hofmeyr	33-39	South	Inland	-31.57	25.97	Grine et al., 2007
58	Klasies River	50-115	South	Coast	-34.10	24.40	Grun et al., 1990; Vogel, 2001; Feathers, 2002; Tribolo et al., 2005; Jacobs et al., 2008a
59	Klein Kliphuis	32-69	South	Inland	-32.07	18.51	Jacobs et al., 2008a
60	Lincoln Cave	118-298	South	Inland	-31.80	20.52	Reynolds et al., 2007
61	Melikane	33-82	South	Inland	-29.95	28.75	Vogel et al., 1986; Jacobs et al., 2008a
62	Ntloana Tsoana	55-73	South	Inland	-29.32	27.82	Jacobs et al., 2008a

Site	Name	Age Range	Region	Coast/Inland	Lat	Long	Reference
63	Pinnacle Point	30-40, 90-130, 160-170	South	Coast	-34.21	22.09	Marean et al., 2010
64	Pockenbank	30-50 ka	South	Inland	-27.22	16.52	Vogelsang, 1998
65	Rose Cottage Cave	20-91	South	Inland	-29.22	27.47	Valladas et al., 2005; Jacobs et al., 2008a; Pienaar et al., 2008
66	Sehonghong	30-60	South	Inland	-29.77	28.78	Jacobs et al., 2008a
67	Sibudu	37-79	South	Inland	-29.00	31.00	Jacobs et al., 2008a, 2008b
68	Umhlatuzana Cave	32-75	South	Inland	-29.48	30.45	Lombard et al., 2010
69	Witkrans	33-106	South	Inland	-27.62	24.63	Butzer et al., 1978; Vogel and Partridge, 1984
70	Wonderwerk Cave	70-220	South	Inland	-27.85	23.56	Vogel 2001; Beaumont and Vogel, 2006

Table A-2. Paleoanthropological sites used in the synthesis.

Proxy	Interpretation	Selected reference
Oceanographic Conditions		
Alkenones	Local SSTs: Uses the alkenone uncertainty index (Uk-37) devised by Prahl et al. 1988	Bard et al., 1997
Mg/Ca	Local SSTs: Measured on planktonic foraminifera after Lea et al. 1999	Weldeab et al., 2007
delta 18O	Global/Local SSTs: Measured on planktonic foraminifera after Wefer and Berger 1991	Van Campo et al., 1982
CaCO3	Indicator of increased primary production, often caused by local upwelling intensity	Leuschner and Sirocko, 2000
Continental precipitation variation		
Pollen	Arboreal pollen abundance increases with relative humidity	Hooghiemstra et al., 1992; Dupont et al. 2000
Groundwater carbonate	Groundwater carbonate abundance increases with relative humidity	Osmond and Dabous, 2004
Diatoms in offshore sites	Wind-borne diatom abundance increases with aridity-induced lake deflation	Pokras & Mix, 1985
Lake water level	Increases or decreases with changes in relative moisture availability; recorded seismically or by strandlines	Scholz et al. 2007; Burrough et al. 2009
Ostracodes	Species diagnostic of particular water conditions/depths	Cohen et al. 2007
Diatoms in continental lakes	Species diagnostic of particular water conditions/depths	Stone et al. 2011
Ratio (total aeolian dust/fluvial mud)	Yields a humidity index: Decreased ratio during times of increased humidity	Stuut and Lamy, 2004; Tjallingii et al. 2008
Dune growth	Active during period of aridity; stabilized with increased humidity	Stokes et al., 1998; Thomas and Shaw, 2003
delta 18O	Paleorainfall amounts and seasonality	Holmgren et al. 1995
delta D	Paleorainfall amounts and seasonality	Bar Matthews et al. 2010
Continental temperature variation		
TEX_{86}	records lake surface temperatures	Tierney et al. 2008

Table A-3. Climate proxies and their interpretations.

Site	PC1	PC2	STP	lat	long
S1a	-0.93	0.51	S	3.18	50.43
S1b	-1.05	0.34	S	0.02	46.03
P3b	-1.05	0.39	P	31.50	35.00
P3a	-0.86	0.65	P	32.58	35.19
S6a	-0.14	0.77	S	-49.01	-12.70
T13c	0.19	0.72	T	-6.60	10.30
T13d	0.02	0.59	T	-11.75	11.70
T12a	0.4	0.99	T	4.80	3.40
S14a	-0.83	0.05	S	38.99	4.02
S14b	-0.96	0.3	S	34.81	23.19
S18a	-0.97	0.31	S	-42.92	8.90
P21c	0.1	-0.29	P	34.90	-7.80
P22a	-0.04	1.26	P	15.00	68.00
P22b	0.02	-1.25	P	-15.00	68.00
S31a	-0.83	-0.01	S	-43.96	49.93
P33a	-0.45	-0.92	P	-25.60	28.08
P33b	-0.76	-0.6	P	-25.60	28.08
S34a	-0.51	-0.12	S	-25.81	12.13
P35b	0.73	0.67	P	-0.20	-23.15
P35a	0.01	-0.38	P	18.40	-21.10
P35c	0.27	0.67	P	-2.28	5.18
P35d	0.59	0.94	P	3.05	-11.82
S36a	-0.91	-0.14	S	55.00	-15.00
S38b	-0.79	0	S	13.70	53.25
S38a	-0.91	-0.47	S	5.07	73.88
S39a	-0.9	-0.03	S	-6.58	10.32
S39b	-1.04	-0.12	S	-11.76	11.68
S39c	-1.06	0.15	S	-20.10	9.18
S42a	-1.07	0.25	S	25.00	-16.00
P44a	0.66	0.16	P	31.30	35.30
P46a	0.67	0.1	P	-11.30	34.45
S59a	-0.84	0.6	S	-0.35	2.50

Table A-4. Principal components (PC) axes 1 and 2 values by site for the 140-30 ka interval. 32 datasets included.

Site	PC1	PC2	STP	Lat	Long
S1a	-0.79	-0.43	S	3.18	50.43
S1b	-0.91	-0.38	S	0.02	46.03
P3b	-0.87	-0.44	P	31.50	35.00
P3a	-0.73	-0.71	P	32.58	35.19
S6a	0.21	0.07	S	-49.01	-12.70
T13c	0.51	-0.62	T	-6.60	10.30
T13d	0.66	-0.09	T	-11.75	11.70
T12a	0.58	-0.72	T	4.80	3.40
T13b	0.75	-0.6	T	-2.20	5.10
T13a	0.29	0.88	T	3.75	-11.40
S14a	-0.71	0.16	S	38.99	4.02
S14b	-0.77	-0.35	S	34.81	23.19
S18a	-0.83	-0.18	S	-42.92	8.90
P21c	0.11	-0.01	P	34.90	-7.80
P22a	0.13	-1.17	P	15.00	68.00
P22b	-0.15	1.16	P	-15.00	68.00
S23a	0.21	0.26	S	17.50	61.50
S31a	-0.7	-0.05	S	-43.96	49.93
P33a	-0.6	0.72	P	-25.60	28.08
P33b	-0.6	0.67	P	-25.60	28.08
S34a	-0.32	-0.06	S	-25.81	12.13
P35b	0.65	-0.73	P	-0.20	-23.15
P35a	0.27	0.75	P	18.40	-21.10
P35c	0.28	-0.58	P	-2.28	5.18
P35d	0.65	-0.68	P	3.05	-11.82
S36a	-0.88	0.22	S	55.00	-15.00
S38b	-0.68	-0.21	S	13.70	53.25
S38a	-0.84	0.1	S	5.07	73.88
S39a	-0.78	0.000	S	-6.58	10.32
S39b	-0.98	0.010	S	-11.76	11.68
S39c	-0.91	-0.170	S	-20.10	9.18
S42a	-0.93	-0.3	S	25.00	-16.00
P44a	0.65	0.10	P	31.30	35.30
P46a	0.79	0.21	P	-11.30	34.45
P47a	0.44	-0.6	P	-20.00	9.26
P53a	-0.73	-0.24	P	20.75	-18.57
S57a	-0.85	-0.4	S	14.40	50.50
S59a	-0.69	-0.42	S	-0.35	2.50

Table A-5. Principal components (PC) axes 1 and 2 values by site for the 115-30 ka interval. 38 datasets included.

Site	PC1	PC2	STP	Lat	Long
S1a	-0.6	-0.03	S	3.18	50.43
S1b	-0.68	0.08	S	0.02	46.03
P3b	-0.81	0.07	P	31.50	35.00
P3a	-0.64	0.4	P	32.58	35.19
S6a	0.08	-0.84	S	-49.01	-12.70
T13c	-0.12	-0.65	T	-6.60	10.30
T13d	0.71	0.37	T	-11.75	11.70
T12a	0.67	-0.22	T	4.80	3.40
T13b	0.41	-0.21	T	-2.20	5.10
T13a	-0.24	-0.31	T	3.75	-11.40
S14a	-0.54	-0.2	S	38.99	4.02
S14b	-0.67	-0.14	S	34.81	23.19
S18a	-0.47	0.01	S	-42.92	8.90
P21c	0.01	0.54	P	34.90	-7.80
P22a	0.63	0.27	P	15.00	68.00
P22b	-0.64	-0.29	P	-15.00	68.00
S23a	-0.04	-0.74	S	17.50	61.50
S31a	-0.15	-0.79	S	-43.96	49.93
P33a	-0.15	-0.37	P	-25.60	28.08
P33b	-0.29	-0.37	P	-25.60	28.08
S34a	0.77	-0.35	S	-25.81	12.13
P35b	-0.23	-0.86	P	-0.20	-23.15
P35a	0.64	-0.67	P	18.40	-21.10
P35c	0.75	-0.43	P	-2.28	5.18
P35d	0.53	0.25	P	3.05	-11.82
S36a	-0.78	-0.03	S	55.00	-15.00
S38b	0.23	0.53	S	13.70	53.25
S38a	-0.51	0.64	S	5.07	73.88
S39a	-0.38	0.64	S	-6.58	10.32
S39b	-0.73	0.41	S	-11.76	11.68
S39c	-0.67	0.49	S	-20.10	9.18
S42a	-0.85	0.13	S	25.00	-16.00
P44a	0.41	-0.16	P	31.30	35.30
P46a	0.5	0.21	P	-11.30	34.45
P47a	0.38	0.7	P	-20.00	9.26
P53a	-0.41	-0.62	P	20.75	-18.57
S57a	-0.54	-0.18	S	14.40	50.50

Site	PC1	PC2	STP	Lat	Long
S59a	-0.68	-0.1	S	-0.35	2.50
S63a	-0.47	-0.32	S	19.00	-20.17
S63b	-0.61	-0.58	S	20.75	-18.58

Table A-6. Principal components (PC) axes 1 and 2 values by site for the 75-30 ka interval. 40 datasets included.

Site	PC1	PC2	STP	Lat	Long
S1a	0.74	0.48	S	3.18	50.43
1b	0.85	0.28	S	0.02	46.03
P3b	0.83	0.23	P	31.50	35.00
P3a	0.82	0.35	P	32.58	35.19
S6a	0.52	0.53	S	-49.01	-12.70
T13c	0.06	0.63	T	-6.60	10.30
T13d	0.22	0.27	T	-11.70	11.70
T12a	-0.17	0.88	T	4.800	3.400
S14a	0.82	-0.21	S	38.99	4.02
S14b	0.85	-0.05	S	34.81	23.19
S18a	0.87	0.03	S	-42.92	8.90
P21a	-0.06	-0.23	P	34.90	-7.80
P21c	0.75	0.43	P	30.00	-10.65
P22a	0.09	0.96	P	15.00	68.00
P22b	-0.08	-0.96	P	-15.00	68.00
S31a	0.71	-0.33	S	-43.96	49.93
P33a	-0.1	-0.82	P	-25.60	28.08
P33b	0.46	-0.36	P	-25.60	28.00
S34a	0.24	-0.23	S	-25.8	12.1
P35b	-0.37	0.48	P	-0.20	-23.15
P35c	-0.56	0.76	P	-2.28	5.180
P35d	-0.49	0.83	P	3.05	-11.82
S36a	0.8	-0.41	S	55.00	-15.00
S38b	0.8	-0.28	S	13.7	53.3
S38a	0.71	-0.59	S	5.1	73.9
S39a	0.62	0.22	S	-6.58	10.32
S39b	0.76	0.03	S	-11.76	11.68
S39c	0.86	0.21	S	-20.10	9.18
P44a	-0.57	0.39	P	31.30	35.30
S52a	0.36	0.82	S	18.10	-21.15
P54a	0.19	0.61	P	-0.90	36.33
S59a	0.8	0.29	S	-0.35	2.5

Table A-S1. Principal components (PC) axes 1 and 2 values by site for the 150-100 ka interval. 32 datasets included.

150-100ka	Eigenvalues	% explained	140-30ka	Eigenvalues	% explained	115-30ka	Eigenvalues	% explained	75-30ka	Eigenvalues	% explained
PC1	*13.88*	*43*	***PC1***	*13.59*	*42*	***PC1***	*16.69*	*44*	***PC1***	*15.34*	*38*
PC2	*7.31*	*23*	***PC2***	*5.19*	*16*	***PC2***	*5.75*	*15*	**PC2**	7.27	18
PC3	3.16	10	**PC3**	2.92	9	**PC3**	3.25	9	**PC3**	4.76	12
PC4	2.89	9	**PC4**	2.37	7	**PC4**	2.82	7	**PC4**	3.63	9
PC5	1.98	6	**PC5**	1.53	5	**PC5**	2.23	6	**PC5**	3.2	8
PC6	1.06	3	**PC6**	1.29	4	**PC6**	1.87	5	**PC6**	1.85	5
PC7	0.71	2	**PC7**	1.02	3	**PC7**	1.39	4	**PC7**	1.58	4
PC8	0.6	2	**PC8**	0.86	3	**PC8**	0.82	2	**PC8**	1.33	3
PC9	0.29	1	**PC9**	0.76	2	**PC9**	0.67	2	**PC9**	1.03	3
PC10	0.12	0	**PC10**	0.64	2	**PC10**	0.58	2			
			PC11	0.49	2	**PC11**	0.47	1			
			PC12	0.31	1	**PC12**	0.4	1			
			PC13	0.24	1	**PC13**	0.35	1			
			PC14	0.18	1	**PC14**	0.29	1			
			PC15	0.15	0	**PC15**	0.21	1			
			PC16	0.13	0	**PC16**	0.12	0			
			PC17	0.12	0	**PC17**	0.09	0			
			PC18	0.08	0						

Table A-S2. Principal components (PC) eigenvalues and the percent of variability explained by each PC axis, according to time interval. Significant PC axes are italicized.

APPENDIX B: MODERN DISTRIBUTION OF OSTRACODES IN THE SOUTHWEST ARM OF LAKE MALAWI

To be submitted to the professional journal: *Hydrobiologia*

APPENDIX B: MODERN DISTRIBUTION OF OSTRACODES IN THE SOUTHWEST ARM OF LAKE MALAWI: IMPLICATIONS FOR PALEOCOLOGICAL STUDIES

Margaret Whiting Blome, Andrew Cohen, Matthew J. Lopez

Abstract

This modern distribution study from the southwest arm of Lake Malawi quantitatively relates variables of the lake environment (e.g. bottom water temperature, dissolved oxygen content, substrate grain size, organic and inorganic carbon content) to surficial ostracode assemblages and other taxa from 102 sites, across a gradient of environmental littoral to shallow profundal conditions. Site locations varied by depth (1-60m) and adjacent shoreline environment. The goal of this research is to use the resultant relationships to help quantify paleoecological interpretations of the fossil record from drill cores. Thirty-three ostracode species are identified from 54 sites including four new, previously un-described species of Cypridopsinae (2) and *Limnocythere* (2). Ostracodes are extremely abundant between 1 and 25 meters water depth, in all three sub-environments, but are rare to absent between 30 and 60 meters. This disappearance in deeper water is presumed to be taphonomic, with steadily decreasing alkalinity beginning at 25 meters causing shell carbonate dissolution in the death assemblage, because abundant live ostracodes have been found in other parts of the lake at greater than 30 meters depth. A detrended correspondence analysis (DCA) of ostracode species abundance at each site suggests that assemblages are more similar by depth than by sub-

environment. This implies that ostracode species niches are determined by ecological factors with specific depth boundaries such as bottom water temperature and dissolved oxygen content.

Introduction

A modern distribution study quantitatively relates variables of the lake environment (e.g. water chemistry, physical limnology) to the taxa present at a variety of sites, over a wide gradient of environmental conditions (Fritz, 1996; Gasse et al. 1995). This type of study determines the range of ecological tolerance of individual taxa based on where they are found at present, and then applies the range determined from modern relationships to fossil assemblage data to interpret paleo-lake conditions. Early approaches to these studies were valuable and informative but only semi-quantitative. This study focuses on the modern distribution of ostracodes specifically within the nearshore (1-60m) environment of Lake Malawi, to identify the relationship between species and the ecological range of their habitat. The relationships between ostracodes and quantifiable variables not observable in sediment cores (e.g. water chemistry, depth), as well as to variables of physical limnology that are measurable in a sediment core (e.g. grain size, organic and inorganic carbon content), will inform future interpretations of the paleoenvironment of Lake Malawi (e.g. Appendix C – this dissertation).

Paleoecological reconstruction from lacustrine fossils is not a new technique. It is a well-tested method that has been used for many years with a variety of indicators.

However, it has not yet been quantitatively applied to ostracodes from Lake Malawi. Researchers have long made inferences about lake paleoecology using an understanding of the relationship between species assemblages and modern environmental conditions (e.g. Fritz, 1996). In addition, a number of these relationships have been used successfully to quantify paleoenvironmental change (e.g. pollen, Vincens et al., 2005; diatoms, Gasse et al., 1995). The usefulness of ostracodes as paleoecological indicators has long been understood (Delorme, 1969). As a result, ostracodes have been used across the globe in quantitative paleoclimatic reconstructions from China (e.g. Mischke et al., 2002) to Europe (e.g. Horne, 2007), and the United States (e.g. Smith, 1993).

Ostracodes are small, bivalved crustaceans with shells of low-magnesium calcite, typically 0.5-3mm long. While the soft inner tissue is not often preserved in the sedimentary record, the outer calcite carapace preserves well in most alkaline environments (pH >7.5) (Holmes, 1992, Cohen, 2003). The shape or size of the valve, the presence or absence of nodes, pores and/or reticulations on the outer surface, and internal valve characteristics readily distinguish the species commonly found in East Africa, and in Lake Malawi in particular (e.g. Martens, 2002; 2003). The environment in which an ostracode lives is determined by the ecological interactions it experiences within a water body and the geology, hydrology and climate of the watershed (Delorme 1969). Ostracode assemblages often reflect lake water chemistry variations with strong correlations to total conductivity and alkalinity (Cohen et al., 1983) and solute composition and concentration (Delorme, 1969, Mezquita et al. 2005). Additionally, lake level histories and water depth can be inferred based on modern analogues and ecological

tolerances (e.g. Mischke et al., 2002; Horne, 2007). The known relationships between ostracodes and their environment increase with each new study, however it is important to remember that these associations are strictly demonstrating a *correlation* and not *causation* between the two groups of data (Fritz 1996).

Lake Malawi, situated between 9-14°S, is the southern-most lake in the East African Rift System (EARS) (Figure B-1 – inset map). It is a large (29,500 km^2), deep (706 m), permanently stratified (meromictic), lake filling the Malawi Rift basin of the EARS. Within the lake, there is both a thermal and chemical stratification throughout much of the year (Patterson and Kachinjika, 1995), however, the lake is located far enough south to have seasonal variations in temperature, wind and precipitation (Eccles, 1974). These variations are caused by the migration of the Intertropical Convergence Zone (ITCZ). The ITCZ is a narrow band of atmospheric convergence and monsoonal precipitation that migrates across the tropics following the location of maximum insolation intensity throughout the year. During the cool, windy season at Lake Malawi (May-August) the ITCZ is sufficiently north of the lake to enhance the SE trade winds at the lake. Sample collection for this study occurred in mid-March specifically to avoid the windy season and capture the variation in lake water chemistry with depth while the lake is stratified. Had these measures been taken later in the year when the surface waters were well mixed, there would have been no chemical gradient with depth (e.g. Patterson and Kachinjika, 1995: figures 1.18, 1.29).

There are a few limitations to be aware of when conducting a modern distribution study within a single lake basin. First, there is very limited water chemistry variance

within the modern lake (Halfman, 1993; Patterson and Kachjinka, 1995). Second, the range of conditions in the modern lake at variable depths only bear a partial relationship to a similar depth range under much lower lake stands and more saline/alkaline lake waters. Third, the environmental gradient lengths are short, and fourth, most of the taxa of modern Lake Malawi are endemics (Martens, 2002), which limits our ability to draw comparative conclusions about the lake under past conditions. A modern distribution study using only the one lake may not be ideal, however, since a number of the ostracode species in the paleo-lake were also endemic (Park and Cohen, 2011; Appendix C, this dissertation), a training set approach using multiple modern lakes would produce no modern analogue for ostracode species assemblages. The environmental variables chosen for this study are ones we hope to be able to reconstruct in the earlier lake conditions.

Methods

Water chemistry and ostracode sample collection

Prior to the March 2010 field season, we acquired detailed bathymetric maps of the Cape MacLear region at the southern end of Lake Malawi from the Department of Surveys – Hydrographic Unit in Malawi (Malawi Government, 2003). Using these maps and Google Earth images of the shoreline, we laid out the locations of numerous depth transects (perpendicular to isobaths). Transects were labeled A-G with A south of Malembo, and G north of Chembe Village (Figure B-1). Transect starting locations were chosen for different types of shoreline environments (Figure B-2): high relief with coarse sandy beach, low relief near river inflow, and low relief near a marshy environment.

Surface sediment samples were collected every 5 meters depth along each transect beginning at the shore (1m, 5m, 10m, 15m, …, 60m) for the northern-most transects (F,G). Transects A-E were sampled at 5-meter intervals from 1-30m and at 1-meter intervals between 30 and 60m due to time constraints in the field. Additional "in-fill" sampling at shallower depths along isobaths (parallel to shore) most commonly occurred at depths of 5 and 20 meters and are labeled with a "Z", followed by the letter of the transect nearest to the site, and then the depth at which the offshoot transect occurred (Table 1). For example, Transect ZA50 occurs near Transect A along the 50m isobath. Samples from Transects A4 and A5 were collected by hand via SCUBA.

At each site, depth was confirmed using a handheld depth finder, and surface pH and water temperature were measured using a Hach pH-meter over the side of the boat. Additionally, at all sites in depths up to 25m, bottom temperature and dissolved oxygen (DO) content were measured using a YSI-83 multi-meter (limited to 25m by the length of the probe cord) (Table 3). Previous research has shown specific conductivity and major ion composition in the upper 25 meters of the modern lake to be relatively invariant (Patterson and Kachinjika, 1995; Halfman, 1993). For this reason we chose not to measure major ion concentrations, and only measured conductivity at a handful of sites (four) to compare to previously reported measurements (Table 3). In addition to temperature, DO, and conductivity measurements, surface sediment samples were collected at each location using a PONAR grab sampler (see Strayer, 2010: fig.5b for example). Arms attached to the grab sampler limited its penetration into the sediment to approximately two centimeters. There were 20 sites where no sample was collected for a

variety of reasons, most commonly due to repeated improper closure of the PONAR sampler. These sites are not included in Table 1. In addition, sites 58-77 were rock surface scrapings taken by SCUBA sampling which yielded insufficient sediment for this study, and are therefore also not included in Table 1. The total number of sites presented in this study is 102, with a relatively even spread over the different shoreline environments and across the depths of interest (Table 2).

Sample preparation: Wet-sieving, grain size laser diffraction, and loss-on-ignition (LOI)

16-20g wet sediment from each sample was split into two aliquots of 12-16g and 4g. The 12-16g split was passed through two wire-mesh sieves, the first with a mesh size of 2mm, the second with a mesh size of 63 μm, yielding sediment splits of >2mm (gravel), 2mm-63μm (sand) and <63μm (silt and clay). The two larger fractions were dried at low temperatures and weighed to determine the percent of each grain size within a sample. The smallest grain size fraction was further prepared by mixing the sediment with 10mL sodium hexametaphosphate (25g/500mL DI water) to ensure complete disaggregation of particles prior to grain size distribution analysis by laser diffraction. This last analysis was used to obtain the fraction of silt and clay-sized particles in each sample.

The 4g aliquot was subjected to sequential heating to estimate the water, organic and inorganic carbon content of the sample (Dean, 1974; Heiri et al., 2001). The samples were first heated for 24-48 hours at 60°C, then weighed to get a dry weight (DW_{60}) and to estimate water content. This was followed by 4 hour burn at 550°C to combust the organic matter in the sample (DW_{550}), followed by a short, high temperature burn at

1000°C for 2 hours of the residual ash to evolve carbon dioxide from the inorganic carbonate in the sample (DW_{1000}). The following calculations were used to determine (1) percent water content to estimate initial dry weight of the sediment, (2) LOI_{550}, which represents the percent weight loss due to combustion of organic matter, and (3) LOI_{1000}, the percent weight loss due to combustion of inorganic carbonate (Heiri et al. 2001).

$$\% \text{ water} = 1-((\text{Initial wet sediment weight})/DW_{60}) \quad (1)$$

$$LOI_{550} = ((DW_{60} - DW_{550})/DW_{60})*100 \quad (2)$$

$$LOI_{1000} = ((DW_{550} - DW_{1000})/DW_{60})*100 \quad (3)$$

Wet-sieved sand-sized residue analysis

Wet-sieved residues were counted for total number of ostracodes per sample, up to ~300 valves, although only 5 of the 102 samples contained >300 valves. All other samples found to contain ostracodes were counted in their entirety. Noted in each sample was the species and taphonomic condition (% broken, whole carapace, adult) of each valve using an Olympus SZH binocular microscope. Ostracode identification followed Martens (2003, 2002, 1988, 1986), Park and Cohen (2011), Rosetti and Martens (1998), Kempf (1980), Howe (1955), Van Harten (1979), Neale (1979), Howe (1955), Klie (1944), Sars (1924, 1910). Additionally, the wet-sieved residues were counted for absolute abundance of other common fossil remains in this same size range including: charred particles, fish (comprising bones, teeth, and scales), mollusc fragments, and the relative abundance of algae (*Botryococcus*) measured as a percentage of sample material. As each sample contained a different mass of sediment analyzed for a number of reasons

from sampling to analysis, each sample was weighed prior to analysis and the "weight picked" was recorded. In this way, taxa abundance can be compared across samples by their density (number/grams dry sediment) (e.g. Cohen et al. 2007). Fossil identifications were confirmed using a Hitachi 3400N SEM and compared to previously described modern material from four other locations in Lake Malawi (Martens 2002).

Stable Isotope Analysis

Stable isotope ratios of oxygen ($^{18}O/^{16}O$) and carbon ($^{13}C/^{12}C$) were measured, and are presented in delta notation ($\delta^{18}O$ and $\delta^{13}C$), the relative deviation of the isotopic ratio of the sample from that of a carbonate standard, PeeDee Formation belemnite (VPDB) (Lister, 1988). Three samples from each sub-environment (and multiple depths) were chosen for isotopic analysis to determine if stable isotopic values differed. Gastropods were used due to their large size and thick shells to ensure sufficient carbonate for analysis. Two specimens per sample were analyzed where available yielding a total n=4, n=6, and n=5 for sand, marsh, and river environments, respectively. In three cases the individuals were so large that they were fragmented and analyzed in parts (samples 35G2, 107G1, and 107G2). In these instances, their results were averaged to make them equivalent to the remaining samples analyzed as whole shells (their shell variability was averaged during the analysis). $\delta^{18}O$ and $\delta^{13}C$ of the carbonates were measured using an automated carbonate preparation device (KIEL-III) coupled to a gas-ratio mass spectrometer (Finnigan MAT 252). Powdered samples were reacted with dehydrated phosphoric acid under vacuum at 70°C. The isotope ratio measurement is

calibrated based on repeated measurements of NBS-19 and NBS-18 and precision is ± 0.10 ‰ for $\delta^{18}O$ and ±0.10‰ for $\delta^{13}C$ (1 sigma).

Detrended Correspondence Analysis (DCA)

We used detrended correspondence analysis (DCA) to better understand the spatial variability of the ostracode assemblages across different depths and environment types. This method of indirect ordination finds the theoretical variable that maximizes the separation of species with unimodal distributions along an environmental gradient while also down-weighting rare species (ter Braak and Prentice, 1988). Therefore, assuming the biological assemblages are controlled by the environment, sites that cluster in ordination space will have similar species composition and come from a similar environment, and vice versa. The significance of the multivariate axes will be examined first by looking at the depths and environments of the sites that cluster to make first order inferences about which variable is more responsible for the observed species distribution. The following constraints were applied to maintain a high level of robustness in our analysis: 1) sites needed to have greater than 5 total ostracodes to be included and 2) species had to be present in more than one site to be included. Following these criteria, five sites (#s 4, 8, 17, 22, and 30) and three species (*Cypridopsine sp.A, Limnocythere s.l. sp.8,* and *Limnocythere sp.B n.sp.*) were removed from analysis. Ostracode percent data were arc-sine transformed prior to analysis to normalize the distribution of the data, and DCA of 30 species and 51 samples was performed using the "*vegan*" package and the program R ©, version 2.12.0 (Jari Oksanan et al. 2011; R Core Development Team, 2010).

Rarefaction Analysis – cross sample comparison of species richness

In order to compare numbers of species/site across samples with differing total ostracode abundances, species richness was standardized to 25 individuals using the computer program "psimpoll" (Bennett, 2007) with an algorithm based on the theory presented by Birks and Line (1992). This was done to account for rarefaction: as abundance increases, so does the likelihood of finding more species in a given sample. All samples with fewer than 25 individuals were excluded from this analysis, yielding a total of 35 sites with a combined 33 species. Twenty-five individuals were chosen as the nearest round number that exceeded the highest number of total species found at any given site (21), allowing the inclusion of as many sites as possible in the analysis.

Results

Limnologic Data

At each site between 1m and 25m water depth the following bottom water temperature (°C) and dissolved oxygen (DO, %) measurements were made in the field. The measured values can be found in Table 3. Bottom temperatures ranged from a maximum of 31°C in the shallowest depths, to a minimum of 24.1°C at 25m depth. Temperatures decreased by an average of at least 1°C every 5 meters, regardless of shoreline environment type (Figure B-3a). Unlike bottom water temperature, DO content in the offshore river environment decreases at a much faster rate than in the other two environments (Figure B-3b). There is also an overall greater variability in DO with

depth. Maximum DO was measured at 5m and the minimum at 25m depth (147% and 21%, respectively).

Grain size distribution

Sample grain sizes were separated into greater than sand, sand, silt, and clay-sized particles with diameters of >2mm, 2mm-63μm, 63-4μm, and <4μm, respectively. The weight percent of each size fraction can be found in Table 3. The largest proportion in most samples was sand-sized or greater, and for this reason we focus on detailed differences in the percentages of the smaller size-fraction of silt and clay in the samples (Figures 4a,b). There is a significantly different distribution of grain size with depth for offshore river sediments than the other two environments. The percentages of both silt and clay increase significantly beginning at ~20m depth and persisting at values higher than the other environments until 50m depth. This can be clearly seen spatially in Figure B-4c, where the transect extending directly offshore from the river inlet has significantly high silt/clay percentages, to the exclusion of larger grain sizes. Between 1m and 15m depth the grain size distribution of all three offshore environment types are similarly scattered across a range from 0-~28% silt and 0-5% clay. In deeper depths there is more variation as offshore sandy-beach sites consistently have less of a fine-grained component than the offshore marsh or river sites from 30-60m.

Weight Percent LOI at 550 °C and 1000 °C

The weight percent lost on ignition (WT%LOI) at 550 °C and 1000 °C (Table 3) is proportional to the organic and inorganic carbon content of the sediments, respectively

(Dean, 1974), and will be referred to as such from here onwards. The organic carbon (OC) content of the sediment at each site shows no discernible pattern of variation by environment type or depth (Figure B-5a), although those sites in the sandy beach category show the greatest variability ranging from 5-29% at 5m to 2-49% at 60m depth. The variance in OC content decreases with increasing depth until ~35m, at which point variance begins to increase again, in almost a "v"-shaped pattern. The increased variance in shallower and deeper depths may reflect increased macrophyte plant debris in the former, and increased algal remains (e.g. *Botryococcus*) in the latter. Inorganic carbon content decreases steadily from a maximum of 24% at 1m water depth to values between 0-2% from 25-60m depth (Figure B-5b), suggesting an increased dissolution of carbonate in deeper water. Noticeable outliers to this trend are two offshore sandy beach sites at 30m and 50m depth with values of 5.9% and 3.5%, respectively. Interestingly these sites were two of the deepest to preserve any (1-3) ostracode valves. There is no particular trend by environment type in this variable.

Stable isotope analysis:

Gastropod shell carbonate from nine samples were analyzed for their stable oxygen and carbon isotope content (Table 4). Two individuals were analyzed for each sample where available, and replicates from the same individual were averaged yielding 15 total data points. The values of $\delta^{18}O$ are remarkably similar for all samples, varying by less than 1.5‰ and ranging from 0.17-1.59‰ (Figure B-6a). These tightly clustered values show no variation by environment or depth, rather the single sample from offshore sandy beach at 60m (0.63‰) is close to the average value for all samples (0.76‰).

Additionally, likely water $\delta^{18}O$ was calculated for each sample using the fractionation at 25°C of Grossman and Ku (1986) as modified by Dettman et al. (1999) for mollusc aragonite (Table 4). Previous studies have shown that no additional biological fractionation is likely in molluscan shell carbonate (Dettman et al., 2005). The average calculated $\delta^{18}O$ value of the water was 1.67‰ with a range from 1.12-2.54‰ (Table 4). The stable carbon isotopic values of the mollusc shells have wider range of values than the oxygen isotopes (-2.53-0.2‰) and offshore marsh values are the most variable, followed by offshore river and sandy beach samples (Figure B-6b). Samples from the sandy beach environment tend to become more enriched in ^{13}C with depth, whereas those offshore of the river inlet were slightly more depleted on average.

Coarse residue counts: Total abundances of biological indicators (charred particles, ostracodes, fish, molluscs and Botryococcus)

These data are presented in terms of abundance per gram of dry sediment to provide a density of each of these taxa per sample and allow their abundances to be comparable across all samples taken (Table 3). Sites offshore from the river inlet typically have orders of magnitude greater charred particle abundance than the other two sites between 1-30m water depth (Figure B-4a). Additionally the highest proportion of sites containing any charred particles (regardless of abundance) are from the offshore river group at most depths (exceptions are 1m, 25-35m and 50m). At 30m the abundance of charred particles at the offshore marsh sites increases rapidly through 50-60m. Offshore high relief, sandy beach sites have the lowest overall charred particle abundance

across all depths, although within that subgroup, there are a greater number of sites with charred particles present in the shallowest 10m than in deeper waters.

Total abundances of ostracode valves, fish bones, molluscs and *Botryococcus* colonies are shown by depth in Table 3 and Figure B-8. Data are plotted on a logarithmic scale for the absolute abundances as they differ from site to site and by taxa by orders of magnitude, and by relative abundance (percent) of *Botryococcus*. There is a marked difference in taxa abundance beginning between 20 and 25m. Above those depths ostracodes, molluscs and to a lesser extent, fish are all quite abundant, with ostracodes being the most abundant taxa at each shallow depth. At 25m, both ostracode frequency of occurrence and total abundance decrease precipitously. From 30-50m ostracodes are found at only 4 sites, and never in densities greater than 3 valves/gram sediment. Below 30m fish bones become much more abundant. *Botryococcus* does not occur above 20m, and gradually increases in relative abundance until 50-60m where its abundance is high, though with significant variability. Like ostracodes, molluscs are quite abundant, and present at numerous sites in water depths less than 25m. Below that depth they become less abundant, and occur in fewer samples overall, although they are present at each sampled depth below 25m, unlike the ostracodes.

Coarse residue counts: Ostracode species abundances

A complete list of all species identified in each sample (including their relative and absolute abundances, and the number of species per sample), can be found in Table 5. For taxonomic references see Appendix C – this dissertation. A list of total number of samples in which each species was recovered can be found in Table 6. For all further

descriptions and analyses, sites with 5 or fewer total ostracode valves and species found in fewer than two sites have been removed. In addition, in order to compare species abundances across multiple sites of the same depth and/or the same offshore environment, average abundances were calculated for each species at each depth and within each environment. This involved calculating the percent abundance of each species within its sample (#species/#total)*100, then grouping samples by category (either depth or environment), and calculating separately the average abundance of each species within each subdivision of that category (e.g. 1m depth, then 5m depth…etc.). This provided an average abundance of each species by each division of depth and environment (Table 7). One sample exceeded the rarity requirements at 25m depth, but because there were no other samples with which to average it, this sample is not included in the average depth dataset (n=50). However, the data from that site is included with the average abundance by environment dataset (n=51), and all further analyses (e.g. DCA).

Based on average species abundances by depth (Figure B-9) it is clear that some species are quite abundant across a wide range of depths (e.g. *Cyprinotinae sp.2* and *G. emyrsi*), whereas others are particularly abundant at a single depth (e.g. *Cypridopsine n.gen. sp.F*, *Cypridopsine n.gen. sp.L*, *Cypridopsine n.gen. sp.P*, and *G. huwi*) or group of depths (e.g. Shallow: *Cyprinotinae sp.1*, *Cyprinotinae sp.3*, *Limnocythere s.l. sp.9*; Deep: *Cypridopsine n.gen. sp.N*, *Limnocythere s.l. sp.1*; or Intermediate: *Cypridopsine n.gen. sp.C*, *Cypridopsine n.gen. sp.K*, *Zonocypris costata*). Still other species have no observable relationship between the depth at which they were found and their abundance

(e.g. *Alicenula serricaudata*, *Candonopsis sp.1*, *Cypridopsine n.gen. sp.O*, and *Ilyocypris sp.1*,).

When comparing species composition by adjacent shoreline environment, *Cyprinotinae spp. 1-3*, *Limnocythere s.l. sp.9* and *G. emyrsi* are the most widespread, occurring at relatively high abundances in all three settings (Figure B-10). By contrast, certain species have comparatively high abundances in a single environmental setting or group of settings (e.g. Marsh: *Cypridopsine n.gen. sp.L*, *Limnocythere s.l. sp.1*, *Limnocythere s.l. sp.2*, *G. irvinei*; River: *Alicenula serricaudata*, *Cypridopsine n.gen. sp.K*, *Cypridopsine n.gen. sp.N*; both Marsh and River: *Ilyocypris sp.1*). The remaining species display no observable adjacent shoreline environmental preference based on their average abundances.

Comparing species richness across sites with differing total abundances of ostracodes required rarefaction analysis. This type of analysis estimates the number of taxa (*t*) one would expect to find in a random sample of individuals (*n*) taken from a larger collection of individuals (*N*) containing *T* taxa (Birks and Line, 1992). *N* and *T* are the actual abundances and number of species found in a given sample, respectively, and *n* is the minimum number of individuals chosen by the researcher and can be based on a number of factors. For our analysis we chose 25 in order to have more individuals than were found in a single sample and to maximize the number of samples included in the analysis. The standardized number of expected taxa (*t*) for each of the 35 samples in the analysis plotted against depth and coded by environment type can be found in Figure B-11. Although the number of sites with at least 25 ostracode valves decreases with depth,

the variance in species richness does not vary significantly with depth between 5 and 20 meters. Additionally, the range of expected number of taxa are similar for all environment types regardless of depth, although it is noticeable that all offshore marsh sites at depths greater than 10 meters have fewer than 25 individuals and are therefore do not appear on this figure. The site with the highest standardized species richness is in the offshore river environment at 20 meters, whereas the sites with the two lowest standardized numbers of taxa are found at 5 meters depth in both offshore marsh and river environments.

DCA of species abundances

Although it is quite informative looking at average abundances of each species by category, a DCA analyzes the actual abundance of each species at each site in multidimensional space and clusters those sites with similar species assemblages (Figure B-12a), and those species that often co-occur (Figure B-12b). The first and second DCA axes explain 15 and 10% of the variance in the dataset and the species and site scores for DCA1 and 2 can be found in Table 8. In Figure B-12b species plotting nearest to each other likely co-occur in multiple samples, and those plotting furthest from each other were less likely to be found in the same sample. A noticeable outlier among the species is *Cypridopsine n.gen. sp.N*, in the lower right quadrant, which was found in the previous section to be most abundant in deep, river front environments (Figure B-12b). On the larger plot of site covariance (Figure B-12a), each point has been coded by shape and color corresponding to the environment and depth of the site, respectively. The extreme lower right quadrant is exclusively sites from 20m depth and riverine environments, and

is also where *Cypridopsine n.gen. sp.N* plots in DCA space. This correspondence between site location and species abundance in the DCA analysis is supported by the results from categorically averaging species abundances in the previous section, and suggests that the DCA is responding to site-to-site differences in species assemblages. There is a clear gradient across the first axis from positive DCA1 values for the deeper sites (purple, blue, and green symbols), to negative DCA1 values for the shallower sites (yellow, orange, and red symbols) (Figure B-12a). There is less of a clear separation among environment categories (symbol types), except where already separated by depth (e.g. marsh and river environments cluster for deeper sites, but not shallow).

Discussion

The interaction of numerous ecological variables affects both the presence/absence and the relative species abundances of the ostracodes living in the benthic environment of modern Lake Malawi. These factors include such features as DO content, temperature, substrate grain size and carbon content (organic and inorganic) measured in this study, as well as other potential factors such as conductivity, local pH and the habitat preferences of potential predators (e.g. fish – Abdallah, 2003) for which we currently lack data. Figures 3-5 and 7 illustrate how each of these factors varied with depth and shore line environment within the study area. Variables such as bottom water temperature, DO, inorganic carbon content, and fish presence (estimated based on abundance of fishbone in samples), changed systematically with depth. Others, including silt/clay content, and charcoal abundance, showed greater variation by environment than by depth. It is useful to consider which of these measured variables, or combination of

variables, are most likely affecting where ostracodes are found, and their specific distribution in the shallow water environments of southern Lake Malawi.

We begin by considering the drastic decrease in both the number of ostracode-bearing samples and total ostracode abundance between 25m-50m depth. Ostracodes are completely absent from samples deeper than 50m. Considering the measured values for temperature and DO in this study, as well as previously reported conductivity and pH values by depth in the southern basin of the lake, could there be an ecological threshold between 20 and 25m inhibiting live ostracode occurrence that explains this change? This is unlikely for three reasons. First, the range of conductivities measured at the four sites in this study (235-247.8 μm/cm, Table 3) are well within the range of those previously reported for the upper 100 meters of Lake Malawi (Patterson and Kachinjika, 1995; Halfman, 1993), suggesting there is no conductivity threshold crossed in the upper 25 meters. Second, the rapidly changing temperature profile from 29-31°C to 24-25°C over 25m depth suggests a relatively shallow thermocline at the time of sampling (mid-March). Two years of cruise data show a similarly shallow thermocline persisting in southern Lake Malawi from December-April, after which the SE trade winds begin thoroughly mixing the surface waters of the lake (Patterson and Kachinjika, 1995). Perhaps a temperature threshold is crossed between 25 and 30 meters (~25°C) below which ostracodes cannot survive in Lake Malawi? This is also unlikely as other researchers sampling Lake Malawi during the same month in 1999 (Martens, 2002) found significant numbers of live ostracodes at depths up to 30m, where temperatures would presumably have been similar to and likely colder than those measured at 25m in our

study (temperature was not explicitly reported). Third, the waters of Lake Malawi do not become anoxic until 200m (Patterson and Kachinjika, 1995), and although measured DO at 25m is on average less than that at 20m, too little oxygen is not a likely cause for the decreased abundance of ostracodes beginning at 25m.

The other variable that decreases systematically with depth is inorganic carbon in the sediment (Figure B-5B). In this study, with the exception of two sites, samples from depths of 25m and greater have less than 2 WT%LOI_{1000}. This corresponds to the depth at which pH begins to decrease rapidly from 8.65 between 0-25m depth, to 8.0 by 75m (Patterson and Kachinjika, 1995: fig 1.26). As carbonate is more soluble in water at lower pH values, it is likely that the disappearance of ostracodes from our record is due to a taphonomic bias – dissolution across a lysocline and thus lack of accumulation below the lake's current carbonate compensation depth (CCD). This would explain why quantities of live ostracodes were recovered from larger sediment samples taken in 30 meters of water elsewhere in Lake Malawi (Martens, 2002): the ostracode is able to preferentially take in carbonate while living, but once dead, the shells dissolve from the record. This situation is in contrast to the supersaturated surface waters of Lake Tanganyika (pH 8.7-9.2) where thin-shelled organisms have been recovered even from cores taken as deep as the oxicline (Alin and Cohen, 2004), although even in this lake a CCD exists at greater depth. This difference in thin-shelled vs. thick-shelled organisms may also explain why gastropods are still present in the dataset (though in lower abundances) below 30m, with a single specimen found at 60m. Smaller, more thinly-walled shells (e.g. ostracode valves) would dissolve faster than larger, thicker shells as

the speed of the reaction would be the same for both, making it more likely to find gastropod shells in deeper surface sediments than ostracodes.

In summary, the data suggest that the sudden decrease in the number of ostracodes recovered from sites deeper than 25m is likely the result of post-depositional dissolution due to carbonate under-saturation and decreased pH at depths greater than 30m (Patterson and Kachinjika, 1995). It is likely, therefore, that our data do not accurately reflect the living assemblage from deeper depths in the modern lake. This also places a clear limit on our ability to extrapolate from these results to times in the past when the lake was shallower and more alkaline than present (e.g. 110-95 thousand years ago – Cohen et al. 2007). It cannot be assumed that ostracodes would not have lived and been preserved at depths greater than 30m during such periods of lowered lake levels, although a deeper CCD may certainly have existed under higher alkalinity conditions than at present.

Post-depositional dissolution may explain the disappearance of ostracodes below 30 meters, however, species assemblage composition changes between 1-25 meters as well. This variability should be explained by ecological factors that also change within that depth range, as suggested by the DCA (Figure B-12A). The DCA suggests that site depth (expressed as color variation on Figure B-12A) is a stronger influence than shoreline environment (symbols) on species distribution. This finding supports a similar assertion by Martens (2002), who found that samples from sites at the same depth in widely separate geographic locations had a higher similarity index (more species in common) than samples from the same location but from different water depths (8m and

30m). Were coastline environment (and its impacts on offshore conditions) the more important factor one would expect sites offshore from the river (squares), marsh (triangles), and sandy beach (circles) to cluster. There is a clustering of sites that are similar in both depth (15-20m) and environment (river), which may relate to the persistent, and increasingly high silt content of the bottom sediments in that environment with depth. With that exception noted, the influence of depth on the ostracode assemblages is most likely the result of crossing species-specific tolerance thresholds in temperature or DO, as these measurements displayed the most consistent change with depth, regardless of environment (Figure B-3a-b). It is also possible that an ecological variable not measured directly in this study contributes to the ostracode assemblage variability such as light penetration which is typically inversely correlated with turbidity (Halfman, 1996). In contrast, for the range of depths in which ostracodes are most abundant (1-20m), silt, clay and organic carbon content are relatively similar (Figures 4a-b, 5a), and are therefore unlikely the driving ecological factors affecting assemblage variation. Although standardized species richness did not vary greatly by either depth or environment type in this study, it may be interesting to compare these modern values with those from samples in the paleo-record to see how ostracode diversity has changed with time.

Other important observations from the dataset include: the distribution of ostracode species in our study compared to a previous report where the majority of modern Malawi ostracodes were initially described (Martens, 2002), the similarity of calculated water $\delta^{18}O$ and that of modern lake water, the covariance in river-influenced

silt and charcoal abundance, and finally, the relationships among the abundances of the biological indicators (specifically ostracodes, fish and *Botryococcus*). These observations are described in detail below.

The largest difference between our results and those of Martens (2002) is that of the five sites he described, species richness was between 7 and 14 species/site. As can be seen in Tables 4 and 6, the average number of species per site in our study was 9, and the maximum was 21. However, this is not an unexpected discrepancy for two reasons. First, Martens (2002) specifically chose to describe those sites with the most diversity, and from which he could describe all of the ostracode species found including those from less species-rich sites. And second, the Martens (2002) report only counted those species that were live, and could therefore have soft-parts of the ostracode preserved for further description. Live assemblages typically have fewer total species because they represent a snapshot in time, whereas live/dead assemblages have the potential to time average ostracode species present over the course of one or more years (Alin and Cohen, 2004). Given the depth of penetration by the grab sampler in this study of ~2cm, and typical unconsolidated sediment accumulation rates in Lake Malawi of ~1mm/year (Pilskaln and Johnson, 1991), it is likely that our samples averaged approximately 20 years of deposition.

Since the purpose of choosing the five sites reported on by Martens (2002) was to maximize overall species diversity (to describe as many new species as were seen in the entire dataset), and the sites chosen were at depths of 7, 8, 10, 11 ("shallow") and 30 ("deep") meters, it is difficult to draw specific comparisons between the two datasets.

However, some general similarities should be highlighted: *Cyprinotinae sp.1* and *sp.2* and *G. emyrsi* are found in multiple "shallow" sites, suggesting they are widespread in terms of environment, as was the case with the different shorelines looked at in this study. Additionally, of the eight species found at the "deep" sites in the live assemblage, four were observed in our study area: *Limnocythere s.l. sp.1*, *Alicenula serricaudata*, *Cyprinotinae sp.1*, and *Cypridopsine n.gen. sp.N*. Three of these four were most abundant in the deeper waters in our study (15-20m depths). A final point concerns the extremely similar distributions of *Limnocythere s.l. sp.9* and *Limnocythere s.l. sp.10* (see Figure B-12B). It was suggested by Martens (2002) that these may, in fact, be males and females of the same species, and given their similar distribution and similar valve attributes (Plate 8, A-F), this seems a reasonable conclusion.

The majority of annual water loss from the lake is through evaporation, which should leave the surface waters significantly enriched over influent waters including precipitation and rivers. The average $\delta^{18}O$ value of the upper 75m of Lake Malawi is +2‰, and the major inflowing rivers (which reflect regional precipitation values) range from -5.4 to -3.1‰ (Branchu et al., 2005). Theoretically, sites at or near the input of a major river should have water $\delta^{18}O$ values somewhere in between depending on the strength of the inflowing river (mass balance of river water to lake water), and the distance and relief between source (precipitation) and the location of the drainage into the lake (longer distances at slower speeds provides opportunity for river waters to become evaporatively enriched). The range of calculated $\delta^{18}O$ lake water values from the measurements on gastropod shell carbonate is +1.12-2.54‰, similar to the measured

value of open, evaporated lake waters, with perhaps a slight negative bias. This is supported by the few near-shore conductivity measurements taken in this study: all are well within the range of those measured from the same depths in the open waters of the modern lake (Patterson and Kachinjika, 1995). Either of the theoretical reasons given above could explain these oxygen isotope values; either a weak river system, or travel over a low relief landscape for long distances. In this case, it is likely a combination of the two. The Lisangadzi River flowing into the lake at the beginning of Transect C is not one of the five major rivers noted by Branchu et al. (2005), and it is flowing slowly over a region of extremely low relief, allowing for evaporation prior to entering the lake.

The percentage of silt and abundance of charcoal also change with depth, however the variation differs further by environment. In sites offshore from the river inlet, the values for both variables increase drastically at ~20m depth and remain high until at least 50m (Figures 4 and 7). This co-variation between variables does not help explain the near-disappearance of ostracodes from the dataset below 25m, but it does suggest two things: 1) grain size distribution in near-shore environments of Lake Malawi is dependent on the sub-environment – offshore channeling (e.g. Figure B-4A, Transect C) from even a small river may redistribute larger grain sizes (silts) to deeper depths than settling velocity models would suggest (e.g. Gibbs et al. 1971); and 2) that macro-charcoal is overwhelmingly supplied to the lake by rivers. The latter point is of particular significance for paleoenvironmental interpretation of sediment cores from the lake, since they indicate that changes in local, rather than distant (wind-borne) fire frequency are responsible for the changes observed in these records.

Important biological indicators often preserved as fossils in paleo-records include ostracodes, fish, and the green alga *Botryococcus*. For this reason, understanding the distribution of these indicators in the modern lake may inform interpretations about the past lake environment (e.g. Appendix C – this dissertation). Since the precipitous decline of ostracodes at ~25 meters in this study is likely caused by taphonomic bias, its potential abundance at deeper depths in shallower, paleo-lakes cannot be assessed. However, the coincidence of decreased ostracode abundance with increased *Botryococcus* should not necessarily be overlooked as this dichotomous relationship has also been observed between the two taxa in the paleo-record of Lake Malawi (Appendix C – this dissertation). There may very likely be an ecological variable that both taxa are responding to but its interpretation is hampered in this study by the taphonomic dissolution of ostracodes. Perhaps future work in a more alkaline modern lake can determine the cause of this nearly exclusive distribution pattern. Fish remains are abundant across all depths sampled in this study. Although the total abundance increases with increased depth, the total variance is similar for all depths (excluding 35, 45 and 55 meter depths due to small sample sizes). It is suggested by Reinthal et al. (2011) that fish are most abundant at intermediate depths, which may indicate abundance may increase with depth until a certain "Goldilocks depth" where conditions were ideal, before decreasing in abundance. However, this study did not sample deep enough to observe this theoretical ideal depth and subsequent decreased abundance. Often in the paleo-record discussed in Appendix C (this dissertation) the highest abundance of fish fossils occur at transitions between ostracode-rich and *Botryococcus*-rich intervals which are

interpreted as relatively shallow and deep lake environments, respectively. It would be interesting for a future study to sample deeper depths in the modern Lake Malawi to find the depth of highest fish abundance, as this value may be directly applicable to past studies.

Conclusions

Modern ecological data from the southwest arm of Lake Malawi including limnological variables, grain size, and organic and inorganic carbonate content of sediments, serve as a data set through which to interpret the paleo-abundance patterns of fish, mollusc, charcoal, *Botryococcus* and ostracodes within the study area. The relationship between modern taxa and modern lake ecology may be useful for paleoenvironmental reconstruction. Interpretations of the data from this study allow the following conclusions to be drawn regarding the distribution and abundance of potentially fossilizeable materials in the littoral zone of modern Lake Malawi.

- The general absence of ostracodes below 30m is likely the result of a taphonomic bias caused by shell dissolution in the undersaturated, lower alkalinity waters below that depth. This is not necessarily a direct reflection of the living ostracode assemblage, although it is probable that ostracodes would be present in lower abundances due to the increased difficulty in calcifying their valves below that depth. It is likely that times in the past when lake level was lower, ostracodes

were more abundant and preserved at deeper depths due to increased alkalinity and therefore a deeper CCD.

- Indirect ordination of ostracode abundance data suggests that assemblages are more similar by depth than by shoreline environment, implying an ecological preference of some species to variables that are the same across a single depth, but vary above and below it. From our dataset, it is most likely that species niches are determined by limnological variables rather than substrate grain size or OC content.
- More species per site were found in this study than Martens (2002) in accordance with predicted time averaging differences between live and live/dead assemblages.
- *Limnocythere s.l. sp.9* and *Limnocythere s.l. sp.10* originally described in Martens (2002) are likely females and males of the same species, respectively.
- Stable oxygen isotopic data from molluscs at different depths and environments suggest shoreline water is as evaporated as the open lake environment, regardless of a potential nearby source of inflowing freshwater. Salinity measurements support the suggestion that the waters surrounding the inflow from the river is no fresher than elsewhere along the shore.
- Even a small inflowing river can significantly affect the particle size distribution of lake sediments, and it can serve as a conduit for macro-charcoal deposition into the basin from the surrounding watershed.

- The distribution by depth of the commonly fossilizable indicators: ostracodes (shallow), fishbone (shallow to intermediate), and *Botryococcus* (intermediate) in the modern lake suggests that changes in their abundances in the past may reflect relative changes in lake level.

Acknowledgements

Funding for the field work for this project was provided by the U.S. National Science Foundation-Earth System History Program (EAR-0602350). Funding for sample preparation and sedimentological analyses was provided to author Lopez by the SAGUARO (Southern Arizona Geosciences Union for Academics, Research and Outreach) program at the University of Arizona. SEM imaging was performed on a Hitachi S-3400N housed in the Geosciences Department at the University of Arizona. Funding for the SEM facility was through the Arizona LaserChron Center grant NSF EAR-0929777. The stable isotope analyses were performed by the Environmental Isotope Laboratory, Geosciences Department, University of Arizona. Lead author Blome would like to thank Howard and Michelle Massey-Hicks and Leonard Kalindekafe for their hospitality and assistance during the 2010 field season in Cape MacLear, Malawi.

References

Abdallah, A.M., 2003. Environmental factors controlling the distributions of benthic invertebrates on rocky shores of Lake Malawi, Africa. Journal of Great Lakes Research 29, 202-215.

Alin, S., Cohen, A.S., 2004. The live, the dead, and the very dead: taphonomic calibration of the recent record of paleoecological change in Lake Tanganyika, East Africa. Paleobiology 30, 44-81.

Bennett, K.D., 2007. psimpoll, version 4.27 ed.

Birks, H.J.B., Line, J.M., 1992. The use of rarefaction analysis for estimating palynological richness from Quaternary pollen-analytical data. The Holocene 2, 1-10.

Branchu, P., Bergonzini, L., Delvaux, D., De Batist, M., Golubev, V., Benedetti, M., Klerk, J., 2005. Tectonic, climatic and hydrothermal control on sedimentation and water chemistry of northern Lake Malawi (Nyasa), Tanzania. Journal of African Earth Sciences 43, 433-446.

Cohen, A.S., Dussinger, R., Richardson, J., 1983. Lacustrine paleochemical interpretations based on eastern and southern African ostracodes. Palaeogeography, Palaeoclimatology, Palaeoecology 43, 129-151.

Cohen, A.S., 2003. Paleolimnology: The History and Evolution of Lake Systems. Oxford University Press, Oxford.

Cohen, A.S., Stone, J.R., Beuning, K.R.M., Park, L.E., Reinthal, P.N., Dettmar, D., Scholz, C.A., Johnsor, T.C., King, J.W., Talbot, M.R., Brown, E.T., Ivory, S.J., 2007. Ecological consequences of early Late Pleistocene megadroughts in tropical Africa. P. Natl. Acad. Sci. USA 104, 16422-16427.

Dean, W.E., 1974. Determination of carbonate and organic matter in calcareous sediments and sdimentary rocks by loss on ignition: comparison with other methods. Journal of Sedimentary Petrology 44, 242-248.

Delorme, L.D., 1969. Ostracodes as Quaternary paleoecological indicators. Can J Earth Sci 6: 1471-1476.

Dettman, D.L., Palacios-Fest, M.R., Nkotagu, H.H., Cohen, A.S., 2005. Paleolimnological investigations of anthropogenic environmental change in Lake Tanganyika: VII. Carbonate isotope geochemistry as a record of riverine runoff. Journal of Paleolimnology 34, 93-105.

Dettman, D.L., Reische, A.K., Lohmann, K.C., 1999. Controls on the stable isotope composition of seasonal growth bands in aragonitic fresh-water bivalves (unionidae). Geochim. Cosmochim. Ac. 63, 1049-1057.

Eccles, D.H., 1974. An outline of the physical limnology of Lake Malawi (Lake Nyasa). Limnol Oceanogr 19, 730-742.

Fritz, S.C., 1996. Paleolimnological records of climatic change in North America. Limnol. Oceanogr. 41, 882-889.

Gasse, F., Juggins, S., Khelifa, L.B., 1995. Diatom-based transfer functions for inferring past hydrochemical characteristics of African lakes. Palaeogeogr, Palaeoclimatol, Palaeogeogr 117, 31-54.

Gibbs, R.J., Matthews, M.D., Link, D.A., 1971. Relationship between sphere size and settling velocity. Journal of Sedimentary Petrology 41, 7-18.

Grossman, E.L., Ku, T.-L., 1986. Oxygen and carbon isotope fractionation in biogenic aragonite: Temperature effects. Chemical Geology: Isotope Geoscience section 59, 59-74.

Halfman, J.D., 1993. Water column characteristics from modern CTD data, Lake Malawi, Africa. Journal of Great Lakes Research 19, 512-520.

Halfman, J.D., 1996. CTD-Transmissometer Profiles from Lakes Malawi and Turkana, in: Johnson, T.C., Odada, E.O. (Ed.), The Limnology, Climatology and Paleoclimatology of the East African Lakes. Gordon and Breach, Amsterdam, pp. 169-182.

Heiri, O., A.F. Lotter, and G. Lemcke, 2001. Loss on ignition as a method for estimating organic and carbonate content in sediments: reporducibility and comparability of results. Journal of Paleolimnology 25, 101-110.

Holmes, J.A., 1992. Nonmarine ostracods as Quaternary palaeoenvironmental indicators. Progress in Physical Geography 16, 405-431.

Horne, D.J., 2007. A Mutual Temperature Range method for Quaternary paleoclimatic analysis using European nonmarine Ostracoda. Quaternary Sci Rev 26: 1398-1415.

Howe, H.V., 1955. Handbook of Ostracod Taxonomy. Louisiana State University Press, Baton Rouge.

Jari Oksanen, F.G.B., Roeland Kindt, Pierre Legendre, Peter R. Minchin, R. B. O'Hara, Gavin L. Simpson, Peter Solymos, M. Henry, H. Stevens and Helene Wagner 2011. vegan: Community Ecology Package, R package version 2.0-1 ed.

Kempf, E.K., 1980. Index and bibliography of nonmarine ostracoda. Geologisches Institut Der Universitaet Zu Koeln, Koeln, Germany.

Klie, W., 1944. Ostracoda, Exploration du Parc National Albert: Mission H. Damas (1935-1936). Instituut der Nationale Parken van Belgisch Congo, Brussels.

Lister, G.S., 1988. Stable isotopes from lacustrine Ostracoda as tracers for continental palaeoenvironments, in: De Deckker, P., Colin, J.-P. and Peypouquet, J.-P. (Ed.), Ostracoda in the earth sciences. Elsevier, Amsterdam, pp. 201-229.

Malawi Government, 2003. Nkhudzi Bay to Malembo. Department of Surveys - Hydrographic Unit, Malawi.

Martens, K., 1986. Taxonomic Revision of the subfamily Megalocypridinae Rome, 1965 (Crustacea, Ostracoda). Paleis der Academien, Brussels.

Martens, K., 1988. Seven new species and two new subspecies of Sclerocypris SARS, 1924 from Africa, with new records of some other Megalocypridinids (Crustacea, Ostracoda). Hydrobiologia 162, 243-273.

Martens, K., 2002. Task 3: taxonomy of invertebrates, in: Irvine, K. (Ed.), The trophic Ecology of the Demersal Fish Community of Lake Malawi/Niassa, Central Africa, pp. 49-59.

Martens, K., 2003. On the evolution of Gomphocythere (Crustacea, Ostracoda) in Lake Nyassa/Malawi (East Africa), with the description of 5 new species. Hydrobiologia 497, 121-144.

Mezquita, F., Roca, J.R., Reed, J.M., Wansard. G., 2005. Quantifying species-environment relationships in non-marine Ostracoda for ecological and palaeoecological studies: Examples using Iberian data. Palaeogeogr Palaeoclimatol Palaeogeogr 225: 93-117.

Mischke, S., Fuchs, D., Riedel, F., Schudack. M.E., 2002. Mid to Late Holocene palaeoenvironment of Lake Eastern Juyanze (north-western China) based on ostracods and stable isotopes. Geobios 35, 99-110.

Neale, J.W., 1979. On the Genus *Cyprinotus* and its Interpretation, in: Krstic, N. (Ed.), Proceedings of VII International Symposium on Ostracodes: Taxonomy, Biostratigraphy and Distribution of Ostracodes. Serbian Geological Society, Beograd, Serbia, pp. 77-85.

Park, L.E., Cohen, A.S., 2011. Paleoecological response of ostracods to early Late Pleistocene lake-level changes in Lake Malawi, East Africa. Palaeogeography, Palaeoclimatology, Palaeoecology 303, 71-80.

Patterson, G., Kachinjika, O., 1995. Limnology and phytoplankton ecology, in: Menz, A. (Ed.), The fishery potential and productivity of the pelagic zone of Lake Malawi/Niassa. Natural Resource Institute, Chatham, UK, pp. 1-67.

Pilskaln, C.H., Johnson, T.C., 1991. Seasonal signals in Lake Malawi sediments. Limnol Oceanogr 36, 544-557.

R Development Core Team, 2010. R: A language and environment for statistical computing, 2.12.0 ed. R Foundation for Statistical Computing, Vienna, Austria.

Reinthal, P.N., Cohen, A.S., Dettman, D.L., 2011. Fish fossils as paleo-indicators of ichthyofauna composition and climatic change in Lake Malawi, Africa. Palaeogeography, Palaeoclimatology, Palaeoecology 303, 126-132.

Rossetti, G., Martens, K., 1998. Taxonomic revision of the Recent and Holocene representatives of the Family Darwinulidae (Crustacea, Ostracoda), with a description of three new genera. Biologie 68, 55-110.

Ryan, W.B.F., S.M. Carbotte, J.O. Coplan, S. O'Hara, A. Melkonian, R. Arko, R.A. Weissel, V. Ferrini, A. Goodwillie, F. Nitsche, J. Bonczkowski, and R. Zemsky, 2009. Global Multi-Resolution Topography synthesis. Geochem. Geophys. Geosyst. 10, Q03014.

Sars, G.O., 1910. Zoological Results of the Third Tanganyika Expedition, conducted. Proceedings of the Zoological Society, London 79, 31-77.

Sars, G.O., 1924. The freshwater Entomostraca of the Cape Province (Union of South Africa). Annals of the south African Museum 20.

Smith, A.J., 1993. Lacustrine ostracodes as hydrochemical indicators in lakes of the north-central United States. J Paleolimnol 8, 121-134.

Strayer, D.L., 2010. Benthic Invertebrate Fauna, Lakes and Reservoirs, in: Likens, G.E. (Ed.), Lake Ecosystem Ecology: A Global Perspective. Elsevier, Amsterdam, pp. 27-41.

ter Braak, C.J.F., Prentice, I.C., 1988. A theory of gradient analysis. Advanced Ecological Research 18, 271-317.

Van Harten, D., 1979. Some new shell characters to diagnose the species of the *Ilyocypris gibba-biplicata-bradyi* group and their ecological significance, in: Krstic, N. (Ed.), Proceedings of VII International Symposium on Ostracodes: Taxonomy, Biostratigraphy and Distribution of Ostracodes. Serbian Geological Society, Geograd, Serbia, pp. 71-76.

Vincens, A., G. Buchet, D. Williamson, and M. Taieb. (2005). A 23,000 year pollen record from Lake Rukwa (8ºS, SW Tanzania): New data on vegetation dynamics and climate in Central Eastern Africa. Review of Palaeobotany and Palynology 137, 147-162.

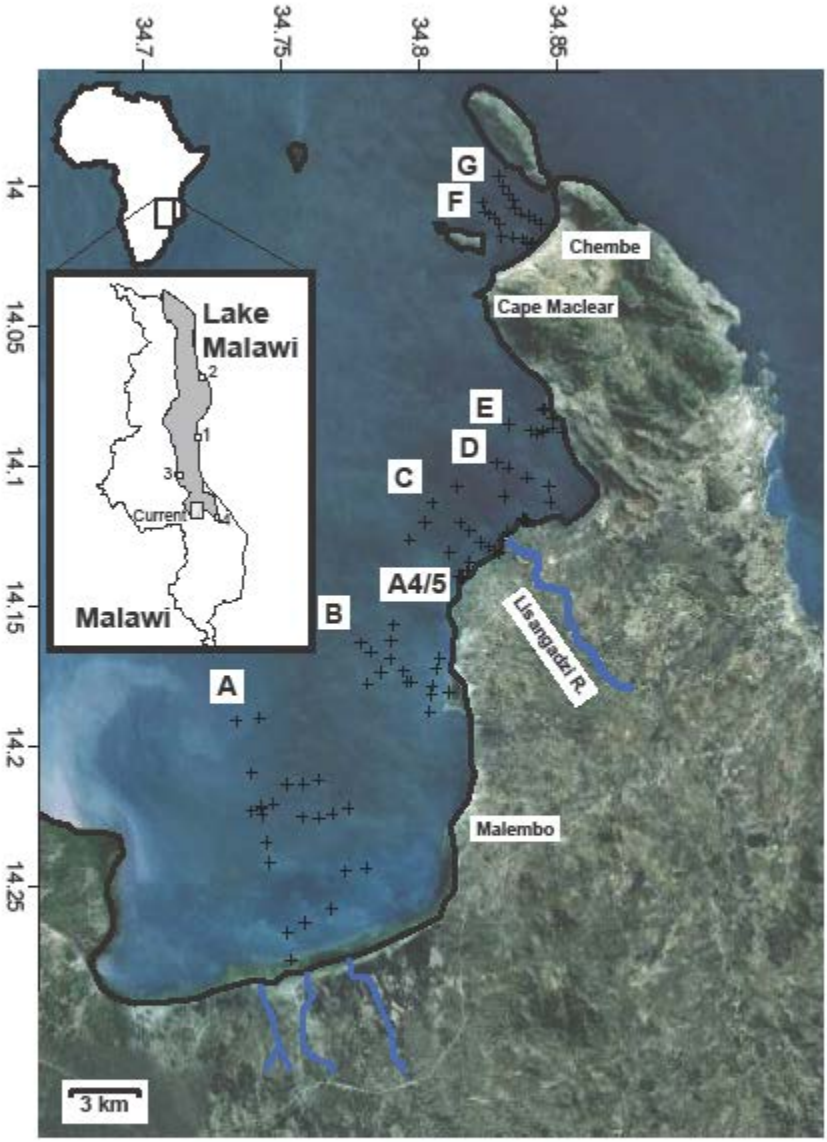

Figure B-1. Site locations for the current study within the southeast arm of the extreme southern end of Lake Malawi. The primary depth transects are labeled A-G, as is the location of the SCUBA transect A4/5. Each cross marks the location of a sample site. Exact coordinates for each site can be found in Table 1. The inset also shows the site locations for a previous study of the ostracodes of modern Lake Malawi (Martens, 2002). Satellite imagery from GeoMapApp (http://www.geomapapp.com).

Figure B-2. Categorization of different offshore environment transects. Sites are divided into "High Relief – Sand", "Low Relief – River", and "Low Relief – Marsh". The first part of the category describes the topography inland of each transect, and the second part of the label describes the immediate shoreline environment: coarse sandy beach, river inflow, and marshland, respectively. The images to the left typify each sub-environment. The middle panel is a digital elevation model (DEM) map (http://www.geomapapp.com, Ryan et al, 2009) of the study area with the main transects illustrated as solid lines from shore to their end at 60m water depth. Extending onto land from each sampled transect is a dotted line showing the location of the topographic transects shown in the panel on the right. Vertical exaggeration (VE) is 15 for transects A-D ("Low Relief"), and VE=3 for transects E, F, and G ("High Relief").

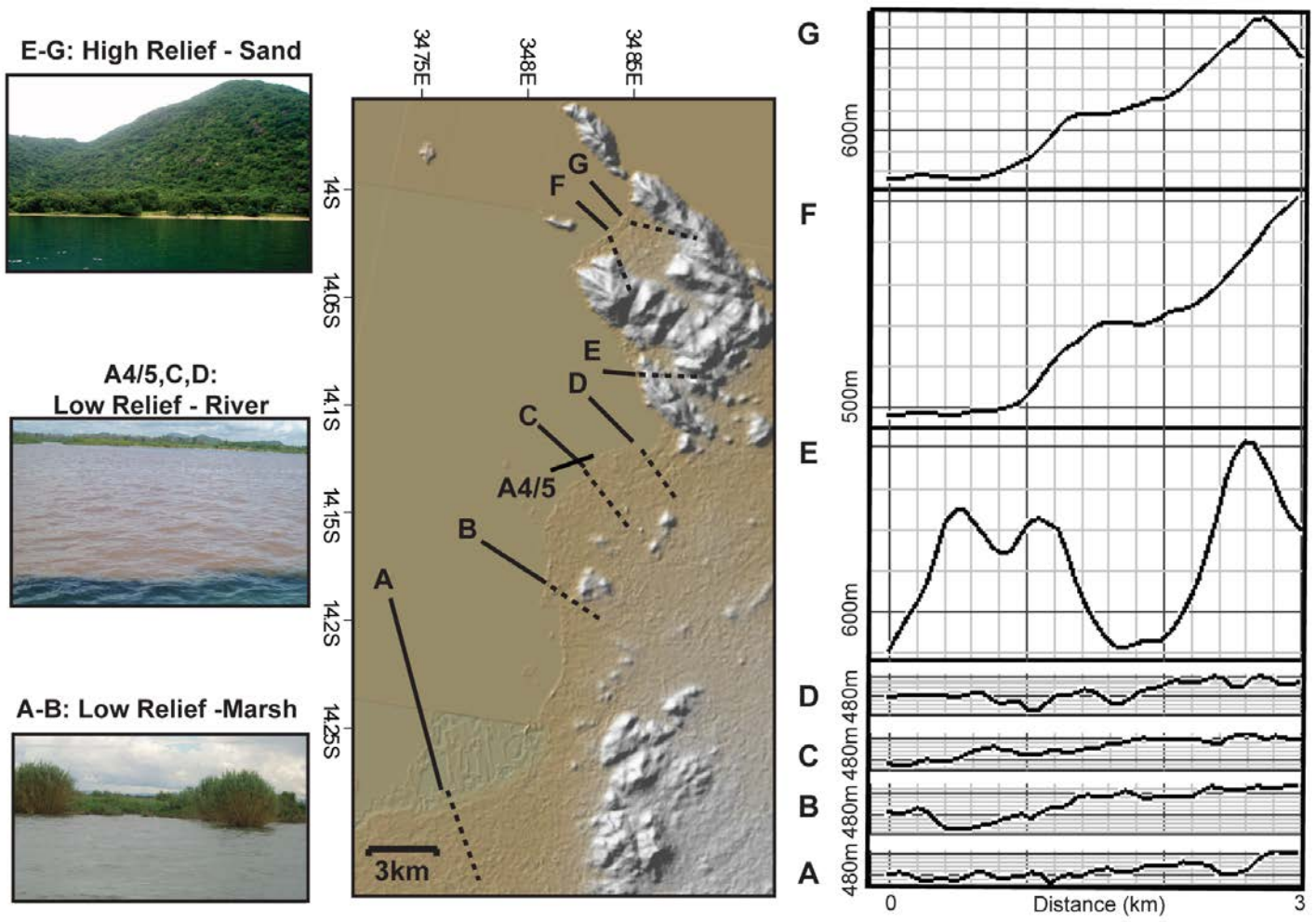
E-G: High Relief - Sand
A4/5,C,D:
Low Relief - River
A-B: Low Relief -Marsh
34.75E
34.8E
34.85E
14S
14.05S
14.1S
14.15S
14.2S
14.25S
G
F
E
D
C
A4/5
B
A
3km
600m
500m
600m
480m
480m
480m
480m
0
Distance (km)
3

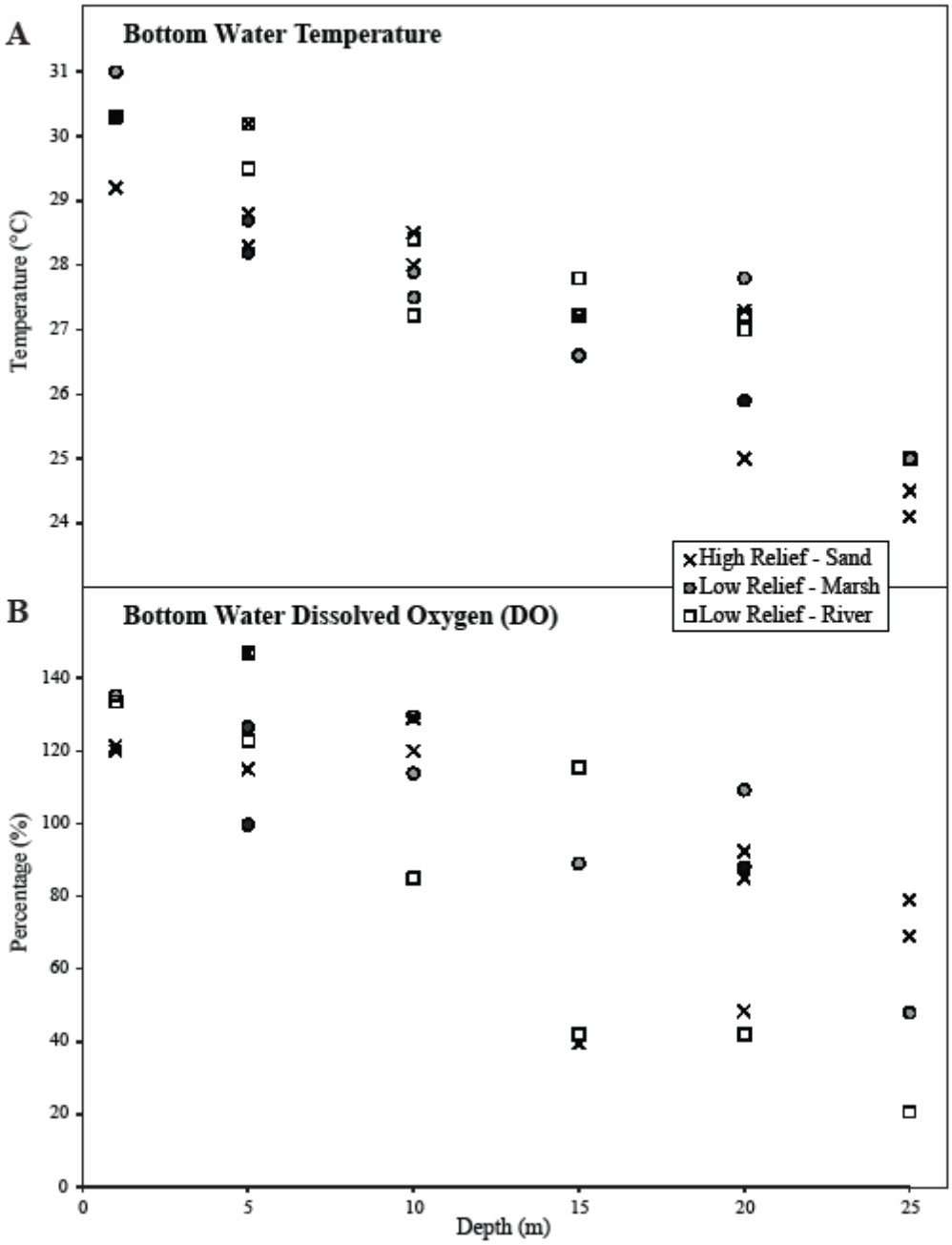

Figure B-3. Limnological results taken from bottom waters along study transects of 1-25 meters water depth and coded by shoreline environment type. A: Bottom water temperature (°C), B. Dissolved Oxygen (DO) (%).

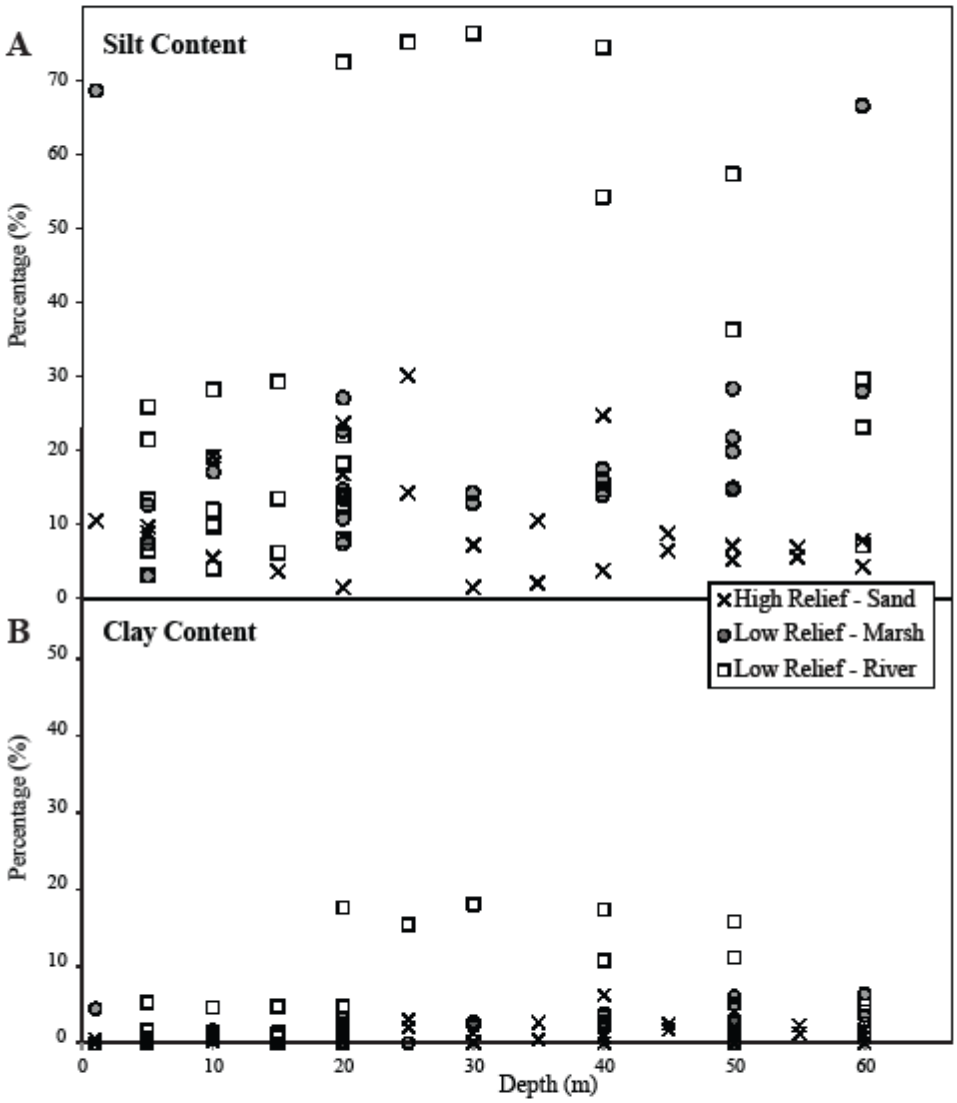

Figure B-4. A-B. Particle size distribution plotted by depth and coded by environment. A. Percentage silt-sized fraction. B. Percentage clay-sized fraction.

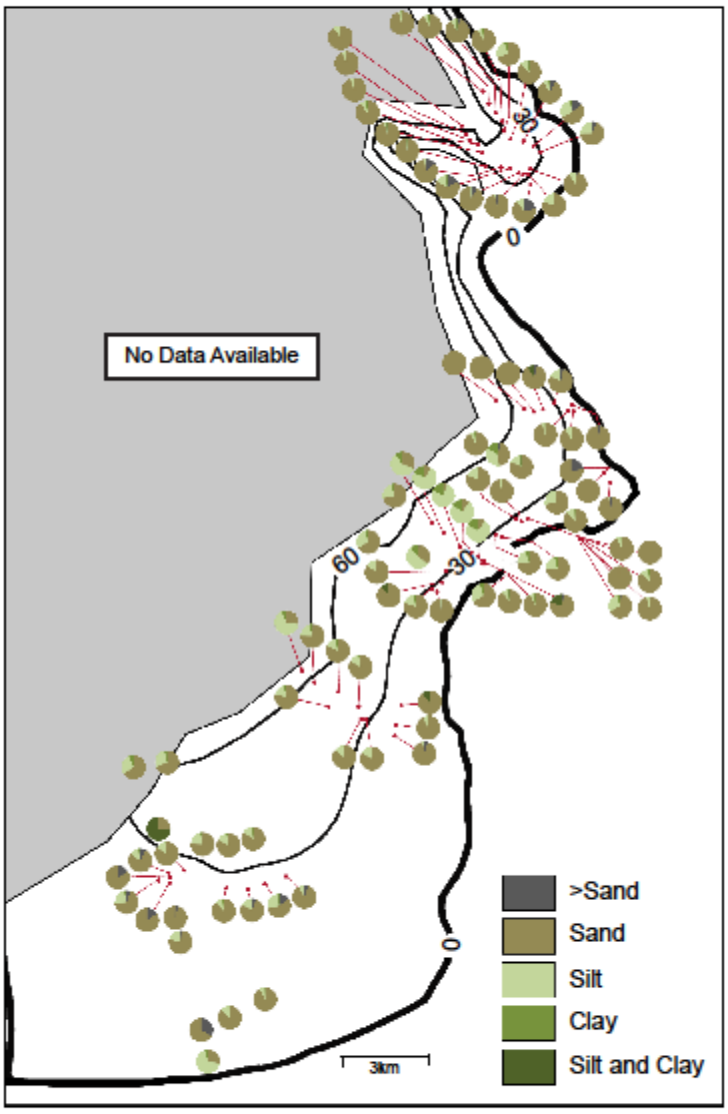

Figure B-4. C. Spatial distribution of sediment grain sizes presented proportionally in a pie graph at each site location.

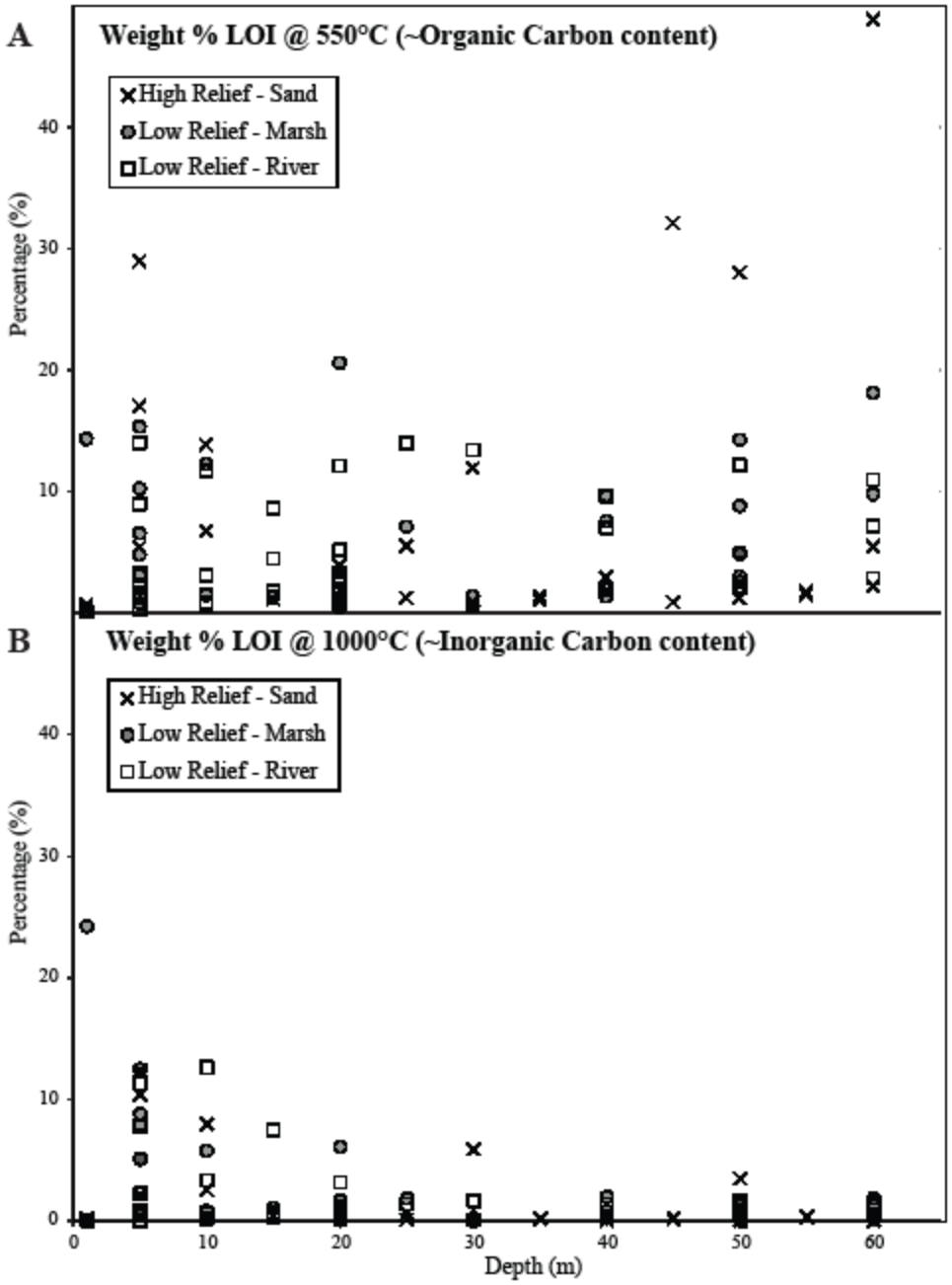

Figure B-5. Loss on ignition (LOI) results. Each sample is plotted by depth and coded by environment. A. Weight percent LOI 550˚C (Organic Carbon Content). B. Weight percent LOI 1000˚C (Inorganic Carbon Content).

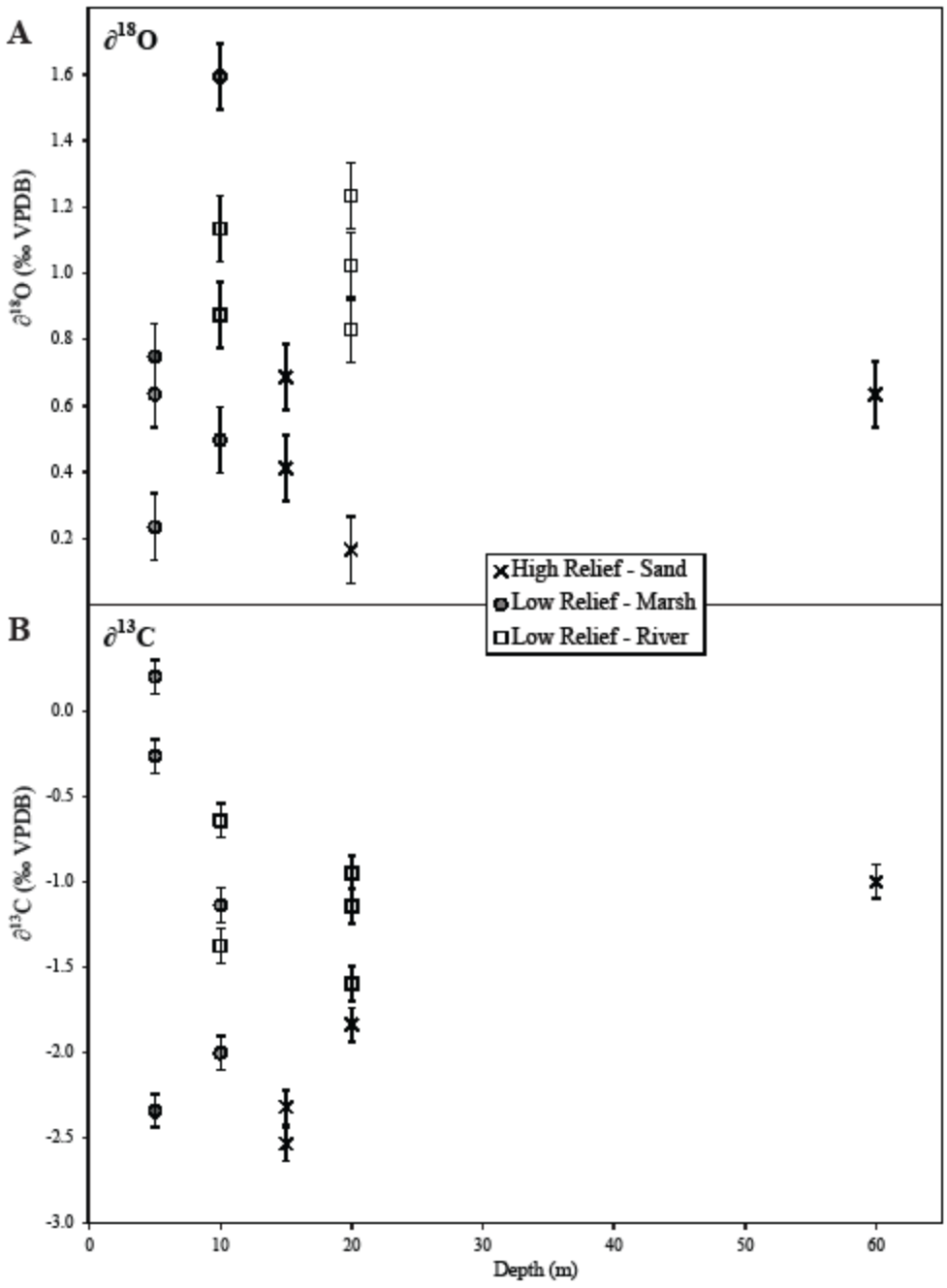

Figure B-6. Stable isotope results. All samples are coded by environment and plotted against sampling depth. A. $\delta^{18}O$ values on mollusc shell. B. $\delta^{13}C$ values on mollusc shell.

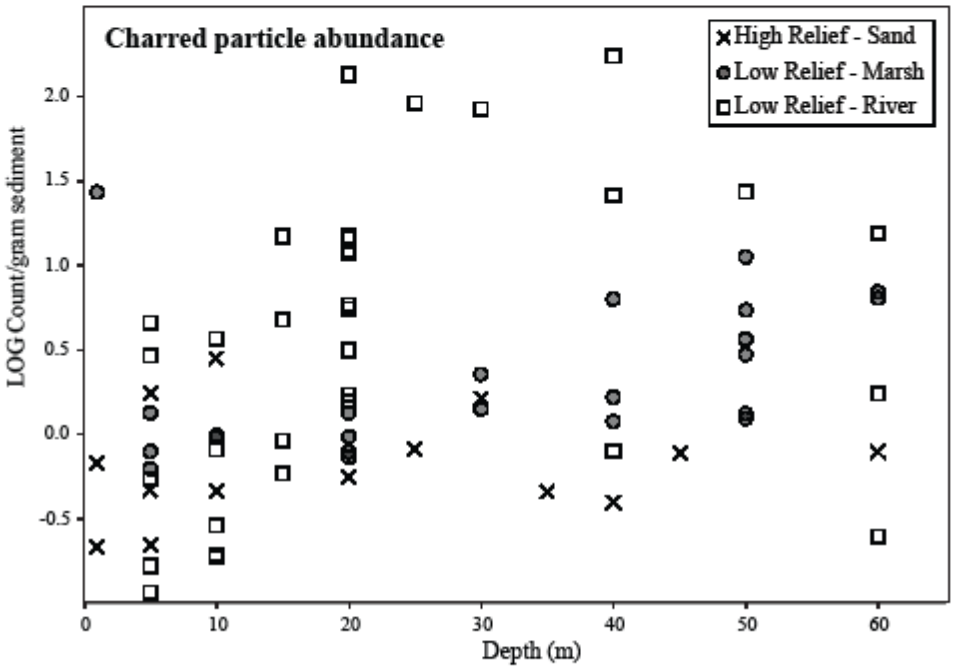

Figure B-7. LOG charred particle abundance plotted by depth and coded by environment. Offshore river sediments have the highest abundance across all depths.

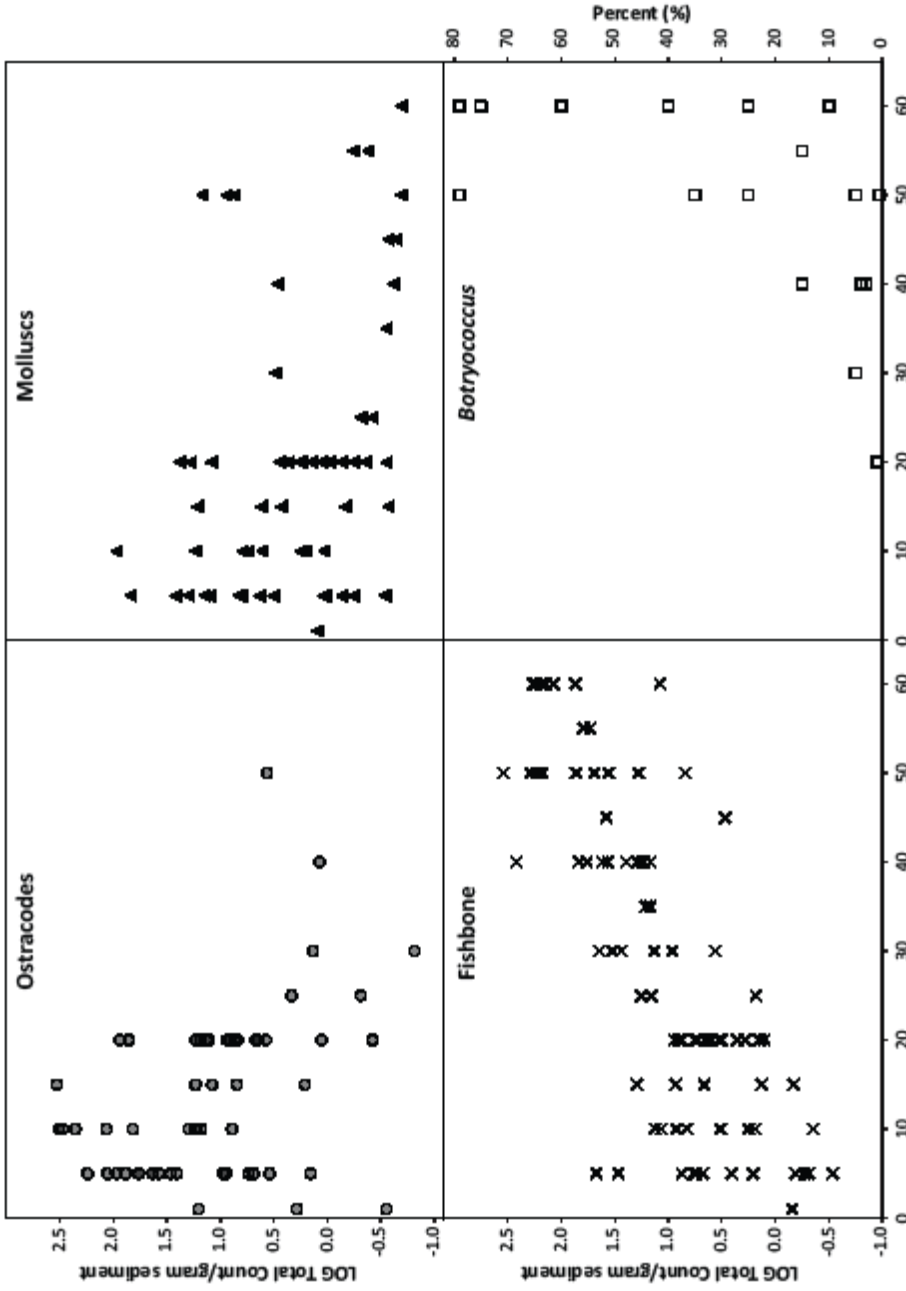

Figure B-8. Biological indicator abundance plotted against depth, with each indicator on its own labeled panel (Ostracodes, Molluscs, Fishbone, and *Botryococcus*). Absolute abundances of ostracodes, molluscs, and fishbones are plotted as the LOG abundance/gram sediment counted (left hand axis). The relative abundance of *Botryococcus* is given as a percentage of the total sample (right hand axis).

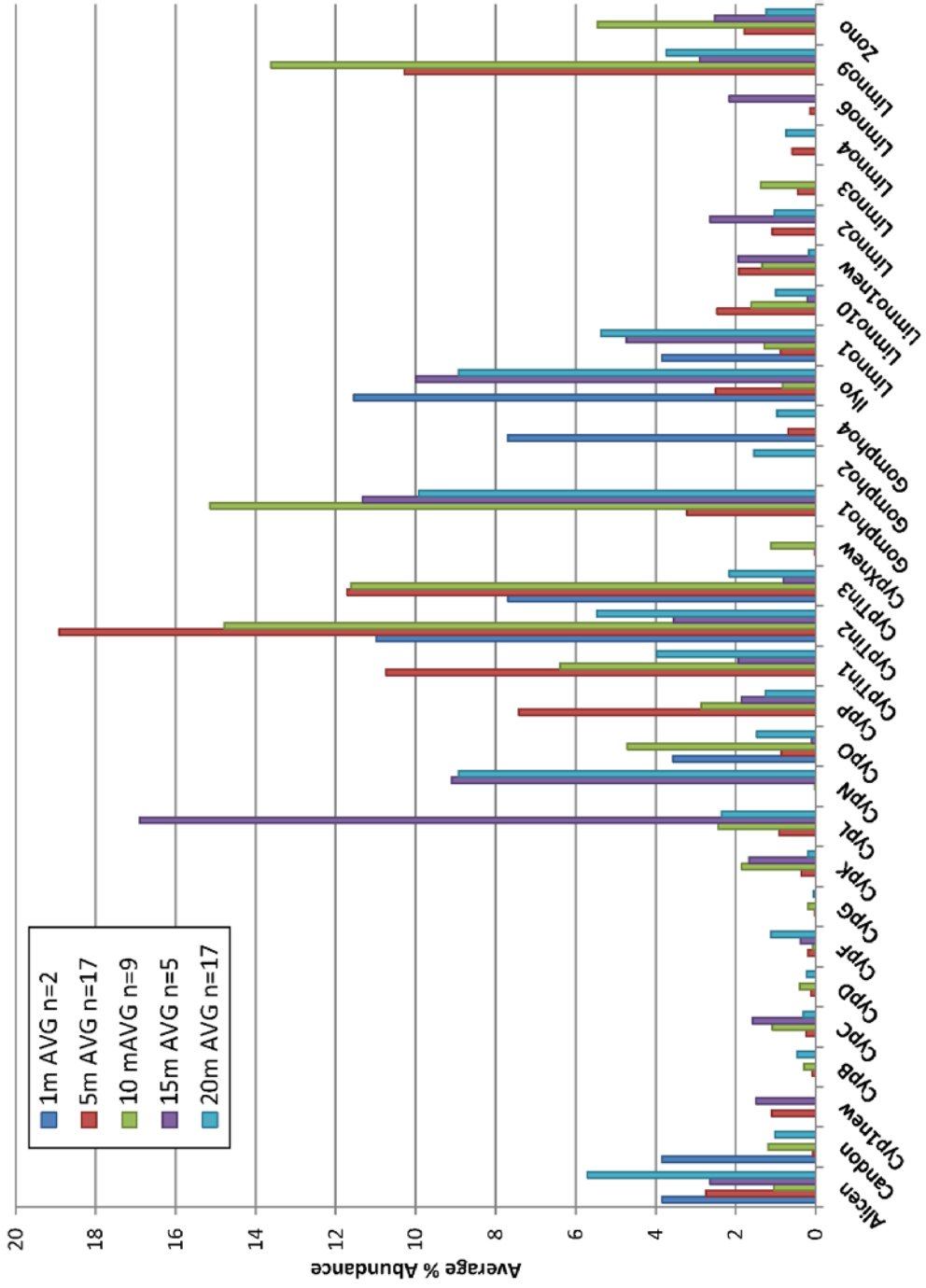

Figure B-9. Average percent abundance of each species at each depth category. Species names are listed alphabetically along the x-axis. Full species names for each shortened ID can be found in Table 8. The total number of samples in each depth category used in the averaging are given in the figure legend.

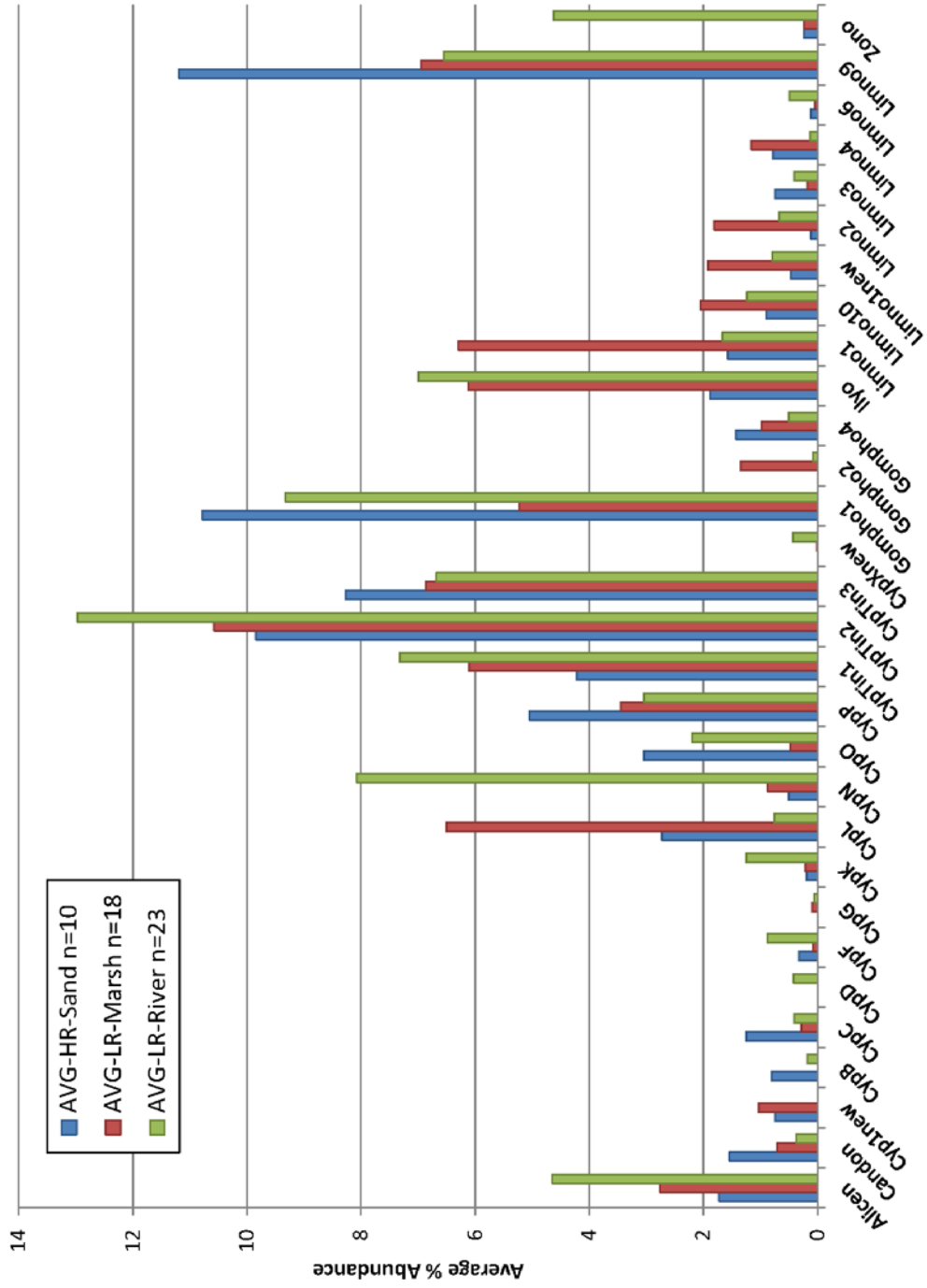

Figure B-10. Average percent abundance of each species at in each offshore environment category. Species names are listed alphabetically along the x-axis. Full species names for each shortened ID can be found in Table 8. The total number of samples in each depth category used in the averaging are given in the figure legend.

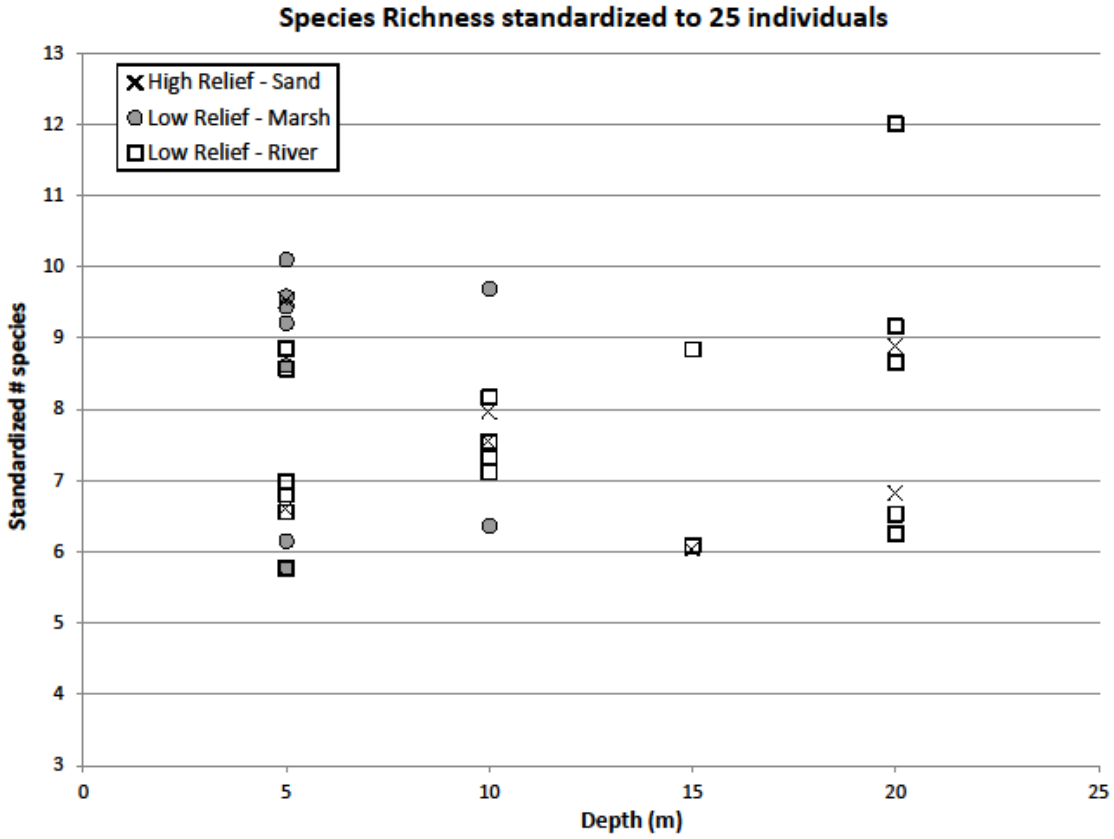

Figure B-11. Standardized species richness (to a minimum of 25 individuals). All samples coded by environment, and plotted against depth.

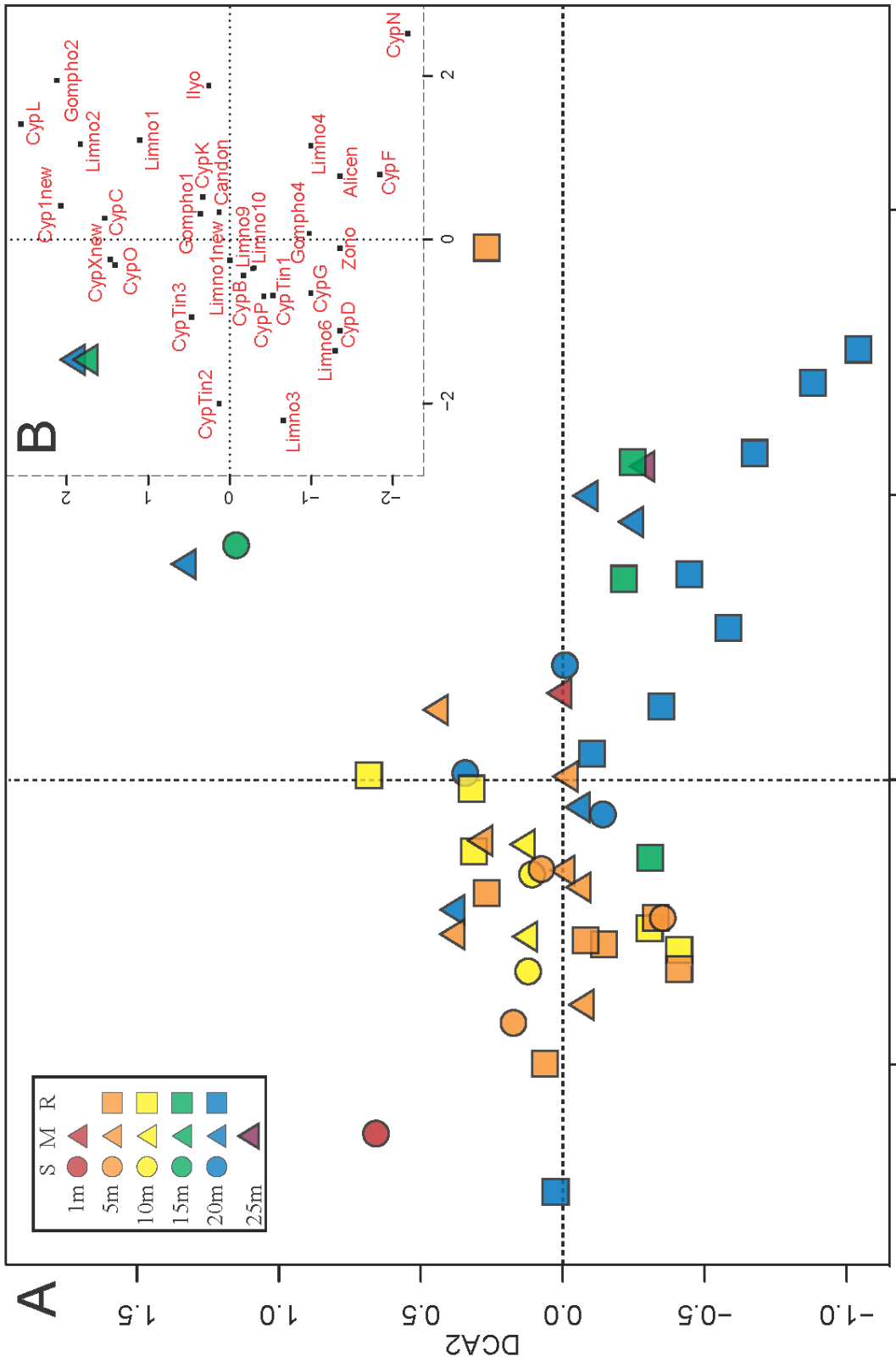
A
B
DCA1
DCA2
S M R
1m
5m
10m
15m
20m
25m
CypL
Gompho2
Cyp1new
Limno2
Limno1
Ilyo
CypXnew
CypC
CypK
Gompho1
Candon
CypO
Limno1new
Limno9
Limno10
CypTin3
CypB
CypP
CypTin1
Gompho4
Limno4
Alicen
CypTin2
Limno3
Limno6
CypG
CypD
Zonio
CypF
CypN

Figure B-12. Detrended Correspondence Analysis (DCA) on all ostracode species found at more than one site, and at all sites with a total number of ostracodes > 5. A. Biplot of site score values on DCA1 and DCA2. Sites that cluster have similar ostracode species assemblages. Each site is color coded by depth and symbol-coded by environment (S = High Relief Sand, M = Low Relief Marsh, R = Low Relief River. B. Bi-plot of species scores on the same axes (DCA1 and DCA2). Species that cluster are more likely to be found in the same sample.

Plates 1-7. Examples of ostracode species found in modern sediments of the SW arm of Lake Malawi. Scale bar applies to all images unless otherwise noted. Carapaces in dorsal or ventral view are oriented with the anterior end pointed in the up direction.

Plate 1. *Cypridopsine n.gen. sp.A* (A-C), *Cypridopsine n.gen. sp.B* (D-E), *Cypridopsine n.gen. sp.D* (F), *Cypridopsine n.gen. sp.C* (G-I), *Cypridopsine n.gen. sp.F* (J-K). A. Right valve, external view, Site 53. B. Carapace, dorsal view, juvenile, Site 78. C. Carapace, left lateral view, juvenile, Site 78. D. Right valve, external view, Site 142. E. Carapace, dorsal view, Site 141. F. Left valve, external view, Site 133. G. Right valve, external view, female, Site 5. H. Carapace, ventral view, Site 5. I. Carapace, dorsal view, Site 5. J. Right valve, external view, Site 133. K. Left valve, external view, juvenile, Site 141.

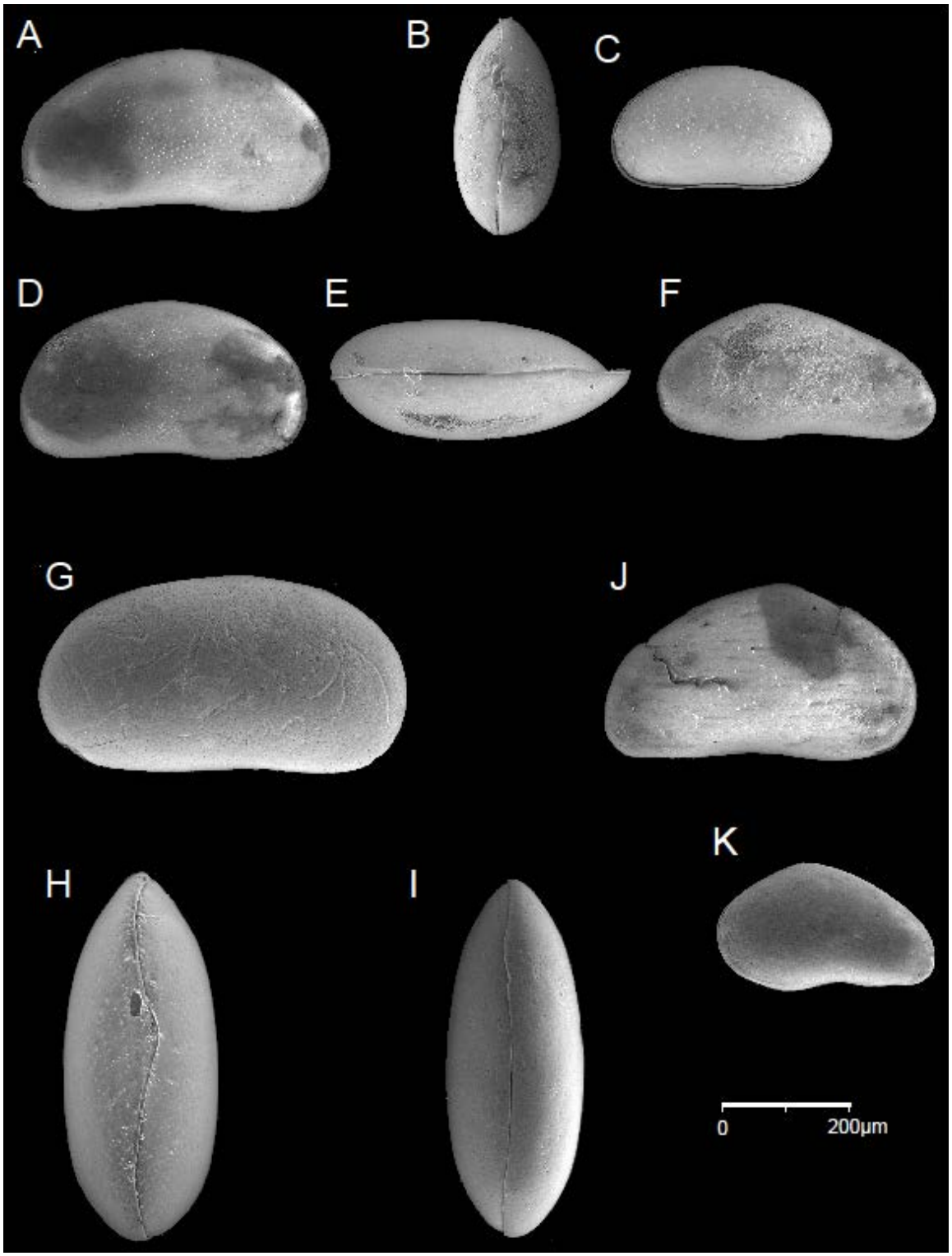
A
B
C
D
E
F
G
J
K
H
I
0
200µm

Plate 2. Examples of ostracode species found in modern sediments of the SW arm of Lake Malawi. *Cypridopsine n.gen. sp.G* (A-B). *Cypridopsine n.gen. sp.K* (C-E). *Cypridopsine n.gen. sp.L* (F-H). *Cypridopsine n.gen. sp.N* (I-L). A. Right valve, external view, Site 83. B. Right valve, internal view, Site 83. C. Left valve, external view, Site 5. D. Right valve, internal view, Site 45. E. Carapace, dorsal view, Site 45. F. Carapace, dorsal view, Site 142. G. Right valve, external view, Site 142. H. Carapace, left lateral view, Site 5. I. Left valve, external view, detail of irregularly shaped nodes – scale below applies only to this image. J. Left valve, external view, Site 133. K. Right valve, internal view, Site 133. L. Carapace, dorsal view, Site 137.

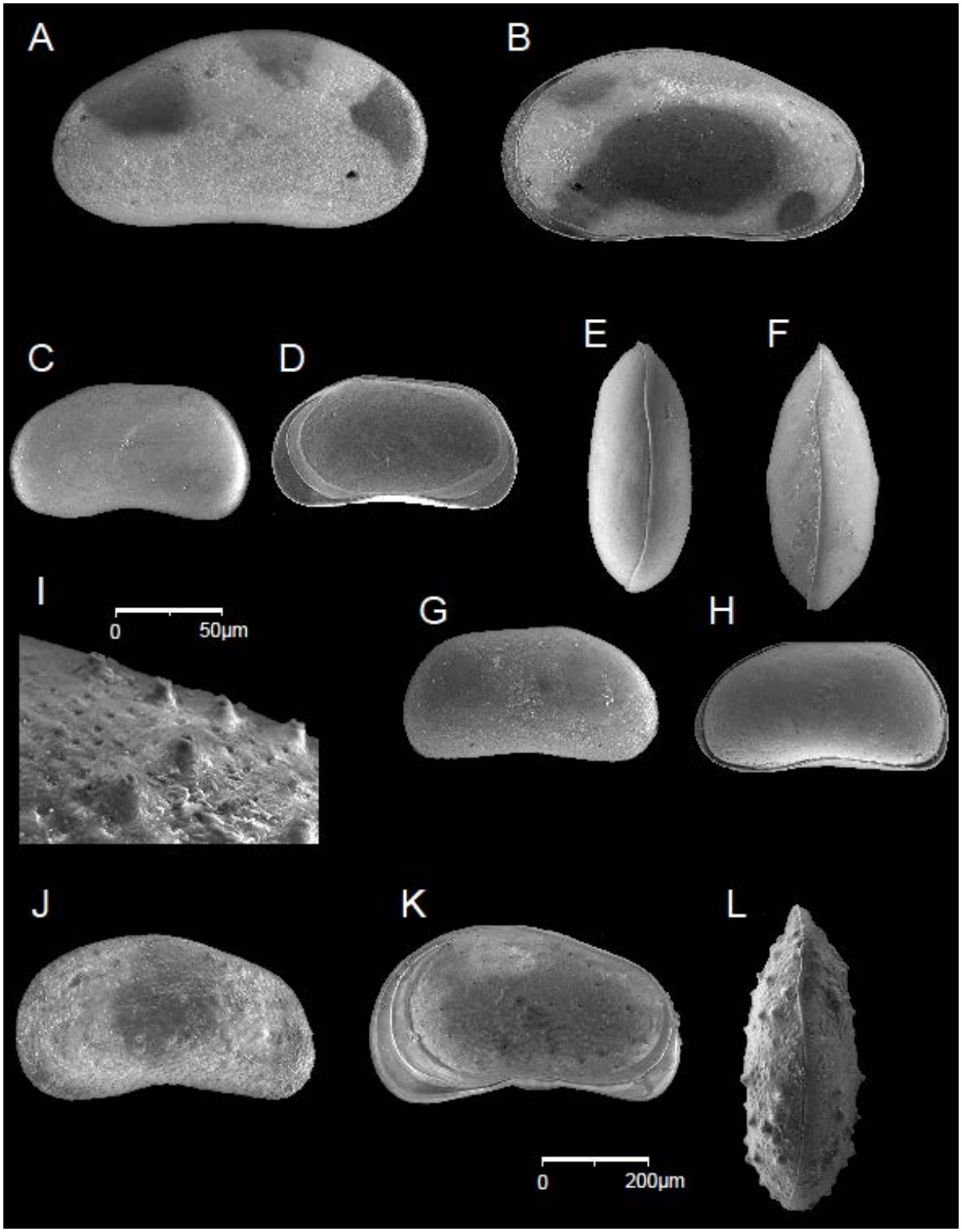
A
B
C
D
E
F
I
0
50µm
G
H
J
K
L
0
200µm

Plate 3. Examples of ostracode species found in modern sediments of the SW arm of Lake Malawi. *Cypridopsine n.gen. sp.O* (A-C). *Cypridopsine n.gen. sp.P* (D-F). *Cypridopsine n.gen. sp.X n.sp.* (G-H). *Cypridopsine n.gen. sp.1* (I-L). A. Right valve, external view, Site 133. B. Right valve, internal view, juvenile, Site 133. C. Carapace, dorsal view, Site 92. D. Left valve, external view, Site 5. E. Left view, internal view, juvenile, Site 132. F. Carapace, dorsal view, Site 90. G. Right valve, external view, Site 142. H. Carapace, left lateral view, Site 142. I. Right valve, external view, Site 102. J. Carapace, dorsal view, Site 102. K. Left valve, internal view, Site 105.

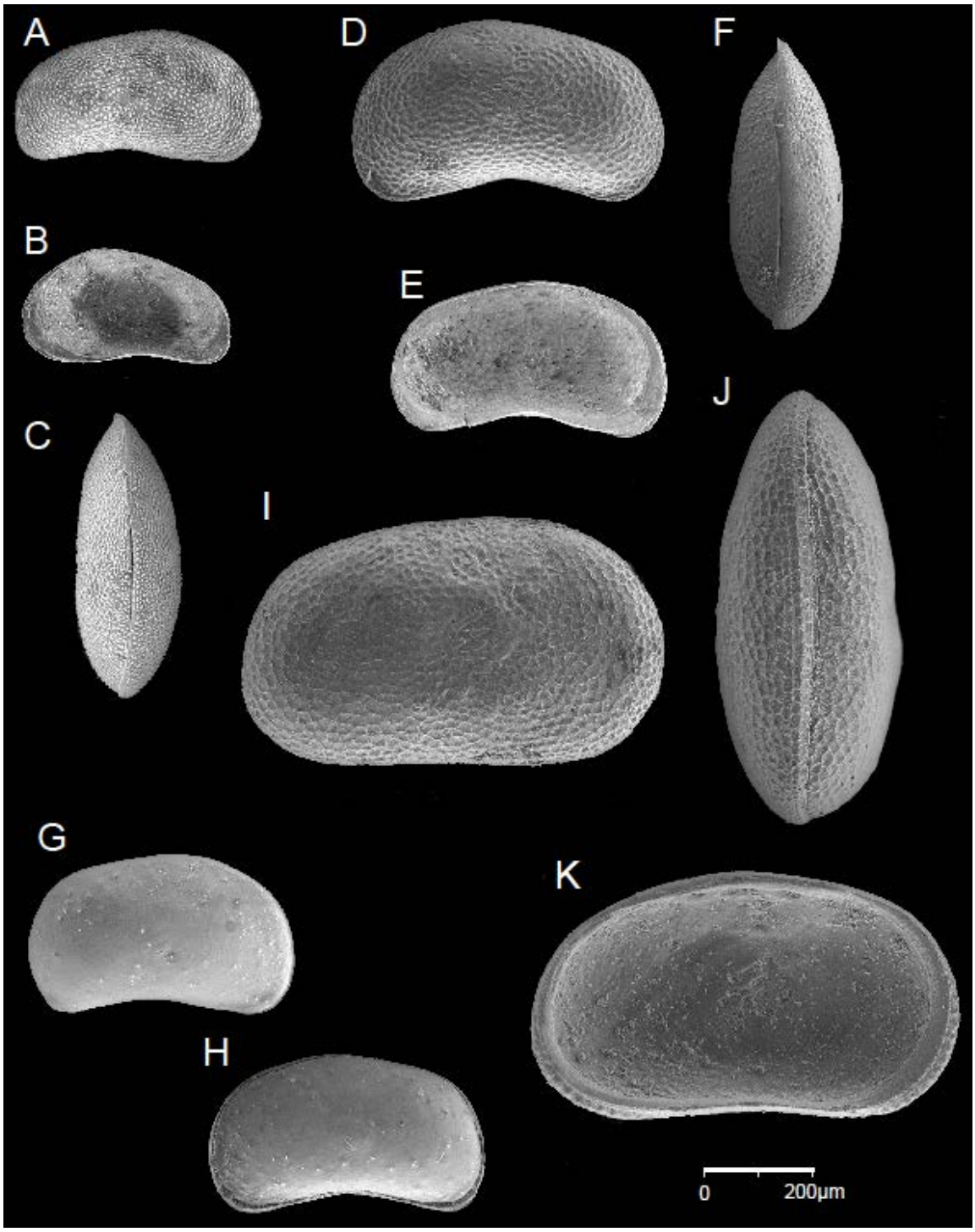
A
D
F
B
E
C
J
I
G
K
H
0
200µm

Plate 4. Examples of ostracode species found in modern sediments of the SW arm of Lake Malawi. *Cyprinotinae n.gen. sp.1* (A-C), *Cyprinotinae n.gen. sp.2* (D-G), *Cyprinotinae n.gen. sp.3* (H-J). A. Right valve, external view, juvenile, Site 35. B. Right valve, internal view, Site 23. C. Left valve, external view, juvenile, Site 35. D. Right valve, external view, Site 35. E. Right valve, internal view, Site 83. F. Carapace, dorsal view, site 94. G. Carapace, ventral view, Site 94. H. Carapace, dorsal view, Site 102. I. Left valve, external view, Site 36. J. Left valve, internal view, Site 23.

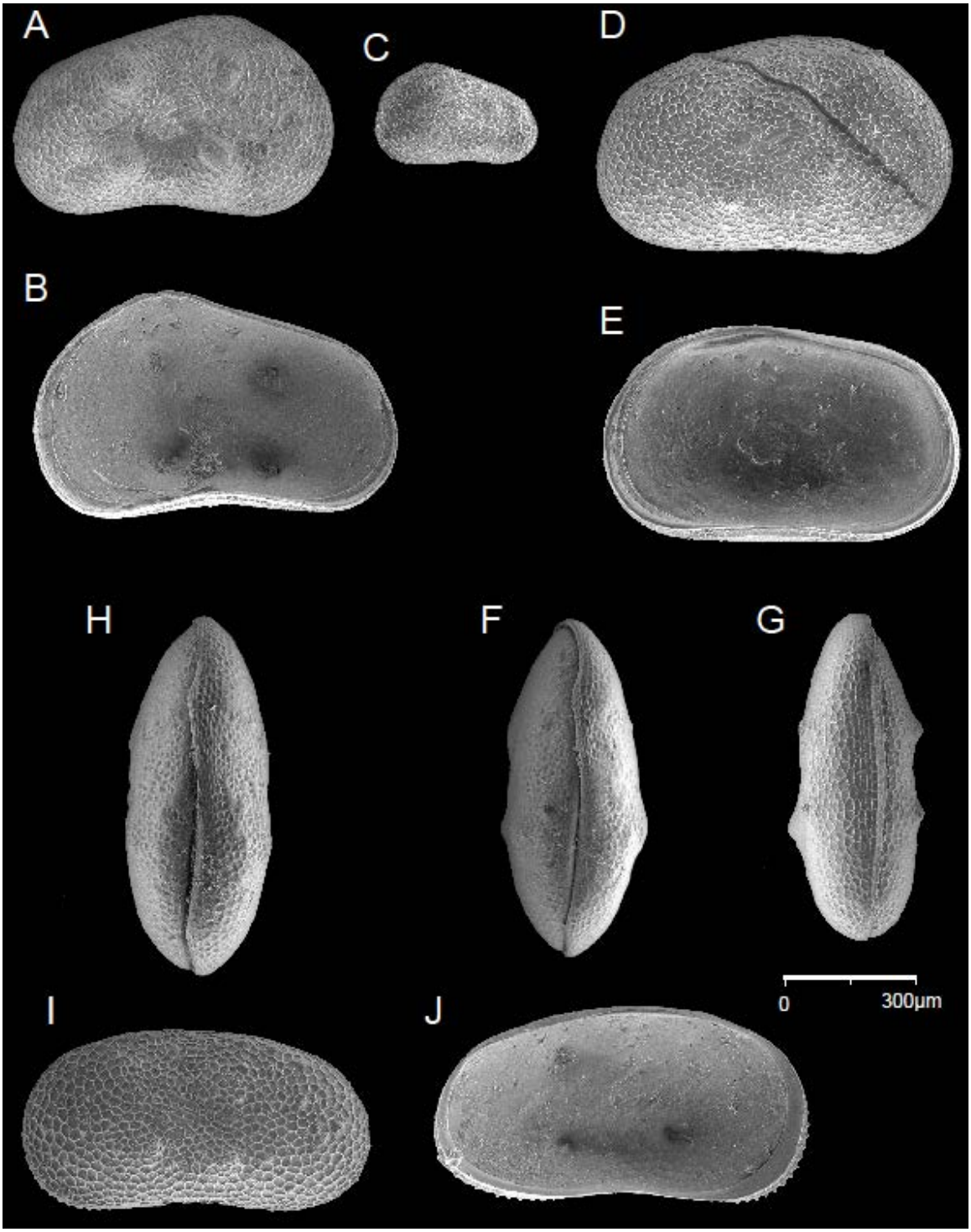
A
C
D
B
E
H
F
G
0
300µm
I
J

Plate 5. Examples of ostracode species found in modern sediments of the SW arm of Lake Malawi. *Gomphocythere emrysi* (A-D), *Gomphocythere irvinei* (E-G), *Gomphocythere huwi* (H-J). A. Right valve, external view, female, Site 94. B. Left valve, ventral view, male, juvenile, Site 83. C. Right valve, external view, male, juvenile, Site 89. D. Carapace, dorsal view, female, Site 141. E. Right valve, ventral view, female, Site 118. F. Right valve, external view, female, Site 118. G. Carapace, dorsal view, male, Site 36. H. Right valve, dorsal view, female, Site 83. I. Left valve, external view, female, juvenile, Site 83. J. Right valve, external view, female, Site 83.

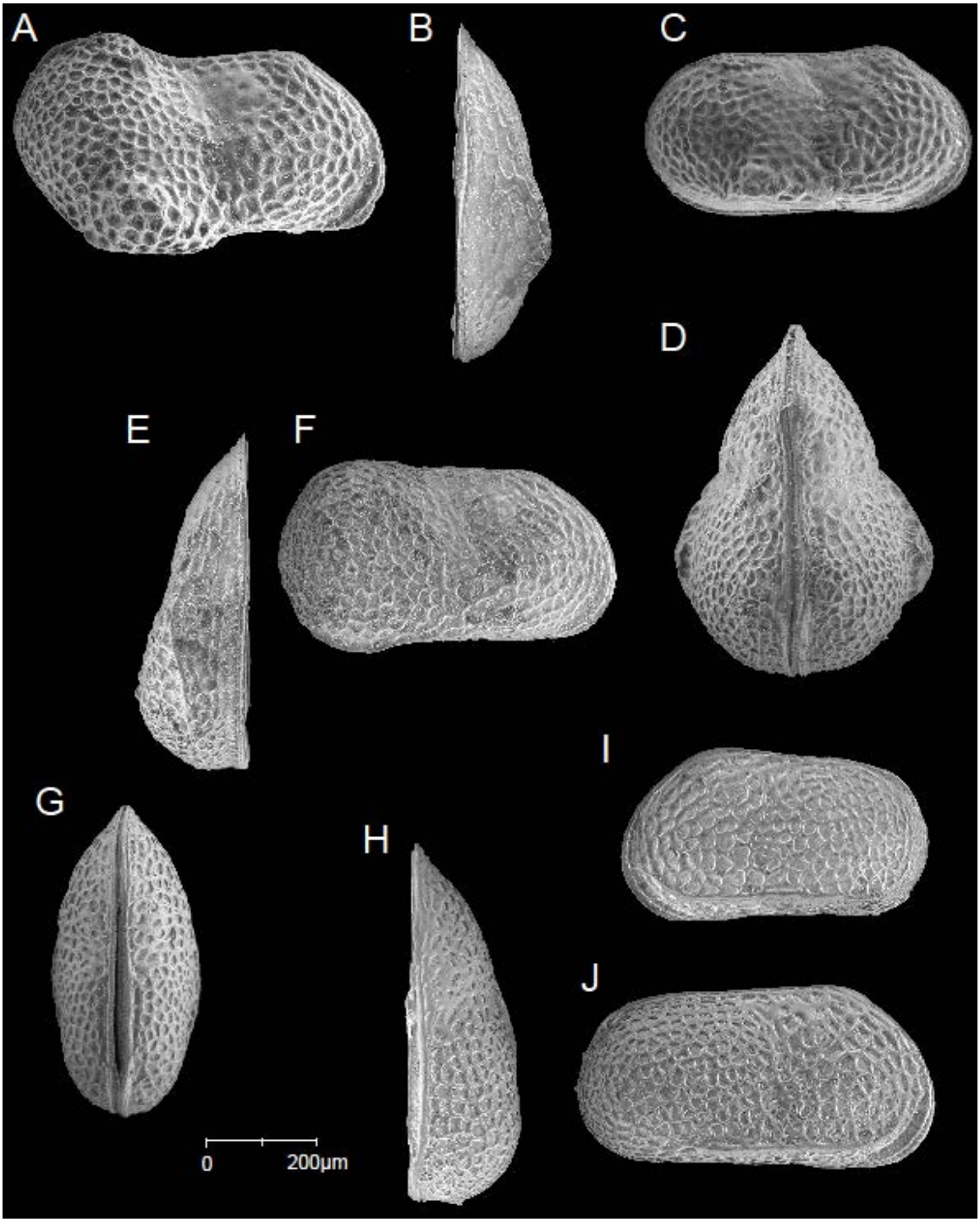
A
B
C
D
E
F
G
H
I
J
0
200µm

Plate 6. Examples of ostracode species found in modern sediments of the SW arm of Lake Malawi. *Alicenula serricaudata* (A-C), *Candonopsis sp.* (D-E), *Ilyocypris sp.1* (F-I), *Zonocypris costata* (J-L). A. Left valve, external view, Site 36. B. Right valve, internal view, Site 36. C. Carapace, dorsal view, juvenile, Site 110. D. Right valve, external view, Site 83. E. Right valve, internal view, Site 83. F. Left valve, external view, Site 34. G. Carapace, dorsal view, Site 134. H. Carapace, ventral view, Site 134. I. Left valve, internal view, Site 133. J. Right valve, external view, Site 136. K. Carapace, dorsal view, Site 36. L. Carapace, ventral view, Site 35.

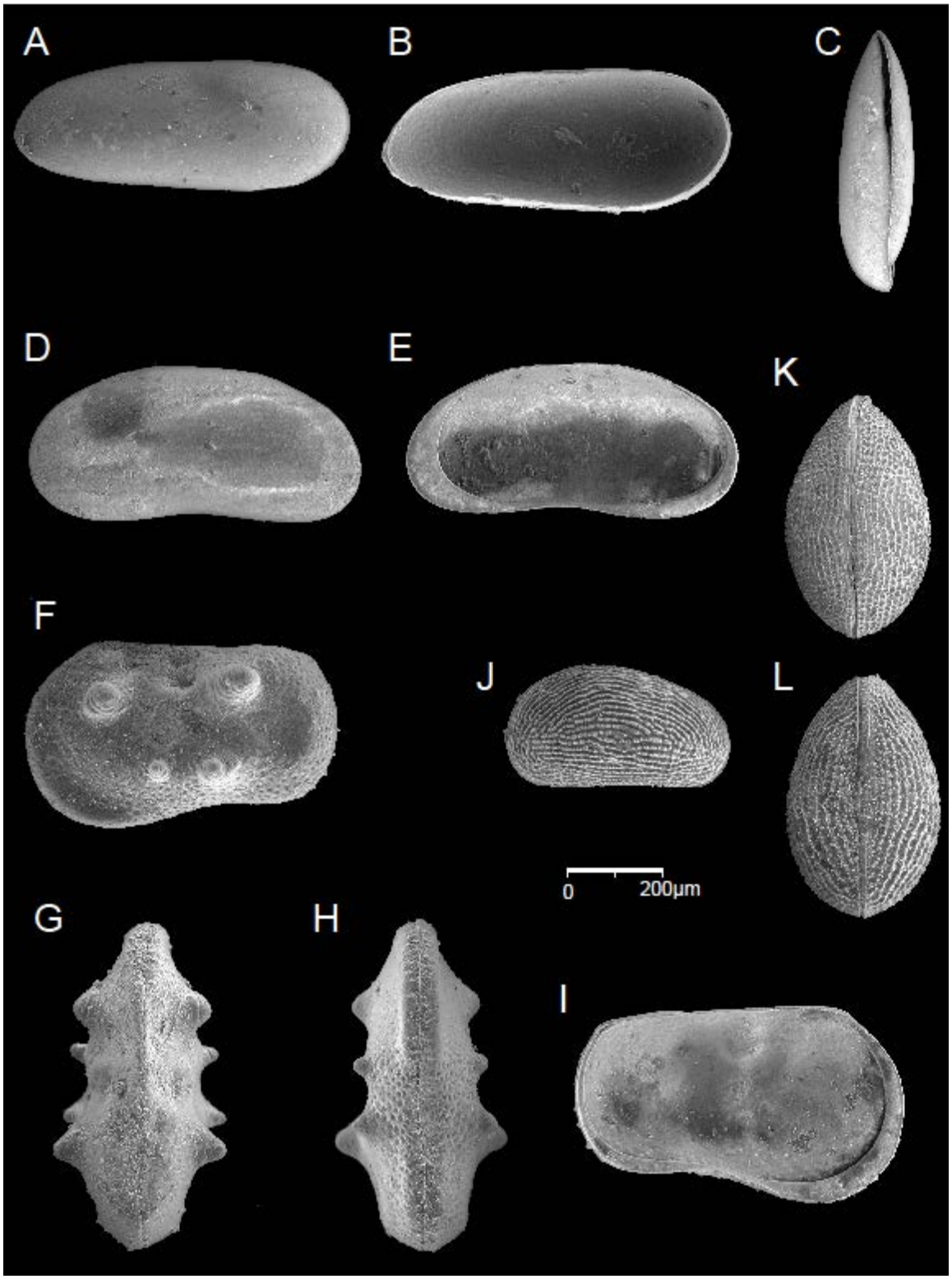
A
B
C
D
E
K
F
J
L
0
200µm
G
H
I

Plate 7. Examples of ostracode species found in modern sediments of the SW arm of Lake Malawi. *Limnocythere s.l. sp.1* (A-F). *Limnocythere s.l. sp.2* (G-H). *Limnocythere s.l. sp.3* (I-J). *Limnocythere s.l. sp.4* (K-L). *Limnocythere s.l. sp.6* (M-N). *Limnocythere s.l. sp.8* (O). A. Left valve, external view, male, Site 23. B. Left valve, external view, female, Site 32. C. Carapace, dorsal view, female, Site 33. D. Left valve, external view, male, juvenile, Site 133. E. Left valve, internal view, female, Site 32. F. Left valve, external view, female, juvenile, Site 80. G. Left valve, external view, female, Site 35. H. Carapace, dorsal view, male, Site 35. I. Carapace, ventral view, female, Site 92. J. Left valve, external view, female, Site 91. K. Right valve, external view, female, Site 92. L. Carapace, dorsal view, male?, Site 133. M. Left valve, external view, male, Site 3. N. Left valve, internal view, male, juvenile, Site 83. O. Right valve, external view, male, Site 105.

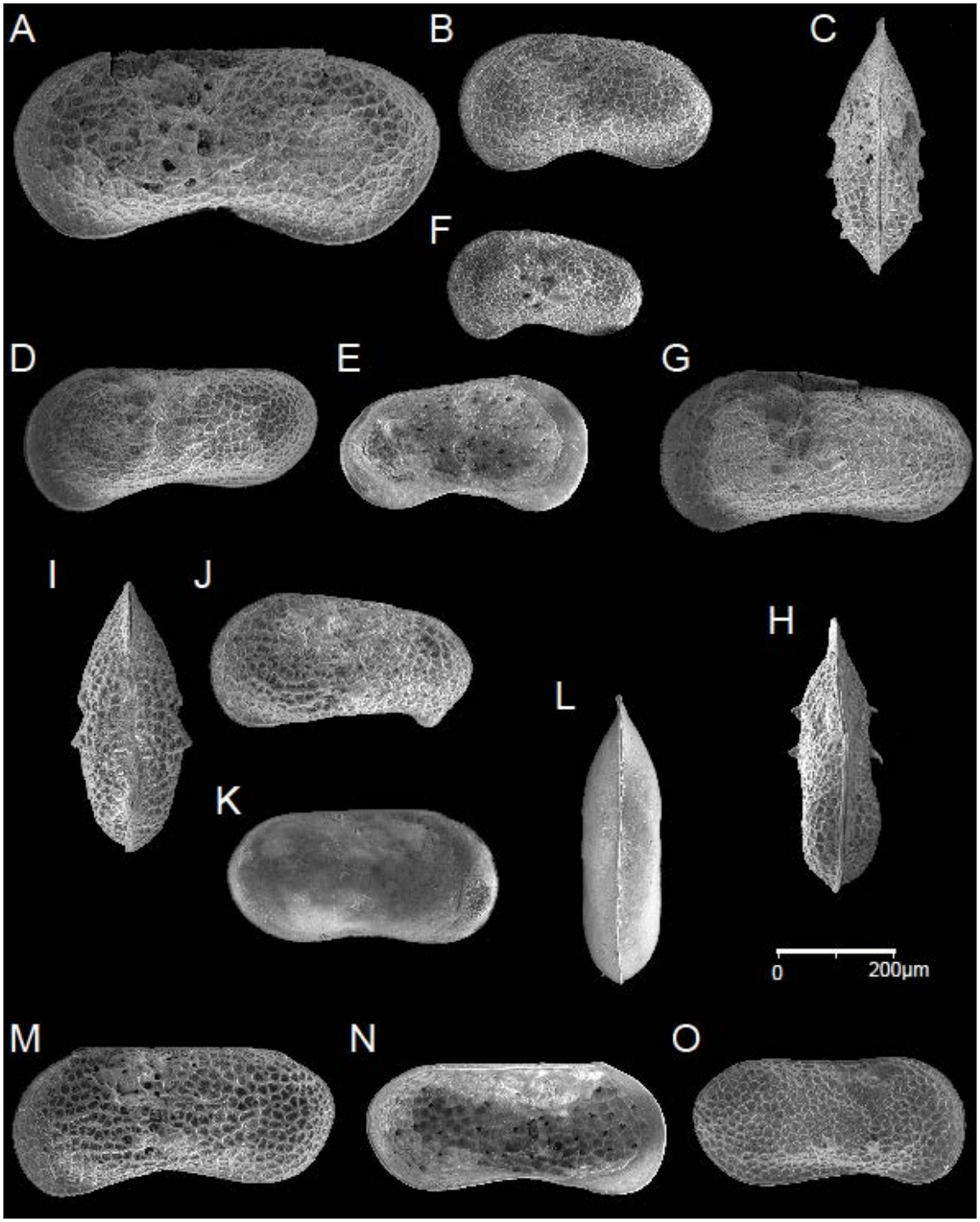
A
B
C
F
D
E
G
I
J
H
L
K
0
200µm
M
N
O

Plate 8. Examples of ostracode species found in modern sediments of the SW arm of Lake Malawi. *Limnocythere s.l. sp.9* (A-C). *Limnocythere s.l. sp.10* (D-F). *Limnocythere s.l. sp.A n.sp.* (G-K). *Limnocythere s.l. sp.B n.sp.* (L). A. Left valve, external view, female, Site 55. B. Carapace, dorsal view, female, Site 90. C. Left valve, external view, female, juvenile, Site 105. D. Left valve, external view, male, Site 138. E. Left valve, internal view, male, Site 90. F. Left valve, external view, male, juvenile, Site 132. G. Right valve, external view, male, Site 90. H. Left valve, internal view, male, Site 90. I. Right valve, external view, female, Site 92. J. Left valve, internal view, female, Site 92. K. Left valve, external view, female, juvenile, Site 106. L. Right valve, external view, female?, Site 133.

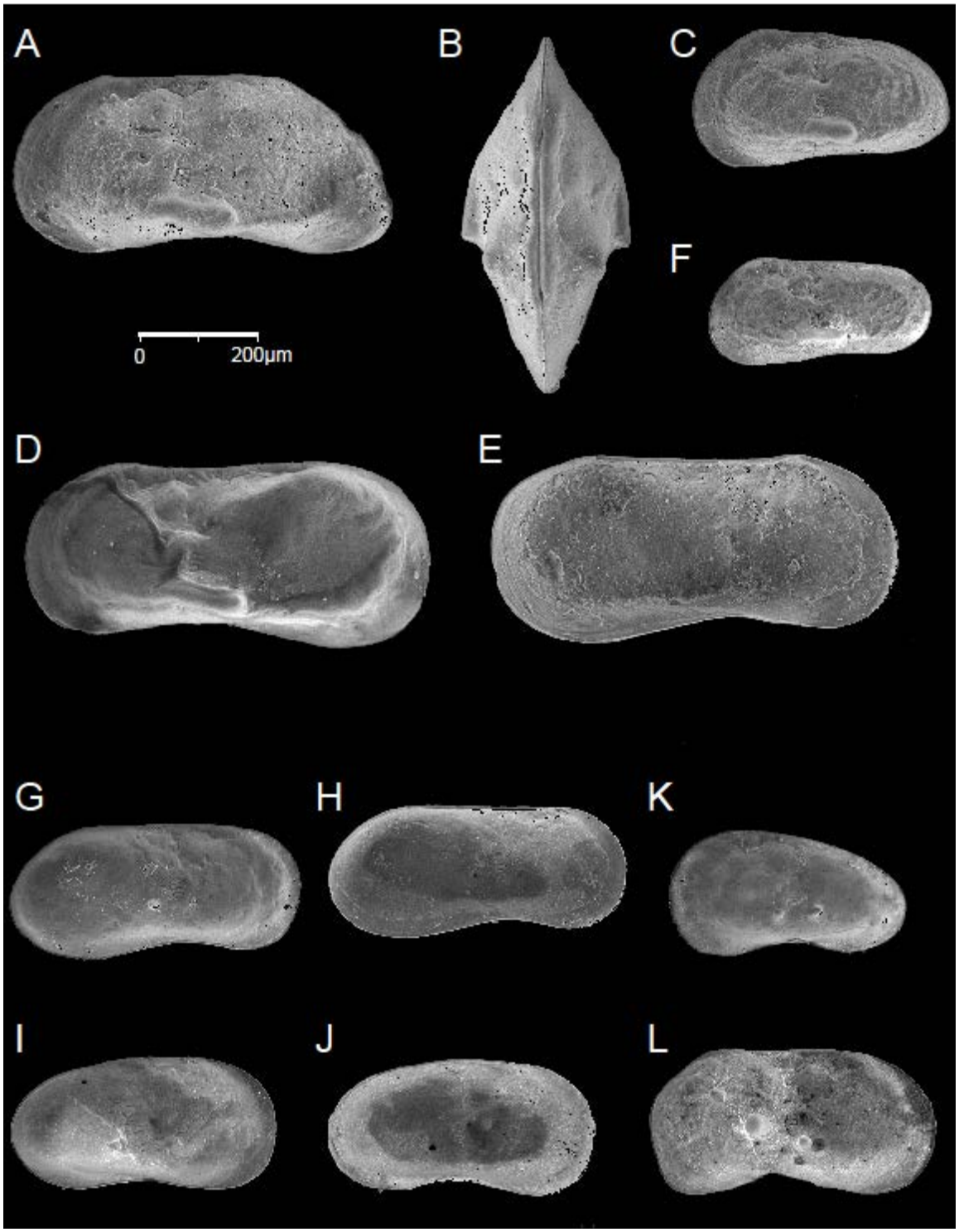
A
B
C
F
0
200µm
D
E
G
H
K
I
J
L

Sample	Locality	Shore Environment	Transect	Depth(m)	Adj Depth(m)	Lat	Long
2	Cape Maclear Bay	HR - Sand	F	9.5	10	-14.020	34.841
3	Cape Maclear Bay	HR - Sand	F	4.7	5	-14.019	34.842
4	Cape Maclear Bay	HR - Sand	F	1	1	-14.023	34.842
5	Cape Maclear Bay	HR - Sand	F	14.9	15	-14.021	34.840
6	Cape Maclear Bay	HR - Sand	F	19.7	20	-14.020	34.839
7	Cape Maclear Bay	HR - Sand	F	24.9	25	-14.019	34.837
8	Cape Maclear Bay	HR - Sand	F	29.7	30	-14.018	34.834
9	Cape Maclear Bay	HR - Sand	F	34.8	35	-14.018	34.830
10	Cape Maclear Bay	HR - Sand	F	39.8	40	-14.014	34.829
11	Cape Maclear Bay	HR - Sand	F	45.1	45	-14.012	34.827
12	Cape Maclear Bay	HR - Sand	F	49.9	50	-14.010	34.825
13	Cape Maclear Bay	HR - Sand	F	54.8	55	-14.009	34.824
14	Cape Maclear Bay	HR - Sand	F	60	60	-14.006	34.823
15	Cape Maclear Bay	HR - Sand	G	60	60	-13.996	34.829
16	Cape Maclear Bay	HR - Sand	G	54.8	55	-14.000	34.830
17	Cape Maclear Bay	HR - Sand	G	49.9	50	-14.003	34.832
18	Cape Maclear Bay	HR - Sand	G	44.9	45	-14.005	34.834
19	Cape Maclear Bay	HR - Sand	G	40.1	40	-14.008	34.834
20	Cape Maclear Bay	HR - Sand	G	35.1	35	-14.010	34.836
21	Cape Maclear Bay	HR - Sand	G	30.1	30	-14.011	34.840
22	Cape Maclear Bay	HR - Sand	G	25.1	25	-14.012	34.842
23	Cape Maclear Bay	HR - Sand	G	19.8	20	-14.014	34.844
28	Off Malembo	LR - Marsh	A	59.9	60	-14.190	34.742
29	Off Malembo	LR - Marsh	A	49.9	50	-14.191	34.734
30	Off Malembo	LR - Marsh	A	39.9	40	-14.221	34.747

Sample	Locality	Shore Environment	Transect	Depth(m)	Adj Depth(m)	Lat	Long
31	Off Malembo	LR - Marsh	A	29.8	30	-14.221	34.743
32	Off Malembo	LR - Marsh	A	24.9	25	-14.223	34.743
33	Off Malembo	LR - Marsh	A	20	20	-14.224	34.743
34	Off Malembo	LR - Marsh	A	15	15	-14.235	34.744
35	Off Malembo	LR - Marsh	A	9.9	10	-14.242	34.746
36	Off Malembo	LR - Marsh	A	5.1	5	-14.267	34.752
37	Off Malembo	LR - Marsh	A	1.2	1	-14.276	34.753
38	Mangombo Bay	LR - River	C	60	60	-14.113	34.805
39	Mangombo Bay	LR - River	C	50	50	-14.120	34.815
40	Mangombo Bay	LR - River	C	40	40	-14.123	34.818
41	Mangombo Bay	LR - River	C	30	30	-14.127	34.822
42	Mangombo Bay	LR - River	C	24.8	25	-14.129	34.825
43	Mangombo Bay	LR - River	C	20.1	20	-14.130	34.827
44	Mangombo Bay	LR - River	C	15.1	15	-14.131	34.828
45	Mangombo Bay	LR - River	C	10.1	10	-14.131	34.829
46	Mangombo Bay	LR - River	C	5	5	-14.131	34.829
47	Mangombo Bay	LR - River	C	0.9	1	-14.132	34.829
48	N. Mangombo Bay	HR - Sand	E	60	60	-14.085	34.832
49	N. Mangombo Bay	HR - Sand	E	49.9	50	-14.087	34.840
50	N. Mangombo Bay	HR - Sand	E	40	40	-14.088	34.843
51	N. Mangombo Bay	HR - Sand	E	30	30	-14.088	34.845
53	N. Mangombo Bay	HR - Sand	E	20	20	-14.086	34.848
55	N. Mangombo Bay	HR - Sand	E	10	10	-14.088	34.852
56	N. Mangombo Bay	HR - Sand	E	5	5	-14.088	34.853
57	N. Mangombo Bay	HR - Sand	E	1	1	-14.087	34.853
78	Pumulani Bay	HR - Sand	ZE5	5	5	-14.106	34.862

Sample	Locality	Shore Environment	Transect	Depth(m)	Adj Depth(m)	Lat	Long
79	Pumulani Bay	HR - Sand	ZE1	1	1	-14.105	34.863
80	Pumulani Bay	LR - River	ZD5	4.9	5	-14.109	34.864
82	Pumulani Bay	LR - River	ZD5	5	5	-14.119	34.852
83	Pumulani Bay	LR - River	ZD5	4.9	5	-14.116	34.849
86	Pumulani Bay	LR - River	D	40	40	-14.104	34.839
87	Pumulani Bay	LR - River	D	50	50	-14.101	34.832
88	Pumulani Bay	LR - River	D	60	60	-14.099	34.828
89	N of Malembo	LR - Marsh	B	20	20	-14.177	34.796
90	N of Malembo	LR - Marsh	B	10	10	-14.177	34.797
91	N of Malembo	LR - Marsh	B	5	5	-14.178	34.805
92	N of Malembo	LR - Marsh	ZB5	5	5	-14.182	34.804
94	N of Malembo	LR - Marsh	ZB5	5	5	-14.173	34.806
97	N of Malembo	LR - Marsh	B	30	30	-14.173	34.794
98	N of Malembo	LR - Marsh	B	40	40	-14.169	34.789
99	N of Malembo	LR - Marsh	B	49.9	50	-14.166	34.782
100	N of Malembo	LR - Marsh	B	60	60	-14.163	34.779
101	N of Malembo	LR - Marsh	ZB40	40	40	-14.174	34.786
105	Off Malembo	LR - Marsh	ZA5	5	5	-14.263	34.758
106	Off Malembo	LR - Marsh	ZA5	5	5	-14.258	34.768
107	Off Malembo	LR - Marsh	ZA5	5.2	5	-14.245	34.773
109	Off Malembo	LR - Marsh	ZA20	20	20	-14.222	34.774
110	Off Malembo	LR - Marsh	ZA20	20	20	-14.224	34.768
111	Off Malembo	LR - Marsh	ZA20	20	20	-14.226	34.764
112	Off Malembo	LR - Marsh	ZA20	20	20	-14.226	34.758
113	Off Malembo	LR - Marsh	ZA20	20	20	-14.223	34.739
114	Off Malembo	LR - Marsh	ZA50	50	50	-14.210	34.739
115	Off Malembo	LR - Marsh	ZA50	50	50	-14.214	34.752
116	Off Malembo	LR - Marsh	ZA50	50	50	-14.214	34.758
117	Off Malembo	LR - Marsh	ZA50	50	50	-14.212	34.763
118	Mangombo Bay	LR - River	ZC20	20	20	-14.140	34.814
119	Mangombo Bay	LR - River	ZC5	5	5	-14.140	34.815

Sample	Locality	Shore Environment	Transect	Depth(m)	Adj Depth(m)	Lat	Long
120	Mangombo Bay	LR - River	ZC5	5	5	-14.137	34.817
121	Mangombo Bay	LR - River	ZC20	20	20	-14.134	34.818
122	Mangombo Bay	LR - River	ZC20	20	20	-14.124	34.832
123	Mangombo Bay	LR - River	ZC5	5.1	5	-14.124	34.832
124	Mangombo Bay	LR - River	ZC20	20	20	-14.119	34.837
125	Mangombo Bay	LR - River	ZC5	5	5	-14.120	34.838
127	Mangombo Bay	LR - River	ZC40	40	40	-14.131	34.811
128	Mangombo Bay	LR - River	ZC60	60	60	-14.126	34.796
131	Mangombo Bay	LR - River	A4	18.8976	20	-14.140	34.814
132	Mangombo Bay	LR - River	A4	17.9832	20	-14.140	34.815
133	Mangombo Bay	LR - River	A4	17.9832	20	-14.140	34.815
134	Mangombo Bay	LR - River	A4	15.3924	15	-14.140	34.815
135	Mangombo Bay	LR - River	A4	12.192	10	-14.140	34.816
136	Mangombo Bay	LR - River	A4	9.144	10	-14.140	34.816
137	Mangombo Bay	LR - River	A5	17.0688	15	-14.119	34.837
138	Mangombo Bay	LR - River	A5	16.764	15	-14.119	34.838
139	Mangombo Bay	LR - River	A5	17.6784	20	-14.119	34.838
140	Mangombo Bay	LR - River	A5	18.5928	20	-14.119	34.838
141	Mangombo Bay	LR - River	A5	11.5824	10	-14.119	34.839
142	Mangombo Bay	LR - River	A5	9.7536	10	-14.120	34.839

Table B-1. Listing of the site location information for each sample taken. “HR” = High Relief“, “LR” = Low Relief. Depth (m)” is the exact measured depth of each sample. “AdjDepth (m)” is the sample depth rounded to the nearest 5 meters, in order to be able to group depths as a categorical variable. All depths were within one-half meter, if taken by PONAR grab-sampler. Depths along SCUBA transects were more continuous between 20m and 5m depth, and are the samples most affected.

Depth	# Sites total	# Sites >5 cods	% Sites >5 cods
1	5	2	40.00
5	18	17	94.44
10	9	9	100.00
15	6	5	83.33
20	20	17	85.00
25	4	1	25.00
30	6	0	0.00
35	2	0	0.00
40	9	0	0.00
45	2	0	0.00
50	11	0	0.00
55	2	0	0.00
60	8	0	0.00

Shoreline Environment	# Sites total	# Sites >5 cods	% Sites >5 cods
High Relief - Sand	32	10	31.25
Low Relief - Marsh	32	18	56.25
Low Relief - River	38	23	60.53

Table B-2. Listing of the total number of sites sampled by depth (above) and shoreline environment (below), number of sites with more than 5 total ostracodes, and the percentage of total sites with more than 5 total ostracodes.

Sample	Transect	AdjDepth	Shore Env	Bottom Temp C	Bottom DO %	Sp. Cond µS/cm	% > Sand	% Sand	% Silt	% Clay	Wt%LOI 550C	Wt%LOI 1000C
2	F	10	HR - Sand	28.0	120			79.89	19.07	1.04	13.85	7.94
3	F	5	HR - Sand	28.3	115		2.12	88.72	8.78	0.39	5.43	2.14
4	F	1	HR - Sand	29.2	121.3		21.99	67.07	10.43	0.51	0.46	0.02
5	F	15	HR - Sand	27.2	39.5		2.87	93.48	3.50	0.15	1.18	0.40
6	F	20	HR - Sand	25.0	48.4		9.08	89.43	1.39	0.10	0.77	0.15
7	F	25	HR - Sand	24.5	69.1		17.45	66.32	14.22	2.01	1.28	0.09
8	F	30	HR - Sand				14.52	83.94	1.35	0.19	0.98	0.09
9	F	35	HR - Sand				2.38	95.16	1.99	0.48	1.42	0.16
10	F	40	HR - Sand				1.84	93.73	3.62	0.81	2.94	
11	F	45	HR - Sand					88.88	8.64	2.48	32.12	0.27
12	F	50	HR - Sand				0.09	93.62	5.10	1.18	28.03	0.38
13	F	55	HR - Sand				0.01	93.31	5.47	1.21	1.79	0.35
14	F	60	HR - Sand				0.12	90.33	7.73	1.82	2.19	0.63
15	G	60	HR - Sand				0.06	94.87	4.16	0.90	48.90	0.43
16	G	55	HR - Sand					91.01	6.74	2.26	1.51	0.22
17	G	50	HR - Sand				3.61	87.59	7.00	1.80	1.25	3.46
18	G	45	HR - Sand				0.12	91.74	6.41	1.73	0.91	0.12
19	G	40	HR - Sand				0.18	68.94	24.67	6.21	1.94	0.18
20	G	35	HR - Sand				0.37	86.55	10.43	2.64	1.09	0.15
21	G	30	HR - Sand				8.07	83.54	7.10	1.29	11.95	0.85
22	G	25	HR - Sand	24.1	79		13.93	53.07	29.98	3.02	5.55	0.57
23	G	20	HR - Sand	25.0	85		5.72	69.10	23.57	1.60	0.73	0.08
28	A	60	LR - Marsh					68.57	27.90	3.53	9.83	1.31
29	A	50	LR - Marsh				0.10	65.60	28.28	6.02	8.84	1.58
30	A	40	LR - Marsh					84.07	13.85	2.08	9.69	1.94
31	A	30	LR - Marsh				7.43	77.60	12.75	2.23	0.64	

Sample	Transect	AdjDepth	Shore Env	Bottom Temp C	Bottom DO %	Sp. Cond µS/cm	% > Sand	% Sand	% Silt	% Clay	Wt%LOI 550C	Wt%LOI 1000C
32	A	25	LR - Marsh	25.0	47.9		17.13	82.87			7.14	1.83
33	A	20	LR - Marsh	25.9	88	235.8	15.56	84.44			20.61	6.11
34	A	15	LR - Marsh	26.6	89		4.13	95.87			1.37	1.03
35	A	10	LR - Marsh	27.5	129.5		1.00	78.44	18.96	1.59	12.29	5.75
36	A	5	LR - Marsh	28.2	99.7		32.88	67.12			3.17	8.79
37	A	1	LR - Marsh	31.0	135.3	247.8		26.99	68.58	4.43	14.37	24.23
38	C	60	LR - River					72.09	23.03	4.88	11.02	1.47
39	C	50	LR - River					31.61	57.25	11.14	12.19	1.65
40	C	40	LR - River					8.18	74.41	17.40	9.67	1.40
41	C	30	LR - River					5.58	76.33	18.09	13.44	1.65
42	C	25	LR - River	25.0	20.6	240.3		9.54	75.08	15.38	14.03	1.36
43	C	20	LR - River	27.0	42			9.92	72.47	17.60	12.14	1.55
44	C	15	LR - River	27.8	115.5	235	0.35	65.76	29.13	4.76	4.47	0.60
45	C	10	LR - River	28.4	85		0.39	88.71	9.53	1.37	1.58	0.61
46	C	5	LR - River	29.5	122.8		0.14	92.00	6.39	1.48	0.33	
47	C	1	LR - River	30.3	133.5		2.23	77.86			0.16	0.03
48	E	60	HR - Sand					100.00			5.53	
49	E	50	HR - Sand					100.00			2.23	*74.35
50	E	40	HR - Sand					100.00			1.69	
51	E	30	HR - Sand				4.16	85.67			0.57	5.88
53	E	20	HR - Sand	27.3	92.3		3.37	78.98	16.70	0.95	3.93	0.41
55	E	10	HR - Sand	28.5	129			94.37	5.40	0.23	6.74	2.54
56	E	5	HR - Sand	28.8	147		0.16	89.93	9.64	0.27	28.98	12.31
57	E	1	HR - Sand	30.3	120		2.92	97.08			0.72	0.21
78	ZE5	5	HR - Sand	30.2	147			100.00			17.06	10.37
79	ZE1	1	HR - Sand	30.3	120		25.64	86.95			0.25	
80	ZE5	5	LR - River	30.2	147		2.44	94.55	2.93	0.08	9.01	7.81

Sample	Transect	AdjDepth	Shore Env	Bottom Temp C	Bottom DO %	Sp. Cond µS/cm	% > Sand	% Sand	% Silt	% Clay	Wt%LOI 550C	Wt%LOI 1000C
82	ZE5	5	LR - River	30.2	147		0.04	72.34	25.83	1.79	14.04	11.28
83	ZE5	5	LR - River	30.2	147			86.12	13.29	0.59	3.21	2.22
86	D	40	LR - River				1.64	80.38	14.57	3.41	2.02	0.28
87	D	50	LR - River				4.11	43.80	36.25	15.84	2.14	0.48
88	D	60	LR - River				0.03	91.63	6.98	1.36	2.87	0.40
89	B	20	LR - Marsh	27.8	109.3			85.36	13.37	1.27	0.88	0.09
90	B	10	LR - Marsh	27.9	113.8			82.51	16.95	0.54	1.49	0.78
91	B	5	LR - Marsh	28.7	126.6			92.50	7.28	0.22	6.58	5.11
92	ZB5	5	LR - Marsh	28.7	126.6		4.58	92.38	2.95	0.09	10.27	7.89
94	ZB5	5	LR - Marsh	28.7	126.6			88.99			0.81	0.41
97	B	30	LR - Marsh					83.17	14.15	2.68	1.40	0.19
98	B	40	LR - Marsh					81.32	16.00	2.68	7.60	0.80
99	B	50	LR - Marsh				0.34	74.92	19.75	5.00	5.02	1.27
100	B	60	LR - Marsh					27.04	66.56	6.40	18.18	1.82
101	ZB40	40	LR - Marsh					78.81	17.36	3.82	1.39	0.34
105	ZA5	5	LR - Marsh	28.2	99.7		0.23	92.29	12.50	0.71	1.53	0.80
106	ZA5	5	LR - Marsh	28.2	99.7			99.50	7.27	0.40	15.35	12.45
107	ZA5	5	LR - Marsh	28.2	99.7		0.87	99.77			4.82	5.06
109	ZA20	20	LR - Marsh	25.9	88		5.78	86.08	7.31	0.82	0.89	1.67
110	ZA20	20	LR - Marsh	25.9	88		15.42	55.26	26.98	2.33	1.08	0.09
111	ZA20	20	LR - Marsh	25.9	88		5.11	78.90	14.55	1.44	1.33	0.17
112	ZA20	20	LR - Marsh	25.9	88		1.17	86.64	10.71	1.48	1.26	0.04
113	ZA20	20	LR - Marsh	25.9	88		5.00	69.23	22.57	3.20	0.50	0.03
114	ZA50	50	LR - Marsh					24.70			14.29	
115	ZA50	50	LR - Marsh				0.16	75.24	21.59	3.01	4.88	0.80
116	ZA50	50	LR - Marsh					82.49	14.81	2.70	3.03	0.64
117	ZA50	50	LR - Marsh					84.19	14.57	1.24	2.61	0.71

Sample	Transect	AdjDepth	Shore Env	Bottom Temp C	Bottom DO %	Sp. Cond µS/cm	% > Sand	% Sand	% Silt	% Clay	Wt%LOI 550C	Wt%LOI 1000C
118	ZC20	20	LR - River	27.0	42		0.10	79.45	17.93	2.51	2.91	0.48
119	ZC5	5	LR - River	29.5	122.8		1.56	97.43	0.96	0.06	1.45	0.84
120	ZC5	5	LR - River	29.5	122.8		0.10	88.95			2.13	0.72
121	ZC20	20	LR - River	27.0	42			84.28	13.75	1.98	1.28	0.44
122	ZC20	20	LR - River	27.0	42		0.12	73.18	21.92	4.78	5.20	1.02
123	ZC5	5	LR - River	29.5	122.8		1.47	71.94	21.33	5.27	3.29	0.56
124	ZC20	20	LR - River	27.0	42		0.11	80.27	18.30	1.32	2.65	0.33
125	ZC5	5	LR - River	29.5	122.8			96.86	2.95	0.20	1.66	0.70
127	ZC40	40	LR - River				1.12	33.95	54.23	10.70	7.06	1.05
128	ZC60	60	LR - River				0.65	65.70	29.51	4.14	7.18	1.17
131	A4	20	LR - River	27.2	42			79.71	18.27	2.02	2.70	0.76
132	A4	20	LR - River	27.2				91.46	7.83	0.72	3.38	1.12
133	A4	20	LR - River	27.2				85.89	12.53	1.58	3.00	3.16
134	A4	15	LR - River	27.2				85.27	13.40	1.33	8.61	7.41
135	A4	10	LR - River	27.2				86.99	11.84	1.17	11.75	12.61
136	A4	10	LR - River	27.2			0.75	88.52	9.92	0.81	3.09	3.34
137	A5	15	LR - River	27.2	42			93.07	6.05	0.87	1.77	0.28
138	A5	15	LR - River	27.2			0.22	99.78			1.80	0.32
139	A5	20	LR - River	27.2			0.54	99.46			1.82	0.26
140	A5	20	LR - River	27.2				85.90	12.14	1.96	1.77	0.29
141	A5	10	LR - River	27.2			1.51	65.82	28.10	4.58	0.82	0.18
142	A5	10	LR - River	27.2			1.71	93.82	3.91	0.56	0.70	0.24

Table B-3 part 1. List of all data discussed in the text, sorted by sample number, with associated transect, adjusted depth and shoreline environment included. Zeros have been removed for readability.

Sample	Tot. Fish/gm	LOG Fish/gm	Charcoal/gm	LOG Charc/gm	Mollusc/gm	LOG Moll/gm	Botryo%	# Cods	Cods/gm	LOG cods/gm	# Cod Species
2	6.69	0.83	2.82	0.45	91.97	1.96		39	65.22	1.81	8
3	5.80	0.76	1.76	0.25				84	3.45	0.54	16
4	0.69	-0.16	0.22	-0.67	0.07	-1.16		3	0.28	-0.55	1
5	8.54	0.93			4.11	0.61		107	16.93	1.23	7
6	7.94	0.90			0.44	-0.36		28	3.74	0.57	7
7	1.52	0.18			0.38	-0.42					
8	3.65	0.56			3.04	0.48		1	0.15	-0.82	1
9	14.69	1.17	0.46	-0.34							
10	14.76	1.17									
11	37.72	1.58	0.78	-0.11	0.27	-0.57					
12	6.92	0.84			0.21	-0.69					
13	61.95	1.79			0.42	-0.38					
14	137.62	2.14	0.79	-0.10	0.20	-0.70					
15	118.19	2.07					25				
16	53.78	1.73			0.57	-0.25	15				
17	72.99	1.86			7.30	0.86		1	3.65	0.56	1
18	2.94	0.47			0.23	-0.65					
19	17.15	1.23	0.39	-0.41	0.24	-0.62					
20	16.20	1.21			0.28	-0.55					
21	27.28	1.44	1.63	0.21							
22	17.93	1.25	0.82	-0.08	0.48	-0.31		1	0.48	-0.31	1
23	8.79	0.94	0.57	-0.25	1.76	0.24		60	7.30	0.86	12
28	186.59	2.27	6.97	0.84			60				
29	168.25	2.23	5.44	0.74							
30	262.32	2.42	6.34	0.80	2.93	0.47		2			2
31	13.57	1.13	1.42	0.15				1			
32	14.42	1.16						33	8.57	0.93	6

Sample	Tot. Fish/gm	LOG Fish/gm	Charcoal/gm	LOG Charc/gm	Mollusc/gm	LOG Moll/gm	Botryo%	# Cods	Cods/gm	LOG cods/gm	# Cod Species
33	7.55	0.88	1.34	0.13				32	15.13	1.18	7
34	19.63	1.29			0.27	-0.57		6	42.57	1.63	3
35	13.28	1.12	0.99	-0.01				113	1.92	0.28	8
36	29.29	1.47			69.00	1.84		162	75.89	1.88	16
37			27.16	1.43	1.22	0.09		13			7
38	153.40	2.19	15.52	1.19			79				
39	193.28	2.29	27.22	1.43	14.71	1.17	79				
40	41.24	1.62	173.61	2.24			4		1.17	0.07	
41	43.96	1.64	84.42	1.93			5		1.36	0.13	
42			91.64	1.96					2.15	0.33	
43			135.14	2.13			1		16.97	1.23	
44			14.86	1.17					1.61	0.21	
45	1.54	0.19	3.70	0.57	4.05	0.61		40	115.42	2.06	8
46									37.26	1.57	
47									15.89	1.20	
48	72.94	1.86					10		15.34	1.19	
49	48.72	1.69							294.72	2.47	
50	19.24	1.28							57.53	1.76	
51	9.15	0.96							172.93	2.24	
53	4.49	0.65						21	9.36	0.97	6
55	3.23	0.51	0.46	-0.34	1.07	0.03		85			10
56			0.47	-0.33	14.02	1.15		9			4
57			0.68	-0.17				14			2
78	4.77	0.68	0.22	-0.65	26.22	1.42		63			8
79											
80	1.61	0.21	0.54	-0.26	19.63	1.29		107	8.83	0.95	9
82			2.93	0.47	0.57	-0.25		199	5.39	0.73	13

Sample	Tot. Fish/gm	LOG Fish/gm	Charcoal/gm	LOG Charc/gm	Mollusc/gm	LOG Moll/gm	Botryo%	# Cods	Cods/gm	LOG cods/gm	# Cod Species
83			0.17	-0.78	6.67	0.82		307	56.97	1.76	13
86	24.63	1.39	0.80	-0.10					6.84	0.84	
87	18.86	1.28					25		16.84	1.23	
88	152.93	2.18	0.25	-0.61			40		4.45	0.65	
89	4.18	0.62						33			5
90	8.47	0.93	0.96	-0.02	5.39	0.73		382	1.13	0.05	17
91			0.79	-0.10	0.29	-0.54		199			14
92	5.43	0.73			3.17	0.50		382			20
94	0.64	-0.19			1.06	0.02		62			7
97	33.44	1.52	2.27	0.36							
98	68.75	1.84	1.66	0.22			3				
99	71.80	1.86	1.33	0.12			35				
100	11.95	1.08	6.41	0.81			10				
101	57.77	1.76	1.19	0.08							
105	46.96	1.67	1.34	0.13	6.16	0.79		105			12
106	7.47	0.87	0.63	-0.20	12.45	1.10		263			16
107	0.54	-0.27			4.32	0.64		211			8
109	3.42	0.53			0.73	-0.14		28	7.72	0.89	5
110	3.93	0.59	0.73	-0.14	1.12	0.05		30			7
111	4.28	0.63			0.95	-0.02		17			3
112	5.58	0.75	0.79	-0.10	0.28	-0.55			28.77	1.46	
113	5.47	0.74	0.97	-0.01	0.94	-0.03		6	112.49	2.05	3
114	346.94	2.54	11.26	1.05			5		93.59	1.97	
115	163.54	2.21	1.24	0.09			1				
116	35.88	1.55	3.66	0.56	8.77	0.94					
117	149.14	2.17	2.97	0.47							
118	1.92	0.28	11.69	1.07				49	8.54	0.93	8

Sample	Tot. Fish/gm	LOG Fish/gm	Charcoal/gm	LOG Charc/gm	Mollusc/gm	LOG Moll/gm	Botryo%	# Cods	Cods/gm	LOG cods/gm	# Cod Species
119					1.03	0.01		171	25.44	1.41	11
120	0.29	-0.54			0.73	-0.14		33	4.88	0.69	6
121	5.43	0.73	1.57	0.19	2.79	0.45		87	12.76	1.11	11
122	2.26	0.35	12.24	1.09	1.81	0.26		10	4.53	0.66	2
123	2.55	0.41	4.60	0.66				9	1.43	0.15	1
124	3.20	0.50	5.85	0.77	0.56	-0.25		2	0.38	-0.42	
125	0.49	-0.31	0.12	-0.94	1.09	0.04		354	42.97	1.63	12
127	36.59	1.56	25.98	1.41			15				
128	172.78	2.24	1.74	0.24			75				
131	3.15	0.50	14.66	1.17	18.90	1.28		272	71.50	1.85	14
132	4.52	0.66	14.89	1.17	23.90	1.38		255	13.29	1.12	12
133	1.41	0.15	3.15	0.50	12.15	1.08		306	86.47	1.94	21
134	4.59	0.66	0.58	-0.23	16.23	1.21		372	335.44	2.53	14
135	11.55	1.06	0.29	-0.54	6.16	0.79		292	224.79	2.35	10
136	1.77	0.25	0.19	-0.71	16.83	1.23		358	317.95	2.50	11
137	1.35	0.13	0.92	-0.03	2.69	0.43		53	11.89	1.08	8
138	0.68	-0.17	4.79	0.68	0.68	-0.17		31	6.98	0.84	10
139	1.39	0.14	5.58	0.75	1.39	0.14		53	8.19	0.91	7
140	1.26	0.10	1.72	0.24	2.32	0.36		22	4.63	0.67	5
141	0.44	-0.35	0.19	-0.72	1.77	0.25		129	19.57	1.29	14
142			0.82	-0.09	1.58	0.20		268	16.96	1.23	12

Table B-3 part 2. List of all data discussed in the text, sorted by sample number. Associated transect, adjusted depth and shoreline environment are listed in part 1. Zeros have been removed for readability.

Sample #	Transect	AdjDepth	Shore Env	SAMPLE ID	d13C VPDB	d18O VPDB	d18O water
5	F	15	HR - Sand	MOD-5G-1	-2.32	0.69	1.64
5	F	15	HR - Sand	MOD-5G-2	-2.53	0.41	1.36
6	F	20	HR - Sand	MOD-6G-1	-1.84	0.17	1.12
14	F	60	HR - Sand	MOD-14G-1	-1.00	0.63	1.58
35	A	10	LR - Marsh	MOD-35G-1	-2.00	0.50	1.45
35	A	10	LR - Marsh	35G2 AVG	-1.14	1.59	2.54
36	A	5	LR - Marsh	MOD-36G-1	-0.26	0.75	1.70
36	A	5	LR - Marsh	MOD-36G-2	0.20	0.24	1.19
45	C	10	LR - River	MOD-45G-1	-1.38	0.87	1.59
45	C	10	LR - River	MOD-45G-2	-0.64	1.14	1.70
107	ZA5	5	LR - Marsh	107G1 AVG	-2.34	0.64	1.59
107	ZA5	5	LR - Marsh	107G2 AVG	-2.34	0.75	1.70
121	ZC20	20	LR - River	MOD-121G-1	-1.60	0.83	1.78
124	ZC20	20	LR - River	MOD-124G-1	-1.14	1.23	2.18
124	ZC20	20	LR - River	MOD-124G-2	-0.95	1.02	1.97

Table B-4. Stable isotope results. Ordered by "Sample ID". Those sites with two individual gastropods sampled are coded as G-1 and G-2. Sites with multiple runs of the same individual are given as averages for each individual, e.g. 107G1 AVG means the average measured values for the first gastropod from sample (site) #107. The last column is calculated water $\delta^{18}O$ values from which the gastropod carbonate would have precipitated at a temperature of 25 °C, using the fractionation of Grossman and Ku (1986) as modified by Dettman et al. (1999).

Sample	Species	Total Cods	Ostracode species	Abundance	% of Sample
2	8	39	*Cyprinotinae sp.2*	3	7.7
2	8	39	*Cyprinotinae sp.3*	16	41.0
2	8	39	*Cypridopsine sp.C*	1	2.6
2	8	39	*Limnocythere sp.3*	2	5.1
2	8	39	*Limnocythere sp.9*	4	10.3
2	8	39	*Gomphocythere emyrsi*	1	2.6
2	8	39	*Alicenula serricaudata*	1	2.6
2	8	39	*Candonopsis sp.*	1	2.6
3	16	84	*Cyprinotinae sp.1*	2	2.4
3	16	84	*Cyprinotinae sp.2*	27	32.1
3	16	84	*Cyprinotinae sp.3*	13	15.5
3	16	84	*Cypridopsine sp.L*	3	3.6
3	16	84	*Cypridopsine sp.P*	2	2.4
3	16	84	*Zonocypris costata*	1	1.2
3	16	84	*Limnocythere sp.1*	2	2.4
3	16	84	*Limnocythere sp.2*	1	1.2
3	16	84	*Limnocythere sp.3*	2	2.4
3	16	84	*Limnocythere sp.4*	1	1.2
3	16	84	*Limnocythere sp.6*	1	1.2
3	16	84	*Limnocythere sp.9*	3	3.6
3	16	84	*Limnocythere sp.10*	1	1.2
3	16	84	*Gomphocythere emyrsi*	1	1.2
3	16	84	*Ilyocypris sp.1*	2	2.4
3	16	84	*Alicenula serricaudata*	6	7.1
4	1	3	*Gomphocythere emyrsi*	3	100.0
5	7	107	*Cypridopsine 1 n.sp.*	8	7.5
5	7	107	*Cypridopsine sp.C*	5	4.7
5	7	107	*Cypridopsine sp.K*	2	1.9
5	7	107	*Cypridopsine sp.L*	19	17.8
5	7	107	*Cypridopsine sp.P*	1	0.9
5	7	107	*Gomphocythere emyrsi*	20	18.7
5	7	107	*Ilyocypris sp.1*	10	9.3
6	7	107	*Cyprinotinae sp.1*	6	5.6
6	7	28	*Cyprinotinae sp.3*	2	7.1
6	7	28	*Cypridopsine sp.C*	1	3.6
6	7	28	*Cypridopsine sp.O*	2	7.1
6	7	28	*Cypridopsine sp.P*	1	3.6
6	7	28	*Gomphocythere emyrsi*	13	46.4
6	7	28	*Ilyocypris sp.1*	2	7.1
8	1	1	*Cypridopsine sp.N*	1	100.0

Sample	Species	Total Cods	Ostracode species	Abundance	% of Sample
17	1	1	*Cyprinotinae sp.2*	1	100.0
22	1	1	*Alicenula serricaudata*	1	100.0
23	12	60	*Cyprinotinae sp.1*	11	18.3
23	12	60	*Cyprinotinae sp.3*	1	1.7
23	12	60	*Cypridopsine sp.B*	2	3.3
23	12	60	*Cypridopsine sp.C*	1	1.7
23	12	60	*Cypridopsine sp.F*	1	1.7
23	12	60	*Cypridopsine sp.N*	3	5.0
23	12	60	*Cypridopsine sp.O*	3	5.0
23	12	60	*Limnocythere sp.1*	8	13.3
23	12	60	*Limnocythere sp.4*	4	6.7
23	12	60	*Limnocythere sp.9*	1	1.7
23	12	60	*Gomphocythere emyrsi*	17	28.3
23	12	60	*Candonopsis sp.*	2	3.3
30	2	2	*Cyprinotinae sp.3*	1	50.0
30	2	2	*Zonocypris costata*	1	50.0
32	6	33	*Cyprinotinae sp.1*	1	3.0
32	6	33	*Cypridopsine sp.N*	3	9.1
32	6	33	*Limnocythere sp.1*	6	18.2
32	6	33	*Limnocythere sp.4*	3	9.1
32	6	33	*Limnocythere sp.9*	4	12.1
32	6	33	*Ilyocypris sp.1*	5	15.2
33	7	32	*Cypridopsine sp.N*	1	3.1
33	7	32	*Limnocythere sp.1*	9	28.1
33	7	32	*Limnocythere sp.4*	1	3.1
33	7	32	*Limnocythere sp.9*	2	6.3
33	7	32	*Limnocythere sp.10*	3	9.4
33	7	32	*Ilyocypris sp.1*	2	6.3
33	7	32	*Alicenula serricaudata*	4	12.5
34	3	6	*Cypridopsine sp.L*	4	66.7
34	3	6	*Limnocythere sp.1*	1	16.7
34	3	6	*Ilyocypris sp.1*	1	16.7
35	8	113	*Cyprinotinae sp.1*	7	6.2
35	8	113	*Cyprinotinae sp.2*	34	30.1
35	8	113	*Cyprinotinae sp.3*	10	8.8
35	8	113	*Cypridopsine sp.G*	2	1.8
35	8	113	*Cypridopsine sp.P*	1	0.9
35	8	113	*Limnocythere sp.1*	7	6.2
35	8	113	*Limnocythere sp.9*	25	22.1
35	8	113	*Gomphocythere emyrsi*	17	15.0
36	16	162	*Cyprinotinae sp.1*	1	0.6

Sample	Species	Total Cods	Ostracode species	Abundance	% of Sample
36	16	162	*Cyprinotinae sp.2*	32	19.8
36	16	162	*Cyprinotinae sp.3*	20	12.3
36	16	162	*Cypridopsine 1 n.sp.*	2	1.2
36	16	162	*Zonocypris costata*	1	0.6
36	16	162	*Limnocythere sp.1*	2	1.2
36	16	162	*Limnocythere sp.2*	2	1.2
36	16	162	*Limnocythere sp.3*	2	1.2
36	16	162	*Limnocythere sp.4*	12	7.4
36	16	162	*Limnocythere sp.9*	6	3.7
36	16	162	*Limnocythere sp.10*	1	0.6
36	16	162	*Gomphocythere emyrsi*	1	0.6
36	16	162	*Gomphocythere huwi*	3	1.9
36	16	162	*Ilyocypris sp.1*	25	15.4
36	16	162	*Alicenula serricaudata*	6	3.7
36	16	162	*Candonopsis sp.*	1	0.6
37	7	13	*Cyprinotinae sp.2*	1	7.7
37	7	13	*Cyprinotinae sp.3*	2	15.4
37	7	13	*Limnocythere sp.1*	1	7.7
37	7	13	*Gomphocythere huwi*	2	15.4
37	7	13	*Ilyocypris sp.1*	3	23.1
37	7	13	*Alicenula serricaudata*	1	7.7
37	7	13	*Candonopsis sp.*	1	7.7
45	8	40	*Cyprinotinae sp.3*	8	20.0
45	8	40	*Cypridopsine sp.C*	1	2.5
45	8	40	*Cypridopsine sp.K*	2	5.0
45	8	40	*Cypridopsine sp.O*	16	40.0
45	8	40	*New Cypridopsine*	4	10.0
45	8	40	*Limnocythere sp.9*	4	10.0
45	8	40	*Ilyocypris sp.1*	3	7.5
45	8	40	*Candonopsis sp.*	2	5.0
53	6	21	*Cyprinotinae sp.3*	1	4.8
53	6	21	*Cypridopsine sp.B*	1	4.8
53	6	21	*Cypridopsine sp.P*	1	4.8
53	6	21	*Gomphocythere emyrsi*	1	4.8
53	6	21	*Gomphocythere huwi*	3	14.3
53	6	21	*Candonopsis sp.*	2	9.5
55	10	85	*Cyprinotinae sp.2*	12	14.1
55	10	85	*Cyprinotinae sp.3*	4	4.7
55	10	85	*Cypridopsine sp.L*	5	5.9
55	10	85	*Cypridopsine sp.P*	2	2.4
55	10	85	*Zonocypris costata*	1	1.2

Sample	Species	Total Cods	Ostracode species	Abundance	% of Sample
55	10	85	*Limnocythere sp.9*	32	37.6
55	10	85	*Limnocythere sp.10*	4	4.7
55	10	85	*Limnocythere sp.A n.sp.*	4	4.7
55	10	85	*Gomphocythere emyrsi*	5	5.9
55	10	85	*Alicenula serricaudata*	1	1.2
56	4	9	*Cyprinotinae sp.2*	2	22.2
56	4	9	*Cypridopsine sp.O*	1	11.1
56	4	9	*Cypridopsine sp.P*	1	11.1
56	4	9	*Limnocythere sp.9*	2	22.2
57	2	14	*Cyprinotinae sp.2*	2	14.3
57	2	14	*Cypridopsine sp.O*	1	7.1
78	8	63	*Cyprinotinae sp.2*	5	7.9
78	8	63	*Cyprinotinae sp.3*	5	7.9
78	8	63	*Cypridopsine sp.A*	2	3.2
78	8	63	*Cypridopsine sp.F*	1	1.6
78	8	63	*Cypridopsine sp.P*	16	25.4
78	8	63	*Limnocythere sp.9*	23	36.5
78	8	63	*Limnocythere sp.10*	2	3.2
78	8	63	*Alicenula serricaudata*	4	6.3
80	9	107	*Cyprinotinae sp.1*	1	0.9
80	9	107	*Cyprinotinae sp.2*	22	20.6
80	9	107	*Cyprinotinae sp.3*	21	19.6
80	9	107	*Cypridopsine sp.P*	6	5.6
80	9	107	*Limnocythere sp.1*	1	0.9
80	9	107	*Limnocythere sp.9*	28	26.2
80	9	107	*Limnocythere sp.10*	7	6.5
80	9	107	*Limnocythere sp.A n.sp.*	2	1.9
80	9	107	*Alicenula serricaudata*	8	7.5
82	13	199	*Cyprinotinae sp.1*	23	11.6
82	13	199	*Cyprinotinae sp.2*	41	20.6
82	13	199	*Cyprinotinae sp.3*	8	4.0
82	13	199	*Cypridopsine sp.B*	3	1.5
82	13	199	*Cypridopsine sp.D*	4	2.0
82	13	199	*Cypridopsine sp.P*	25	12.6
82	13	199	*Zonocypris costata*	17	8.5
82	13	199	*Limnocythere sp.3*	4	2.0
82	13	199	*Limnocythere sp.6*	1	0.5
82	13	199	*Limnocythere sp.9*	18	9.0
82	13	199	*Limnocythere sp.A n.sp.*	3	1.5
82	13	199	*Gomphocythere emyrsi*	4	2.0
82	13	199	*Alicenula serricaudata*	10	5.0

Sample	Species	Total Cods	Ostracode species	Abundance	% of Sample
83	13	307	*Cyprinotinae sp.1*	32	10.4
83	13	307	*Cyprinotinae sp.2*	71	23.1
83	13	307	*Cyprinotinae sp.3*	34	11.1
83	13	307	*Cypridopsine sp.G*	1	0.3
83	13	307	*Cypridopsine sp.P*	27	8.8
83	13	307	*Zonocypris costata*	46	15.0
83	13	307	*Limnocythere sp.1*	2	0.7
83	13	307	*Limnocythere sp.10*	36	11.7
83	13	307	*Limnocythere sp.A n.sp.*	4	1.3
83	13	307	*Gomphocythere emyrsi*	11	3.6
83	13	307	*Gomphocythere huwi*	25	8.1
83	13	307	*Alicenula serricaudata*	9	2.9
83	13	307	*Candonopsis sp.*	1	0.3
89	5	33	*Cypridopsine sp.L*	1	3.0
89	5	33	*Cypridopsine sp.O*	2	6.1
89	5	33	*Limnocythere sp.1*	2	6.1
89	5	33	*Gomphocythere emyrsi*	3	9.1
89	5	33	*Gomphocythere irvinei*	8	24.2
90	17	382	*Cyprinotinae sp.1*	13	3.4
90	17	382	*Cyprinotinae sp.2*	70	18.3
90	17	382	*Cyprinotinae sp.3*	25	6.5
90	17	382	*Cypridopsine sp.C*	6	1.6
90	17	382	*Cypridopsine sp.K*	2	0.5
90	17	382	*Cypridopsine sp.L*	18	4.7
90	17	382	*Cypridopsine sp.N*	1	0.3
90	17	382	*Cypridopsine sp.O*	3	0.8
90	17	382	*Cypridopsine sp.P*	47	12.3
90	17	382	*Zonocypris costata*	9	2.4
90	17	382	*Limnocythere sp.1*	2	0.5
90	17	382	*Limnocythere sp.9*	41	10.7
90	17	382	*Limnocythere sp.10*	12	3.1
90	17	382	*Limnocythere sp.A n.sp.*	25	6.5
90	17	382	*Gomphocythere emyrsi*	57	14.9
90	17	382	*Alicenula serricaudata*	8	2.1
90	17	382	*Candonopsis sp.*	3	0.8
91	14	199	*Cyprinotinae sp.1*	32	16.1
91	14	199	*Cyprinotinae sp.2*	16	8.0
91	14	199	*Cyprinotinae sp.3*	13	6.5
91	14	199	*Cypridopsine sp.C*	4	2.0
91	14	199	*Cypridopsine sp.P*	35	17.6
91	14	199	*Zonocypris costata*	1	0.5

Sample	Species	Total Cods	Ostracode species	Abundance	% of Sample
91	14	199	*Limnocythere sp.2*	10	5.0
91	14	199	*Limnocythere sp.3*	3	1.5
91	14	199	*Limnocythere sp.6*	1	0.5
91	14	199	*Limnocythere sp.9*	26	13.1
91	14	199	*Limnocythere sp.10*	3	1.5
91	14	199	*Limnocythere sp.A n.sp.*	13	6.5
91	14	199	*Gomphocythere emyrsi*	8	4.0
91	14	199	*Alicenula serricaudata*	15	7.5
92	20	382	*Cyprinotinae sp.1*	45	11.8
92	20	382	*Cyprinotinae sp.2*	94	24.6
92	20	382	*Cyprinotinae sp.3*	30	7.9
92	20	382	*Cypridopsine sp.C*	5	1.3
92	20	382	*Cypridopsine sp.F*	6	1.6
92	20	382	*Cypridopsine sp.K*	1	0.3
92	20	382	*Cypridopsine sp.L*	2	0.5
92	20	382	*Cypridopsine sp.O*	7	1.8
92	20	382	*Cypridopsine sp.P*	47	12.3
92	20	382	*New Cypridopsine*	1	0.3
92	20	382	*Zonocypris costata*	3	0.8
92	20	382	*Limnocythere sp.2*	16	4.2
92	20	382	*Limnocythere sp.3*	2	0.5
92	20	382	*Limnocythere sp.4*	5	1.3
92	20	382	*Limnocythere sp.6*	1	0.3
92	20	382	*Limnocythere sp.9*	44	11.5
92	20	382	*Limnocythere sp.10*	12	3.1
92	20	382	*Limnocythere sp.A n.sp.*	13	3.4
92	20	382	*Gomphocythere emyrsi*	27	7.1
92	20	382	*Alicenula serricaudata*	21	5.5
94	7	62	*Cyprinotinae sp.1*	22	35.5
94	7	62	*Cyprinotinae sp.2*	12	19.4
94	7	62	*Cyprinotinae sp.3*	8	12.9
94	7	62	*Cypridopsine sp.P*	4	6.5
94	7	62	*Limnocythere sp.9*	1	1.6
94	7	62	*Limnocythere sp.A n.sp.*	4	6.5
94	7	62	*Gomphocythere emyrsi*	2	3.2
105	12	105	*Cyprinotinae sp.3*	7	6.7
105	12	105	*Cypridopsine 1 n.sp.*	3	2.9
105	12	105	*Cypridopsine sp.L*	4	3.8
105	12	105	*Cypridopsine sp.P*	8	7.6
105	12	105	*Limnocythere sp.1*	8	7.6
105	12	105	*Limnocythere sp.2*	1	1.0

Sample	Species	Total Cods	Ostracode species	Abundance	% of Sample
105	12	105	*Limnocythere sp.8*	1	1.0
105	12	105	*Limnocythere sp.9*	15	14.3
105	12	105	*Limnocythere sp.10*	12	11.4
105	12	105	*Limnocythere sp.A n.sp.*	11	10.5
105	12	105	*Gomphocythere emyrsi*	1	1.0
105	12	105	*Ilyocypris sp.1*	9	8.6
106	16	263	*Cyprinotinae sp.1*	23	8.7
106	16	263	*Cyprinotinae sp.2*	67	25.5
106	16	263	*Cyprinotinae sp.3*	40	15.2
106	16	263	*Cypridopsine 1 n.sp.*	7	2.7
106	16	263	*Cypridopsine sp.C*	1	0.4
106	16	263	*Cypridopsine sp.K*	8	3.0
106	16	263	*Cypridopsine sp.P*	13	4.9
106	16	263	*Limnocythere sp.1*	3	1.1
106	16	263	*Limnocythere sp.2*	12	4.6
106	16	263	*Limnocythere sp.9*	19	7.2
106	16	263	*Limnocythere sp.10*	5	1.9
106	16	263	*Limnocythere sp.A n.sp.*	3	1.1
106	16	263	*Gomphocythere emyrsi*	20	7.6
106	16	263	*Ilyocypris sp.1*	13	4.9
106	16	263	*Alicenula serricaudata*	1	0.4
106	16	263	*Candonopsis sp.*	1	0.4
107	8	211	*Cyprinotinae sp.1*	52	24.6
107	8	211	*Cyprinotinae sp.2*	33	15.6
107	8	211	*Cyprinotinae sp.3*	36	17.1
107	8	211	*Cypridopsine 1 n.sp.*	25	11.8
107	8	211	*Cypridopsine sp.L*	3	1.4
107	8	211	*Limnocythere sp.9*	3	1.4
107	8	211	*Gomphocythere emyrsi*	12	5.7
107	8	211	*Gomphocythere huwi*	1	0.5
109	5	28	*Cyprinotinae sp.2*	6	21.4
109	5	28	*Cyprinotinae sp.3*	4	14.3
109	5	28	*Cypridopsine sp.L*	1	3.6
109	5	28	*Gomphocythere emyrsi*	3	10.7
109	5	28	*Alicenula serricaudata*	1	3.6
110	8	30	*Cypridopsine sp.N*	1	3.3
110	8	30	*Limnocythere sp.1*	6	20.0
110	8	30	*Limnocythere sp.9*	1	3.3
110	8	30	*Gomphocythere emyrsi*	1	3.3
110	8	30	*Ilyocypris sp.1*	1	3.3
110	8	30	*Alicenula serricaudata*	2	6.7

Sample	Species	Total Cods	Ostracode species	Abundance	% of Sample
110	8	30	*Candonopsis sp.*	1	3.3
111	3	17	*Limnocythere sp.9*	3	17.6
111	3	17	*Limnocythere sp.10*	1	5.9
111	3	17	*Gomphocythere emyrsi*	2	11.8
113	3	6	*Cypridopsine sp.L*	2	33.3
113	3	6	*Limnocythere sp.2*	1	16.7
113	3	6	*Ilyocypris sp.1*	1	16.7
118	8	49	*Cypridopsine sp.F*	3	6.1
118	8	49	*Cypridopsine sp.K*	1	2.0
118	8	49	*Cypridopsine sp.N*	16	32.7
118	8	49	*Zonocypris costata*	2	4.1
118	8	49	*Gomphocythere emyrsi*	2	4.1
118	8	49	*Gomphocythere irvinei*	1	2.0
118	8	49	*Ilyocypris sp.1*	17	34.7
118	8	49	*Alicenula serricaudata*	5	10.2
119	11	171	*Cyprinotinae sp.1*	61	35.7
119	11	171	*Cyprinotinae sp.2*	28	16.4
119	11	171	*Cyprinotinae sp.3*	11	6.4
119	11	171	*Cypridopsine sp.O*	3	1.8
119	11	171	*Cypridopsine sp.P*	6	3.5
119	11	171	*Zonocypris costata*	5	2.9
119	11	171	*Limnocythere sp.2*	2	1.2
119	11	171	*Limnocythere sp.9*	31	18.1
119	11	171	*Limnocythere sp.10*	1	0.6
119	11	171	*Gomphocythere emyrsi*	10	5.8
119	11	171	*Gomphocythere huwi*	2	1.2
120	6	33	*Cyprinotinae sp.1*	3	9.1
120	6	33	*Cyprinotinae sp.2*	14	42.4
120	6	33	*Cyprinotinae sp.3*	10	30.3
120	6	33	*Cypridopsine sp.K*	1	3.0
120	6	33	*Cypridopsine sp.P*	2	6.1
120	6	33	*Limnocythere sp.9*	1	3.0
121	11	87	*Cyprinotinae sp.1*	4	4.6
121	11	87	*Cyprinotinae sp.3*	3	3.4
121	11	87	*Cypridopsine sp.F*	3	3.4
121	11	87	*Cypridopsine sp.K*	1	1.1
121	11	87	*Cypridopsine sp.N*	9	10.3
121	11	87	*Cypridopsine sp.P*	1	1.1
121	11	87	*Limnocythere sp.1*	2	2.3
121	11	87	*Limnocythere sp.4*	2	2.3
121	11	87	*Gomphocythere emyrsi*	22	25.3

Sample	Species	Total Cods	Ostracode species	Abundance	% of Sample
121	11	87	*Ilyocypris sp.1*	3	3.4
121	11	87	*Alicenula serricaudata*	2	2.3
122	2	10	*Cyprinotinae sp.2*	5	50.0
122	2	10	*Limnocythere sp.9*	1	10.0
123	1	9	*Ilyocypris sp.1*	1	11.1
125	12	354	*Cyprinotinae sp.1*	54	15.3
125	12	354	*Cyprinotinae sp.2*	82	23.2
125	12	354	*Cyprinotinae sp.3*	91	25.7
125	12	354	*Cypridopsine sp.C*	2	0.6
125	12	354	*Cypridopsine sp.F*	1	0.3
125	12	354	*Cypridopsine sp.L*	22	6.2
125	12	354	*Cypridopsine sp.P*	6	1.7
125	12	354	*Zonocypris costata*	3	0.8
125	12	354	*Limnocythere sp.1*	4	1.1
125	12	354	*Limnocythere sp.9*	12	3.4
125	12	354	*Gomphocythere emyrsi*	46	13.0
125	12	354	*Alicenula serricaudata*	2	0.6
131	14	272	*Cyprinotinae sp.1*	9	3.3
131	14	272	*Cyprinotinae sp.2*	13	4.8
131	14	272	*Cyprinotinae sp.3*	4	1.5
131	14	272	*Cypridopsine sp.F*	1	0.4
131	14	272	*Cypridopsine sp.N*	47	17.3
131	14	272	*Cypridopsine sp.P*	5	1.8
131	14	272	*Zonocypris costata*	15	5.5
131	14	272	*Limnocythere sp.1*	2	0.7
131	14	272	*Limnocythere sp.9*	15	5.5
131	14	272	*Limnocythere sp.A n.sp.*	5	1.8
131	14	272	*Gomphocythere emyrsi*	15	5.5
131	14	272	*Gomphocythere huwi*	6	2.2
131	14	272	*Ilyocypris sp.1*	53	19.5
131	14	272	*Alicenula serricaudata*	28	10.3
132	12	255	*Cyprinotinae sp.1*	27	10.6
132	12	255	*Cyprinotinae sp.2*	23	9.0
132	12	255	*Cyprinotinae sp.3*	7	2.7
132	12	255	*Cypridopsine sp.F*	10	3.9
132	12	255	*Cypridopsine sp.O*	14	5.5
132	12	255	*Cypridopsine sp.P*	2	0.8
132	12	255	*Limnocythere sp.1*	8	3.1
132	12	255	*Limnocythere sp.9*	16	6.3
132	12	255	*Limnocythere sp.10*	2	0.8
132	12	255	*Gomphocythere emyrsi*	23	9.0

Sample	Species	Total Cods	Ostracode species	Abundance	% of Sample
132	12	255	*Ilyocypris sp.1*	32	12.5
132	12	255	*Alicenula serricaudata*	30	11.8
133	21	306	*Cyprinotinae sp.1*	15	4.9
133	21	306	*Cyprinotinae sp.2*	24	7.8
133	21	306	*Cyprinotinae sp.3*	4	1.3
133	21	306	*Cypridopsine sp.D*	12	3.9
133	21	306	*Cypridopsine sp.F*	11	3.6
133	21	306	*Cypridopsine sp.G*	3	1.0
133	21	306	*Cypridopsine sp.N*	11	3.6
133	21	306	*Cypridopsine sp.O*	4	1.3
133	21	306	*Cypridopsine sp.P*	11	3.6
133	21	306	*Zonocypris costata*	29	9.5
133	21	306	*Limnocythere sp.1*	13	4.2
133	21	306	*Limnocythere sp.2*	3	1.0
133	21	306	*Limnocythere sp.4*	2	0.7
133	21	306	*Limnocythere sp.9*	28	9.2
133	21	306	*Limnocythere sp.10*	3	1.0
133	21	306	*Limnocythere sp.A n.sp.*	4	1.3
133	21	306	*LimnoNew2*	1	0.3
133	21	306	*Gomphocythere emyrsi*	18	5.9
133	21	306	*Ilyocypris sp.1*	40	13.1
133	21	306	*Alicenula serricaudata*	30	9.8
133	21	306	*Candonopsis sp.*	3	1.0
134	14	372	*Cyprinotinae sp.1*	36	9.7
134	14	372	*Cyprinotinae sp.2*	59	15.9
134	14	372	*Cyprinotinae sp.3*	8	2.2
134	14	372	*Cypridopsine sp.F*	7	1.9
134	14	372	*Cypridopsine sp.O*	2	0.5
134	14	372	*Cypridopsine sp.P*	24	6.5
134	14	372	*Zonocypris costata*	35	9.4
134	14	372	*Limnocythere sp.1*	2	0.5
134	14	372	*Limnocythere sp.6*	40	10.8
134	14	372	*Limnocythere sp.9*	23	6.2
134	14	372	*Limnocythere sp.10*	4	1.1
134	14	372	*Gomphocythere emyrsi*	86	23.1
134	14	372	*Ilyocypris sp.1*	7	1.9
134	14	372	*Alicenula serricaudata*	13	3.5
135	14	372	*Cyprinotinae sp.1*	67	18.0
135	10	292	*Cyprinotinae sp.2*	68	23.3
135	10	292	*Cyprinotinae sp.3*	20	6.8
135	10	292	*Cypridopsine sp.F*	2	0.7

Sample	Species	Total Cods	Ostracode species	Abundance	% of Sample
135	10	292	*Cypridopsine sp.P*	11	3.8
135	10	292	*Zonocypris costata*	51	17.5
135	10	292	*Limnocythere sp.1*	12	4.1
135	10	292	*Limnocythere sp.9*	38	13.0
135	10	292	*Limnocythere sp.10*	10	3.4
135	10	292	*Alicenula serricaudata*	1	0.3
136	11	358	*Cyprinotinae sp.1*	52	14.5
136	11	358	*Cyprinotinae sp.2*	44	12.3
136	11	358	*Cyprinotinae sp.3*	7	2.0
136	11	358	*Cypridopsine sp.D*	13	3.6
136	11	358	*Zonocypris costata*	95	26.5
136	11	358	*Limnocythere sp.3*	26	7.3
136	11	358	*Limnocythere sp.9*	33	9.2
136	11	358	*Limnocythere sp.10*	6	1.7
136	11	358	*Limnocythere sp.A n.sp.*	3	0.8
136	11	358	*Gomphocythere emyrsi*	65	18.2
136	11	358	*Alicenula serricaudata*	2	0.6
137	8	53	*Cyprinotinae sp.2*	1	1.9
137	8	53	*Cyprinotinae sp.3*	1	1.9
137	8	53	*Cypridopsine sp.N*	19	35.8
137	8	53	*Cypridopsine sp.P*	1	1.9
137	8	53	*Limnocythere sp.2*	7	13.2
137	8	53	*Limnocythere sp.9*	1	1.9
137	8	53	*Gomphocythere emyrsi*	1	1.9
137	8	53	*Ilyocypris sp.1*	10	18.9
138	10	31	*Cypridopsine sp.C*	1	3.2
138	10	31	*Cypridopsine sp.K*	2	6.5
138	10	31	*Cypridopsine sp.N*	3	9.7
138	10	31	*Zonocypris costata*	1	3.2
138	10	31	*Limnocythere sp.1*	2	6.5
138	10	31	*Limnocythere sp.9*	2	6.5
138	10	31	*Limnocythere sp.A n.sp.*	3	9.7
138	10	31	*Gomphocythere emyrsi*	4	12.9
138	10	31	*Ilyocypris sp.1*	1	3.2
138	10	31	*Alicenula serricaudata*	3	9.7
139	7	53	*Cypridopsine sp.N*	14	26.4
139	7	53	*Cypridopsine sp.P*	3	5.7
139	7	53	*Zonocypris costata*	1	1.9
139	7	53	*Limnocythere sp.1*	7	13.2
139	7	53	*Limnocythere sp.9*	2	3.8
139	7	53	*Ilyocypris sp.1*	9	17.0

Sample	Species	Total Cods	Ostracode species	Abundance	% of Sample
139	7	53	*Alicenula serricaudata*	11	20.8
140	5	22	*Cyprinotinae sp.1*	1	4.5
140	5	22	*Cypridopsine sp.N*	11	50.0
140	5	22	*Gomphocythere emyrsi*	1	4.5
140	5	22	*Ilyocypris sp.1*	4	18.2
140	5	22	*Alicenula serricaudata*	2	9.1
141	14	129	*Cyprinotinae sp.2*	13	10.1
141	14	129	*Cyprinotinae sp.3*	3	2.3
141	14	129	*Cypridopsine sp.B*	2	1.6
141	14	129	*Cypridopsine sp.C*	4	3.1
141	14	129	*Cypridopsine sp.K*	9	7.0
141	14	129	*Cypridopsine sp.L*	4	3.1
141	14	129	*Cypridopsine sp.O*	2	1.6
141	14	129	*Cypridopsine sp.P*	5	3.9
141	14	129	*Zonocypris costata*	2	1.6
141	14	129	*Limnocythere sp.1*	1	0.8
141	14	129	*Limnocythere sp.9*	9	7.0
141	14	129	*Gomphocythere emyrsi*	61	47.3
141	14	129	*Alicenula serricaudata*	3	2.3
141	14	129	*Candonopsis sp.*	1	0.8
142	12	268	*Cyprinotinae sp.1*	28	10.4
142	12	268	*Cyprinotinae sp.2*	46	17.2
142	12	268	*Cyprinotinae sp.3*	33	12.3
142	12	268	*Cypridopsine sp.B*	1	0.4
142	12	268	*Cypridopsine sp.K*	11	4.1
142	12	268	*Cypridopsine sp.L*	22	8.2
142	12	268	*Cypridopsine sp.P*	7	2.6
142	12	268	*Limnocythere sp.9*	7	2.6
142	12	268	*Limnocythere sp.10*	4	1.5
142	12	268	*Gomphocythere emyrsi*	87	32.5
142	12	268	*Alicenula serricaudata*	1	0.4
142	12	268	*Candonopsis sp.*	4	1.5

Table B-5. Full listing of all ostracode species found by site number, as well as number of species (species richness), total number of ostracodes, the abundance of each species, and the percent abundance of that species.

Species	# sites/species	Plate	Image
Alicenula serricaudata	31	6	A-C
Candonopsis sp.	13	6	D-E
Cypridopsine n.gen. sp.A	1	1	A-C
Cypridopsine n.gen. sp.B	5	1	D-E
Cypridopsine n.gen. sp.C	12	1	G-I
Cypridopsine n.gen. sp.D	3	1	F
Cypridopsine n.gen. sp.F	11	1	J-K
Cypridopsine n.gen. sp.G	3	2	A-B
Cypridopsine n.gen. sp.K	11	2	C-E
Cypridopsine n.gen. sp.L	14	2	F-H
Cypridopsine n.gen. sp.N	14	2	I-L
Cypridopsine n.gen. sp.O	13	3	A-C
Cypridopsine n.gen. sp.P	30	3	D-F
Cypridopsine n.gen. sp.X n.sp.	2	3	G-H
Cypridopsine n.gen. sp.1 n.sp.	5	3	I-L
Cyprinotinae n.gen. sp.1	27	4	A-C
Cyprinotinae n.gen. sp.2	33	4	D-G
Cyprinotinae n.gen. sp.3	36	4	H-J
Gomphocythere emyrsi	37	5	A-D
Gomphocythere irvinei	2	5	E-G
Gomphocythere huwi	7	5	H-J
Ilyocypris sp.1	24	6	F-I
Limnocythere s.l. sp.1	25	7	A-F
Limnocythere s.l. sp.2	10	7	G-H
Limnocythere s.l. sp.3	7	7	I-J
Limnocythere s.l. sp.4	8	7	K-L
Limnocythere s.l. sp.6	5	7	M-N
Limnocythere s.l. sp.8	1	7	O
Limnocythere s.l. sp.9	37	8	A-C
Limnocythere s.l. sp.10	20	8	D-F
Limnocythere s.l. sp.A n.sp.	14	8	G-L
Limnocythere s.l. sp.B n.sp.	1	8	L
Zonocypris costata	20	6	J-L

Table B-6. List of the number of sites in which each species was found. Also included in this list are the references for the plate and image numbers for each species.

SampleID	AVG-HR-Sand n=10	AVG-LR-Marsh n=18	AVG-LR-River n=23	SampleID	1m AVG n=2	5m AVG n=17	10 mAVG n=9	15m AVG n=5	20m AVG n=17
Alicen	1.723	2.758	4.651	**Alicen**	3.846	2.742	1.048	2.634	5.703
Candon	1.542	0.712	0.373	**Candon**	3.846	0.078	1.180	0.000	1.010
Cyp1new	0.748	1.033	0.000	**Cyp1new**	0.000	1.094	0.000	1.495	0.000
CypB	0.810	0.000	0.183	**CypB**	0.000	0.089	0.300	0.000	0.476
CypC	1.248	0.293	0.408	**CypC**	0.000	0.251	1.082	1.580	0.308
CypD	0.000	0.000	0.416	**CypD**	0.000	0.118	0.403	0.000	0.231
CypF	0.325	0.087	0.883	**CypF**	0.000	0.202	0.076	0.376	1.125
CypG	0.000	0.098	0.057	**CypG**	0.000	0.019	0.197	0.000	0.058
CypK	0.187	0.213	1.250	**CypK**	0.000	0.373	1.845	1.664	0.188
CypL	2.721	6.504	0.762	**CypL**	0.000	0.914	2.434	16.885	2.349
CypN	0.500	0.878	8.079	**CypN**	0.000	0.000	0.029	9.105	8.926
CypO	3.040	0.482	2.202	**CypO**	3.571	0.865	4.704	0.108	1.471
CypP	5.051	3.450	3.037	**CypP**	0.000	7.413	2.866	1.855	1.256
CypTin1	4.214	6.110	7.325	**CypTin1**	0.000	10.745	6.391	1.935	3.983
CypTin2	9.840	10.578	12.977	**CypTin2**	10.989	18.907	14.783	3.549	5.475
CypTin3	8.272	6.869	6.679	**CypTin3**	7.692	11.715	11.619	0.807	2.166
CypXnew	0.000	0.015	0.435	**CypXnew**	0.000	0.015	1.111	0.000	0.000
Gompho1	10.785	5.225	9.330	**Gompho1**	0.000	3.224	15.146	11.320	9.927
Gompho2	0.000	1.347	0.089	**Gompho2**	0.000	0.000	0.000	0.000	1.546
Gompho4	1.429	0.984	0.501	**Gompho4**	7.692	0.685	0.000	0.000	0.970
Ilyo	1.887	6.116	7.000	**Ilyo**	11.538	2.496	0.833	9.998	8.930
Limno1	1.571	6.302	1.662	**Limno1**	3.846	0.888	1.289	4.731	5.362
Limno10	0.907	2.055	1.230	**Limno10**	0.000	2.460	1.604	0.215	1.001
Limno1new	0.471	1.919	0.797	**Limno1new**	0.000	1.923	1.343	1.935	0.185
Limno2	0.119	1.813	0.668	**Limno2**	0.000	1.078	0.000	2.642	1.038
Limno3	0.751	0.181	0.403	**Limno3**	0.000	0.450	1.377	0.000	0.000
Limno4	0.786	1.163	0.128	**Limno4**	0.000	0.583	0.000	0.000	0.750
Limno6	0.119	0.042	0.489	**Limno6**	0.000	0.145	0.000	2.151	0.000
Limno9	11.187	6.947	6.557	**Limno9**	0.000	10.288	13.620	2.904	3.742
Zono	0.237	0.237	4.628	**Zono**	0.000	1.788	5.454	2.527	1.233

Table B-7. Lists of the calculated average abundances of each species by environment on the left, and depth on the right. Total number of sites included in each average is given in the column heading (n=). The shortened name under "sample ID" is matched to full species name in Table 8.

Species	Species ID	DCA1	DCA2
Alicenula serricaudata	Alicen	2.24	-0.31
Candonopsis sp.	Candon	1.81	1.18
Cypridopsine n.gen. sp.B	CypB	1.06	0.88
Cypridopsine n.gen. sp.C	CypC	1.74	2.59
Cypridopsine n.gen. sp.D	CypD	0.4	-0.31
Cypridopsine n.gen. sp.F	CypF	2.26	-0.8
Cypridopsine n.gen. sp.G	CypG	0.85	0.05
Cypridopsine n.gen. sp.K	CypK	1.99	1.38
Cypridopsine n.gen. sp.L	CypL	2.88	3.61
Cypridopsine n.gen. sp.N	CypN	3.94	-1.14
Cypridopsine n.gen. sp.O	CypO	1.18	2.46
Cypridopsine n.gen. sp.P	CypP	0.81	0.63
Cypridopsine n.gen. sp.X n.sp.	CypXnew	1.25	2.52
Cypridopsine n.gen. sp.1 n.sp.	Cyp1new	1.89	3.13
Cyprinotinae n.gen. sp.1	CypTin1	0.82	0.52
Cyprinotinae n.gen. sp.2	CypTin2	-0.47	1.18
Cyprinotinae n.gen. sp.3	CypTin3	0.56	1.52
Gomphocythere emyrsi	Gompho1	1.79	1.41
Gomphocythere irvinei	Gompho2	3.38	3.18
Gomphocythere huwi	Gompho4	1.56	0.07
Ilyocypris sp.1	Ilyo	3.32	1.31
Limnocythere s.l. sp.1	Limno1	2.67	2.16
Limnocythere s.l. sp.2	Limno2	2.62	2.89
Limnocythere s.l. sp.3	Limno3	-0.67	0.39
Limnocythere s.l. sp.4	Limno4	2.6	0.05
Limnocythere s.l. sp.6	Limno6	0.16	-0.25
Limnocythere s.l. sp.9	LimnoAnew	1.24	1.05
Limnocythere s.l. sp.10	Limno10	1.15	0.75
Limnocythere s.l. sp.A n.sp.	Limno9	1.14	0.77
Zonocypris costata	Zono	1.38	-0.31

Site Scores	DCA1	DCA2
2S10	0.78	1.16
3S5	1.14	1.11
5S15	2.28	2.19
6S20	1.48	1.38
23S20	1.85	1.03
32M25	2.55	0.76
33M20	2.36	0.79
34M15	2.93	2.73
35M10	0.9	1.16
36M5	1.46	1.02
37M1	1.76	1.04
45R10	1.47	1.72
53S20	1.33	0.9
55S10	1.12	1.15
56S5	0.6	1.21
57S1	0.21	1.7
78S5	0.97	0.68
80R5	0.88	0.91
82R5	0.78	0.63
83R5	0.97	0.71
89M20	2.21	2.37
90M10	1.22	1.17
91M5	1.07	0.97
92M5	1.13	1.03
94M5	0.66	0.97
105M5	1.7	1.48
106M5	1.23	1.32
107M5	0.91	1.42
109M20	0.99	1.42
110M20	2.45	0.95
111M20	1.36	0.98
113M20	2.93	2.74
118R20	2.85	0.15
119R5	0.89	0.96
120R5	0.45	1.1
121R20	2.17	0.59
122R20	0	1.06
123R5	3.32	1.31
125R5	1.05	1.3
131R20	1.98	0.46
132R20	1.54	0.94
133R20	1.7	0.69
134R15	1.17	0.73

Eigenvalues			
DCA1	DCA2	DCA3	DCA4
0.34	0.24	0.14	0.13

Percent variance explained %			
DCA1	DCA2	DCA3	DCA4
14.63	10.1	5.78	5.64

Table B-8. Detrended Correspondence Analysis (DCA) results. The upper left table lists the species scores for the first two DCA axes, including the full species name matched to its shortened ID. To the right is the listing of site scores for the first two DCA axes. The ID contains the sample number followed by a letter denoting environment type (S = HR Sand, M = LR Marsh, R = LR River), followed by another number which is the adjusted depth (1m, 5m, 10m, etc.). On this page are the eigenvalues and the percent variance explained by each axis.

APPENDIX C: A LONG PALEOECOLOGICAL DRILL CORE RECORD FROM LAKE MALAWI (1250-147 KA) AND ITS PALEOENVIRONMENTAL IMPLICATIONS

To be submitted to the professional journal: *Palaeogeography, Palaeoclimatology, Palaeoecology*

A LONG PALEOECOLOGICAL DRILL CORE RECORD FROM LAKE MALAWI (1250-147 KA) AND ITS PALEOENVIRONMENTAL IMPLICATIONS

Margaret Whiting Blome, Andrew S. Cohen

Abstract

Sedimentary records from rift basin environments can provide continuous and high resolution histories of past environments. Analysis of the sand-sized fraction of sediment between 380.7 and 82 meters below lake floor (mblf) recovered from Core MAL05-1B in the central basin of Lake Malawi forms the basis for reconstructing the paleohydrology and paleoecology of Lake Malawi between 1.25 million and 147 thousand years ago. We present the absolute abundances of fossil indicators, including ostracodes, fish, charred particles, molluscs, green algae and fern spores, the relative abundances of ostracode taxa taphonomic variables of ostracode preservation, and sand fraction mineralogy. These data are grouped into seven biological and five minerogenic facies assemblages. Facies changes throughout the core characterize five distinct and recurrent paleoenvironmental states at the core site. These include a major transition from river to non-river influenced local environments occurring between 230-203 mblf (~800-660 ka), as evidenced by a unidirectional shift in dominant ostracode species assemblages and minerogenic content. This change was likely caused by intra-basinal tectonics cutting off a riverine sediment supply to the core site. In addition, a principal components analysis (PCA) performed on 23 of these variables shows a strong correlation between the first axis of variance (PC1) and depth-dependent indicators, and is thus interpreted as representing relative lake level

though time. Ecological variability constrained in the PC1 stratigraphic time series has a clear environmental interpretation as major changes in facies are coincident with observed shifts in the curve.

Introduction:

The paleoclimatic and paleoenvironmental history of Africa has become an increasingly important issue for many reasons, not the least of which is the current concern over global climate change. One of the most pressing questions is what impact anthropogenic climate change will have on tropical Africa and specifically, what is the sensitivity of this climatically vulnerable region? To answer these questions, (paleo)climatologists are studying the history of climate change in the tropics at various time scales to determine the natural variability of climate through time (e.g. Tjallingi et al. 2008, Russell et al. 2003). Reconstructing paleoenvironmental conditions for terrestrial Africa from sediments found in marine cores can be useful, although these records are often collected at a considerable distance from the area of interest (e.g. Hooghiemstra et al., 1992). In contrast, continental sediment archives from ancient lakes can span more than 1,000,000 years, and can provide valuable information about long term environmental history closer to the region of interest (Melles et al. 2012; Stone et al., 2011; Cohen et al. 2007).

Rift basin lakes considered especially good candidates for paleoclimatic studies for the following reasons. First, they tend to be deep and therefore contain long and rarely interrupted sedimentation records; second, their sediments often preserve abundant

fossils and other useful paleoclimate indicators; and third, when they are "closed", they are hydrologically sensitive to variations in water balance (P-E), which is in turn coupled to local climate (Nicholson, 1998). Tropical Lake Malawi satisfies these three conditions, thereby making it an ideal location for studies of continental African paleoclimate.

In 2005 seven sediment cores were drilled from two locations in Lake Malawi. The first site was in the central basin at 592 meters water depth. Four cores were recovered from this site, MAL05-1A-1D (hereafter Core(s)-1A-1D), the longest of which was Core 1B (380.7 meters). A shorter core, Core 1C, covers the Middle-Late Pleistocene interval from ~144 to 10 thousand years ago (ka) and has been extensively described elsewhere (e.g. Cohen et al., 2007; Scholz et al., 2007; Lyons et al., 2011; Park and Cohen, 2011; Reinthal et al., 2011; Scholz et al., 2011a,b; Stone et al., 2011). In this paper we summarize the ecological and environmental history of Lake Malawi from 1.25 million years ago (Ma) to 147 ka, as inferred from biological and mineralogical indicators found in the sand-sized sediment fraction from Core 1B, and the implications of that history for the region's paleohydrology and paleoclimatology.

Location and geologic setting

Lake Malawi, situated between 9-14°S, is the southern-most lake in the East African Rift System (EARS) (Figure C-1a). The EARS comprises a series of aligned tectonic basins, each 100s of kilometers long and 10s of kilometers wide, which individually contain sediment packages thousands of meters thick (Chorowicz, 2005, Rosendahl et al., 1992). The Malawi rift basin is part of the western branch of the EARS.

Regionally there is evidence for magmatic activity in the latest Paleogene (see Roberts et al., 2012), although rifting in the Malawi basin likely began in the Late Miocene, and has progressively moved northward through time (Tiercelin and Lezzar, 2002; Scholz et al. 2011b). The Malawi rift occupies a series of alternating, asymmetric, tilted half-grabens, which are flanked by uplifted shoulders along border faults (Ebinger et al., 1987, Chorowicz, 2005). These border faults accommodate offsets of up to seven kilometers, and are responsible for the topographic pattern of high relief "shoulders" next to deep, sediment filled basins (Ebinger et al., 1987). The sedimentation pattern in this region is controlled by the interaction between the underlying geological structure of the basin and the regional climatology (Tiercelin et al. 1988; Chorowicz, 2005). For example, the uplifted "shoulders" provide opportunity for enhanced orographic precipitation which, when combined with the steep slopes, also increases physical and chemical erosion of the highlands. At the same time the graben basins focus drainage and sedimentation. The high relief areas also divert much of the eroded material from the rift uplifts *away* from immediate deposition in the lake, though due to the asymmetry of the system, material often reenters the rift along an adjacent hanging wall rift segment (Tiercelin et al., 1988). The position and course of influent rivers in the Malawi basin are also strongly controlled by the evolution and structural geology of the local rift segments, which may change over time (Flannery and Rosendahl, 1990).

The Core 1B site is located on the southeast side of Lake Malawi's central basin depocenter (Figure C-1b), on the flank of a structural basement high, which precluded significant accumulation of sediment at the site due to gravity flows (Scholz et al.,

2011a). This location also has one of the thickest accumulations of sediments in the lake (~1.8km), and is in the deepest basin in the lake (Ebinger et al., 1987). Further, evidence from seismic data suggest the stratigraphic section at the site lacks any significant unconformities or time-gaps in the record (Scholz et al., 2011a). The geological structure of the Malawi rift basin makes it an excellent depositional environment for the continuous accumulation of sediments over long periods of time, and is part of what makes it an excellent location for studying continental paleoclimate.

Lake Malawi: Limnology and Climatology

Lake Malawi is a large (29,500 km^2), deep (706 m), permanently stratified (meromictic) lake filling the Malawi Rift basin of the EARS. Within the lake, there is both a thermal and chemical stratification (Patterson et al., 2000): a thermocline at 40-100 meters depth separates surface (epilimnion) waters with temperatures that vary seasonally between 23-28°C from the deeper, homothermal (metalimnion and hypolimnion) layers at 22-23°C. A permanent oxicline at 230-250 meters depth separates the anoxic hypolimnion from the layers above in the modern lake (Eccles, 1974; Eccles; 1988, Patterson and Kachinjika, 1995; Bootsma and Hecky, 1999).

Although tropical, the lake is located far enough south to have seasonal variations in temperature. The lake also experiences strong seasonality in wind and precipitation (Eccles, 1974), caused by the migration of the Intertropical Convergence Zone (ITCZ) (Figure C-1a). The ITCZ is a narrow band of atmospheric convergence and precipitation that migrates across the tropics following the location of maximum insolation intensity throughout the year. During the cool, windy season at Lake Malawi (May-August) the

ITCZ is sufficiently north of the lake to enhance the SE trade winds at the lake. Due to the morphology and orientation of the lake basin, these strong southeasterly winds cause stacking of surface water in the northern basin and enhanced upwelling in the southern basin (Eccles, 1974). Cooler surface waters and wind combine to decrease the temperature-dependent water density difference, essentially tilting the thermocline, and allowing the epilimnion to deepen to ~150 m (Patterson and Kachinjika, 1995; Wüest et al., 1996; Bootsma and Hecky, 1999). This seasonal mixing is essential for the redistribution of nutrients from the anoxic hypolimnion to the epilimnion where they are accessible to phytoplankton and other biota and increase lake productivity (Eccles, 1974). In this way, the lake's ecology may reflect changes in the position of the ITCZ through time.

The water budget of Lake Malawi reflects the inflows to and outflows from the lake. There are seven major inflowing rivers to the lake (Bootsma and Hecky, 1999), however ~62% of the annual input to the lake is from direct precipitation onto the lake surface (Spigel and Coulter, 1996). Similarly, 82% of the outflow from the lake is through evaporation from the lake surface, with the remaining 18% outflowing via the Shire River in the south. To become a completely closed basin, the surface level of modern Lake Malawi would need to fall a mere four meters for the lake to be cut off from its outflow (Hecky et al., 1996). This amount of change may have happened repeatedly in the past two centuries (observations from 1900 and 1969 indicate 6m change; Eccles, 1974; Hecky et al, 1996), and since its current level is likely the highest it has been in the

past 60kyrs (Stone et al., 2011), it is likely that the lake was a closed basin for most of the record presented here.

Furthermore, the modern lake level can vary over a range of 0.4-1.8 m in a single year (Ribbink, 1994) suggesting the modern hydroclimate of Lake Malawi is primarily controlled by the difference between precipitation and evaporation (P-E) in the watershed which, when the basin is closed, is the dominant driver of water depth. The amount of evaporation from the lake, is in turn, a function of its surface area, insolation and regional humidity and wind intensity. In the low-latitudes, precipitation amount, intensity, and seasonality is driven primarily by the location of the ITCZ. However there is evidence to suggest that high- and low-latitude forcing are not mutually exclusive drivers of African climate, and at times in the past it has been affected by both, e.g. global ice cover and regional-global sea surface temperatures (SSTs) which can affect the position and strength of the ITCZ (deMenocal and Rind, 1993; Tierney et al. 2008; Blome et al., 2012). For these reasons, hydrologic changes in Lake Malawi may be linked to changes in regional and/or global climate.

Paleoecological indicators used in this study

This study is part of a larger research project detailing the geochronology, sedimentology, geochemistry and paleoecology of Lake Malawi using samples recovered from Core 1B. Paleoecological/geochemical indicators studied by other researchers that will not be discussed in depth as a part of this study include: pollen and diatom assemblages, water temperature (as reconstructed using TEX_{86}), and sediment C/N ratios, total organic carbon (TOC) and calcium content. This study focuses on the biota and

mineral content of the sand-sized fraction from Core 1B. A summary of previous (paleo)-ecological interpretations of each indicator used in the analyses of this study can be found in Table 1, with a brief introduction to each below.

Ostracodes are used in this study to infer paleo-water depth, and in particular the occurrence of "shallow" lake conditions (e.g. littoral-profundal depths above any permanent oxicline), and furthermore, to differentiate shallow lake habitats based on discrete species assemblages and taphonomic considerations. A complete list of all ostracode species ever found in Lake Malawi, including whether they are known from sediment cores, modern sediments, are endemic, and/or are present in this study, can be found in Table 2. Ostracodes are benthic, bivalved crustaceans, which in lakes live primarily just above the sediment-water interface or burrow interstitially between sediment grains (Cohen, 2003). Their calcitic shells preserve well in the sediment record (De Deckker and Forester, 1988), and species-level identification is possible from the shape, ornamentation, and muscle scar patterns on the valve (Holmes, 1992). Ostracodes require oxygen to survive, and therefore cannot live in stratified lakes below the oxicline (Delorme, 1969). The presence of life assemblages of ostracodes in a sediment core is therefore evidence of past bottom-water oxygenation, and suggests a maximum lake depth: i.e. the lake must have been shallower than the depth at which it would become permanently stratified, or meromictic (Cohen et al., 2007; Stone et al., 2011). In addition, ostracode life assemblages are regulated by such limnological and hydrological variables as the nature of the water body (its size/shape, depth, energy level, orientation to dominant wind direction), and substrate type, as well as the temperature and chemistry

of the water (Holmes, 1992). Many of these factors co-vary with water depth and many previous studies have found ostracode species composition to differ within a given lake along depth gradients (e.g. Mourguiart et al., 1986).

The taphonomy of the ostracode shell can also provide useful information about the mechanical energy, redox and carbonate saturation conditions of the depositional environment. For this analysis we include percentage adults, whole carapaces, broken valves, and carbonate coatings. Juvenile valves of a species tend to be weakly calcified (Park et al., 2003; Park and Cohen, 2011) and are thus more prone to break in higher energy environments, and less likely to be preserved in the sedimentary record. Stratigraphic intervals in which sediments are dominated by adult valves (and often high numbers of broken, unidentifiable juveniles) can therefore be interpreted as having formed in higher energy, shallow water (Whatley, 1988; Brouwers, 1988). Carbonate coatings on ostracodes are more likely to occur in shallow waters that are (super)-saturated with respect to carbonate (Alin and Cohen, 2004), and may indicate post-depositional reworking of the valve. Although not included in the analysis, oxidation and reduction staining on ostracode valves are diagenic taphonomic features indicative of post-burial deposition in oxidizing (possibly subaerial) and anoxic environments, respectively.

Ostracode taxa used for the analyses in this study include un-described endemic genera of Cypridopsinae, plus various species of *Limnocythere, Candonopsis, Ilyocypris* and *Sclerocypris*. The fact that most of these species are apparently endemic to Lake Malawi precludes making species-specific quantitative assessments of many of the

habitat variables (e.g. major ion water chemistry) we would normally like to reconstruct based on a regional training set analysis, although a within-lake modern distribution study is used in our assessment of species level changes (Appendix B – this dissertation). Interpretations described below are most applicable when each of these taxa dominate the record: Cypridopsine species often indicate open, deeper water conditions (Holmes, 1992; Park and Cohen, 2011; Appendix B – this dissertation); *Candonopsis* may indicate an oligo-saline lake, possibly transitioning to fresher waters (Holmes 1992); *Limnocythere* species (especially when forming monospecific assemblages), are indicative of highly saline, and typically alkaline conditions (Cohen et al., 1983); *Ilyocypris* is indicative of fluvio-deltaic and marsh environments (Holmes, 1992; Appendix B – this dissertation); and *Sclerocypris* has been found in a wide range of environments from shallow, fishless ponds to crater lakes (Martens, 1986). For this study, the basis for paleoenvironmental interpretation will include a suite of co-occurring biota and minerals (biologic and minerogenic-facies) (Balch et al., 2005), and will not rely solely on ostracode species abundances.

Other biota include molluscs (bivalves and gastropods), which indicate littoral-profundal conditions above a permanent oxicline. Intact mollusc shells were rarely recovered from the core, however large fragments could be counted. The green algae *Botryococcus* and *Pediastrum* are commonly preserved in lake sediments as a result of the high silica content in their cell walls (Cohen, 2003). *Botryococcus* has previously been interpreted as representing a wide range of environments from arid/semi-arid to fresh water conditions, and is thought to out-compete other organisms in rapidly

changing environments (Guy-Ohlson, 1992). *Pediastrum* is common in warm, mesotrophic to eutrophic lakes (Jankovska and Komarek, 2000). *Polypodiaceae* ferns have a wide modern distribution from semideciduous forests in East Africa (Kreier and Schneider, 2006) to humid tropical rainforests in India (Panigrahi and Patnaik, 1961) and West Africa (Kreier and Schneider, 2006). Based on these distributions, abundant fern sori of *Polypodiaceae* are interpreted here as indicative of a relatively humid, though possibly seasonally dry, forested watershed. Chaoborids (lake-fly larvae) are common in lakes with anoxic bottom waters that provide refuge from fish predation, and are currently abundant in the stratified, deep waters of Lake Malawi (Dawidowicz et al, 1990; Irvine, 1995). Fish fossil abundance in Lake Malawi cores has elsewhere been interpreted as indicative of shallow lake depths, or widely fluctuating lake levels (Renithal et al., 2011). Finally, charred particle abundance is a reflection of fire frequency in the watershed. The frequency of fire and therefore charred particles is assumed here to be unimodal in terms of effective moisture balance requiring conditions that are arid enough for fires to start, but not so arid as to preclude sufficient vegetative cover to maintain fires (Whitlock and Millspaugh, 1996; Bird et al., 2004; Cohen et al., 2007). Modern distributions of sand-sized charred particles (macro-charcoal) in Lake Malawi suggest their abundance is representative of the local fire history and is delivered from the watershed to the lake via rivers (Appendix B – this dissertation), whereas micro-charcoal may be windborne, and therefore more indicative of regional fire history (e.g. Thevenon et al., 2003).

Mineral indicators used in this study include the relative abundance of authigenic and diagenic pyrite and siderite, and terrigenous quartz, mica and ooids (coated grains) retained in the sieved coarse fraction of lake sediment. Pyrite and siderite form in reducing environments either in the water column (often framboidal pyrite; Wilkin and Barnes, 1997), or within the pore space between the sediments (Postma, 1982). They are most likely to form in environments with high organic matter content (Taylor and Macquaker, 2011), such as swamps, marshes, and deltas (Postma, 1982; Moore et al., 1992; Sapota et al. 2006). Siderite also forms in the absence of pyrite in non-organic-rich environments with low concentrations of sulfur (Kelts and Hsu, 1978; Giresse et al., 1991). Calcium carbonate ooids form in a very narrow range of water depths and energy conditions (Heller et al., 1980; Wilkinson et al., 1980), requiring medium sand for nucleation, and sufficient bottom-water energy for the grain to be entrained and buffeted along the lake floor (upper 5m in lakes). Sand-sized mica flakes are often concentrated in distal-deltaic environments where they settles out hydrodynamically (Park and Cohen, 2012). High percentages of terrigenous quartz grains are indicative of shallow, littoral, possibly wave-dominated environments (Jones and Bowser, 1978; Cohen, 2003).

Methods

Core recovery, description and geochronology

The Lake Malawi Drilling Project recovered seven sediment cores from two sites in the lake during 2005. Details of the drilling operations are provided in Scholz et al (2006). This paper focuses on the sedimentary record preserved in the 380.7m-long Core

1B (11.3°S, 34.44°E, 592m depth). Previous papers have described in detail the core collection and description of the shorter core from the deep-water site, Core MAL05-1C (Scholz et al. 2011a) and the same methods were followed in the recovery and description of Core 1B. All cores of the Lake Malawi Scientific Drilling Project were described and imaged at the National Lacustrine Core Repository (LacCore) in Minneapolis, Minnesota. Dating of the sediments required the use of multiple methods due to the length of the cores, and the paucity of volcanic ash in the sediment. These methods included radiocarbon, optically stimulated luminescence (OSL), paleomagnetism (correlation of paleo-intensity and inclination records), tephra correlation and Argon-Argon geochronology. The age model used in this study will be published elsewhere (Lyons et al., *in prep*.)

Wet-sieved residue methods

Sediment samples (n=1945) were taken at 16cm intervals (average inter-sample resolution ~570 years). Sediment treatment followed a variant of the methods described in Forester et al. (1994). Samples were split into two aliquots; the first was weighed then disaggregated using deionized (DI) water and freeze-thaw treatment (often requiring multiple cycles), and finally washed through 63μm mesh stainless steel sieves to recover all material sand-sized and greater. The second aliquot was weighed wet, oven-dried at 60°C for at least 48 hours, and re-weighed to determine water content. This calculated water content was then used to determine the dry weight of the sieved aliquot.

Wet-sieved residues were counted for total number of ostracodes per sample (normalized to abundance/gram dry weight), taphonomic condition (% broken, whole

carapace, adult, carbonate coated, oxidation/reduction stained), and each valve was identified to the species level where possible, using an Olympus SZH binocular microscope. Ostracode identification followed Martens (2003, 2002, 1988, 1986), Park and Cohen (2011), Rosetti and Martens (1998), Kempf (1980), Howe (1955), Van Harten (1979), Neale (1979), Howe (1955), Klie (1944), Sars (1924, 1910). Additionally, the wet-sieved residues were counted for absolute abundance of other common fossil remains in this same size range (chaoborid fragments, charred particles, fish (including bones, teeth, and scales), algae (*Pediastrum* and *Botryococcus*), *Polypodiaceae* sori, and the relative abundance of mollusk fragments, and both monomineralic and lithic grains in the sand fraction (specifically: quartz, mica, pyrite, siderite, vivianite, aragonite needles and ooids). Fossil identifications were confirmed using a Hitachi 3400N SEM and compared to modern material from Lake Malawi (Martens, 2002). Mineral identifications were confirmed using an Oxford EDS/EBSD system in conjunction with the SEM.

Data screening and statistical analysis

Before any analysis we plotted raw data from all samples chronologically against depth and age. Prior to multivariate statistical analysis, we removed 12 samples that contained none of the indicators sought (remaining n=1933). The count-data were log-transformed prior to analysis. At this point we performed an indirect ordination detrended correspondence analysis (DCA) on all samples containing ostracodes identified to the species level to determine if grouping by higher taxonomic level was justified (ter Braak and Prentice, 1988). Further analyses group ostracodes by genus or subfamily (Cypridopsinae). Before the next analysis, we removed those indicators that were present

in fewer than 90 total samples in the dataset (< 5% occurrence). These rare indicators included the monospecific genera *Gomphocythere* and *Zonocypris*, oxidation and reduction staining of valves, aragonite needles and vivianite. Using the absolute and relative abundance data of the remaining indicators, zonation of the paleoecological record was determined using stratigraphically-constrained cluster analysis (CONISS) (Grimm, 1987). The data were square-root transformed prior to the cluster analysis using the software program Tilia ©, version 1.7.16 (Grimm, 1992). The number of important stratigraphic zones (8) was determined subjectively based on the branching of the dendrogram (Figure C-2b). Stratigraphic zones spanning less than 10 thousand years (kyrs), or less than 1% of the record, were grouped with the most similar neighboring zone. All 8 major zones are significant according to the broken-stick model (Bennett, 2006) generated using the "*rioja*" package of the program R ©, version 2.12.0 (Juggins, 2009; R Development Core Team, 2010). Significant zones are numbered MAL1-8 with subzones designated by letters (a-c).

In addition to stratigraphic zonation, we were interested in how the multiple indicators correlated with each other and the patterns that could be drawn from those correlations (ter Braak and Prentice, 1988). Due to the variety of data types in the dataset we used a principal components analysis (PCA) on the indicators not excluded above. These included: the relative abundance of the ostracode taxa Cypridopsines, *Limnocythere*, *Candonopsis*, *Ilyocypris*, and *Sclerocypris*, their taphonomic condition (broken, whole carapace, adult, carbonate coated), the LOG-concentrations of chaoborid fragments, charred particles, fish (including bones, teeth, and scales), algae (*Pediastrum*

and *Botryococcus*), *Polypodiaceae* sori, and the relative abundance mollusk fragments and authigenic and terrigenous mineral grains in the sand fraction (quartz, mica, pyrite, siderite, and ooids). As a result of the prevalence of siderite in both anoxic shallow and deep water environments (Taylor and Macquaker, 2011; Postma, 1982), and the prevalence of pyrite (± siderite) in shallow anoxic environments (Postma, 1982, Chowdhury and Noble 1996) its utility as a hydrologic indicator was minimal. To maximize its use, we separated the relative percentage of "siderite" into "organic matter-rich (OM)" and "basinal" depending on the presence (OM-rich) or absence (basinal) of pyrite in the same sample. PCA of 23 variables and 1933 samples was performed using the "*vegan*" package and the program R ©, version 2.12.0 (Jari Oksanan et al. 2011; R Development Core Team, 2010).

Stable Isotope Analysis

Stable isotope ratios of oxygen ($^{18}O/^{16}O$) and carbon ($^{13}C/^{12}C$) were measured on a small sample set of ostracode and mollusk shells. Stable isotope data are expressed in delta notation ($\delta^{18}O$ and $\delta^{13}C$) relative to the PeeDee Formation belemnite (PDB) standard (Lister, 1988). Twenty three samples were run on six ostracode species and two samples were run on mollusc shell carbonate. Depending on estimated valve mass, between 8 and 20 ostracode valves were picked per species for each sample. Samples including species with thicker, larger valves (e.g. *Sclerocypris c.f. jenkinae*) or a high percentage of adult valves, required fewer total valves analyzed. Samples were chosen based on total number of ostracodes present, genera diversity, and location in the core in order to maximize spatial coverage and to include each major genus represented in the

core. Further, likely lake-water $\delta^{18}O$ values were calculated, taking into consideration temperature-dependent fractionation effect between water and carbonate, and an average ostracode fractionation effect (for the ostracode samples) of 1.2‰ (D. Dettman, personal communication, 10/9/12). These water values were calculated only for carbonate $\delta^{18}O$ samples with 1-sigma errors of 0.10‰. $\delta^{18}O$ and $\delta^{13}C$ of the carbonates were measured using an automated carbonate preparation device (KIEL-III) coupled to a gas-ratio mass spectrometer (Finnigan MAT 252). Powdered samples were reacted with dehydrated phosphoric acid under vacuum at 70°C. The isotope ratio measurement is calibrated based on repeated measurements of NBS-19 and NBS-18 and precision is ± 0.10 ‰ for $\delta^{18}O$ and ±0.10‰ for $\delta^{13}C$ (1 sigma) except for the following the following: All measurements of $\delta^{18}O$ and $\delta^{13}C$ listed in Table 3 with larger than 0.10‰ error have been corrected after the analysis for low voltage, which occurs when low amounts of CO_2 are evolved from the carbonate in the sample. This affected the measurements of *Candonopsis sp.*, both species of *Limnocythere*, one sample of *I. alta* and *Cypridopsine n.gen. sp.2*.

Results:

Stratigraphy – Raw data

Zone 1: 380-341 mblf (1.25-1.18 Ma)

Zone 1a: 380-358 mblf (1.25-1.21 Ma)

This subzone is characterized by faintly laminated to massive, greenish-grey muds and silts interbedded with massive, fine to medium quartz sand (Figure C-2a).

Diatoms are absent from smear slide observations throughout this interval. The base of the core (380-374 m) is the sandiest interval, with the lowermost two meters characterized by poorly-sorted, medium-grained sands interbedded with massive silts. Above this the sands are fine-grained, cross-bedded, and well sorted (~378-374 m), and interbedded with massive silts and muds. From 374-360 m the intervals of interbedded muds are characterized by fine, faint lamina composed of either white carbonate or siderite. Locally these laminations are up to ~5mm thick.

The mineralogy of this subzone is characterized by high proportions of all mineral grains (mostly quartz and mica) with lesser abundances siderite, pyrite, ooids and aragonite needles (Figure C-2b). Quartz and mica dominate the sand fraction at the base of the core described above (374-380 m), with less abundant siderite. This is followed by peaks in the abundance of both ooids and aragonite needles between ~372-365 m, and then a return to mica dominance with lesser quartz and siderite (365-360m). This is the only interval in which aragonite needles are found. The subzone ends at ~358 mblf with a spike in the abundance of both pyrite and quartz.

Ostracode presence in this subzone is sporadic but where present they are dominated by *Ilyocypris alta* and *Sclerocypris sp.* with less abundant and less frequent *Candonopsis sp.*, and one or more unidentifiable species of Cypridopsine and *Limnocythere* (Figure C-3a). The latter two taxa are unidentifiable at the species level in this subzone because they are represented by juveniles and coated and broken valves. Higher percentages of adults occurs in the same intervals where *I. alta* is abundant,

whereas *Sclerocypris sp.* abundance is coincident with increased percentage of carbonate coatings on ostracode fossils (~370 m) (Figure C-3b).

Aside from ostracodes few other fossils were found at the base of the core (~375-380 m) (Figure C-2c), although there is a thin interval where fish are present, though not abundant (376-378 m). This is followed by the sudden appearance and persistence of charred particles and chaoborid fragments in the record (375-360 m). Their appearance is coincident with a thin interval of high abundance of the green algae *Botryococcus* and *Pediastrum* (375-365 m). The abundance of charred particles increases into the next subzone, whereas the other biota decline in abundance or disappear entirely (e.g. *Botryococcus*).

Zone 1b: 358-353 mblf (1.21-1.20 Ma) 10 kyrs

Subzone 1b is characterized by faintly to coarsely laminated, banded, greenish-grey silty clay (Figure C-2a). Locally, these lamina are aragonitic (e.g. 355-356 m). Diatoms are absent from smear slide observations throughout this interval. The relative abundance of all mineral grains is significantly less in subzone 1b than the previous interval (Figure C-2b). Quartz and mica are absent from this interval. Pyrite is present throughout the subzone, though at low abundances (~10%), and there is a thin (<0.5 m) interval where siderite peaks in abundance between 354 and 353 mblf. Ooids and aragonite needles are absent from this interval.

Ostracodes have a more consistent presence during this subzone, however the dominant taxa remain the same: *I. alta* and *Sclerocypris sp.* (Figure C-3a). The subordinate taxa are also similar to those in Subzone 1a: *Candonopsis sp.*, and one or

more unidentifiable species of Cypridopsines. There are also two species that appear for the first time in this subzone, Cypridopsine n.gen. sp. B at 356 m, and *Gomphocythere huwi* at 354 m. Neither of these species persists throughout the interval. A significant difference between the previous subzone and Subzone 1b is in the taphonomic condition of the ostracodes. There is no evidence of carbonate coatings preserved in this interval (Figure C-3b). In addition, samples in this interval had higher percentages of juveniles and were more consistently broken than in Subzone 1a.

The defining characteristic of this subzone that distinguishes it from those above and below is the abundance of the green algae *Botryococcus* and *Pediastrum* throughout the 5-meter interval (Figure C-2c). *Polypodiaceae* sori are rare over this interval and disappear entirely from the record for the next ~125 meters. Charred particles, chaoborid fragments and total fish fossils are present throughout.

Zone 1c: 353-341 mblf (1.20-1.18 Ma)

Subzone 1c is characterized two different lithologies. From 353-347 mblf it is the same as in Subzone 1b, faintly to coarsely laminated, banded, greenish-grey silty clay. This is overlain by faintly laminated, greenish-black, silty clay interbedded with massive, very fine sand from 347-343 mblf, at which point the interbedded sands disappear, and silty clays again dominate into the next subzone (Figure C-2a). As in the previous two subzones, diatoms are absent from smear slide observations throughout this interval.

Sand-sized mineral grains are again present in this subzone, particularly quartz and mica, which continue at high abundances throughout the interval, and siderite, which peaks during a thin interval (~346 m), and then persists at lower abundances for the

remainder of the interval (Figure C-2b). Pyrite and ooid grains are rare or absent for much of the interval, followed by significant peak in abundance marking the end of the interval (~342-341 m). These minerals are increasingly abundant above the lithologic change from silty clay to interbedded silts, and sands. In addition, subsequent subzones lack significant quantities of ooids, quartz or mica until ~290 mblf.

Ostracodes are again consistently present throughout this subzone, and the dominant taxa remain unchanged: *I. alta* and *Sclerocypris sp.* (Figure C-3a). The subordinate taxa are also similar to those in Subzone 1a and 1b: *Candonopsis sp.* and one or more unidentifiable species of *Limnocythere*. However, unlike previous intervals, *Candonopsis* sp. is continuously present, comprising ~25-35% of the ostracode assemblage throughout this subzone. *G. huwi* and *I. propinqua* are rare. Ostracodes in this subzone are increasingly carbonate coated up-section, and are represented mostly by juveniles until ~343-341 mblf (Figure C-3b). Similar to the preceding interval, there is a high proportion of broken valves throughout the subzone, with the exception of an extremely thin interval (344 m) where a number of whole carapaces are also found.

Whereas the ostracode fossil assemblage in this interval is similar to the previous one, the other fossils are noticeably different, particularly the precipitous decline in green algae at the beginning of Subzone 1c (Figure C-2c). Mollusc fragments are present though rare until 350 mblf. Their disappearance from the record is coincident with the beginning of a rapid decrease in charred particle abundance to a complete absence of such fossils by 345 mblf. Fish fossils and chaoborid fragments are present, though at lower abundances than the preceding interval.

Zone 2: 340-286 mblf (1.18-1.03 Ma)

Zone 2a: 340-321 mblf (1.18-1.14 Ma)

Subzone 2a is a faintly laminated to massive, greenish-grey silty clay (340-333 m) overlain by finely laminated, greenish-grey silty clay and mud (grain size alternates at 1-3m resolution between 333 and 321 m) (Figure C-2a). Unlike Zone 1, diatoms are present in this subzone, though it is locally diatom-poor. A 5-meter interval of core from 325-330 mblf is disturbed in this interval. In stark contrast to Zone 1 which was dominated by sand-sized mineral grains throughout, subzone 2a lacks any significant accumulation of such sediment (Figure C-2b). There is a thin peak in pyrite abundance at ~336 mblf, and mica and siderite are present, though rare throughout this subzone.

Ostracodes are abundant in specific sub-intervals of Zone 2a, 337-334 m and 330-321m (Figure C-3a). Where present, the dominant taxa are similar to those in Zone, *I. alta* and *Sclerocypris sp.*, however the subordinate taxa are quite different. *Limnocythere s.l. sp.4* is quite abundant in the lower sub-interval, its first appearance in the record. There are also rare occurrences of *Limnocythere s.l. sp.1*, *Cypridopsine n.gen. sp.2 n.sp.*, *Candonopsis sp.*, *G. sp. 3* and one or more unidentifiable species of both *Limnocythere* and Cypridopsines. Subzone 2a has the most diverse assemblage of ostracode taxa to this point in the core. Notably different from the previous interval is the appearance and abundance of *L. s.l. sp.4* and decreased abundance of *Candonopsis sp.*. Zone 2a ostracodes are rarely carbonate coated, are frequently broken, are represented more often by adult valves than in the previous zone, and in the lower sub-interval are represented by a significant number of whole carapaces (Figure C-3b).

Other fossils in this subzone include *Botryococcus*, fish, charred particles and chaoborid and mollusk fragments (Figure C-2c). *Botryococcus* is present in discrete horizons, whereas fish, chaoborids and charred particles are consistently present throughout the interval. Mollusc fragments are rare. Total fish abundance increases across the subzone in contrast to chaoborids and charred particles which increase in abundance until 330 mblf, and subsequently decrease. This peak in abundance between 333 and 330 mblf is coincident with peaks in fish and *Botryococcus* fossils as well.

Zone 2b: 321-299 mblf (1.14-1.07 Ma)

Zone 2b is characterized by alternately finely laminated to massive, greenish-grey silty clay and mud (Figure C-2a). Like the previous interval, grain size alternates at 1-3 meter resolution throughout. From the smear slides, diatoms are few or rare in the massive interval from 312-308 mblf. The only sand-sized mineral grains with any significant presence in this subzone are authigenic pyrite and siderite, which appear to alternate in abundance: where siderite is abundant (321-315 and 305-303 mblf), pyrite is rare, and vice versa (Figure C-2b).

The ostracodes of Zone 2b are dominated by *Candonopsis sp.* with lesser *I. alta* across the entire subzone (Figure C-3a). This is the first and only subzone in which *Candonopsis sp.* is the single dominant species. The subordinate other taxa in this interval are *Sclerocypris sp.* and all *Limnocythere* from 321-315 mblf, followed by a marked shift to *Cypridopsine n.gen. sp.B* and one or more unidentifiable species of Cypridopsines from 306-300 mblf. Zone 2b ostracodes include the highest proportions of adult valves (throughout) and whole carapaces (esp. 309-300 mblf) of any other intervals

in the core (Figure C-3b). Overall, broken valves and carbonate coatings are less common in this subzone than previous zones.

Total fish, chaoborid fragments, charred particles and *Botryococcus* are found throughout this subzone at relatively constant abundances (Figure C-2c). However there are a few thin intervals of peak abundances: in fish fossils from 315-313 mblf and in both charred particles and *Botryococcus* at 321 and 319-314 mblf. Mollusc fragments are also found in this subzone, although sporadically and in low abundance. *Pediastrum* are present at discrete depths in moderate abundances (315, 309, 301 mblf).

Zone 2c: 299-286 mblf (1.07-1.03 Ma)

This 13-meter subzone is faintly laminated to massive, greenish-grey mud until 296 mblf where it changes to finely laminated to massive, greenish-grey silty clay (Figure C-2a). From 289-287 mblf the laminations are aragonitic and/or sideritic. This interval is locally diatom-poor. Similar to the rest of Zone 2, the mineralogy of the Zone 2c coarse fraction is predominately pyrite and siderite in varying abundances throughout, although there is no apparent oscillation between the two minerals in this subzone (Figure C-2b). There is a thin interval at the top of 2c in which mica dominates the sand fraction (290-286 mblf).

Ostracodes are rare in this subzone (Figure C-3a), and no one taxon dominates over the entire interval. Rather, the presence of individual taxa appears to alternate, beginning with *Limnocythere sp.1* (299-295 mblf), then *Cypridopsine n.gen. sp.B* and one or more unidentifiable Cypridopsines (295-292 mblf), followed by *Candonopsis sp.* and *I. alta* (290-288 mblf) and finally *Sclerocypris sp.*, *G. huwi* and *Candonopsis sp.* (288-

286 mblf). Throughout this interval, carbonate coating is infrequent, but where it occurs, 100% of the assemblage is coated (Figure C-3b). In addition, where adult valves are present, they compose a majority of the assemblage. Within this interval whole carapaces are preserved at 295 and 292 mblf, coincident with decreased broken valves.

Other fossils preserved in Subzone 2c are similar to those from 2b (Figure C-2c). Mollusc fragments, *Pediastrum* and *Botryococcus* occur sporadically, with coincident increases in the two green algae. Charred particle and chaoborid abundance decrease over this interval whereas the abundance of fish fossils increases in the latter half of 2c (~294-287 mblf). The peak abundance of fish fossils coincides with spikes in green alga1 abundance. Zone 2c is the last subzone in the 1B core record in which mollusc fragments comprise greater than 5% of the sand-sized fraction.

Zone 3: 286-255 mblf (1.03 Ma – 933 ka)

Zone 3a: 286-255 mblf (1.03 Ma – 933 ka)

Zone 3a is composed entirely of greenish-grey mud that is alternately massive (280-276 and 270-256 mblf), finely laminated (276-270 mblf), and coarsely laminated (286-280 mblf) (Figure C-2a). The majority of the mud in this zone is diatomaceous, although there is a thin diatom-poor interval from ~264-260 mblf. The mineralogy of the sand-sized fraction in Zone 3a is dominated primarily by pyrite and siderite, and as in Zone 2b these minerals are alternately dominant from the base of the zone to 260 mblf, at which point they co-occur for ~2 meters (Figure C-2b). The most striking feature of the suite of grain types in this subzone is the reappearance of ooids and their dominance of the sand sized fraction in the thin intervals where they occur (at 285, 278-276, 260, and

256-255 mblf). Vivianite appears in low abundances for the first time in the core, just after the lowermost spike in ooid abundance (~284-280 mblf). Mica abundance is negligible throughout.

Starting in this zone, ostracodes are present (and likewise absent) in discrete intervals (Figure C-3a). For example, in Zone 3a ostracodes are found at the following depths but are absent from the record in between: 286-282 m, 280-276 m, sporadically between 276 and 270 m, 268-266 m, and 261-255 m. As in the previous subzone, there is no single dominant taxa. *Sclerocypris sp.* is the only species present across the entire interval, but it appears intermittently. Four taxa occur separately in only one horizon throughout Zone 3a: *Limnocythere sp.1*, *G. huwi*, unidentifiable Cypridopsines, and *Candonopsis sp.* (listed from bottom to top of 3a). Additionally, unidentifiable *Limnocythere* are sporadically abundant from the base of 3a to ~272 mblf. The top of this zone is dominated by *I. alta* with lesser *I. propinqua* beginning at 261 mblf. Taphonomically, ostracode valves in this zone are dominantly broken juveniles that lack carbonate coatings and are seldom preserved as an entire carapace (Figure C-3b).

Charred particles are the only fossils present across all of Zone 3a (Figure C-2c). Abundances of fish fossils, chaoborid fragments, charred particles and *Botryococcus* peak over the same sub-interval, ~275-270 mblf. Below this peak, fish fossils are scarce to absent. Above this depth chaoborids and *Botryococcus* disappear from the record, and fish fossils and charred particles decrease in abundance, until the start of the next zone.

Zone 4: 255-203 mblf (933-657 ka)

Zone 4a: 255-244 mblf (933-872 ka)

This subzone is characterized by finely laminated, greenish-grey, diatomaceous silty clay from 254-247 mblf (Figure C-2a). Thin intervals at the top and bottom of the subzone (255-254 and 247-244 mblf) are composed of greenish-black to grey, diatomaceous mud. The sand fraction mineralogy of Zone 4a is dominated by siderite, with lesser pyrite until ~249 mblf (Figure C-2b). The disappearance of pyrite at this depth is coincident with the appearance of trace amounts of vivianite.

Ostracodes are found in this subzone only from 256-250 mblf (Figure C-3a), and are mostly unidentifiable fragments. Where recognizable, the taxa were indistinguishable Cypridopsine species at 255 and 251 mblf, and *I. alta* and *Sclerocypris sp.* at 253 mblf. Zone 4a ostracodes were typically uncoated, broken, juveniles (Figure C-3b).

Other fossils in this subzone are the same as Zone 3a (Figure C-2c). *Botryococcus* is abundant just at the transition from 3a, ~256 mblf, and again beginning at 250 mblf. Across subzone 4a, abundance of charred particles increases whereas that of chaoborid fragments decreases. There is no trend to the fish fossil data, though fish fossil abundance is widely variable on a sub-meter scale.

Zone 4b: 244-228 mblf (872-791 ka)

This subzone is characterized by finely laminated (244-234 mblf), and massive (234-230 mblf), greenish-grey, diatomaceous mud (Figure C-2a). The mineralogy of the sand fraction is limited to siderite (dominant until 235 mblf) and pyrite (dominant above 235 mblf). This change in mineralogy is coincident with the change in bedding type. Mica is negligible throughout (Figure C-2b).

Total ostracode abundance decreases from the beginning of Zone 4b to a thin interval where they are absent from the record at ~ 236 mblf, above which their abundance gradually increases to the end of the zone. The ostracode assemblage in subzone 4b is quite diverse compared to 4a (Figure C-3a). Unidentifiable Cypridopsine and *Ilyocypris* species alternate dominance between 244-235 mblf. At 235 mblf the assemblage changes to one composed of *I. alta*, *Sclerocypris sp.*, *G. huwi* and one or more unidentifiable species of Cypridopsines until 230 mblf, where Cypridopsines become the dominant taxa, specifically *Cypridopsine n.gen. sp.B* and *Cypridopsine n.gen. sp.2*, with minor *Candonopsis sp.*, until the end of the subzone. Zone 4b ends with an abrupt cessation of ostracode deposition. Ostracodes in this zone are carbonate coated and occasionally broken from 254-250 mblf, and are represented by mostly juveniles until ~237 mblf. Between 250-234 mblf the ostracodes are infrequently broken, and from 237-234 mblf, are frequently represented by adult valves and whole carapaces (Figure C-3b). Between 232 and 228 mblf the assemblage is represented by juveniles, occasionally whole carapaces, and are infrequently carbonate coated. Additionally, at 230 mblf ~30% of the assemblage is reduction stained, and at the transition to Zone 4c the majority are oxidation stained (228 mblf).

Other fossils in Zone 4b include fish, chaoborids, charred particles, and both green algae (Figure C-2c). Fish fossils increase in abundance over this interval, as charred particle abundance decreases. Chaoborid abundance gradually increases to a maximum between ~236-234 mblf, after which point it decreases through the top of the zone. *Botryococcus* peaks between 239 and 235 mblf and is scarce to absent in the zone

outside of those depths. *Pediastrum* is found sporadically throughout the subzone, in low abundances.

Zone 4c: 228-203 mblf (791-657 ka)

Zone 4c is characterized by finely laminated to massive, greyish-brown silty clay (228-215 mblf), overlain by an interval of rapidly alternating (<1.5 m resolution), massive, brown silty -clay and mud (Figure C-2a). This subzone is locally disturbed (~220-217 and 207-202 mblf) and locally diatom-poor (228 and 208 mblf). The mineralogy of the sand-sized fraction is similar to the other subzones of Zone 4 until 210 mblf (Figure C-2b). Below this depth, siderite is the dominant mineral, with negligible mica. Above this depth ooids reappear in the record for the final time. They are the co-dominant minerals between 210 and the top of Zone 4c (203 mblf).

Ostracodes are largely absent from the record in this zone until ~215 mblf, and they remain abundant until ~205 mblf (Figure C-3a). *I. alta* and other unidentifiable *Ilyocypris* taxa dominate the assemblage with lesser *Sclerocypris sp.*, *Cypridopsine n.gen. sp.2* and other unidentifiable Cypridopsines. Trace *I. propinqua* is found at ~208 mblf. This is the final zone in which *Ilyocypris* or *Sclerocypris* species are found in great abundance over an interval greater than 1 meter. The ostracodes in Zone 4c are predominantly juveniles, and are rarely carbonate coated and/or reduction stained (only between 207-205 mblf) (Figure C-3b). Similar to the rapidly alternating grain size described above for this interval, the percentage of broken valves in a sample varies rapidly from less than 5% to 100% at sub-meter resolution.

With the exception of mollusc fragments (last seen in the record at ~285 mblf), all other indicator fossils are found in Zone 4c including fish, chaoborids, charred particles, *Polypodiaceae*, *Pediastrum* and *Botryococcus* (Figure C-2c). There are two peaks in abundance that are coincident across all of these fossils; the first, at the base of the subzone between 228-223 mblf, the second from 216-213 mblf. Above this, there is a less pronounced peak in the abundance of fish, chaoborids and charred particles from 209-206 mblf. *Polypodiaceae* sori and *Pediastrum* are absent from these depths, and *Botryococcus* is intermittently present at low abundances.

Zone 5: 203-191 mblf (657-595 ka)

Zone 5a: 203-191 mblf (657-595 ka)

Zone 5a is predominantly characterized by massive, brown silty clay (203-196 mblf), overlain by finely laminated, brown, diatomaceous silty clay (195-191 mblf) (Figure C-2a). There are few diatoms noted in smear slide observations in the lower unit at ~198 mblf. The mineralogy of the sand fraction in Zone 5a is dominated by mica at ~202 mblf, above which it is composed of siderite and mica (200-195 mblf), and finally quartz and pyrite, with lesser mica and siderite at the top of the zone (193-191 mblf) (Figure C-2b).

Ostracodes are less abundant in Zone 5a than in any other zone in the core, even though they are present throughout the entire interval. Zone 5a is the only zone in which *Cypridopsine n.gen. sp.1* dominates the assemblage (Figure C-3a). It is one of the main distinguishing features of this zone. This species is extremely abundant from 202-199 mblf, above which it is sporadically abundant. Subordinate species in this subinterval are

Limnocythere sp.1, *Candonopsis sp.*, *I. alta* and *G. huwi*. Between 199-192 mblf the majority of ostracodes are unidentifiable Cypridopsines and infrequently *Cypridopsine n.gen. sp. 1*, with lesser *Cypridopsine n.gen. sp.B, Cypridopsine n.gen. sp.2*, *Candonopsis sp.*, *I. alta*, and unidentifiable species of *Limnocythere* and *Ilyocypris*. This zone contains a very diverse assemblage, although throughout the interval none of the "lesser" species listed above ever compose more than 50% of the assemblage. Intervals dominated by *Cypridopsine n.gen. sp.1* are more likely to be represented by unbroken (and possibly whole carapaces), adult, occasionally carbon coated valves (Figure C-3b). Broken valves are more common in the upper sub-interval of this zone (199-192 mblf). Reduction staining of valves at ~198 mblf is coincident with increased *Ilyocypris* abundance.

The other fossils present in this zone are the same as those in Zone 4c (Figure C-2c). Fish fossils and chaoborid fragments increase in abundance from the base of the zone to the top. Charred particles, *Polypodiaceae* and *Botryococcus* peak in abundance between ~196 and 199 mblf. *Botryococcus* has a secondary peak at the top of the zone from 194-192 mblf, coincident with increased *Pediastrum* abundance.

Zone 6: 191-154 mblf (595-401 ka)

Zone 6a: 191-165 mblf (595-460 ka)

Zone 6a is composed of diatomaceous silty clay throughout. It is finely laminated to massive, and greyish-brown from 191-183 mblf, and faintly to finely laminated, grey to greyish-brown between 183-165 mblf (Figure C-2a). The sediment is disturbed from 189-187 and 171-169 mblf. The mineralogy of the sand fraction in Zone 6a is entirely dominated by siderite, the abundance of which varies in a pulse-like fashion throughout

the zone (Figure C-2b). Siderite is noticeably absent from the record between 185-180 and 176-173 mblf. Pyrite and quartz are present in negligible amounts until 174 mblf, above which they are both absent. Mica is abundant sporadically throughout the entire interval, reaching maximum abundances of ~10% of the sand fraction.

Ostracodes of Zone 6a are found solely between 185-170 mblf, with maximum abundance and most continual presence from 180-173 mblf (Figure C-3a). No single taxon is particularly dominant over the entire subzone. One or more species of *Limnocythere* and *Ilyocypris* are found between 185-180 mblf. At this point there is a noticeable change to a more diverse assemblage composed primarily of indistinguishable Cypridopsines and *Limnocythere*, with sporadic contributions from *Cypridopsine n.gen. sp.J*, *Cypridopsine n.gen. sp.2*, *Limnocythere sp.1* and *Candonopsis sp.* from 180-173 mblf. The majority of ostracodes in this interval are identifiable only to the genus level, likely due to the high percentage of broken, carbonate coated, juvenile valves preserved, particularly above 180 mblf (Figure C-3b). Where dominated by *Limnocythere* and *Ilyocypris* below that depth, the ostracodes are commonly reduction stained, represented by juveniles, and occasionally broken.

Chaoborid fragments, charred particles and fish fossils are continuously present throughout this interval, with no significant peaks in abundance (Figure C-2c). In contrast, the occurrence of *Polypodiaceae* sori, *Pediastrum* and *Botryococcus* is very punctuated. All three of these indicators peak between 190-185 and 173-170 mblf. *Botryococcus* is also abundant from 181-177 and above 170 mblf until the top of the subzone, at which point its abundance decreases precipitously.

Zone 6b: 165-154 mblf (460-401 ka)

Zone 6b is characterized by faintly to coarsely laminated, grey, diatom-poor mud (Figure C-2a). There is a thin interval of disturbance between 162-159 mblf. This interval appears largely devoid of all sand-sized mineral grains (Figure C-2b). However, there are trace (< 1%) abundances of quartz and mica throughout, and slightly higher (< 5%) abundances of mica and pyrite at 162 and 157 mblf, respectively.

Ostracodes are increasingly abundant over the length of Zone 6b (Figure C-3a). Similar to the previous interval, Zone 6b ostracodes are diverse, particularly below 160 mblf where no single taxon dominates the assemblage. This lower sub-interval includes *Cypridopsine n.gen. sp.2*, *Cypridopsine n.gen. sp. B*, *Limnocythere sp.1* and *sp.4*, *Candonopsis sp.* and one or more unidentifiable species of Cypridopsine and *Limnocythere*. The upper interval (160-154 mblf) assemblage is primarily composed of *Limnocythere* (undifferentiated and both unique species) and *Candonopsis sp.* There are also minor contributions from *Cypridopsine n.gen. sp.2* and unidentifiable Cypridopsines. Taphonomically, the ostracodes of the lower sub-interval are comparatively less broken, and more often represented by juveniles (Figure C-3b). High percentages of ostracodes from both intervals are carbonate coated.

Zone 6b is distinguished by the absence or rarity of *Polypodiaceae* sori, and both green algae (Figure C-2c). The abundance of fish fossils and chaoborid fragments neither increase nor decrease over the interval, whereas charred particles increase in overall abundance. The apparent gap in the record of fish fossils and chaoborid fragments is caused by the disturbed interval (162-159 mblf) mentioned earlier.

Zone 7: 154-125 mblf (401-278 ka)

Zone 7a: 154-145 mblf (401-355 ka)

Zone 7a is characterized by faintly laminated, grey, diatomaceous mud (Figure C-2a). The sediment is disturbed between 154-152 mblf. The interval is dominated by widely variable amounts of siderite, and a constant low abundance of mica (Figure C-2b). Quartz is found in trace amounts at ~150 mblf.

Ostracodes are extremely rare in Zone 7a (Figure C-3a). Where present (150 mblf), they are not at all abundant, and are represented by unidentifiable fragments in one instance, and by a single, adult, unidentifiable *Limnocythere* carapace in the other (Figure C-3b). This carapace showed signs of abrasion, but no coatings.

This interval is distinguished from its neighboring strata by its other fossils (Figure C-2c). This interval is dominated by extremely high abundances of both *Botryococcus* and *Pediastrum*, charcoal, and the continuous presence of *Polypodiaceae* sori. This is the only interval when the majority of these variables rise simultaneously to very high abundances over the entirety of the zone. On the other hand, the abundance of chaoborid fragments and fish fossils inversely varies with the abundance of the other fossils.

Zone 7b: 145-125 mblf (355-278 ka)

Zone 7b is characterized by coarsely laminated grey to brownish-grey mud from 145-136 mblf, and faintly laminated, grey, diatomaceous mud between 136-125 mblf (Figure C-2a). The interval is locally diatom-poor (139-136 mblf). In addition, there are two thin, intervals of disturbed sediment, 133-132 and 129-127 mblf. This change in

bedding type is coincident with changes in the sand fraction mineralogy in this zone (Figure C-2b). The lower sub-interval has minimally abundant pyrite and quartz, with trace mica present; the upper sub-interval is dominated by siderite, and also has trace amounts of mica.

This division of Zone 7b is apparent in the ostracode record as well (Figure C-3a). Ostracodes are abundant in the lower sub-interval (145-136 mblf) and are rare to absent in this zone above 136 mblf. *Limnocythere sp.1* is particularly abundant at the base of this subzone (145-142 mblf), though this dominance quickly gives way to its co-dominance with *Candonopsis sp.*, *Cypridopsine n.gen. sp.B* and *sp.2* and one or more unidentifiable species of Cypridopsine and *Limnocythere* (142-136 mblf). Zone 7b is the first interval in which *Zonocypris costata* is found (~142-140 mblf). Present in the record either discontinuously or at low abundances are: *Cypridopsine n.gen. sp.1* (142 mblf), *Limnocythere sp.4* (140 mblf), *Sclerocypris sp.* (144 and 137 mblf), *G. huwi* (137 mblf) and one or more unidentifiable species of *Ilyocypris* (137 mblf). This zone has the most diverse assemblage in the record in terms of total number of species represented. Taphonomically, the ostracodes of Zone 7b are represented by often broken, carbonate coated valves between 139-135 mblf (Figure C-3b). They are increasingly represented by adults up-section, and although rare between 135-133 mblf, are commonly reduction stained and preserved as a whole carapace in that sub-interval.

In Zone 7b the abundances of fish fossils and chaoborid fragments co-vary as do the abundances of charred particles, *Botryococcus* and *Polypodiaceae* sori (Figure C-2c). However, these two subgroups of other fossils vary in opposition to one another: Fish

fossils and chaoborids decrease in abundance throughout this interval, whereas charred particles, *Botryococcus* and *Polypodiaceae* sori increase.

Zone 8: 125-82 mblf (278-147 ka)

Zone 8a: 125-111 mblf (278-238 ka)

Zone 8a is composed of finely laminated, grey, diatomaceous mud (Figure C-2a). There is a thin interval of disturbed sediment between 113-111 mblf. Smear slide observations suggest minimal vivianite abundance at the base of this interval, although vivianite was not seen in the sand fraction component (Figure C-2b). In fact, Zone 8a lacks continuous abundance of any minerogenic sand-sized grains with the exception of 120-117 mblf where mica, siderite and trace amounts of pyrite are present.

There are two peaks in total ostracode abundance in Zone 8a centered on 123 and 115 mblf (Figure C-3a). Between these peaks, ostracodes are absent from the record at between 121-118 mblf. The lower sub-interval of Zone 8a is dominated by *Cypridopsine n.gen. sp.2* and one or more unidentifiable species of Cypridopsines and *Limnocythere*, with lesser *Candonopsis sp.*, and trace *Limnocythere sp.1*. The upper sub-interval from 118- 115 mblf is dominated by *Limnocythere sp.4* and other indistinguishable *Limnocythere* with significant *Cypridopsine n.gen. sp.2* and *Candonopsis sp.* and minor *Z. costata* and *I. alta*. Above 115 mblf, the zone is dominated by undifferentiated Cypridopsines, to the exclusion of everything else. Zone 8a ostracodes are more likely to be represented by adults, and are less likely to be broken in the lower sub-interval (125-121 mblf), than in the upper (118-111 mblf) (Figure C-3b). A small fraction of the ostracodes at ~123 mblf are reduction stained.

Other fossils in Zone 8a include fish, chaoborids, charred particles, *Polypodiaceae* sori, and *Botryococcus* (Figure C-2c). The abundance of fish fossils is similar in pattern to that of the ostracode fossils, with two peaks in the zone; the first centered at 123 mblf, the second at 115 mblf. These peaks are coincident with minimum *Botryococcus* abundance over this interval. The abundances of both *Polypodiaceae* sori and *Botryococcus* peak at ~119 mblf. Chaoborids become more abundant over this interval, whereas charred particle abundance exhibits no trend, but rather maintains an intermediate abundance throughout the zone.

Zone 8b: 111-82 mblf (238-147 ka)

Zone 8b is characterized by faintly laminated, grey, diatomaceous mud (111-100 mblf), faintly to coarsely laminated, grey to greenish-grey, diatomaceous silty clay (100-91 mblf), and faintly to finely laminated, grey, locally diatom-poor silty clay (91-82 mblf) (Figure C-2a). Vivianite was observed in smear slides at ~96 and 83-82 mblf, respectfully, but was not found in the sand-sized fraction mineral assemblage in this zone (Figure C-2b). Rather, siderite dominates the mineralogy with minimally abundant mica from 111-98 mblf. Between 98-89 mblf, mica is present in low abundance. From 86-89 mblf quartz, mica and siderite are simultaneously abundant, and above 86 mblf mica and pyrite are moderately abundant.

Ostracodes are rare to absent from Zone 8b between 111-97 and 92-85 mblf (Figure C-3a). Where present within those depths, they are represented solely by broken, unidentifiable fragments. From 97-92 mblf Zone 8b ostracodes are dominated by *Candonopsis sp.* and *Limnocythere sp.1* with lesser contributions from *Cypridopsine*

n.gen. sp.2 and one or more unidentifiable species of Cypridopsines, *Limnocythere*, and *Ilyocypris*. The top of the zone (85-82 mblf) is dominated by *Cypridopsine n.gen. sp.2* and *sp.B* with minor *Limnocythere sp.1* and *Candonopsis sp.* The lowest sub-interval of abundant ostracodes are more likely to be represented by unbroken, adult specimens, and are rarely carbonate coated (Figure C-3b). Above 92 mblf the majority of ostracodes are uncoated, broken juveniles, with the exception of a few samples at ~83 mblf where a small percentage of ostracodes are represented by whole carapaces, adults, and are either carbonate coated or oxidation stained.

All other fossil indicators are found in Zone 8b (Figure C-2c). *Pediastrum* are uncommon, occurring at the base and top of the zone, but nowhere in between. Mollusc fragments are found in trace amounts at ~91 mblf. The other five fossils are continuously present for the entire interval (or nearly continuously in the case of *Polypodiaceae* sori). As in the previous zone, peaks in the abundance of *Botryococcus*, charred particles, and *Polypodiaceae* sori are coincident. In Zone 8b, there are two such peaks centered on ~104 and 89 mblf. Chaoborid abundance displays muted peaks at those depths, in addition to a thin interval of highest abundance coincident with abundant fish fossils at ~90 mblf.

Stable Isotope Results

Twenty-five samples were successfully analyzed for their stable oxygen- and carbon-isotope content. Six ostracode species in 23 samples and two mollusc samples are represented in the dataset. Previous studies have used $\delta^{18}O$ and $\delta^{13}C$ ratios from ostracodes valves to infer changes in basin hydrology (e.g. open vs. closed lake basin),

changes in water chemistry (e.g. salinity), and habitats of different species (e.g. Forester et al., 1994; Holmes et al., 1997; Ricketts et al., 2001). The measured isotopic results and calculated lake water $\delta^{18}O$ are described below and listed in Table 3. Low voltage errors affected the precision of measurements for of *Candonopsis sp.*, both species of *Limnocythere*, one sample of *I. alta* and *Cypridopsine n.gen. sp.2*. However, as these are the only stable isotopic measurements on these species from Lake Malawi, these data are shown to provide a reference point for further research, despite their higher level of uncertainty.

The $\delta^{18}O$ and $\delta^{13}C$ values are evaluated by species versus the depth of the sample in the core (Figures 4a and 4b; error bars of ±1-sigma are shown). The range in $\delta^{18}O$ values is quite large between 0.34 and 9.09‰, with the most extreme values measured on different species of the same sample (315.435 mblf). When considering only those samples with the least uncertainty, the range shrinks to between ~+2.0 to +4.4‰, with an outlier at over +6‰. Although there is quite a range in values at each depth, even within a single species, it is interesting to note that the calculated water values for these samples fall between +2.9 and +5.2‰ at ~315 mblf and 200-208 mblf. These values are significantly more enriched in ^{18}O than the modern lake (+2.0‰ – Branchu et al., 2005), which is to be expected. In order for ostracodes to be present at the core site, the lake must have been ~400 meters lower than it is currently, implying a significantly more arid environment. This would shrink the overall lake size, and increase the evaporative enrichment of the remaining lake water. The intra-species variation within a single sample precludes the assessment of any species-specific vital effects.

The carbon-isotope results show much less intra-specific variation than the oxygen isotopes (Figure C-4b). Additionally, where the same species were measured at different core depths, their range of $\delta^{13}C$ values overlap. Given this, it is interesting that there is a distinct separation between the range of $\delta^{13}C$ values for *Cypridopsine n.gen. sp.1* (more positive) and those of *Sclerocypris c.f. jenkinae* and *I. alta* (more negative). Carbon isotopic measurements are frequently inferred to be measures of lake productivity with organisms drawing down the ^{12}C in the surface waters (enriching ^{13}C), then upon death and burial in bottom sediments, the ^{12}C is released back into the immediate environment, decreasing the water $\delta^{13}C$ (Lister, 1988). Organisms living in environments with a lot of organic matter deposition and oxidation, or authigenic carbonate precipitated in such environments, are more likely to have more negative $\delta^{13}C$ values (Lister, 1988; Ricketts and Johnson, 1996). The genus *Ilyocypris* is commonly found in modern river and marsh environments (e.g. Mezquita et al., 1999, Appendix B – this dissertation). Marsh and deltaic environments typically are areas of higher organic matter accumulation, which is also suggested from the core material with the co-occurrence of *Ilyocypris* species and framboidal pyrite. It is possible that the differences in the range of $\delta^{13}C$ values for these three taxa is caused by their living in different environments within the lake, and that *Ilyocypris* and *Sclerocypris* are both found in marsh/deltaic environments.

Multivariate analysis - Detrended Correspondence Analysis (DCA)

A DCA was performed on ostracode data including only species that had been identified to the species level, as a potential source of data reduction, to determine if

different species of the same genera often co-occurred in samples throughout the core. The DCA analyzes the actual abundance of each species at each site in multidimensional space and clusters sites with similar species assemblages (not figured), and those species that often co-occur (Figure C-3c). The first and second DCA axes each explain 14% of the variance in the dataset. The eigenvalues and percentage variance explained for all DCA axes are listed in Table 4, in addition to species scores for DCA1 and 2. In Figure C-3c, species plotting nearest to each other likely co-occur in multiple samples, and those plotting furthest from each other were less often found in the same sample. Noticeably, rare species in each genera plot to the outside of the graph, suggesting that where they occur, they generally do not co-occur with other species. Looking back at the raw data for the intervals in which each of these species was most abundant, this is the case for *Cypridopsine n.gen. sp.1, G. huwi,* and *Limnocythere s.l. sp.4*, which may explain the variance in DCA axis 1. The species separate primarily by genera or subfamily along DCA axis 2 suggesting assemblage variability in the dataset may be fully described at the genus (or subfamily) level. From this point on, analyses and descriptions will be by taxa, and will include abundances of ostracodes that were not able to be identified to the species level (e.g. those taxa in Figure C-3a listed as "undifferentiated" will be included with identified species of the same genus, or subfamily in the case of Cypridopsines).

Facies Identification and Cluster Analysis

Six distinct minerogenic facies are identified based on commonly associated sand-fraction mineralogy. Similarly, seven biofacies are delineated based on commonly associated fossils (Figure C-5). Each facies has a dominant indicator or group of

indicators, and a facies change occurs when indicator dominance shifts. These determinations were made looking solely at the co-occurring indicators, without reference to either the stratigraphic zonation supplied by the cluster analysis or the stratigraphic time series of principal component axis 1 (PC1) described below, to avoid researcher bias. A detailed description of each facies can be found in Table 5, however, notable indicator associations include: *Ilyocypris* with *Sclerocypris*, Cypridopsines with both *Candonopsis* and *Limnocythere*, *Botryococcus* with *Pediastrum* and *Polypodiaceae*, "basinal" siderite with minimal mica and little else, and the co-occurrence of all mineral grains (quartz, mica, siderite, pyrite, ooids).

Using a stratigraphically-constrained cluster analysis of the indicators shown in Figure C-5, we delineated eight significant zones and six sub-zones of stratigraphic similarity (see dendrogram, Figure C-2b). Zone boundaries were placed at significant branches in the dendrogram, and "sub-zones" are separated at less substantial branching locations. Biofacies and minerogenic facies changes commonly occur at these zone boundaries, suggesting the defined zones are accurately distinguishing regions of commonly associated indicators in the record. Furthermore, the zonation corresponds well with major changes in abundances of taxa thought to react strongly to environmental changes, and water depth (particularly presence/absence of ostracodes as a whole, versus *Pediastrum* and *Botryococcus*).

Multivariate analysis – Principal Component Analysis (PCA)

Eigenvalues and percentage variance explained for all principal component axes are listed in Table 6. The first two principal components (PC1, PC2) cumulatively

account for 23% of the variation in this dataset. We interpret PC1, which explains the most variation (14%), as primarily a water-depth gradient. The positive loadings on this axis include previously interpreted shallow water indicators such as percentage broken and adult valves, and all ostracode species (Figure C-6: Biofacies 3/4, 6/7). The negative loadings include biological and mineralogical indicators of both open waters and a generally more humid watershed conditions, including *Botryococcus* and basinal siderite, as well as charred particle abundance (Figure C-6: Biofacies 1, Minerogenic facies 5). PC2 (explains 9% variation) appears to maximize variance among the shallower water indicators, separating the ostracode taxa into two groups (Figure C-6: Biofacies 3/4 and Biofacies 6/7). Additionally, major shifts in PC1 values through time are in good agreement with the zonation described above, separating sections of core with similar taxa and similar environmental interpretations, supporting the interpretation that PC1 is likely correlated with changes in precipitation, which is strongly correlated with water depth. Interpretations made from this point forward are based on the facies associations described above, and like the major zonation boundaries, changes in facies are also in good agreement with major variation in the PC1 curve through time.

Interpretation (Figure C-7)

Zone 1: 380-341 mblf (1.25-1.18 Ma)

Zone MAL1a 380-358 mblf (1.25Ma – 1.18Ma)

This zone is represented by Minerogenic Facies 1, characterized by high percentages of all sand-sized terrigenous and authigenic mineral grains excluding ooids,

and Biofacies 3, dominated by *Ilyocypris* and *Sclerocypris* ostracodes, brief occurrences of *Candonopsis* or *Limnocythere*, and with *Botryococcus, Pediastrum,* and *Polypodiaceae* rare to absent. We interpret this combination of biologic and minerogenic facies as characteristic of a deltaic paleoenvironment. Given the co-dominance of these minerals, and the lithology of Zone 1a is described as interbedded sands, silts, and muds, it is likely that the environment at the core site shifted between distal and proximal deltaic throughout this interval.

Zone 1b: 358-353 mblf (1.21-1.20 Ma)

This zone is also represented by Minerogenic Facies 1, as described above, and Biofacies 4, which is characterized by the same dominant species as Biofacies 3, *Ilyocypris* and *Sclerocypris*, though now with brief occurrences of cypridopsine ostracodes instead of *Limnocythere* or *Candonopsis*. In addition, *Botryococcus* and *Pediastrum* are present in short, punctuated intervals. This zone is still interpreted as a deltaic environment based on Minerogenic Facies 1, and the dominant ostracode taxa. During the course of deposition of this subzone, it is probable that there was some degree of delta lobe migration allowing short periods when more open water biota flourished. This does not imply a change in lake level, but rather a transient change in areas of deltaic sedimentation.

Zone 1c: 353-341 mblf (1.20-1.18 Ma)

This zone is the last interval to be characterized by Minerogenic Facies 1. It is also characterized by Biofacies 3, as was Zone 1a, and differs from Zone 1b by the

disappearance of green algae as well as cypridopsine ostracodes. For these reasons, this subzone is interpreted as a return to a proximal deltaic environment.

Zone 2: 340-286 mblf (1.18-1.03 Ma)

Zone 2a: 340-321 mblf (1.18-1.14 Ma)

This zone is characterized by Minerogenic Facies 2, defined by rapidly alternating "basinal" siderite to pyrite dominance of the sand fraction mineralogy, with lesser amounts of mica. Like the underlying zone, it is characterized by Biofacies 3, though *Sclerocypris* is considerably more dominant than *Ilyocypris* in this interval. We interpret this facies combination representing a period of rapidly fluctuating environments between a nearshore marsh and an offshore sublittoral/profundal environment. Where pyrite is the dominant mineral (e.g. 340-330 mblf, ~1.18-1.16 Ma) the environment at the core site was more marsh-like, and when basinal siderite is more abundant the core site was farther offshore. The interval dominated by pyrite is occasionally massive possibly due to plant or benthic animal bioturbation, whereas the siderite interval is finely laminated supporting the interpretation of deeper water deposition. This was a period of numerous transitions on time scales of <4 kyr.

Zone 2b: 321-299 mblf (1.14-1.07 Ma)

This zone is characterized by Minerogenic Facies 2, described above, and Biofacies 5, the only facies assemblage where *Candonopsis* is dominant, although *Ilyocypris* is also quite abundant over the entire interval. *Limnocythere* and *Sclerocypris* are both somewhat abundant for the first half of the zone (321-310 mblf, ~1.14-1.1 Ma) at which point Cypridopsine ostracodes become more abundant. In addition,

Botryococcus is quite abundant in samples throughout the entire interval, although, the samples containing ostracodes are distinct from those with *Botryococcus*. We interpret this facies combination similar to Zone 2a: a rapidly fluctuating marsh to sublittoral/profundal environment, supported by the lithologic character of this unit which fluctuates at a 1-3 meter resolution between the two sub-environments described in 2a. Given the abundance of *Botryococcus* during the periods of deeper waters, the lake is also interpreted as having been highly productive at this time, as well as being extremely variable in depth.

Zone 2c: 299-286 mblf (1.07-1.03 Ma)

This zone is still characterized by Minerogenic Facies 2, described above, and Biofacies 4 which is dominated by *Ilyocypris* and *Sclerocypris* ostracodes. *Botryococcus* and *Pediastrum* are rare. The lithologic character does not fluctuate in grain size during this interval, though it does vary between laminated and massive. This facies combination is interpreted as reflecting alternations between sublittoral/profundal and marsh environments.

Zone 3: 286-255 mblf (1.03 Ma – 933 ka)

Zone 3a: 286-255 mblf (1.03 Ma – 933 ka)

This zone is characterized by two distinct minerogenic and biofacies assemblages. The first is Minerogenic Facies 3 characterized by alternating pyrite and ooid dominance, with Biofacies 4, described above. This assemblage occurs between 286-275 mblf and 265-255 mblf. This portion of the zone is interpreted as predominantly a shallow (< 5m deep considering ooid formation), marsh to offshore marsh environment. Despite the

shallow depth, these intervals are predominately coarsely laminated to massive mud, which may indicate that coarser, river-transported material was bypassing the core site at these times (as seen in modern Lake Tanganyika: Soreghan and Cohen, 1996). In between, from 275-265 mblf (~1.0-0.96 Ma), the zone is characterized by Minerogenic Facies 2, rapidly alternating between pyrite and siderite, and composed entirely of faintly laminated muds. Additionally, this zone is characterized by Biofacies 1, which is dominated by *Botryococcus* and charred particles, with lesser amounts of *Pediastrum, Polypodiaceae* sori, and lacking significant ostracode abundance. This is the first zone with a significant gap in ostracode presence (275-273 mblf), and corresponds to the most negative excursion of PC1 (deeper water, more humid environment) thus far in the record. This combination of facies assemblages and lithology in the middle of the zone is interpreted as changing from very deep (>200m due to lack of ostracodes) sublittoral/profundal environment back to marsh conditions.

Zone 4: 255-203 mblf (933-657 ka)

Zone 4a: 255-244 mblf (933-872 ka)

This zone is characterized by Minerogenic Facies 2, with alternations of abundant basinal siderite and pyrite throughout. There is a shift at 250 mblf (~900 ka) from Biofacies 4 to Biofacies 1, caused by a switch in the dominant fossil biota, from ostracodes prior to 900 ka, to *Botryococcus* with no ostracodes from 250-244 mblf (~900-872 ka). This shift is coincident with a change in lithology from silty clay to black mud. Chaoborids also peak at this time, indicating the core site may have been located at or just below the oxicline prior to the transition to fully anoxic waters. This zone is

interpreted as changing from an offshore marsh environment (silty clays) to an anoxic profundal environment at 250m (900ka), possibly with significant organic matter accumulation (black mud). It also marks a striking decrease in the frequency of variation between deep and shallow water environments.

Zone 4b: 244-228 mblf (872-791 ka)

This zone is characterized by Minerogenic Facies 2 and Biofacies 4. By this time (244 mblf, 872 ka) ostracodes are once again present in the record, and are dominantly *Ilyocypris* and *Sclerocypris* with greater amounts of cypridopsine ostracodes beginning around 235 mblf (~825 ka). The increase in cypridopsines is coincident with a lithologic change from finely laminated to massive sediments, which would be expected in shallower environments with greater potential for bioturbation. *Botryococcus* is minimally abundant throughout this zone. This zone is interpreted as shallowing upward from the previous zone and changing gradually from sublittoral/profundal to marsh and offshore marsh environments by 235 mblf.

Zone 4c: 228-203 mblf (791-657 ka)

This zone is characterized by two separate facies assemblages. From 228-210 mblf (791-700 ka) the zone is characterized by Minerogenic Facies 4, with minerogenic sand-sized grains dominated exclusively by basinal siderite in faintly laminated silty clay (the mineralogy of the sediments no longer alternates between pyrite and siderite), and Biofacies 1, with abundant *Botryococcus* and *Pediastrum*, minimal *Polypodiaceae* and no ostracodes. This period is the longest continuous negative excursion in PC1 to this point in the record, suggesting this was a time of a relatively stable, deep, "basinal" lake

environment, likely with increased humidity in the watershed as indicated by the fern spores. Given the presence of *Polypodiaceae* in the basin surrounding the modern lake, it is possible that conditions during this period were similar to the present day for the first time in the record. From 210-203 mblf (700-657 ka) the lithologic character rapidly alternates between silty clay and mud, though is consistently massive throughout suggesting benthic bioturbation. In addition, Minerogenic Facies 3 dominated by pyrite and ooid abundance, and Biofacies 4 characterize this interval, suggesting a return to very shallow shelf environment adjacent to a marsh (e.g. offshore modern Ruzizi River in Lake Tanganyika: Soreghan and Cohen, 1996). This corresponds to a significant change in the PC1 curve to more positive values. This is the last zone in which river/marsh ostracodes *Ilyocypris* and *Sclerocypris* dominate the record, signifying a change of state from river-influenced to an absence of a nearby, large river influence after 203 mblf (657 ka).

Zone 5: 203-191 mblf (657-595 ka)

Zone 5a: 203-191 mblf (657-595 ka)

This zone is characterized by Minerogenic Facies 5 which is characterized by extremely low abundances of sand-sized mineral grains, and Biofacies 7, which is the only biofacies where cypridopsines are the dominant ostracode taxa, with lower abundances of *Candonopsis, Limnocythere,* and *Ilyocypris*. Notably, this is the only zone in which *Cypridopsine n.gen. sp.1* occurs, and *Botryococcus* and *Pediastrum* are likewise abundant. This zone is interpreted as changing between sublittoral (ostracode dominance from 203-200 mblf) to basinal (ostracodes are rarer from 200-195 mblf) and back to

sublittoral to the end of the zone. The shift to back to an ostracode-dominated environment at 195 mblf coincides with a change from massive to finely laminated silty clays. Interestingly, in the modern lake *Cypridopsine n.gen. sp.1* is found mostly in very shallow (5-10 meters) water (Appendix B – this dissertation), and in the core it is interpreted to have lived in a much deeper, open water environment based on co-occurring indicators and laminated core lithology. However, due to taphonomic dissolution of ostracode carbonate in the undersaturated waters below 30m in the modern lake, our ability to make direct inferences to past conditions is somewhat limited.

Zone 6: 191-154 mblf (595-401 ka)

Zone 6a: 191-165 mblf (595-460 ka)

Beginning with Zone 6, at 191 mblf (595 ka), the facies assemblages throughout the rest of the 1B record alternates between Minerogenic Facies 4, in which basinal siderite dominates the sand minerogenic fraction, and Minerogenic Facies 5, lacking any significant sand-sized minerogenic grains. Most often associated with Minerogenic Facies 4 is Biofacies 2, with high abundances of green algae, *Polypodiaceae* sori, and charred particles. This biofacies differs from Biofacies 1 in that peaks in the abundance of fish fossils and chaoborids are now anti-correlated with peaks in green algae, *Polypodiaceae* sori, and charred particles. Most often occurring with Minerogenic Facies 5 is Biofacies 6, in which *Limnocythere, Candonopsis* and cypridopsine ostracodes are co-dominant and the fossils typically associated with deeper water conditions (the siliceous green algae and fern sori) are rare to absent.

Zone 6a is characterized by Minerogenic Facies 4 and Biofacies 2, interrupted by an excursion from 181-175 mblf (540-520 ka) with abundant, carbonate coated cypridopsine ostracodes (Biofacies 6) occurring in finely laminated to massive silty clay. This zone is interpreted as basinal lacustrine from 191-181 and 175-165 mblf (595-540 and 520-460 ka), with a 20 kyr period of littoral (non-river influenced) environment between. The return to basinal conditions at 175 mblf is coincident with a change in lithology where the silty clays are no longer massive, suggesting this later period may represent a slightly deeper environment than the earlier sub-interval.

Zone 6b: 165-154 mblf (460-401 ka)

This zone is characterized by Minerogenic Facies 5 and Biofacies 6 indicative of a shallow, littoral lake environment. This is interpretation is supported by the taphonomic condition of the ostracodes, with high percentage broken and coated valves at this time, although the lithologic character suggests a less turbid environment with a return to predominately faintly laminated muds in this zone. It is also corresponds to an extended period of positive PC1 values. The transition between Zone 6a and 6b is sharp, and is followed by a comparatively long period of stability. This is seen again at the transition from Zone 6b to 7a, where indicator abundance (and therefore minerogenic and bio-facies assemblages) changes in a step-like fashion. This suggests that the core site was likely not at or near the oxicline during the entire interval, but rather deepened or shallowed rapidly and then remained at that state. Had the core site been close to the oxicline throughout, the smallest perturbations in the hydrology of the lake would have

been enough to push it back and forth repeatedly, causing a more tooth-like, or gradual signal of environmental change.

Zone 7: 154-125 mblf (401-278 ka)

Zone 7a: 154-145 mblf (401-355 ka)

Zone 7a is characterized by Minerogenic Facies 4 and Biofacies 2 and is exclusively characterized by faintly laminated mud. It is the period of highest abundance of both green algae taxa, and the most persistent abundance of *Polypodiaceae* sori. There are a few samples in which adult *Limnocythere* are present but scarce within this interval, which would suggest that they were transported to the core site, though there is no description of turbidites at this depth in the initial core description (ICD) and the fossils showed no sign of abrasion. In addition, charred particles are particularly abundant over this interval, which likely reflects higher fire frequency. This would suggest there was a higher vegetative fuel load as it was overall a wetter period, so during the annual arid season fire frequency was also high. There is a slight time-lag between the disappearance of ostracodes (shallow water, arid environment) at the end of 6b, and the peak in charred particle abundance, which may be explained by the amount of time necessary to sufficiently increase the vegetative cover in the watershed. This interval is interpreted as a highly productive, basinal lacustrine environment with correspondingly increased humidity in the watershed.

Zone 7b: 145-125 mblf (355-278 ka)

Zone 7b is characterized by Minerogenic Facies 5 and Biofacies 6 from ~145-135 mblf (350-310 ka) which transitions gradually to Minerogenic Facies 4 and Biofacies 2

from 135-125 mblf (355-278 ka). There is a lithologic change from coarsely laminated mud to faintly laminated mud that occurs just before the change in facies assemblages (~137 mblf). This zone is interpreted as a littoral environment that gradually deepens past the oxicline at 135 mblf. This is supported by the disappearance of carbonate coating on valves and an increase in percentage whole carapaces preserved prior to the disappearance of ostracodes from the record in this zone.

Zone 8: 125-82 mblf (278-147 ka)

Zone 8a: 125-111 mblf (278-238 ka)

Zone 8a is characterized by Minerogenic Facies 5 and predominantly by Biofacies 6, indicative of a littoral lake environment, although there is a brief interval (121-118 mblf, ~270-260 ka) where the Biofacies 2 assemblage with minimal to moderate abundances of *Botryococcus* and *Polypodiaceae* sori. The entire interval is characterized by finely laminated mud suggesting cyclic productivity and a lack of bioturbation by burrowing benthos. This zone is interpreted as a littoral lake environment with intermediate levels of productivity, which shifts rapidly into and out of a more basinal, productive lake environment, with increased humidity.

Zone 8b: 111-82 mblf (238-147 ka)

Zone 8b is characterized Minerogenic Facies 4 and Biofacies 2 assemblages, and faintly laminated mud from 111-100 mblf (238-200 ka) where ostracodes are absent from the record. It is then characterized by Minerogenic Facies 5 and faintly laminated silty clays through the top of the record, although the biological assemblage changes between Biofacies 2 (97-92 mblf, 197-180 ka; 85-82 mblf, 152-147 ka) and 6 (92-85 mblf, 180-

152 ka) depending chiefly on relative ostracode and *Botryococcus* abundances and the co-occurrence of basinal siderite with the decreased numbers of ostracodes. This zone is interpreted as a period of uneven, short, step-like changes in lake depth and watershed hydrology from humid, with a deep, productive lake with anoxic bottom water, to a deeper littoral environment, especially in the uppermost sub-section where there were massive quantities of thin juvenile valves, typical of deeper environments.

Discussion

In this dataset, the best indicator of specific lake depth over time is the concentration of ostracodes because their presence is constrained by the depth of the oxicline. Although this depth may change during prolonged periods of deeper ventilation due to increased windiness and/or colder temperatures (e.g. 62-64ka; Scholz et al., 2007; Stone et al., 2011), in the modern deep lake the oxicline has remained relatively constant at around 250 meters (Eccles, 1974; Patterson and Kachjinka, 1995). This suggests lake levels lower than half the current depth of 592 meters would be required for ostracodes to survive at the core site, especially as there is very little evidence for significant downslope transport of ostracodes in the core. In the nearshore environment of modern Lake Malawi, ostracode abundance and diversity are high between 1-20 meters water depth after which point both decrease dramatically with no ostracodes recovered by 55 meters depth (Appendix B – this dissertation). However, this relatively shallow disappearance observed in the modern training set is likely a reflection more of decreased pH levels at depths beginning at 25m and, as a result, increased post-depositional

carbonate dissolution of ostracode valves. At times when the core site had oxygenated bottom waters, the lake would have been much smaller, more alkaline, and would have preserved ostracode shell carbonate from deeper waters.

The variability of indicators used in the wet-sieved dataset is defined by five minerogenic facies assemblages of commonly co-occurring minerals, and seven biofacies of different combinations of commonly occurring biota. From these facies assemblages, we delineate five discrete paleoenvironmental conditions of the basin, three of which are influenced by a river inflow near the core site, two of which are not (Figure C-7). The "Basinal" environment is defined by the presence of anoxic bottom water, high algal productivity, and an absence of ostracode fauna. Interestingly, in the modern dataset, there is also an observable dichotomy between ostracode and *Botryococcus* abundance even at shallow depths; as ostracode abundances decrease with depth, the algal abundance increases (Appendix B – this dissertation), suggesting that extreme depth is not required for algae to bloom, but it is more a reflection of nutrients in the water (Patterson and Kachinjika, 1995). Therefore in the core record, we interpret zones of abundant *Botryococcus* and *Pediastrum* as indicative of elevated lake productivity and nutrient availability. However, their co-occurrence throughout the record with "deep" siderite, an indicator of anoxic bottom waters (Kelts and Hsu, 1978; Giresse et al. 1991), and their abundance at times when ostracodes are absent from the record (another indication of bottom water anoxia), suggest that paleo-lake depth is correlated with lake productivity: as the lake deepened it also became more productive. This has been observed in modern environments when a reservoir basin is flooded and soils from the

drowned landscape release nutrients into the lake water (Talbot et al., 2006). Although this happens on a geologically instantaneous scale, it is hypothesized by Talbot et al. (2006) that lake transgressions in the past would have similarly flooded the surrounding landscape, covering significant surface area where shore relief is low. Further, they suggest that this initial burst of productivity may then maintained through two related processes: increased river-supplied nutrients as the climate became wetter (likely causing lake level to rise in the first place), and the generation of a deep water nutrient pool once the lake is deep enough to be chemically stratified. Once stratified, seasonal mixing could maintain high levels of productivity, as is the case in the modern lake (Hecky et al., 1996; Patterson and Kachjinka, 1995). These seasonal, though persistent, increases in productivity would then be recorded in the sedimentary record and correlate with high lake level and humid watershed conditions.

The "Littoral" interpreted paleoenvironment is defined by the dominance of cypridopsine, *Limnocythere* and *Candonopsis* ostracodes with varying amounts of charred particles and fish, but lacking high abundances of green algae. These environments likely spanned a wider range of depths than those covered in the modern training set, but always maintained oxygenated bottom waters. This interpretation suggests increased aridity in the watershed in order to drop lake level over 400 meters from present. However, these conditions were not desert-like , in contrast to some of the younger megadrought intervals (Cohen et al, 2007). This is evident from the increased charred particle deposition immediately following many of these intervals, suggesting higher fire frequency under conditions of sufficient vegetative ground cover to support

fires (Bird et al., 2004). Additionally, further evidence that the "Littoral" paleoenvironments interpreted in Core 1B in this study were never extremely or persistently arid, is the lack of any interval in this portion of the record dominated exclusively by *Limnocythere*, in contrast to the Megadrought phases of the 1C core (Park and Cohen, 2011). Where it occurs in 1B below 82 meters it is always co-dominant with or subordinate to other ostracodes, particularly *Candonopsis* and Cypridopsines.

The transition from a river influenced to non-river influenced environment at the core site starting about 800 ka is interpreted to have happened over a 27 meter interval (~140 kyrs). This transition zone begins where framboidal pyrite (precipitated in OM-rich, anoxic environments, typical of marshes; Postma, 1982) ceases being a dominant indicator in the record at ~230 mblf . The transition period ends at ~203 mblf (660 ka) after which point the intervals rich in ostracodes are no longer dominated by *Ilyocypris* and *Sclerocypris*. This change of state observed in the record was likely caused by a reconfiguration of the local watershed hydrology, probably related to local tectonic controls rather than regional climate. To test this interpretation, the PCA was re-run removing the ostracode taxa indicative of river-influenced shallow water environments (*Ilyocypris* and *Sclerocypris*). The remaining indicators maintain the same positions in covariance (PC) space relative to one another despite the removal (Figure C-S1a), and the stratigraphic time series is nearly identical to the original series with peaks and troughs in the same locations (Supplemental Figure C-S1b). This suggests that PC1 is responding primarily to basin-wide changes in lake level (specifically oxygenated vs. anoxic bottom waters) rather than local ecological variability driven by the presence or absence of an

influent river near the core site. This interpretation is further supported by the fact that the watershed continues to vary between humid (deeper lake – no ostracodes) and arid (shallower lake – with ostracodes) after this change, but without riverine sediment or riverine/marsh biotic inputs. This sort of change has been observed in seismic records from Lakes Tanganyika and Malawi interpreted for the past 25,000 years (Scholz and Rosendahl, 1988). In these records there was evidence for rotation of individual fault blocks within each half-graben causing variable estimates of paleoshoreline levels in different structural units. Such a rotation along any of the 26 mapped faults within the basin north of the core site (Rosendahl et al., 1988) could have potentially cut off sediment transport from a southerly flowing river, most likely from either the paleo-Ruhuhu or Songwe rivers, thereby impounding these sediments well to the north of the drill site. To date we have been unable to identify a single fault or group of faults that may have been be responsible for this change. However, we strongly suggest this as a future research objective if improvements can be made in either the quality of the legacy Project PROBE seismic data sets for these older parts of the record, or with new multifold seismic data collection.

The deepest interpreted river-influenced paleoenvironment is "Sublittoral/Profundal" which is really a combination of two lake floor environments, with sublittoral being the transition between littoral (shallower) and profundal (deeper). The reason for the combination is that where this occurs in the record, there is extremely rapid variation (less than the average ~500 yr sampling step) between pyrite (forming in anoxic, though OM-rich environments nearer the shore - sublittoral) and siderite (forming

away from the OM-rich sediment - profundal). These variations are often on a sub-meter scale and were therefore grouped into a single description since they cannot be resolved with our current sampling resolution.

The next river-influenced paleoenvironment is "Deltaic" which is defined by high percentages of quartz (proximal) and mica (distal) as well as pyrite and OM-rich siderite, which likely form in the anoxia produced by the combination of plant matter decay and burial with rapid clastic sedimentation. It is also defined by the co-dominance of *Ilyocypris* and *Sclerocypris* (as are most of the river-influenced bio-assemblages, where ostracodes are present). Changes in biofacies within this paleoenvironmental category to one more typical of open waters (higher cypridopsines and higher algal productivity), should not be interpreted as a sudden deepening of the lake but rather a local change in deltaic sedimentation. This paleoenvironment spans the entire interval where diatoms are missing for an extended period from smear-slide samples in the ICD (Figure C-2a). Their absence can be the result of a number of factors, but in this instance it is likely the result of either: 1) high sedimentation rates, where diatoms may be present, but in low numbers compared to the clastic sediment influx, or 2) post-depositional dissolution due to high pH, or a combination of the two (J. Stone, personal communication, 8/22/2012).

The final interpreted paleoenvironment is "Marsh". This environment likely occurs laterally along a shoreline near an inflowing river or small stream (as seen in the modern lake). The core site need not be located directly in the marsh (1-3m depth) but would still affect species assemblages even if positioned in deeper water directly offshore from such an environment (e.g. Appendix B – this dissertation). Like the interpreted

"Deltaic" paleoenvironment, the ostracode assemblage of the "Marsh" paleoenvironment is also dominated by the river/marsh favoring ostracodes *Ilyocypris* and *Sclerocypris*. The $\delta^{18}O$ values on *Ilyocypris* and *Sclerocypris*, though more negative than one of the cypridopsinae species, are still more positive than would be expected in a strictly meteoric/river water environment. This could happen if the core site was located further from the river and neighboring marshes, or if the mass balance between the river inflow and the evaporated lake water was unequal. Both are equally probable. This environment has a high abundance of framboidal pyrite, and at times significant ooid accumulation, suggesting the lake must have been significantly shallower than at present for ooids to form (typically in depths of 5 meters or less). A similar environment has been described off the Ruzizi River delta front in Lake Tanganyika where a shallow carbonate shelf accumulates ooids, just offshore from marshland (Soreghan and Cohen, 1996).

It is important to remember that although PC1 is most influenced by the presence or absence of ostracodes in the record, which is depth dependent (anchored at ~200 m), it is not strictly speaking a curve of specific lake depths through time. Rather it describes the variability within the record, and although the positive PC1 values are correlated with indicators living in shallower environments, and negative PC1 values with those in deeper or anoxic environments, indicators like *Botryococcus* are not themselves depth-specific. Instead they tend to occur at times when ostracodes do not, and are therefore anti-correlated with those indicators requiring oxygenated bottom water (or shallower) environments. It is better to think of PC1 as a record of the state of the basin: when the

environment is extremely variable (e.g. rapidly alternating between pyrite and basinal siderite precipitation), the values of PC1 are similarly extremely variable. When there are periods of relative stasis in the record and particular assemblages remain dominant for extended periods of time, the PC curve will behave more in a step-like manner (e.g. Zone 6b to Zone 7a transition, Figure C-7). PC1 does accurately describe where ostracodes are (positive) or are not (negative) found in the record, and may be thought of as a representation of *relative* lake level, or lake level change, through time.

Connections to regional and global climate

Using this record of local humidity and lake level change for the past 1.25 Ma from Lake Malawi, we are now able to compare a continental record of climate change to offshore records of terrestrial African climate change (Larrasoaña et al., 2003; Hooghiemstra et al., 2006; Dupont et al., 2001) in addition to global glacial/interglacial cycles from the Vostok ice core (Jouzel et al., 2007) and local Southern Hemisphere insolation at 15°S (Laskar et al., 2004) (Figure C-8). The three records of terrestrial climate change were chosen to cover a large portion of the African continent and include two pollen records from offshore northwest and tropical Africa (Hooghiemstra et al., 2006 and Dupont et al., 2001, respectively), and the third is a record of aridity and dust accumulation from northeast Africa from a core recovered from the eastern Mediterranean Sea (Larrasoaña et al., 2003). All terrestrial records are oriented so that interpreted arid conditions are to the right of the figure.

The three records that encompass the period from 1.25 Ma to 800 ka (Congo Basin, Lake Malawi, and Eastern Mediterranean) all show a distinct change in the

frequency of variability between 1000-900ka, possibly coincident with changes evident in the Mid-Pleistocene Revolution (e.g. Elderfield et al, 2012; Raymo et al., 1997). Between 800 and 600 ka (the limit of the Congo Basin record) climate change in the Lake Malawi basin are coincident with those recorded in the pollen record of the Congo Basin which reflects changing vegetation in central Africa. These regions show similar climate synchronicity between 150 and 35 ka (Blome et al., 2012). Between 700 and 350 ka changes in lake level at Lake Malawi are coincident with latitudinal fluctuations in the border between the Sahara and Sahel environments of northern Africa. Synchronicity between these two regions occurred less frequently over the last 150 ka (Blome et al., 2012), though this is a period of somewhat more muted insolation variability, which could explain why global glacial/interglacial cycles seem to have an influence on tropical African climate over this period. However, this does not mean that local insolation intensity and variability had no effect on the climate at Lake Malawi. When comparing our record to the offshore dust record in the eastern Mediterranean (primarily reflecting Northern Hemisphere insolation variability driving the North African monsoon) there are times when the two are in phase (e.g. ~810 ka) and others when the two are clearly out of phase (e.g. ~325 ka). This is likely a reflection of insolation intensity – when intensity is high the records from the two hemispheres are more often out of phase, when it is low, they are occasionally in phase.

This initial comparison of the million-year long record of climate record from Lake Malawi to records other records of African climate change shows some of the regional patterns and synchronicity that might be expected from patterns observed in the

more recent record (Blome et al., 2012). It also illustrates the competing effects of high and low-latitude climate forcing mechanisms on Lake Malawi, which highlights the need to consider both global teleconnections as well as local insolation for tropical continental records. Future refinement of the age-model and an analysis of the PC1 time series will allow for a more certain interpretation of synchronicity between the east African tropics and the other geographical regions of Africa, as well as provide precise data with regards to the frequencies of variability seen in the record.

Conclusions:

The main purpose of this study was to determine if the ecological variability in Core 1B could be constrained by a single multivariate axis, in order to model changes in basin hydrology through time. The results of this study demonstrate a clear environmental interpretation of the variability in the 1B record constrained by the PC1 axis with indicators living in shallow water environments (e.g. ostracodes) positively loaded on PC1, and those indicators of deeper water environments (e.g. "basinal" siderite), negatively loaded on PC1. This correlation suggests that the stratigraphic time series of PC1 from this study can be used as a single variable representing the relative lake level of Lake Malawi through time in future analyses of regional environmental variability in East Africa.

Based on the shape of the PC1 curve, there is an overall trend toward wetter, deeper lake environments, although with considerable scatter ($R^2 = 0.10$) (Figure C-8). With the exception of the Megadrought events between 120 and 90ka, data from the

shorter 1C core suggest that this trend would continue to the present day (Stone et al., 2011; Park and Cohen, 2011). There is also a change of state from river to non-river influenced between 230-203 mblf (~800-660 ka) as evidenced by a transition in dominant ostracode species assemblages. The cause of this change is likely driven by local tectonics, with movement on a fault or set of faults north of the core site cutting off sediment supply from either the Songwe or Ruhuhu paleo-rivers. Additionally, this state change is *not* observable in the PC1 curve, suggesting that the curve is responding more to the presence or absence of ostracodes, and the overall variability in the record, but not to the level of the individual ostracode species. At a more detailed, descriptive level than the PC1 curve, five minerogenic facies and seven biofacies describe the commonly associated indicators in the record. From these facies associations, five distinct paleoenvironments were defined: "Basinal" and "Littoral" from the upper, non-river influenced section of the core, and "Sublittoral/Profundal", "Deltaic" and "Marsh" from the river-influenced, lower section of the core.

Finally, comparison of this paleoenvironmental record of past climate variability shows remarkable similarity to other regional African climate records and suggests that both high and low-latitude forcing mechanisms alternately affect the regional precipitation history of eastern tropical Africa. Additionally, there appears to be a change in the frequency of variability in PC1 beginning ~1.025 Ma, from higher frequency to lower. These qualitative observations will be further assessed once a final age-model has been defined for the core. At that point, a time series analysis will be performed to

determine the exact frequencies of variation and how those frequencies change through time in the core.

Acknowledgements:

Funding for this project was provided by the U.S. National Science Foundation-Earth System History Program (EAR-0602350), the International Continental Scientific Drilling Program, and the Smithsonian Institution. Initial core processing and sampling was carried out at LacCore, the National Lake Core Repository at the University of Minnesota. Partial support during sample preparation and analysis received from multiple sources including: DOSECC Inc. (Drilling, Observation and Sampling of the Earth's Continental Crust), and Chevron and BP summer scholarships. Sample processing conducted by Devin Gaugler, Chris Johnson, Jeanine Ash, and Claire DeCelles with partial funding through the SAGUARO (Southern Arizona Geosciences Union for Academics, Research and Outreach) program at the University of Arizona. SEM imaging was performed on a Hitachi S-3400N housed in the Geosciences Department at the University of Arizona. Funding for the SEM facility was through the Arizona LaserChron Center grant NSF EAR-0929777. The stable isotope analyses were performed by the Environmental Isotope Laboratory, Geosciences Department, University of Arizona.

References:

Alin, S., Cohen, A.S., 2004. The live, the dead, and the very dead: taphonomic calibration of the recent record of paleoecological change in Lake Tanganyika, East Africa. Paleobiology 30, 44-81.

Baker, A.L., Baker, K.K., Tyler, P.A., 1985. Close interval sampling of migrating Chaoborus larvae across the chemocline of meromictic Lake Fidler, Tasamania. Archiv Fur Hydrobiologie 103, 51-59.

Balch, D.P., Cohen, A.S., Schnurrenberger, D.W., Haskell, B.J., Valero Garces, B.L., Beck, J.W., Cheng, H., Edwards, R.L., 2005. Ecosystem and paleohydrological response to Quaternary climate change in the Bonneville Basin, Utah. Palaeogeography, Palaeoclimatology, Palaeoecology 221, 99-122.

Bennett, K., 2006. Determination of the number of zones in a biostratigraphical sequence. New Phytologist 132, 155-170.

Bird, M.I., Veenendaal, E.M., Lloyd, J.J., 2004. Soil carbon inventories and $\delta^{13}C$ along a moisture gradient in Botswana. Global Change Biology 10, 342-349.

Blome, M.W., Cohen, A.S., Tryon, C.A., Brooks, A.S., Russell, J., 2012. The environmental context for the origins of modern human diversity: a synthesis of regional variability in African climate 150,000-30,000 years ago. J Hum Evol 62, 563-592.

Bootsma, H.A., Hecky, R.E., 1999. Water Quality Report. Lake Malawi/Nyasa Biodiversity Conservation Project, Senga Bay, Malawi.

Branchu, P., Bergonzini, L., Delvaux, D., De Batist, M., Golubev, V., Benedetti, M., Klerkx, J., 2005. Tectonic, climatic and hydrothermal control on sedimentation and water chemistry of northern Lake Malawi (Nyasa), Tanzania. Journal of African Earth Sciences 43, 433-446.

Brouwers, E.M., 1988. Sediment transport detected from the analysis of ostracod population structure: an example from the Alaskan continental shelf, in: De Deckker, P., Colin, J.-P. and Peypouquet, J.-P. (Ed.), Ostracoda in the earth sciences. Elsevier, Amsterdam, pp. 231-244.

Carbonel, P., Colin, J.P., Danielopol, D.L., 1988. Paleoecology of limnic ostracodes: a review of some major topics. Palaeogeography, Palaeoclimatology, Palaeoecology 62, 413-461.

Castaneda, I.S., Werne, J.P., Johnson, T.C., 2009. Influence of climate change on algal community structure and primary productivity of Lake Malawi (East Africa) from the Last Glacial Maximum to present. Limnol Oceanogr 54, 2431-2447.

Chorowicz, J., 2005. The East African rift system. Journal of African Earth Sciences 43, 379-410.

Chowdhury, A.H., Noble, J.P.A., 1996. Organic carbon and pyrite sulphur relationships as evidences of bottom water conditions of sedimentation, Albert Formation fine-grained lacustrine sediments, New Brunswick, Canada. Marine and Petroleum Geology 13, 79-90.

Cohen, A.S., Dussinger, R., Richardson, J., 1983. Lacustrine paleochemical interpretations based on eastern and southern African ostracodes. Palaeogeography, Palaeoclimatology, Palaeoecology 43, 129-151.

Cohen, A.S., 2003. Paleolimnology: The History and Evolution of Lake Systems. Oxford University Press, Oxford.

Cohen, A.S., Stone, J.R., Beuning, K.R.M., Park, L.E., Reinthal, P.N., Dettmar, D., Scholz, C.A., Johnsor, T.C., King, J.W., Talbot, M.R., Brown, E.T., Ivory, S.J., 2007. Ecological consequences of early Late Pleistocene megadroughts in tropical Africa. P. Natl. Acad. Sci. USA 104, 16422-16427.

Dawidowicz, P., Pijanowska, J., Ciechomski, K., 1990. Vertical migration of chaoborus larvae is induced by the presence of fish. Limnol Oceanogr 35, 1631-1637.

De Deckker, P., Forester, R.M, 1988. The use of ostracods to reconstruct continental palaeoenvironmental records, in: De Deckker, P., Colin, J.-P. and Peypouquet, J.-P. (Ed.), Ostracoda in the earth sciences. Elsevier, Amsterdam, pp. 175-199.

Delorme, L.D., 1969. Ostracodes as Quaternary paleoecological indicators. Can J Earth Sci 6: 1471-1476.

Dettman, D.L., Reische, A.K., Lohmann, K.C., 1999. Controls on the stable isotope composition of seasonal growth bands in aragonitic fresh-water bivalves (unionidae). Geochim. Cosmochim. Ac. 63, 1049-1057.

deMenocal, P., Rind, D., 1993. Sensitivity of Asian and African Climate to Variations in Seasonal Insolation, Glacial Ice Cover, Sea Surface Temperature, and Asian Orography. J. Geophys. Res. 98, 7265-7287.

deMenocal, P., Ruddiman, W., Pokras, E., 1993. Influences of High- and Low-Latitude Processes on African Terrestrial Climate:Pleistocene Eolian Records from Equatorial Atlantic Ocean Drilling Program Site 663. Paleoceanography 8, 209-242.

Dillon, R.T., 2000. The Ecology of Freshwater Molluscs. Cambridge University Press, Cambridge.

Dupont, L.M., Donner, B., Schneider, R., Wefer, G., 2001. Mid-Pleistocene environmental change in tropical Africa began as early as 1.05 Ma. Geology 29, 195-198.

Ebinger, C., Rosendahl, B., Reynolds, D., 1987. Tectonic model of the Malaŵi rift, Africa. Tectonophysics 141, 215-235.

Eccles, D., 1988. A quarter century of great lakes research in Africa. Journal of the Limnological Society of Southern Africa 14, 41-48.

Eccles, D.H., 1974. An outline of the physical limnology of Lake Malawi (Lake Nyasa). Limnol Oceanogr 19, 730-742.

Elderfield, H., Ferretti, P., Greaves, M., Crowhurst, S., McCave, I.N., Hodell, D., Piotrowski, A.M., 2012. Evolution of Ocean Temperature and Ice Volume Through the Mid-Pleistocene Climate Transition. Science 337, 704-709.

Flannery, J.W., Rosendahl, B., 1990. The seismic stratigraphy of Lake Malawi, Africa: implications for interpreting geological processes in lacustrine rifts. Journal of African Earth Sciences (and the Middle East) 10, 519-548.

Forester, R.M., Colman, S.M., Reynolds, R.L., Keigwin, L.D., 1994. Lake Michigan's Late Quaternary Limnological and Climate History From Ostracode, Oxygen Isotope, and Magnetic Susceptibility. Journal of Great Lakes Research 20, 93-107.

Friedman, I., O'Neil, J.R., 1977. Compilation of stable isotope fractionation factors of geochemical interest. U.S. G.P.O., Washington, D.C.

Giresse, P., Maley, J., Kelts, K., 1991. Sedimentation and paleoenvironment in crater lake Barombi Mbo, Cameroon during the last 25,000 years. Sedimentary Geology 71, 151-175.

Grimm, E., 1987. CONISS: a FORTRAN 77 program for stratigraphically constrained cluster analysis by the method of incremental sum of squares. Computers & Geosciences 13, 13-35.

Grimm, E.C., 1992. Tilia and Tilia-graph: pollen spreadsheet and graphics programs, Program and Abstracts, 8th International Palynological Congress, Aix-en-Provence [France].

Guy-Ohlson, D., 1992. Botryococcus as an aid in the interpretation of palaeoenvironment and depositional processes. Review of Palaeobotany and Palynology 71, 1-15.

Hecky, R.E., Bootsma, H.A., Mugidde, R.M., Bugenyi, F.W.B., 1996. Phosphorus pumps, nitrogen sinks, and silicon drains: plumbing nutrients in the African Great Lakes, in: Johnson, T.C., Odada, E.O. (Ed.), The limnology, climatology, and paleoclimatology of the East African lakes. Gordon and Breach Publishers, Amsterdam, pp. 205-224.

Heller, P.L., Komar, P.D., Pevear, D.R., 2005. Transport Processes in Ooid Genesis. Journal of Sedimentary Petrology 50, 943-951.

Holmes, J.A., 1992. Nonmarine ostracods as Quaternary palaeoenvironmental indicators. Progress in Physical Geography 16, 405-431.

Holmes, J.A., Street-Perrott, F.A., Allen, M.J., Fothergill, P.A., Harkness, D.D., Kroon, D., Perrott, R.A., 1997. Holocene palaeolimnology of Kajemamm Oasis, Northern Nigeria: an isotopic study of ostracodes, bulk carbonate and organic carbon. Journal of the Geolgoical Society, London 154, 311-319.

Hooghiemstra, H., Stalling, H., Agwu, C.O.C., Dupont, L., 1992. Vegetational and climatic changes at the northern fringe of the Sahara 250,000-5000 years BP: evidence from 4 marine pollen records located between Portugal and the Canary Islands. Rev. Palaeobotany and Palynology 74, 1-52.

Hooghiemstra, H., Lezine, A.M., Leroy, S.A.G., Dupont, L., Marret, F., 2006. Late Quaternary palynology in marine sediments: A synthesis of the understanding of pollen distribution patterns in the NW African setting. Quatern Int 148, 29-44.

Irvine, K., 1995. Ecology of the Lakefly, *Chaoborus edulis*, in: Menz, A. (Ed.), The fishery potential and productivity of the pelagic zone of Lake Malawi/Niassa. Natural Resources Institute, Chatham, UK, pp. 109-140.

Jankovska, V., Komarek, J., 2000. Indicative value of Pediastrum and other coccal green algae in palaeoecology. Folia Geobotanica 35, 59-82.

Jari Oksanen, F.G.B., Roeland Kindt, Pierre Legendre, Peter R. Minchin, R. B. O'Hara, Gavin L. Simpson, Peter Solymos, M. Henry, H. Stevens and Helene Wagner 2011. vegan: Community Ecology Package, R package version 2.0-1 ed.

Jones, B.F., Bowser, C.J., 1978. The mineralogy and related chemistry of lake sediments, in: Lerman, A. (Ed.), Lakes: Chemistry, Geology, Physics. Springer-Verlag, New York, pp. 179-235.

Jouzel, J., Masson-Delmotte, V., Cattani, O., Dreyfus, G., Falourd, S., Hoffmann, G., Minster, B., Nouet, J., Barnola, J.M., Chappellaz, J., Fischer, H., Gallet, J.C., Johnsen, S., Leuenberger, M., Loulergue, L., Luethi, D., Oerter, H., Parrenin, F., Raisbeck, G., Raynaud, D., Schilt, A., Schwander, J., Selmo, E., Souchez, R.,

Spahni, R., Stauffer, B., Steffensen, J.P., Stenni, B., Stocker, T.F., Tison, J.L., Werner, M., Wolff, E.W., 2007. Orbital and Millennial Antarctic Climate Variability over the Past 800,000 Years. Science 317, 793-796.

Juggins, S., 2009. rioja: Analysis of Quaternary Science Data, R package version 0.5-6.

Kelts, K., Hsu, K.J., 1978. Freshwater carbonate sedimentation, in: Lerman, A. (Ed.), Lakes: Chemistry, Geology, Physics. Springer-Verlag, New York, pp. 295-324.

Komarek, J., Jankovska, V., 2001. Review of the Green Algal Genus Pediastrum: Implication for Pollenanalytical Research. J. Cramer, Berlin.

Kreier, H.P., Schneider, H., 2006. Phylogeny and biogeography of the staghorn fern genus Platycerium (Polypodiaceae, Polypodiidae). Am J Bot 93, 217-225.

Larrasoaña, J.C., Roberts, A.P., Rohling, E.J., Winklhofer, M., Wehausen, R., 2003. Three million years of monsoon variability over the northern Sahara. Clim. Dyn. 21, 689-698.

Laskar, J., Robutel, P., Joutel, F., Gastineau, M., Correia, A.C.M., Levrard, B., 2004. A long-term numerical solution for the insolation quantities of the Earth. Astron. Astrophys. 428, 261-265.

Lister, G.S., 1988. Stable isotopes from lacustrine Ostracoda as tracers for continental palaeoenvironments, in: De Deckker, P., Colin, J.-P. and Peypouquet, J.-P. (Ed.), Ostracoda in the earth sciences. Elsevier, Amsterdam, pp. 201-229.

Lyons, R.P., Scholz, C.A., Buoniconti, M.R., Martin, M.R., 2011. Late Quaternary stratigraphic analysis of the Lake Malawi Rift, East Africa: An integration of drill-core and seismic-reflection data. Palaeogeography, Palaeoclimatology, Palaeoecology 303, 20-37.

Martens, K., 1986. Taxonomic Revision of the subfamily Megalocypridinae Rome, 1965 (Crustacea, Ostracoda). Paleis der Academien, Brussels.

Martens, K., 2002. Task 3: taxonomy of invertebrates, in: Irvine, K. (Ed.), The trophic Ecology of the Demersal Fish Community of Lake Malawi/Niassa, Central Africa, pp. 49-59.

Melles, M., Brigham-Grette, J., Minyuk, P.S., Nowaczyk, N.R., Wennrich, V., DeConto, R.M., Anderson, P.M., Andreev, A.A., Coletti, A., Cook, T.L., Haltia-Hovi, E., Kukkonen, M., Lozhkin, A.V., Rosen, P., Tarasov, P., Vogel, H., Wagner, B., 2012. 2.8 Million Years of Arctic Climate Change from Lake El'gygytgyn, NE Russia. Science 337, 315-320.

Mezquita, F., Tapia, G., Roca, J., 1999. Ostracoda from springs on the eastern Iberian Peninsula: ecology, biogeography and palaeolimnological implications. Palaeogeography, Palaeoclimatology, Palaeoecology 148, 65-85.

Moore, S.E., Ferrell, R.E., Aharon, P., 1992. Diagentic siderite and other ferroan carbonates in a modern subsiding marsh sequence. Journal of Sedimentary Petrology 62, 357-366.

Mourguiart, P., Carbonel, P., Peypouquet, J.-P., Wirrmann, D. and Vargas, C., 1986. Quaternary palaeohydrology of Lake Huinaymarca (Bolivia). Hydrobiologia 143, 191-197.

Nicholson, S.E., 1998. Historical fluctuations of Lake Victoria and other lakes in the northwestern Rift Valley of East Africa. In: Lehman, J.T., (Ed.), Environmental Change and Response in East African Lakes. Kluwer Academic Publishers, Netherlands, pp. 7-35.

Panigrahi, G., Patnaik, S.N., 1961. Cytology of some genera of *Polypodiaceae* in Eastern India. Nature 191, 1207-1208.

Park, L.E., Cohen, A.S., 2011. Paleoecological response of ostracods to early Late Pleistocene lake-level changes in Lake Malawi, East Africa. Palaeogeography, Palaeoclimatology, Palaeoecology 303, 71-80.

Park, L.E., Cohen, A.S., Martens, K., 2003. The impact of taphonomic processes on interpreting paleoecologic changes in large lake ecosystems: ostracodes in Lakes Tanganyika and Malawi. Journal of Paleolimnology 39, 127-138.

Patterson, G., Kachinjika, O., 1995. Limnology and phytoplankton ecology, in: Menz, A. (Ed.), The fishery potential and productivity of the pelagic zone of Lake Malawi/Niassa. Natural Resource Institute, Chatham, UK, pp. 1-67.

Patterson, G., Hecky, R.E., Fee, E.J., 2000. Effect of hydrological cycles on planktonic primary production in Lake Malawi/Niassa, in: Rossiter, A., Kawanabe, H. (Ed.), Ancient Lakes: Biodiversity, Ecology and Evolution. : Advances in Ecological Research. Academic Press, New York, pp. 421-429.

Postma, D., 1982. Pyrite and siderite formation in brackish and fresh-water swamp sediments. American Journal of Science 282, 1151-1183.

R Development Core Team, 2010. R: A language and environment for statistical computing, 2.12.0 ed. R Foundation for Statistical Computing, Vienna, Austria.

Raymo, M.E., Oppo, D.W., Curry, W., 2007. The mid-Pleistocene climate transition: A deep sea carbon isotopic perspective. Paleoceanography 12, 546-559.

Reinthal, P.N., Cohen, A.S., Dettman, D.L., 2011. Fish fossils as paleo-indicators of ichthyofauna composition and climatic change in Lake Malawi, Africa. Palaeogeography, Palaeoclimatology, Palaeoecology 303, 126-132.

Ribbink, A.J., 1994. Lake Malawi, in: Martens, K.G., B.; Coulter, G. (Ed.), Speciation in Ancient Lakes. Arch. Hydrobiol. Beih. Ergebn. Limnol., Stuttgart, pp. 27-33.

Ricketts, R.D., Johnson, T. C., 1996. Early Holocene Changes in Lake Level and Productivity in Lake Malawi as interpreted from Oxygen and Carbon Isotopic Measurements of Authigenic Carbonates, in: Johnson, T.C., Odada, E.O. (Ed.), The Limnology, Climatology and Paleoclimatology of the East African Lakes. OPA, Amsterdam, pp. 475-493.

Ricketts, R.D., Johnson, T.C., Brown, E.T., 2001. The Holocene paleolimnology of Lake Issyk-Kul, Kyrgyzstan: Trace element and stable isotope composition of ostracodes. Palaeogeography, Palaeoclimatology, Palaeoecology 2001, 207-227.

Roberts, E.M., Stevens, N.J., O'Connor, P.M., Dirks, P., Gottfried, M.D., Clyde, W.C., Armstrong, R.A., Kemp, A.I.S., Hemming, S., 2012. Initiation of the western branch of the East African Rift coeval with the eastern branch. Nat. Geosci. 5, 289-294.

Rosendahl, B.R., Versfelt, J.W., Scholz, C.A., Woods, L.D. (Ed.), 1988. Seismic Atlas of Lake Tanganyika, Project PROBE. Duke University, Durham, NC.

Rosendahl, B., Kilembe, E., Kaczmarick, K., 1992. Comparison of the Tanganyika, Malawi, Rukwa and Turkana Rift zones from analyses of seismic reflection data. Tectonophysics 213, 235-256.

Russell, J.M., Johnson, T.C., Talbot M.R., 2003. A 725 yr cycle in the climate of central Africa during the late Holocene. Geology 31, 677-680.

Sapota, T., Aldahan, A., Al-Aasm, I., 2006. Sedimentary facies and climate control on formation of vivianite and siderite microconcretions in sediments of Lake Baikal, Siberia. Journal of Paleolimnology 36, 245-257.

Scholz, C.A., Rosendahl, B.R., 1988. Low lake stands in Lakes Malawi and Tanganyika, East Africa, delineated with multifold seismic data. Science 240, 1645-1648.

Scholz, C.A., Cohen, A.S., Johnson, T.C., King, J.W., Moran, K., 2006. The Lake Malawi Scientific Drilling Project. Scientific Drilling 2, 17-19.

Scholz, C.A., Johnson, T.C., Cohen, A.S., King, J.W., Peck, J.A., Overpeck, J.T., Talbot, M.R., Brown, E.T., Kalindekafe, L., Amoako, P.Y.O., Lyons, R.P., Shanahan, T.M., Castañeda, I.S., Heil, C.W., Forman, S.L., McHargue, L.R., Beuning, K.R.,

Gomez, J., Pierson, J., 2007. East African megadroughts between 135 and 75 thousand years ago and bearing on early-modern human origins. Proc. Natl. Acad. Sci. 104, 16416–16421.

Scholz, C.A., Cohen, A.S., Johnson, T.C., King, J., Talbot, M.R., Brown, E.T., 2011a. Scientific drilling in the Great Rift Valley: The 2005 Lake Malawi Scientific Drilling Project — An overview of the past 145,000years of climate variability in Southern Hemisphere East Africa. Palaeogeography, Palaeoclimatology, Palaeoecology 303, 3-19.

Scholz, C.A., Talbot, M.R., Brown, E.T., Lyons, R.P., 2011b. Lithostratigraphy, physical properties and organic matter variability in Lake Malawi Drillcore sediments over the past 145,000years. Palaeogeography, Palaeoclimatology, Palaeoecology 303, 38-50.

Soreghan, M.J., Cohen, A.S., 1996. Textural and compositional variability across littoral segments of Lake Tanganyika: The effects of asymmetric basin structure on sedimentation in large rift lakes. AAPG Bulletin 80, 382-409.

Spigel, R.H., Coulter, G.W., 1996. Comparison of hydrology and physical limnology of the East African Great Lakes: Tanganyika, Malawi, Victoria, Kivu and Turkana (with reference to some North American Great Lakes), in: Johnson, T.C., Odada, E.O. (Ed.), The limnology, climatology, and paleoclimatology of the East African lakes. Gordon and Breach Publishers, Amsterdam, pp. 103-139.

Stone, J.R., Westover, K.S., Cohen, A.S., 2011. Late Pleistocene paleohydrography and diatom paleoecology of the central basin of Lake Malawi, Africa. Paleogeogr. Paleoclimatol. Paleoecol. 303, 51-70.

Stratton, M.A., Kesler, D.H., 2007. The role of light and oxygen in Chaoborus punctipennis (Insecta : Diptera) diel vertical migration. J. Freshw. Ecol. 22, 101-106.

Sweeney, R.E., Kaplan, I.R., 1973. Pyrite framboid formation – laboratory synthesis and marine sediments. Economic Geology 68, 618-634.

Talbot, M.R., Jensen, N.B., Laerdal, T., Filippi, M.L., 2006. Geochemical responses to a major transgression in giant African Lakes. Journal of Paleolimnology 35, 467-489.

Taylor, K.G., Macquaker, J.H.S., 2011. Iron Minerals in Marine Sediments Record Chemical Environments. Elements 7, 113-118.

ter Braak, C.J.F., Prentice, I.C., 1988. A theory of gradient analysis. Advanced Ecological Research 18, 271-317.

Thevenon, F., Williamson, D., Vincens, A., Taieb, M., Merdaci, O., Decobert, M., Buchet, G., 2003. A late-Holocene charcoal record from Lake Masoko, SW Tanzania: climatic and anthropologic implications. Holocene 13, 785-792.

Tiercelin, J.J., Lezzar, K.E., 2002. A 300 million years history of rift lakes in Central and East Africa; an updated broad review, in: Odada, E.O., Olago, D.O. (Ed.), The East African Great Lakes: Limnology, Paleolimnology and Biodiversity. Kluwer, Dordrecht, pp. 3-60.

Tiercelin, J.J., Chorowicz, J., Bellon, H., Richert, J.P., Mwanbene, J.T., Walgenwitz, F., 1988. East African rift system: offset, age and tectonic significance of the Tanganyika-Rukwa-Malawi intracontinental transcurrent fault zone. Tectonophysics 148, 241-252.

Tierney, J.E., Russell, J.M., Huang, Y., Damste, J.S., Hopmans, E.C., Cohen, A.S., 2008. Northern hemisphere controls on tropical southeast African climate during the past 60,000 years. Science 322, 252-255.

Tjallingii, R., Claussen, M., Stuut, J.B.W., Fohlmeister, J., Jahn, A., Bickert, T., Lamy, F., Rohl, U., 2008. Coherent high- and low-latitude control of the northwest African hydrological balance. Nat. Geosci. 1, 670-675.

Voss, S., Mumm, H., 1999. Where to stay by night and day: Size-specific and seasonal differences in horizontal and vertical distribution of Chaoborus flavicans larvae. Freshw. Biol. 42, 201-213.

Whatley, R., 1988. Population structure of ostracods: some general principles for the recognition of palaeoenvironments, in: De Deckker, P., Colin, J.-P. and Peypouquet J.-P. (Ed.), Ostracoda in the earth sciences. Elsevier, Amsterdam, pp. 245-256.

Whitlock, C., Millspaugh, S.H., 1996. Testing the assumptions of fire history studies: An examination of modern charcoal accumulation in Yellowstone National Park, USA. Holocene 6, 7-15.

Wilkin, R.T., Barnes, H.L., 1997. Pyrite formation in an anoxic estuarine basin. American Journal of Science 297, 620-650.

Wilkinson, B.H., Pope, B.N., Owen, R.M., 1980. Nearshore ooid formation in a modern temperate region marl lake. The Journal of Geology 88, 697-704.

Wüest, A., Piepke, G., Halfman, J.D., 1996. Combined effects of dissolved solids and temperature on the density stratification of Lake Malawi, in: Johnson, T.C., Odada, E.O. (Ed.), The limnology, climatology, and paleoclimatology of the East African lakes. Gordon and Breach Publishers, Amsterdam, pp. 183-204.

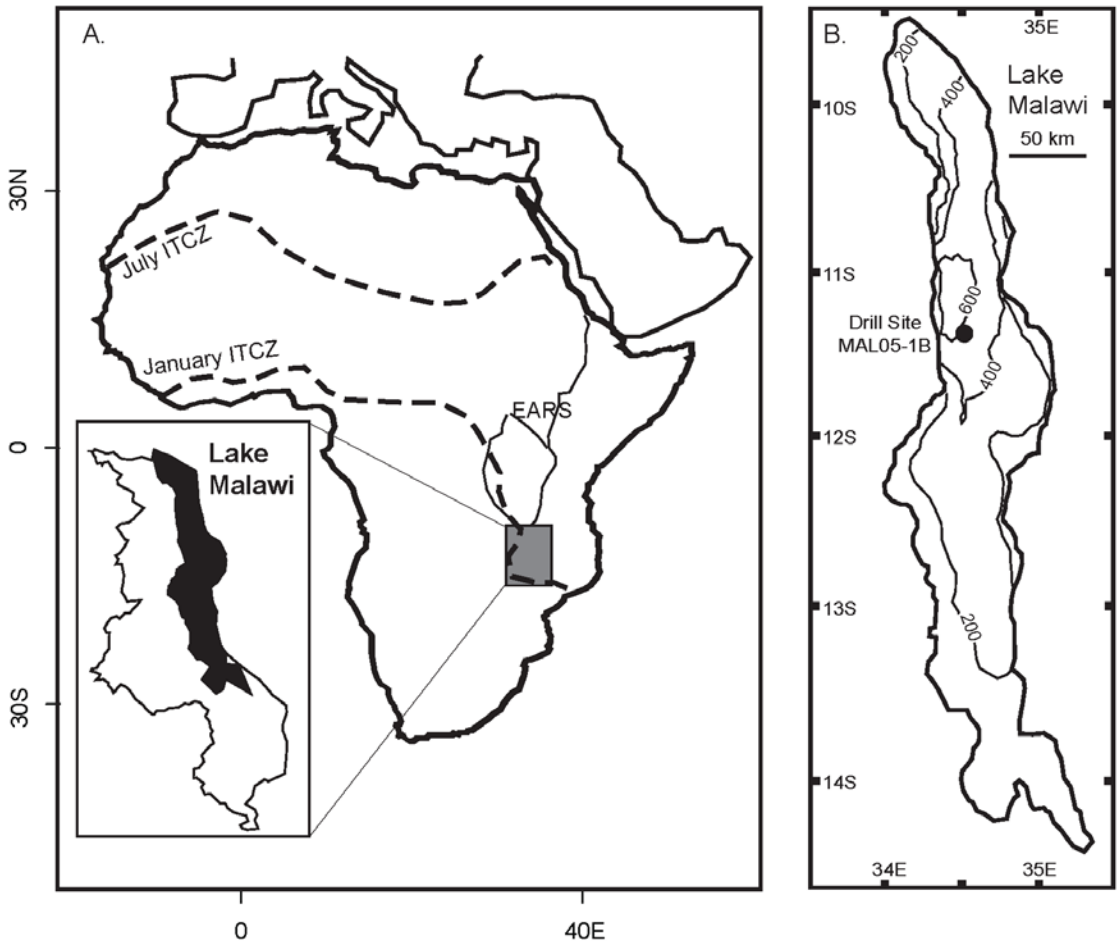

Figure C-1. A. Location of Lake Malawi, East Africa, in relation to the extent of the Inter-Tropical Convergence Zone (ITCZ) and the East African Rift System (EARS). B. Lake Malawi bathymetry (modified from Ribbink, 1994) and site location of core MAL05-1B (Core 1B).

Figure C-2. A. Lithologic description by stratigraphic zone for the section of Core 1B between 80-380 mblf. Generated using the Initial Core Description (ICD). Resolution is ~2 meters.

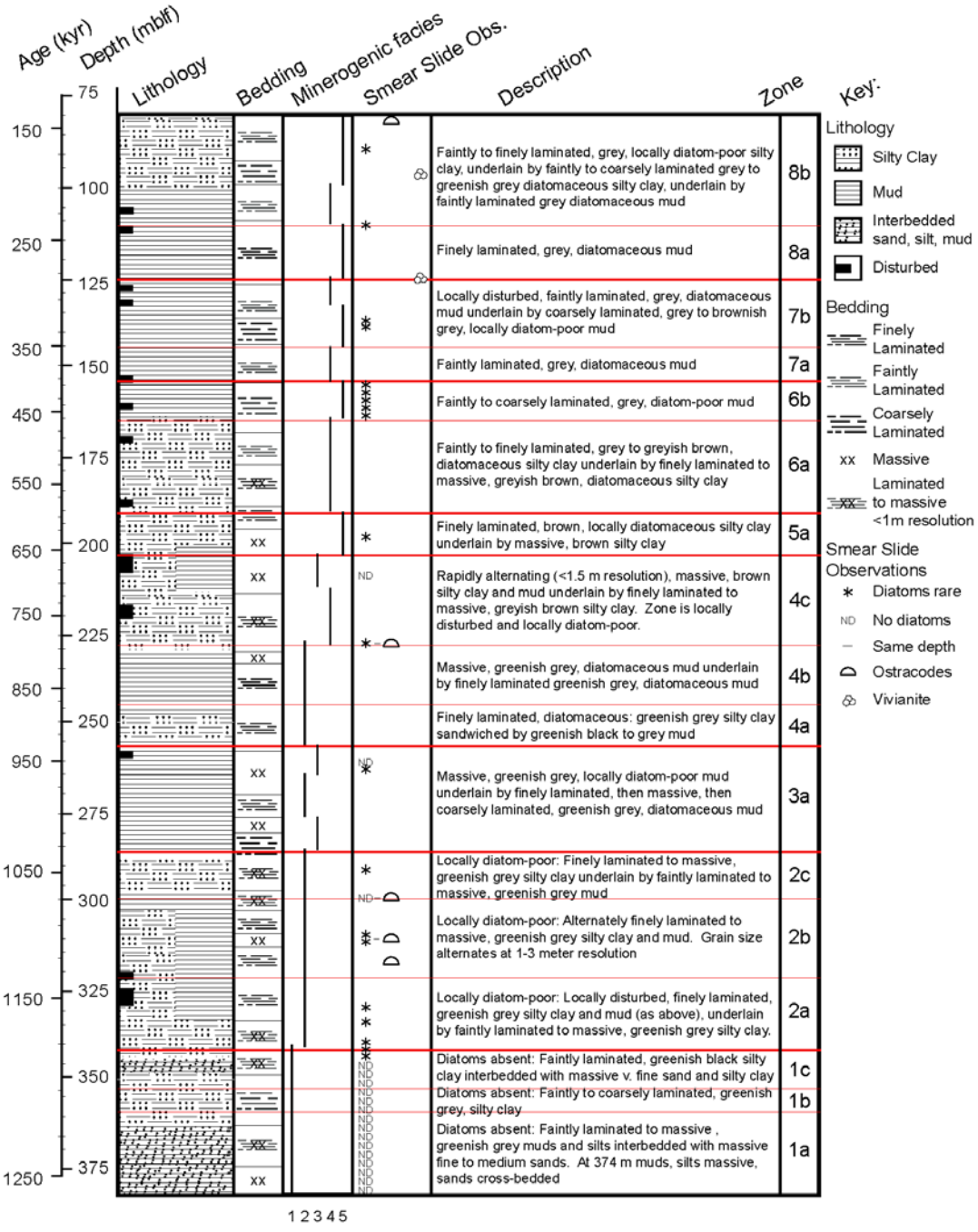
Age (kyr)
Depth (mblf)
Lithology
Bedding
Minerogenic facies
Smear Slide Obs.
Description
Zone
Key:
Lithology
Silty Clay
Mud
Interbedded sand, silt, mud
Disturbed
Bedding
Finely Laminated
Faintly Laminated
Coarsely Laminated
xx Massive
Laminated to massive <1m resolution
Smear Slide Observations
* Diatoms rare
ND No diatoms
– Same depth
Ostracodes
Vivianite
75
100
125
150
175
200
225
250
275
300
325
350
375
150
250
350
450
550
650
750
850
950
1050
1150
1250
Faintly to finely laminated, grey, locally diatom-poor silty clay, underlain by faintly to coarsely laminated grey to greenish grey diatomaceous silty clay, underlain by faintly laminated grey diatomaceous mud
8b
Finely laminated, grey, diatomaceous mud
8a
Locally disturbed, faintly laminated, grey, diatomaceous mud underlain by coarsely laminated, grey to brownish grey, locally diatom-poor mud
7b
Faintly laminated, grey, diatomaceous mud
7a
Faintly to coarsely laminated, grey, diatom-poor mud
6b
Faintly to finely laminated, grey to greyish brown, diatomaceous silty clay underlain by finely laminated to massive, greyish brown, diatomaceous silty clay
6a
Finely laminated, brown, locally diatomaceous silty clay underlain by massive, brown silty clay
5a
Rapidly alternating (<1.5 m resolution), massive, brown silty clay and mud underlain by finely laminated to massive, greyish brown silty clay. Zone is locally disturbed and locally diatom-poor.
4c
Massive, greenish grey, diatomaceous mud underlain by finely laminated greenish grey, diatomaceous mud
4b
Finely laminated, diatomaceous: greenish grey silty clay sandwiched by greenish black to grey mud
4a
Massive, greenish grey, locally diatom-poor mud underlain by finely laminated, then massive, then coarsely laminated, greenish grey, diatomaceous mud
3a
Locally diatom-poor: Finely laminated to massive, greenish grey silty clay underlain by faintly laminated to massive, greenish grey mud
2c
Locally diatom-poor: Alternately finely laminated to massive, greenish grey silty clay and mud. Grain size alternates at 1-3 meter resolution
2b
Locally diatom-poor: Locally disturbed, finely laminated, greenish grey silty clay and mud (as above), underlain by faintly laminated to massive, greenish grey silty clay.
2a
Diatoms absent: Faintly laminated, greenish black silty clay interbedded with massive v. fine sand and silty clay
1c
Diatoms absent: Faintly to coarsely laminated, greenish grey, silty clay
1b
Diatoms absent: Faintly laminated to massive , greenish grey muds and silts interbedded with massive fine to medium sands. At 374 m muds, silts massive, sands cross-bedded
1a
1 2 3 4 5

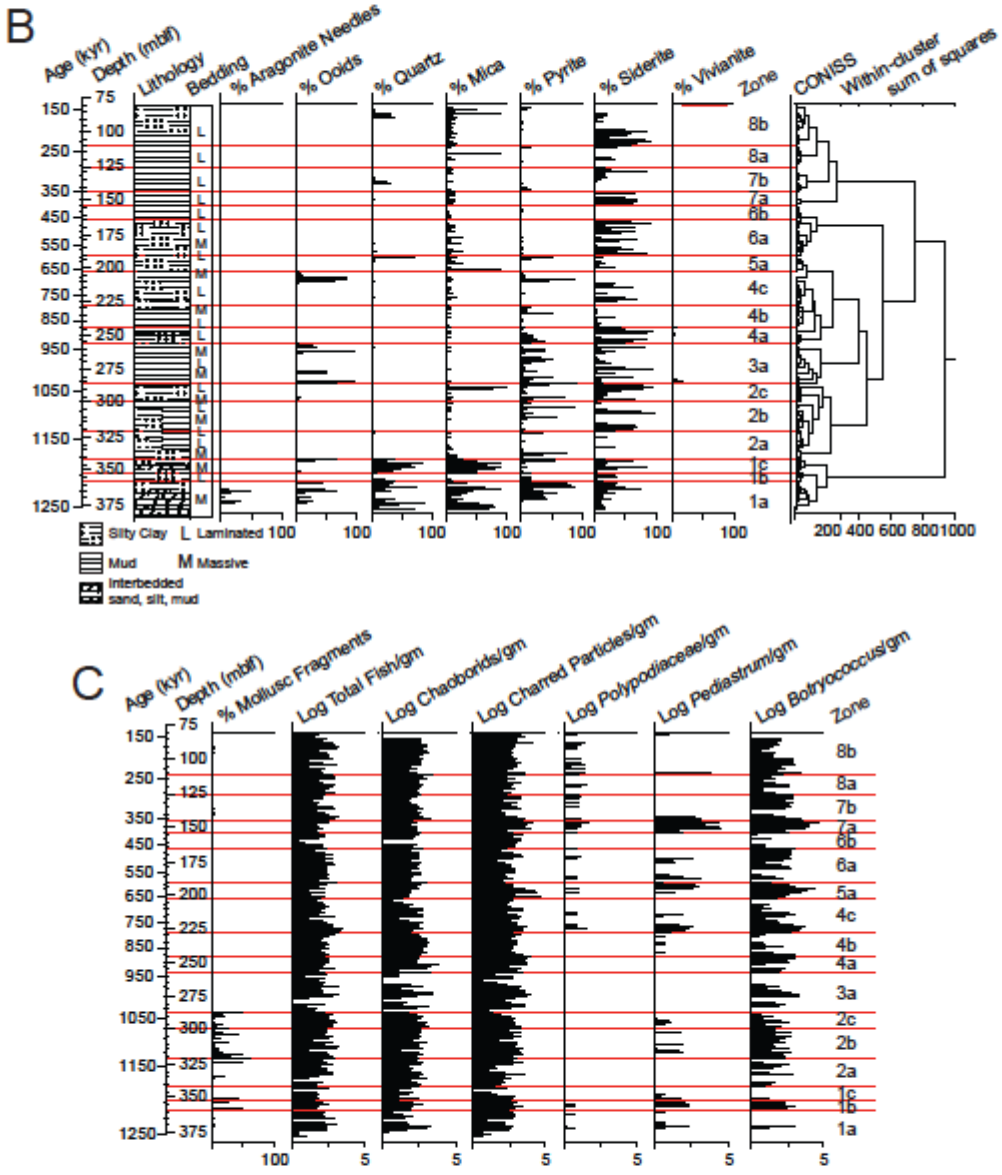

Figure C-2. B. Raw Data: The relative abundance of sand-sized minerals in Core 1B sediments. A summary of the lithologic description is provided to the left of the graphs. To the right is the stratigraphically constrained cluster analysis dendrogram used to delineate stratigraphic zones of similar composition. This cluster analysis used only the indicators shown in Figure 6, but is shown here for context. C. Raw Data: The relative and absolute abundances of all biological indicators used in this study with the exception of ostracodes

Figure C-3. A. Raw Data: The absolute abundance of total ostracodes (normalized to abundance/gram dry sediment), and the relative abundances of each ostracode species found in the core. B. Relative percentages of taphonomic variables affecting ostracodes. C. Detrended Correspondence Analysis (DCA) of all ostracode taxa identified to species level. DCA1 explains 14.39% of the variance and DCA2 explains 14.38%. Those species present in at least 0.5% of samples are noted with an asterisk. Given the separation between the species of *I. alta, I. propinqua* and *Sclerocypris c.f. jenkinae* versus the Cypridopsines and *Limnocythere sp. 1* and *sp.2*, a determination was made to group ostracode taxa by the next highest group, which was genus-level for all but the Cypridopsines (sub-family level).

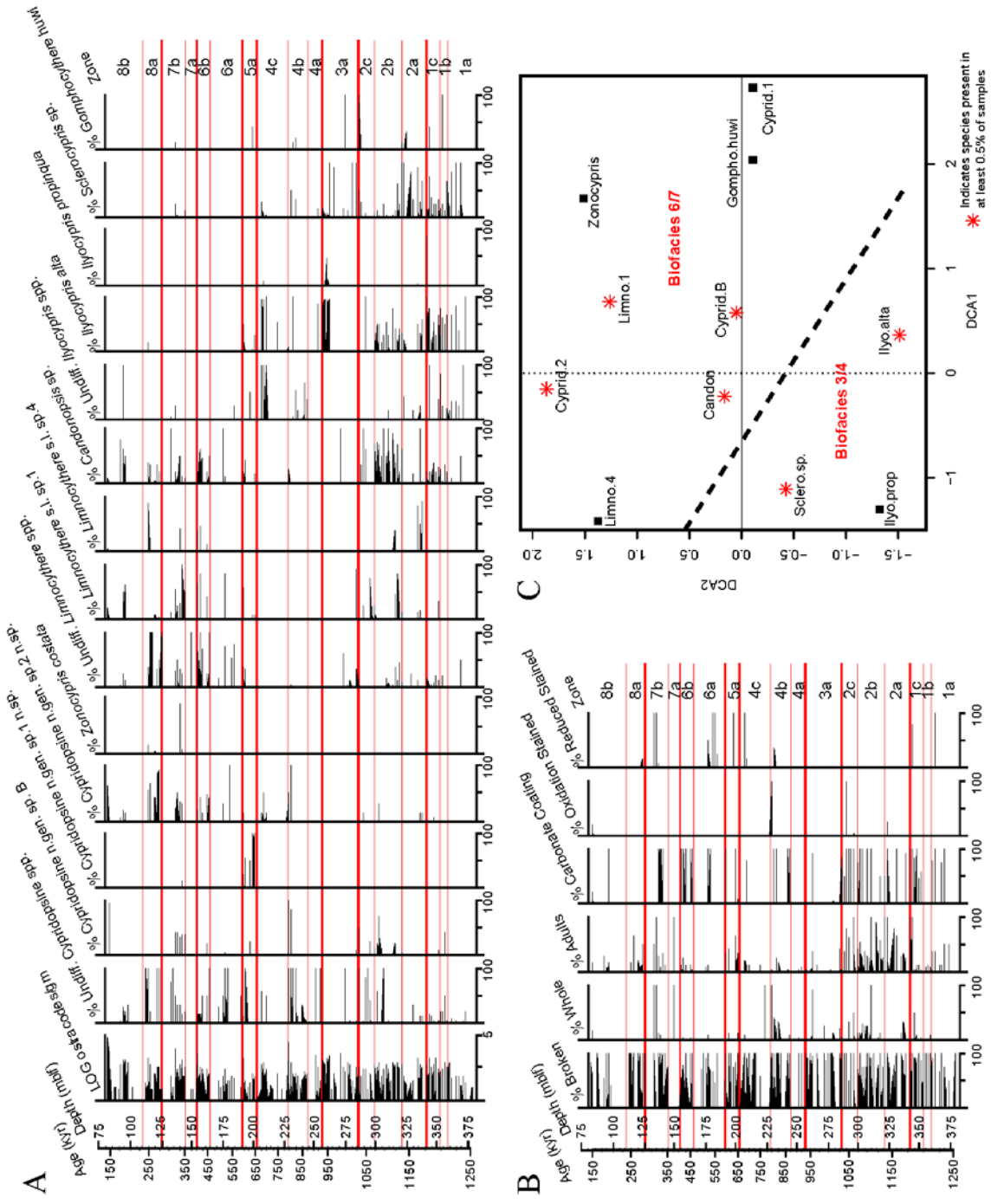
A
Age (kyr)
Depth (mbsf)
LOG Sta6code5stm
% Undiff. Cyprid.
% Cyprid.B
% Candon
% Cypridopsine n.gen. sp. B
% Cypridopsine n.gen. sp.1 n.sp.
% Undiff. Limnocythere spp.
% Zonocypris costata
% Undiff. Limnocythere s.l. sp.1
% Limnocythere s.l. sp.4
% Candonopsis sp.
% Undiff. Ilyocypris spp.
% Ilyocypris alta
% Sclerocypris prophigua
% Gomphocythere hunti
Zone
8b
8a
7b
7a
6b
6a
5a
4c
4b
4a
3a
2c
2b
2a
1c
1b
1a
B
Age (kyr)
Depth (mbsf)
% Stocken
% WMhole
% Adults
% Carbonate Coating
% Oxidation
% Reduced Stained
Zone
C
DCA2
DCA1
Cypria.2
Limno.4
Limno.1
ZonoCypris
Biofacies 6/7
Cyprid.B
Candon
Gompho.huwi
Cyprid.1
Sclero.sp.
Biofacies 3/4
Ilyo.prop
Ilyo.alta
Indicates species present in at least 0.5% of samples

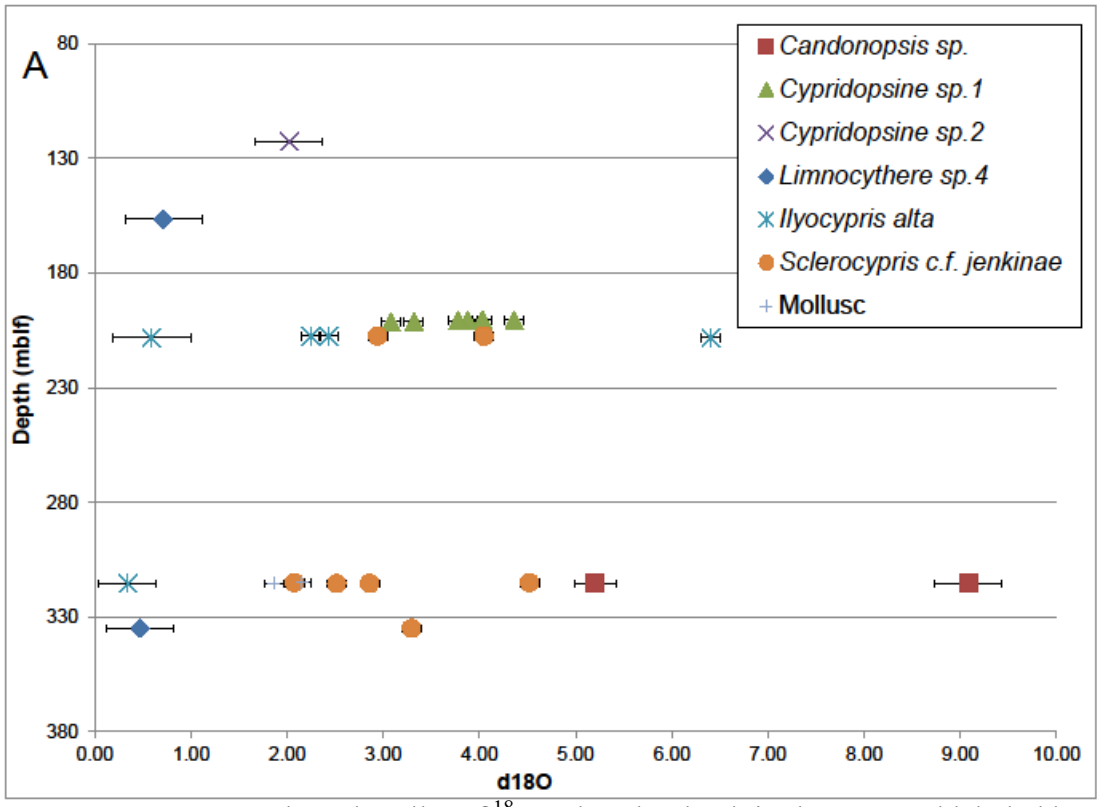

Figure C-4. A. Ostracode and mollusc $\delta^{18}O$ values by depth in the core and labeled by species/taxa. Error bars are ± 1-sigma. Samples with the lowest precision are mostly outliers, whereas the majority of those with the least amount of uncertainty fall between 1.86 and 4.36 ‰.

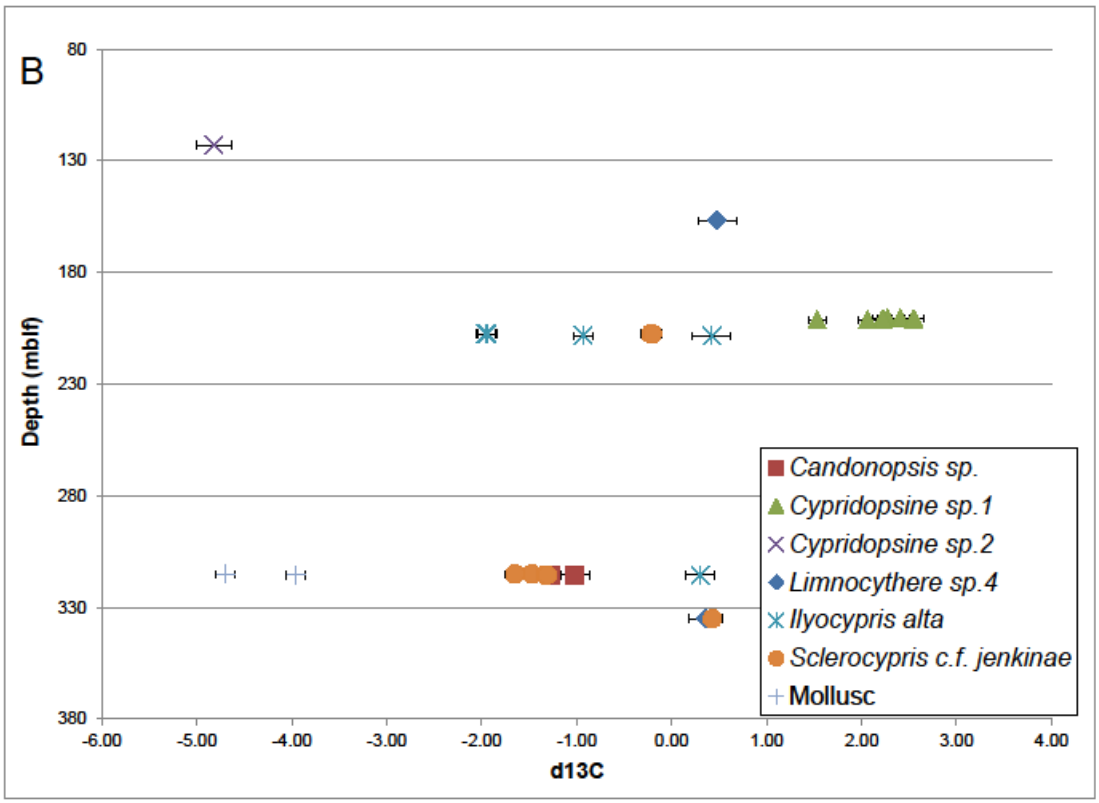

Figure C-4. B. Ostracode and mollusc $\delta^{13}C$ values by depth in the core and labeled by species/taxa. Intraspecific variation among ostracodes is significantly decreased, with the ranges of *Sclerocypris c.f. jenkinae* and *I. alta* overlapping even at significantly different depths in the core. This is interpreted to mean they likely live in the same bottom water environment, one containing abundant organic matter decay producing the more negative $\delta^{13}C$ values compared to *Cypridopsine n.gen. sp.1*.

Figure C-5. Minerogenic and biofacies determination. Using the presence, absence, and abundance of the indicators to the right of the figure, five distinct minerogenic facies and seven biofacies capture the variation of indicators throughout the core. The separation of facies was undertaken without referencing the curve shown in PC1 or the stratigraphic zonations, to avoid researcher bias. Facies boundaries often fall at zone boundaries or at major changes in the PC1 curve. The descriptions of dominant and co-dominant taxa or mineralogy can be found in Table 4.

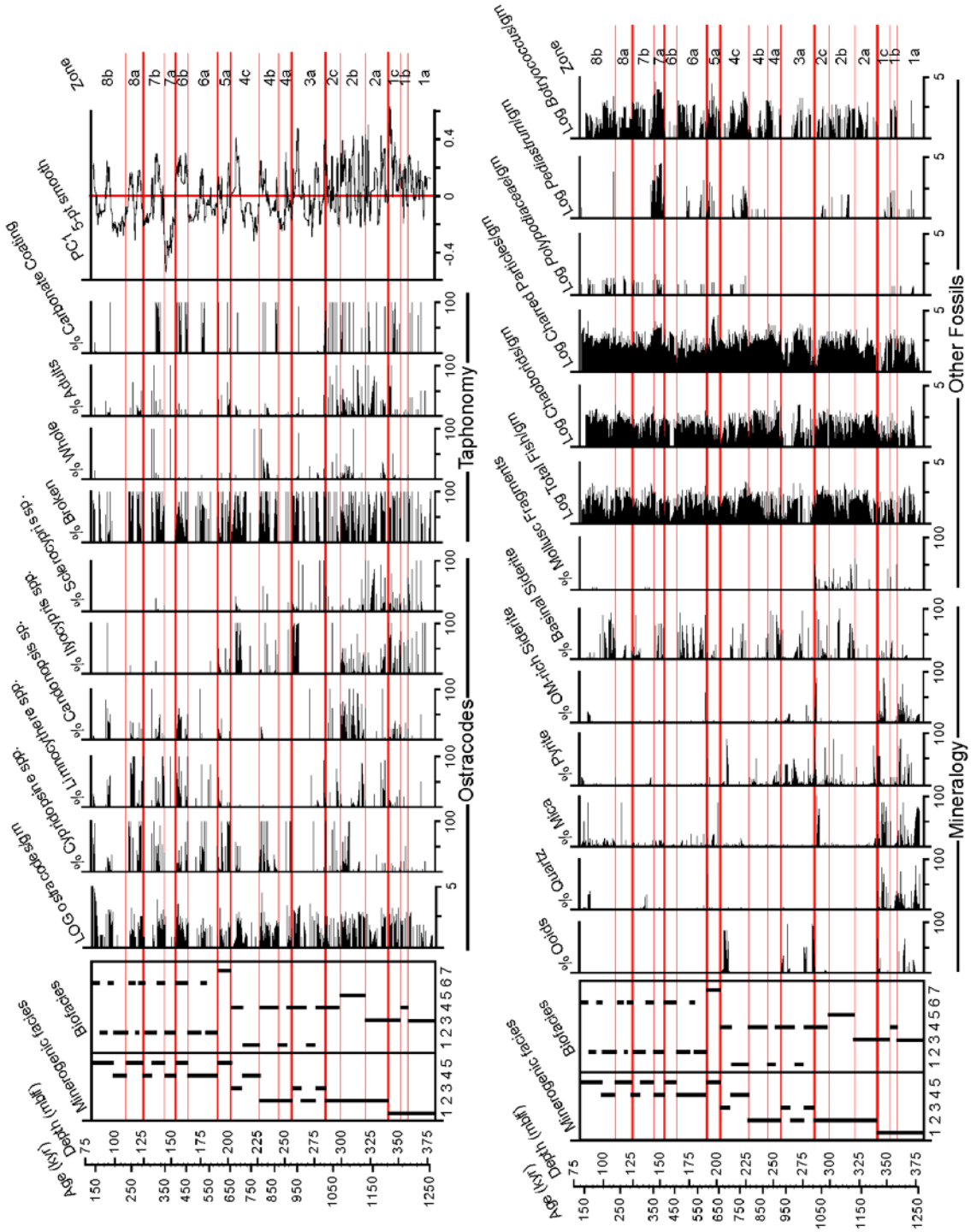
Age (kyr)
Depth (mbsf)
Mineralogenic facies
Biofacies
LOG Ostracode/gm
% Cytheridopsina spp.
% Limnocythere spp.
% Candonopsis spp.
% Ilyocypris spp.
% Sclerocypris sp.
% Broken
% Whole
% Adults
% Carbonate coating
PC1 5-pt smooth
Zone
Ostracodes
Taphonomy
% Ooids
% Quartz
% Mica
% Pyrite
% OM-rich Siderite
% Basinal Siderite
% Mollusc Fragments
Log Total Fish/gm
Log Chaobontids/gm
Log Charred Patricles/gm
Log Polypodiaceae/gm
Log Pediastrum/gm
Log Botryococcus/gm
Mineralogy
Other Fossils

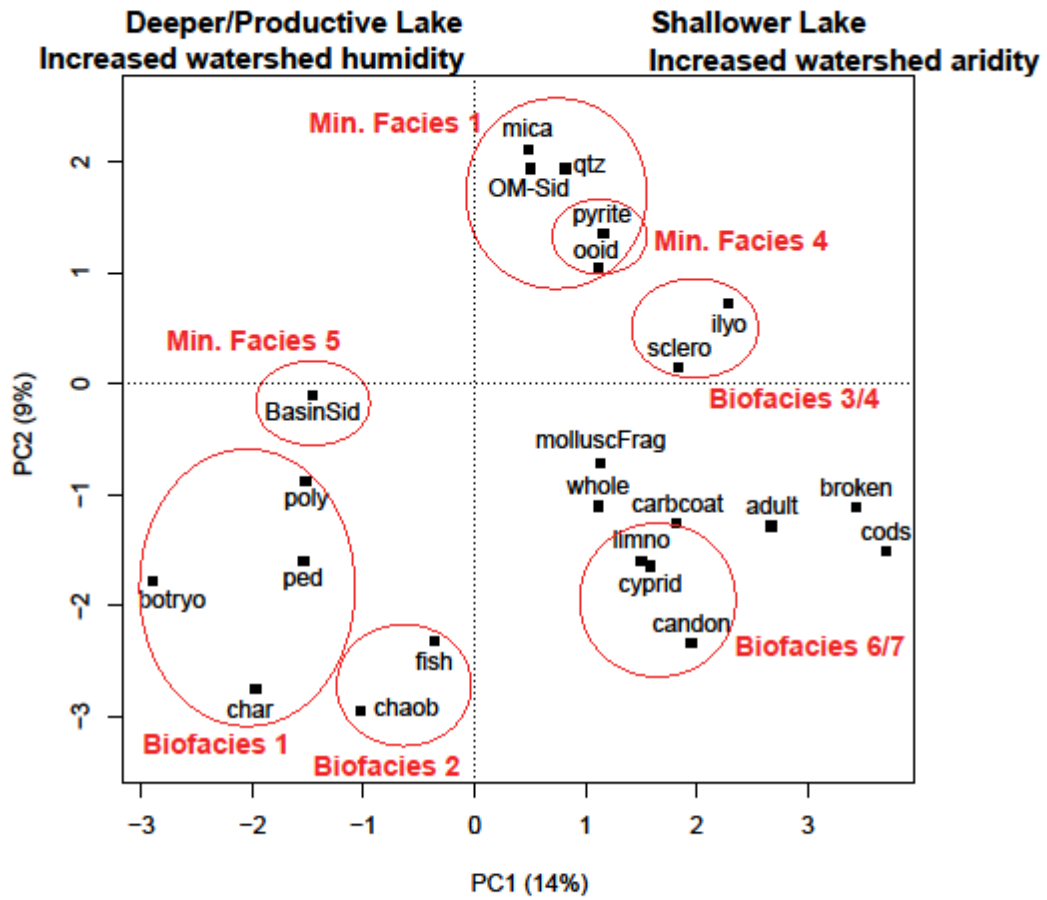

Figure C-6. Principal Components Analysis (PCA) for all indicators graphed in Figure 5, with facies assemblages noted. PC1 explains 14.27% of the variance in the record, and PC2 explains 8.83%. PC1 separates indicators of shallower environments from those found in deeper or more productive lake environments. The full indicator name for the shortened ID used here can be found in Table C-6.

Figure C-7. Environmental interpretation: In the graph, to the left are the defined depths of the minerogenic and bio-facies described in Table 4. The middle is a 5pt smoothed graph of the PC1 scores through time. To the right of the graph is the interpreted lake environment at each time in the record. The depths interpreted as river influenced or not are noted, and the grey rectangle shows the transition zone between the two. To the right of the graph are the important features of each interpreted paleoenvironment including their associated minerogenic and bio-facies, the defining indicators, and a cartoon of each environment in relation to the core site.

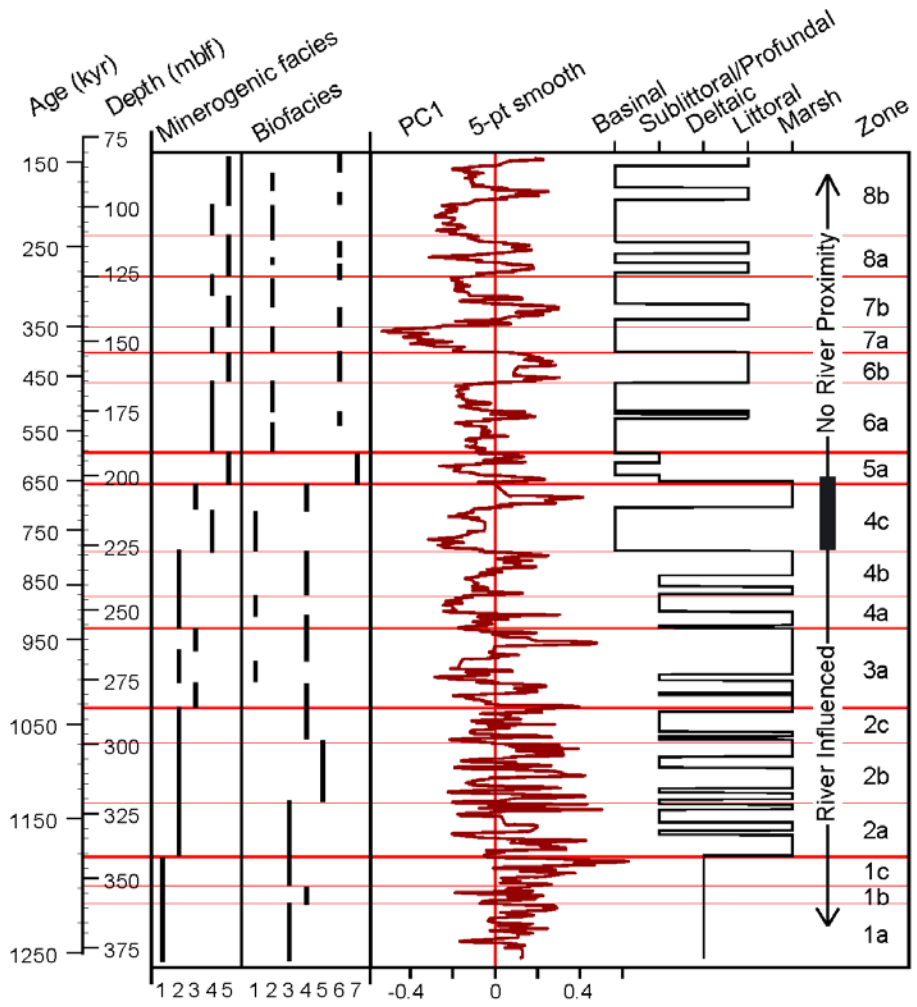
Age (kyr)
Depth (mblf)
Minerogenic facies
Biofacies
PC1
5-pt smooth
Basinal
Sublittoral/Profundal
Deltaic
Littoral
Marsh
Zone
75
100
125
150
175
200
225
250
275
300
325
350
375
150
250
350
450
550
650
750
850
950
1050
1150
1250
1 2 3 4 5
1 2 3 4 5 6 7
-0.4
0
0.4
8b
8a
7b
7a
6b
6a
5a
4c
4b
4a
3a
2c
2b
2a
1c
1b
1a
No River Proximity
River Influenced

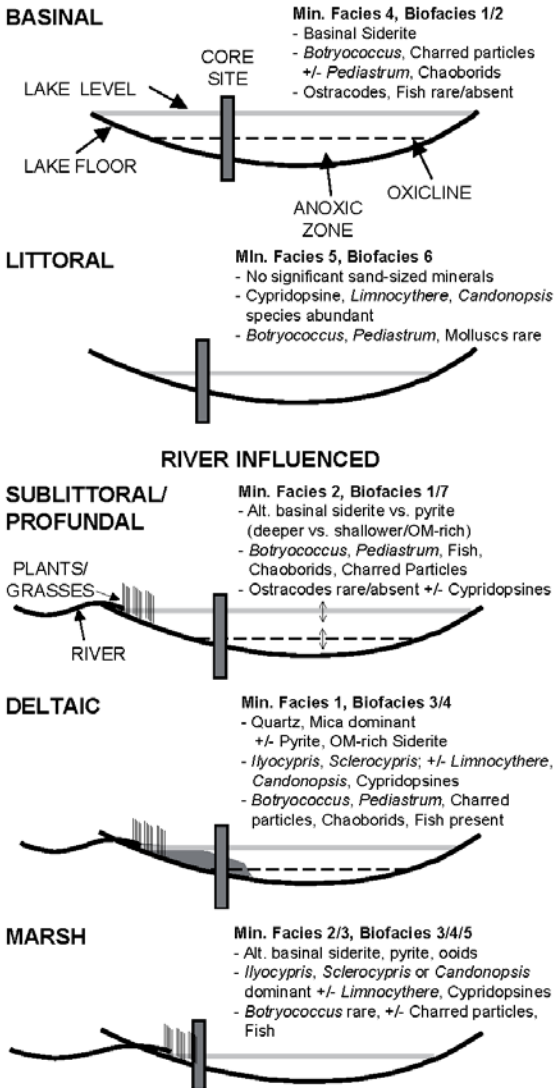
BASINAL
Min. Facies 4, Biofacies 1/2
- Basinal Siderite
- Botryococcus, Charred particles
+/- Pediastrum, Chaoborids
- Ostracodes, Fish rare/absent
CORE SITE
LAKE LEVEL
LAKE FLOOR
ANOXIC ZONE
OXICLINE
LITTORAL
Min. Facies 5, Biofacies 6
- No significant sand-sized minerals
- Cypridopsine, Limnocythere, Candonopsis species abundant
- Botryococcus, Pediastrum, Molluscs rare
RIVER INFLUENCED
SUBLITTORAL/ PROFUNDAL
Min. Facies 2, Biofacies 1/7
- Alt. basinal siderite vs. pyrite (deeper vs. shallower/OM-rich)
- Botryococcus, Pediastrum, Fish, Chaoborids, Charred Particles
- Ostracodes rare/absent +/- Cypridopsines
PLANTS/ GRASSES
RIVER
DELTAIC
Min. Facies 1, Biofacies 3/4
- Quartz, Mica dominant +/- Pyrite, OM-rich Siderite
- Ilyocypris, Sclerocypris; +/- Limnocythere, Candonopsis, Cypridopsines
- Botryococcus, Pediastrum, Charred particles, Chaoborids, Fish present
MARSH
Min. Facies 2/3, Biofacies 3/4/5
- Alt. basinal siderite, pyrite, ooids
- Ilyocypris, Sclerocypris or Candonopsis dominant +/- Limnocythere, Cypridopsines
- Botryococcus rare, +/- Charred particles, Fish

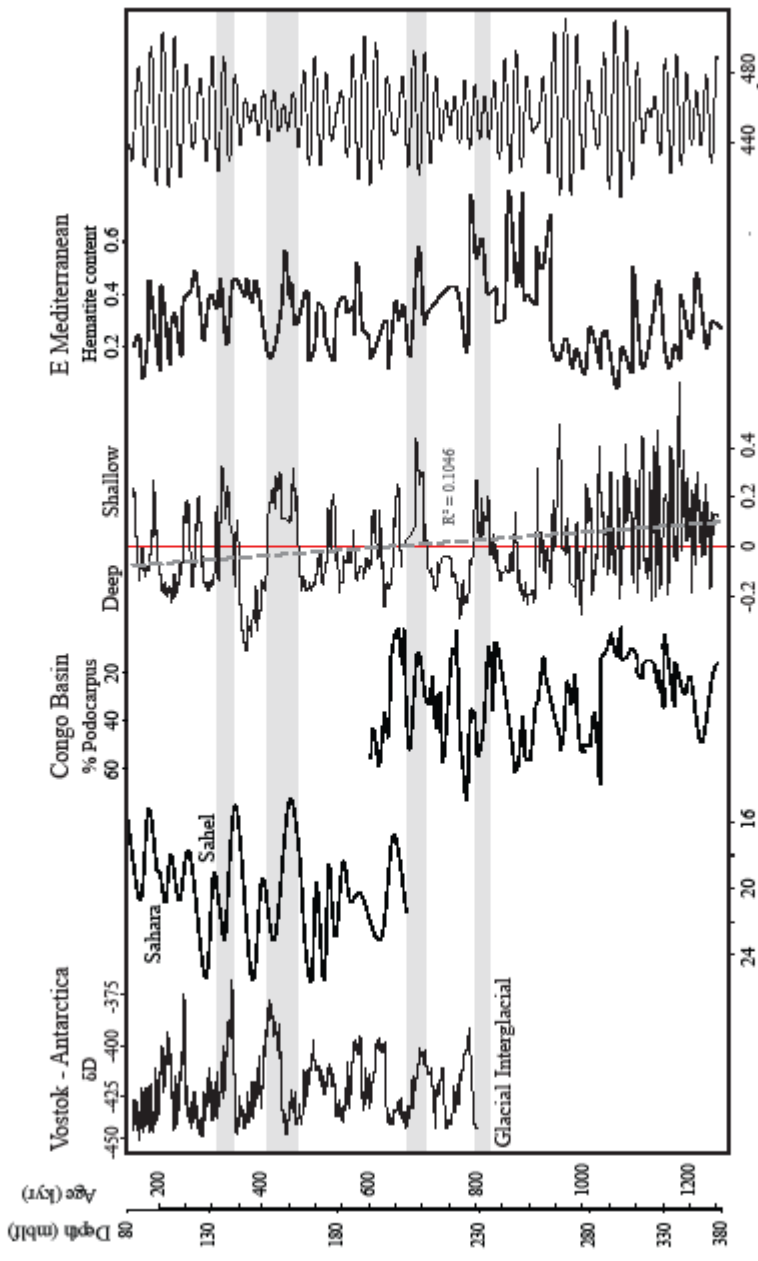

Figure C-8. Regional and global climate comparison: The graphs are now plotted linearly versus age as opposed to depth as in previous graphs. Shaded rectangles indicate arid excursions at Lake Malawi of at least 25kyrs. The dotted grey line is a linear regression (R^2 shown) through all data in the PC1 stratigraphic time series. Reference information as follows - Vostok ice core record (Jouzel et al. 2007); NW African Coast, ODP Site 658, 21°N, 19°W (Hooghiemstra et al., 2006); Congo Basin, ODP Site 1075, 5°S, 10°E (Dupont et al., 2001); Lake Malawi (this study); Eastern Mediterranean, ODP Site 967, 34°N, 33°E; Insolation at 15°S (Laskar et al., 2004).

Figure C-S1. A. Stratigraphic time series of PC1 plotted linearly against time for all data included in this analysis (black line) and for all data excluding the genera *Ilyocypris* and *Sclerocypris* (grey line). B. Covariance plot of axes PC1 and PC2 of the original data (black boxes) and of all indicators excluding *Ilyocypris* and *Sclerocypris* ostracodes. The labels are placed so that the nearest black and grey box are accurately labeled. The full indicator name for the shortened ID used here can be found in Table C-6.

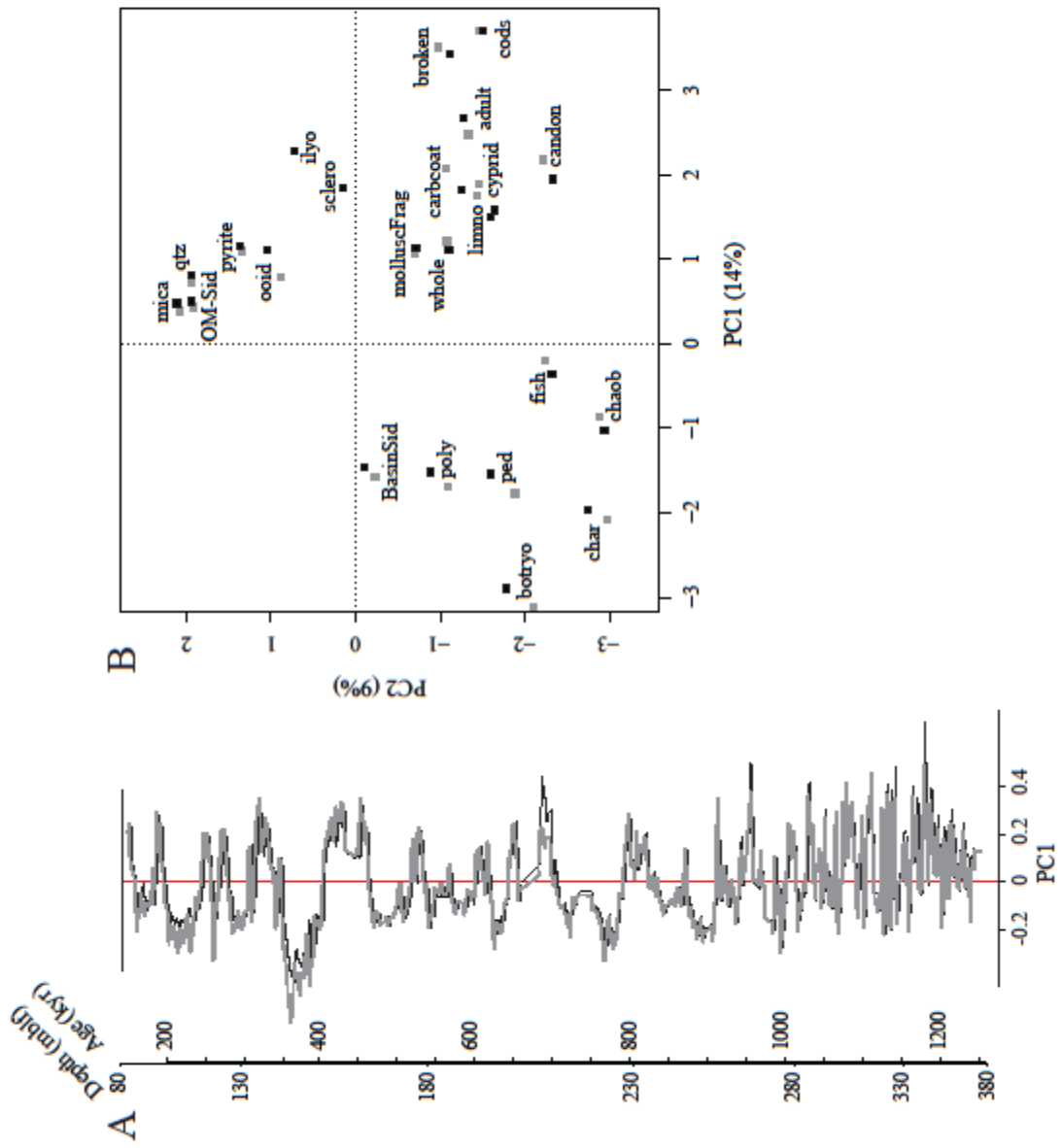
A
Depth (mblf)
Age (kyr)
80
130
180
230
280
330
380
200
400
600
800
1000
1200
-0.2
0
0.2
0.4
PC1
B
PC2 (9%)
PC1 (14%)
mica
qtz
OM-Sid
pyrite
ooid
ilyo
sclero
mollusc Frag
carbcoat
whole
limno
cyprid
adult
broken
cods
candon
fish
chaob
BasinSid
poly
ped
botryo
char

Plate C-1. Plate showing examples of ostracode species found throughout Core 1B: A. *Sclerocypris c.f. jenkinae* – Left valve, external view from 71E-2 0-1; B. *Sclerocypris c.f. jenkinae* – Left valve, external view, juvenile, from 45E-4 17.5-18.5; C. *Gomphocythere huwi* – Left valve, external view, male, from 68E-2 16-17; D. *Gomphocythere c.f. huwi* – Left valve, external view, juvenile, from 68E-2 32-33; E. *Gomphocythere c.f. huwi* – Left valve, internal view, juvenile, from 117E-3 16-17; F. *Limnocythere s.l. sp.4* – Left valve, external view, female, from 123E-2 96-97; G. *Limnocythere s.l. sp.1* – Left valve, external view, male, from 51E-1 32-33; H. *Limnocythere s.l. sp.1* – Left valve, external view, female, from 59E-3 16.1-17.4.

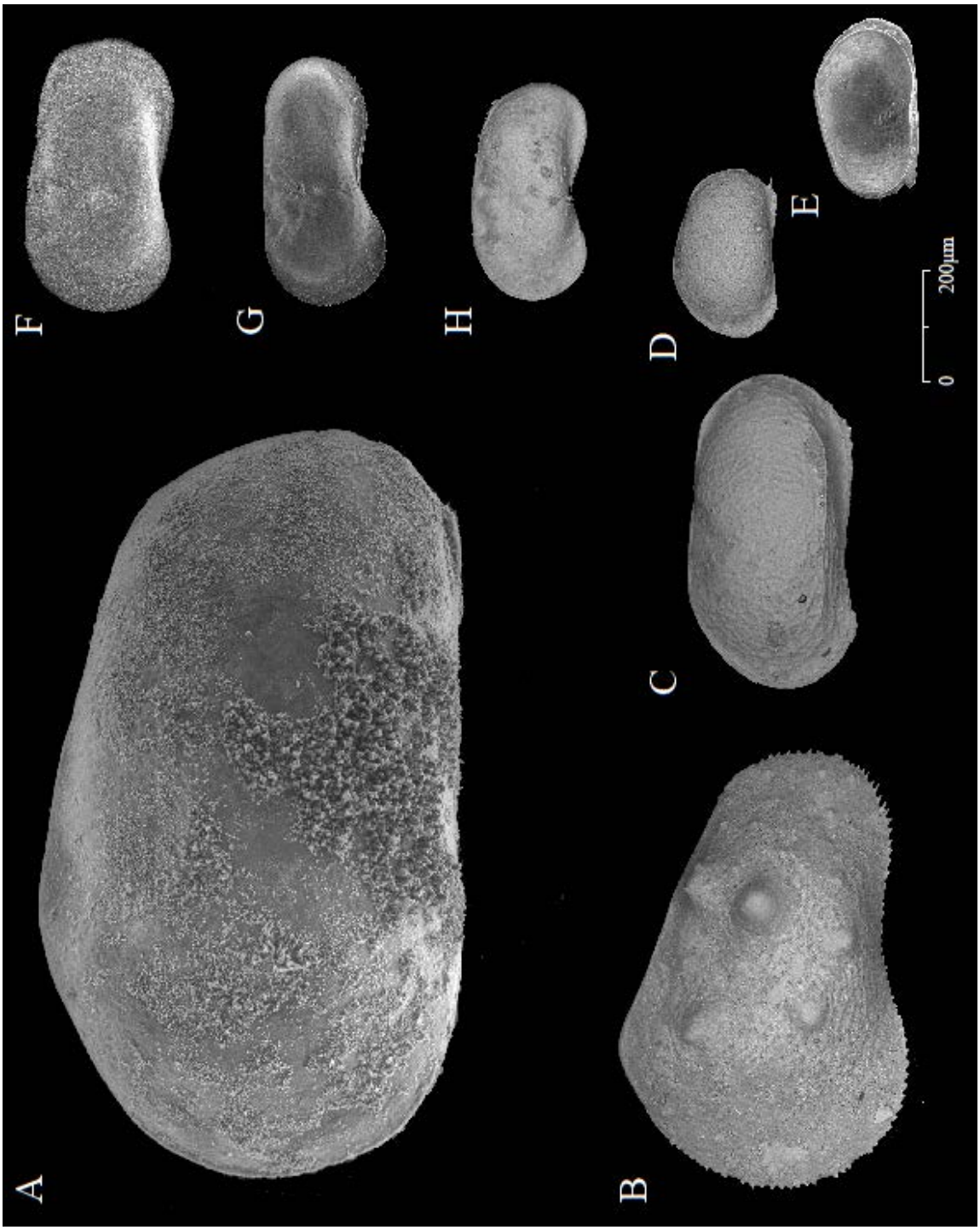
A
B
C
D
E
F
G
H
0
200µm

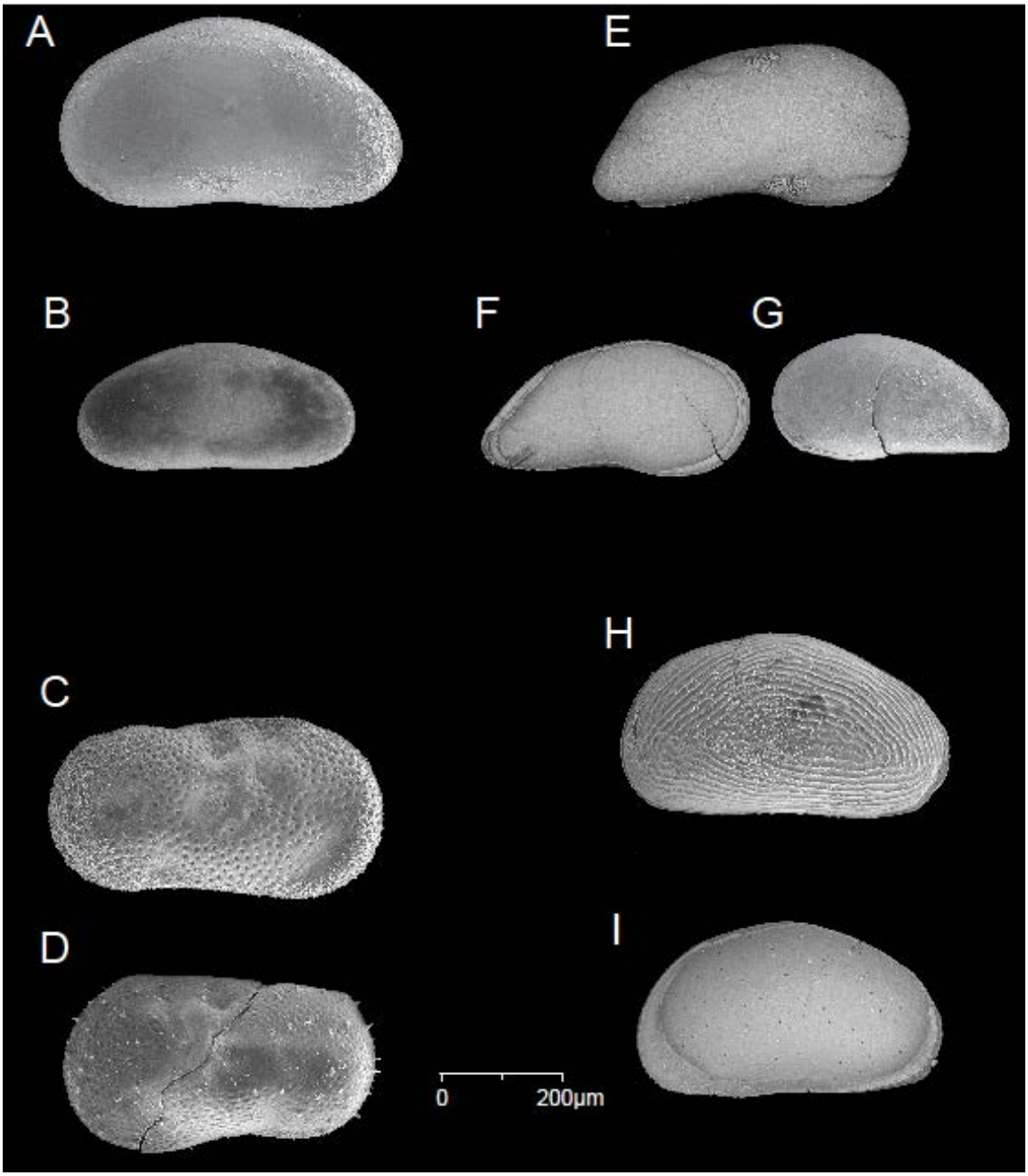

Plate C-2. Plate showing examples of ostracode species found throughout Core 1B: A. *Cypridopsine n.gen. sp.B* – Left valve, external view, from 27E-1 112-113; B. *Candonopsis sp.* – Right valve, external view, from 26E-2 0-1; C. *Ilyocypris propinqua* – Right valve, external view, from 126E-3 16-17; D. *Ilyocypris alta* – Left valve, external view, from 124E-1 96-97; E-G. *Cypridopsine n.gen. sp.2 n.sp.*: E. Right valve, external view, from 71E-4 16.4-17.4; F. Left valve, internal view, juvenile, from 71E-4 32.3-33.3; G. Left valve, external view, juvenile, from 43E-2 48.4-49.4; H-I: *Zonocypris costata*, H. Left valve, external view, from 44E-2 64-65; I. Right valve, internal view, from 45E-2 2.5-3.

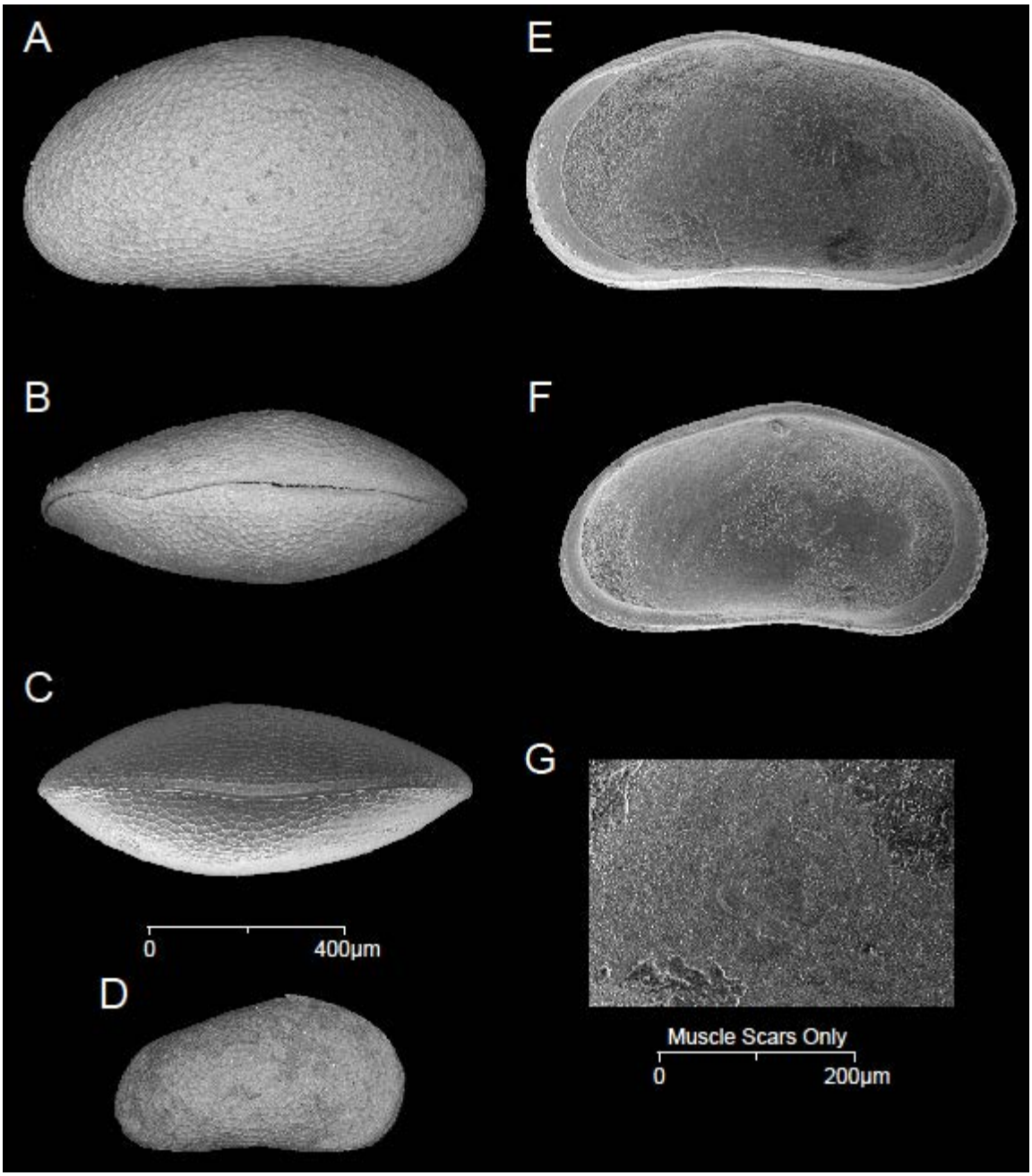

Plate C-3. Plate showing all aspects of the undescribed species *Cypridopsine n.gen. sp.1* found in Core 1B. A. Right valve, external view, from 68E-2 32-33; B. Carapace, dorsal view, from 68E-2 64-65; C. Carapace, ventral view, from 68E-2 64-65; D. Right valve, external view, juvenile, from 68E-2 32-33; E. Right valve, internal view, from 68E-1 80-81; F. Left valve, internal view, juvenile, from 68E-3 32-33; G. Adductor muscle scars from same ostracode as Plate 3-E.

Type	Previous Interpretations	Reference
Ostracodes		
Total number	Oxygenated bottom water, alkaline (preservation of shell material), littoral-profundal environments	Cohen 2003
Limnocythere	Highly saline/alkaline lake, littoral zone	Cohen et al., 1983; Carbonel et al. 1988; Cohen et al. 2007
Ilyocypris	Littoral zone; moving water possible; Most abundant in offshore riverine and marsh environments in modern Lake Malawi	Holmes, 1992; Mezquita et al., 1999; Appendix B - this dissertation
Sclerocypris	Littoral zone; fishless ponds; *S. jenkinae*found in both lakes and pools in Kenya	Martens, 1986
Candonopsis	Oligosaline lake, possibly transitional to deeper waters; sometimes interpreted as fresh water indicator	Holmes, 1992; Holmes et al. 1997
Cypridopsines	Can be found in multiple environments, but when found in conjunction with high numbers of intact, juveniles, has been interpreted as indicating deeper, freshwater lake conditions	Holmes, 1992; Cohen et al. 2007; Park and Cohen 2011
Taphonomy		
% Broken	Highest energy environment; reworked; possible waves	Brouwers, 1998; Cohen et al. 2007
% Adult	Higher energy environment; littoral zone	Brouwers, 1998; Park et al., 2003; Cohen et al. 2007
% Carbonate Coated	Carbonate (super)saturated/alkaline environment; likely reworked; littoral zone	Alin and Cohen, 2004; Cohen et al. 2007
% Whole	Lower energy or less shallow environment	Whatley, 1988; Holmes, 1992; Park et al., 2003; Cohen et al,. 2007; Park and Cohen, 2011
Other Biota		
Mollusk Fragments	Oxygenated bottom water, alkaline (preservation of shell material)	Dillon, 2000
Fish	Shallow and/or widely fluctuating lake depth	Reinthal et al., 2011
Charcoal	Reflection of fire frequency that can go up as things are getting more arid from a very wet starting point, or when things get wetter starting from a very arid condition	Whitlock and Millspaugh, 1996; Bird et al., 2004; Cohen et al. 2007
Botryococcus	Has been found in shallow water environments in arid, semi-arid regions; also in fresh and brackish water in the tropics (including	Guy-Ohlson, 1992; Casteneda et al., 2009; Appendix B - this dissertation

Type	Previous Interpretations	Reference
	modern Lake Malawi); Indicator of primary productivity in lake	
Pediastrum	Nutrient-rich, freshwater conditions; warm, mesotrophic to eutrophic lakes; Indicator of primary productivity in lake	Jakovska and Komarek, 2000; Komarek and Jankovska, 2001
Polypodiaceae sori	Not used in previous paleoecological interpretations, however the plant is found in humid, tropical rainforest environments	Panigrahi and Patnaik, 1961; Kreier and Schneider, 2006
Chaoborus	Presence of anoxic bottom water (a refuge from predatory fish during diurnal migrations), Abundant in open waters of the central basin in present day Lake Malawi, less abundant in the shallower southern end of the lake with	Baker et al. 1985; Dawidowicz et al. 1990; Irvine, 1995; Voss and Mumm, 1999; Stratton and Kessler, 2007
Mineralogy		
Pyrite	Bottom water anoxia; reducing environment with Fe and sulfates available (e.g. marshes or estuarine environments); often forms framboids or euhedral crystals	Sweeney and Kaplan, 1973; Postma, 1982; Chowdhury and Noble, 1996; Wilkin and Barnes, 1997; Taylor and Macquaker, 2011
Ooids	Alkaline environment with medium sand-sized particles on which to nucleate carbonate; shallow enough for frequent agitation and/or transport with bedload	Wilkinson et al., 1980; Heller et al., 1980
Quartz	Higher mechanical energy environments; turbulent mixing, sediment winnowing environments (e.g. river inflow-deltaic or wave action-beach)	Jones and Bowser, 1978; Cohen, 2003
Shallow Siderite	Bottom water anoxia; reducing environment with Fe and (often) bacterially generated CO2; forms in modern swamps, marshes and deltaic environments; Fe/Ca ratio > 0.05	Kelts and Hsu, 1978; Postma, 1982; Moore et al. 1992; Sapota et al. 2006; Taylor and Macquaker, 2011; Park and Cohen, 2011
Deep Siderite	Bottom water anoxia; reducing environment with Fe and (often) bacterially generated CO2; low concentrations of sulfur and sulfate; Fe/Ca ratio > 0.05	Kelts and Hsu, 1978; Giresse et al., 1991
Mica	Distal deltaic deposits	Park and Cohen, 2012

Table 1. A summary of the previous ecological interpretations of each indicator used for analysis in this study and associated references.

Hierarchical Level	Name	Reference	Plate	Image
Class	Ostracoda	Latreille, 1806		
Subclass	Podocopa	G.W. Müller, 1894		
Order	Podocopida	Sars, 1866		
Suborder	Podocopina	Sars, 1866		
Superfamily	Cypridoidea	Baird, 1845		
Family	Candonidae	Kaufmann, 1900		
Subfamily	Candoninae	Kaufmann, 1900		
♦ +	*Candonopsis africana s.l.*	Kaufmann, 1900		
+ *	*Candonopsis sp.1*	Martens, 2002		
† ♦	*Candonopsis sp.*		**2**	**B**
Subfamily	Cyclocypridinae	Kaufmann, 1900		
+	*Cypria lenticularis*	Müller, 1898		
+	*Physocypria castanea*	Brady, 1904		
Family	Cyclocyprididae	Kaufmann, 1900		
♦	possible *Allocypria* sp.1			
♦	possible *Allocypria* sp.2			
Family	Cyprididae	Baird, 1845		
Subfamily	Cypricercinae	Sars, 1895		
+	*Cypricerus inermis*	Brady, 1904		
+	*Neocypridella fossulata*	Daday, 1910		
+	*Strandesia laticauda*	Daday, 1910		
Subfamily	Cypridopsinae	Bronstein, 1947		
	Cypridopsinae n.gen. cunningtoni	Sars, 1910		
♦ + *	*Cypridopsinae n.gen. sp.A*	Martens, 2002		
† ♦ + *	*Cypridopsinae n.gen. sp.B*	Martens, 2002	**2**	**A**
+ *	*Cypridopsinae n.gen. sp.C*	Martens, 2002		
+ *	*Cypridopsinae n.gen. sp.D*	Martens, 2002		
+ *	*Cypridopsinae n.gen. sp.F*	Martens, 2002		
♦ + *	*Cypridopsinae n.gen. sp.G*	Martens, 2002		
+ *	*Cypridopsinae n.gen. sp.K*	Martens, 2002		
+ *	*Cypridopsinae n.gen. sp.L*	Martens, 2002		
+ *	*Cypridopsinae n.gen. sp.N*	Martens, 2002		
♦ + *	*Cypridopsinae n.gen. sp.O*	Martens, 2002		
+ *	*Cypridopsinae n.gen. sp.P*	Martens, 2002		
+ *	*Cypridopsinae n.gen. sp.Q*	Martens, 2002		
+ *	*Cypridopsinae n.gen. sp.X n.sp.*	(undescribed)		
† ♦ + *	*Cypridopsinae n.gen. sp.1 n.sp.*	(undescribed)	**3**	**A-G**
† ♦ + *	*Cypridopsinae n.gen. sp.2 n.sp.*	(undescribed)	**2**	**E-G**
+	*Cypridopsis vidua*	Müller, 1776		

Hierarchical Level	Name	Reference	Plate	Image
+	*Pleisiocypridopsis fulleborni*	Daday, 1910		
† ♦ + *	*Zonocypris costata*	Vavra, 1897	**2**	**H, I**
Subfamily	Cyprinotinae	Bronstein, 1947		
+ *	*Cyprinotinae n. gen. sp.1*	Martens, 2002		
+ *	*Cyprinotinae n. gen. sp.2*	Martens, 2002		
+ *	*Cyprinotinae n. gen. sp.3*	Martens, 2002		
Subfamily	Herpetocypridinae	Kaufmann, 1900		
+	*Acocypris platybasis*	Lowndes, 1932		
+	*Chrissia fasciculata*	Daday, 1910		
+	*Chrissia fullborni*	Daday, 1910		
+	*Chrissia marginata*	Daday, 1910		
+	*Chrissia perarmata*	Brady, 1904		
+	*Chrissia sinuate*	Müller, 1898		
+	*Chrissia stagnalis*	Daday, 1910		
+	*Humphcypris sp.1*	Martens, 1998		
+	*Stenocypris major*	Baird, 1859		
Subfamily	Megalocyprinae	Rome, 1965		
† ♦	*Sclerocypris jenkinae*	Klie, 1933	**1**	**A, B**
Family	Ilyocyprididae	Kaufmann, 1900		
† ♦	*Ilyocypris alta*	Sars, 1910	**2**	**D**
† ♦	*Ilycypris propinqua*	Sars, 1910	**2**	**C**
+ *	*Ilyocypris sp.1*	Martens, 2002		
Family	Notodromadidae	Kaufmann, 1900		
Subfamily	Oncocypridinae	DeDeckker, 1979		
+	*Oncocypris mulleri*	Daday, 1910		
Superfamily	Cytheroidea	Baird, 1850		
Family	Limnocytheridae	Klie, 1938		
Subfamily	Limnocytherinae	Klie, 1938		
+ *	*Limnocythere jocquei*	Martens, 1990		
† ♦ + *	*Limnocythere s.l. sp.1*	Martens, 2002	**1**	**G, H**
♦ + *	*Limnocythere s.l. sp.2*	Martens, 2002		
♦ + *	*Limnocythere s.l. sp.3*	Martens, 2002		
† ♦ + *	*Limnocythere s.l. sp.4*	Martens, 2002	**1**	**F**
+ *	*Limnocythere s.l. sp.5*	Martens, 2002		
♦ + *	*Limnocythere s.l. sp.6*	Martens, 2002		
+ *	*Limnocythere s.l. sp.7*	Martens, 2002		
♦ + *	*Limnocythere s.l. sp.8*	Martens, 2002		
+ *	*Limnocythere s.l. sp.9*	Martens, 2002		
+ *	*Limnocythere s.l. sp.10*	Martens, 2002		

Hierarchical Level	Name	Reference	Plate	Image
♦ *	*Limnocythere s.l. sp.11*	(undescribed)		
♦ *	*Limnocythere s.l. sp.12*	(undescribed)		
♦ *	*Limnocythere s.l. sp.13*	(undescribed)		
♦ *	*Limnocythere s.l. sp.14*	(undescribed)		
♦ *	*Limnocythere s.l. sp.15*	(undescribed)		
♦ *	*Limnocythere s.l. sp.16*	(undescribed)		
+ *	*Limnocythere sp.A n.sp.*	(undescribed)		
+ *	*Limnocythere sp.B n.sp.*	(undescribed)		
Subfamily	Timiriaseviinae	Mandelstam, 1960		
+ *	*Gomphocythere emrysi*	Martens, 2003		
† ♦ + *	*Gomphocythere huwi*	Martens, 2003	**1**	**C-E**
+ *	*Gomphocythere irvinei*	Martens, 2003		
+ *	*Gomphocythere lisae*	Martens, 2003		
+ *	*Gomphocythere piriformis*	Martens, 2003		
Superfamily	Darwinuloidea	Brady and Norman, 1889		
Family	Darwinulidae	Brady and Norman, 1889		
+ *	*Alicenula inversa*	Rossetti and Martens, 1998		
+ *	*Alicenula serricaudata*	Rossetti and Martens, 1998		
+	*Darwinula stevensoni*	Brady and Robertson, 1870		
+ *	*Penthesiluna gr.incae*	Rossetti and Martens, 1998		

Key:

- ♦ Fossil species in core material
- \+ Species found in modern Lake Malawi
- * Endemic species
- † Species found in current study

Table 2. Species list of modern and fossil ostracodes found within Lake Malawi. Symbols denote those found in the current study, endemic species, which are found as fossils in core records, and which are found in the modern lake (see key). The plate and image number for those ostracodes found in this study are given in the two right hand columns. Note that many of these species are not described and identified only by informal letter and numerical designations that refer to Martens' (2002) report. New species found in the core or modern sediments not previously identified are listed as "n.sp." This table updates information found in Park and Cohen (2011). Additional taxonomic information from Martens (1984; 1986).

D18O #	Depth	Taxa	d13C VPDB	d18O VPDB	d18O corr	calculated water d18O	C std dev	O std dev	Voltage
34	315.435	*Candonopsis sp.*	-1.27	9.09			0.18	0.35	0.77
11	315.435	*Candonopsis sp.*	-1.02	5.20			0.15	0.22	0.86
38	122.908	*Cypridopsine sp.2*	-4.82	2.02			0.18	0.35	0.77
8	200.571	*Cypridopsine sp.1*	2.27	4.36	3.16	5.20	0.10	0.10	1.63
4	200.571	*Cypridopsine sp.1*	2.41	4.03	2.83	4.90	0.10	0.10	2.02
9	200.696	*Cypridopsine sp.1*	2.55	3.88	2.68	4.70	0.10	0.10	2.10
3	200.696	*Cypridopsine sp.1*	2.22	3.78	2.58	4.60	0.10	0.10	2.20
2	201.317	*Cypridopsine sp.1*	1.54	3.08	1.88	4.00	0.10	0.10	1.47
10	201.317	*Cypridopsine sp.1*	2.06	3.32	2.12	4.20	0.10	0.10	2.29
30	207.519	*Ilyocypris alta*	-1.94	2.25	1.05	3.10	0.10	0.10	1.13
1	207.519	*Ilyocypris alta*	-1.96	2.43	1.23	3.30	0.10	0.10	1.50
32	208.39	*Ilyocypris alta*	0.42	0.59			0.20	0.40	0.72
33	208.39	*Ilyocypris alta*	-0.93	6.41	5.21	7.30	0.10	0.10	0.99
36	315.435	*Ilyocypris alta*	0.30	0.34			0.15	0.30	0.82
5	156.721	*Limnocythere sp.4*	0.48	0.71			0.20	0.40	0.69
8	335.042	*Limnocythere sp.4*	0.36	0.47			0.18	0.35	0.78
31	315.027	*Mollusc*	-4.70	2.15		3.10	0.10	0.10	1.35
30	315.435	*Mollusc*	-3.96	1.86		2.80	0.10	0.10	2.38
34	207.519	*Sclerocypris c.f. Jenkinae*	-0.22	2.94	1.74	3.90	0.10	0.10	1.33
11	207.519	*Sclerocypris c.f. Jenkinae*	-0.20	4.05	2.85	4.90	0.10	0.10	1.96
33	315.027	*Sclerocypris c.f. Jenkinae*	-1.47	2.07	0.87	2.90	0.10	0.10	1.54
32	315.027	*Sclerocypris c.f. Jenkinae*	-1.65	4.52	3.32	5.40	0.10	0.10	2.45

9	315.435	*Sclerocypris c.f. Jenkinae*	-1.33	2.51	1.31	3.40	0.10	0.10	1.79
35	315.435	*Sclerocypris c.f. Jenkinae*	-1.31	2.86	1.66	3.80	0.10	0.10	1.84
7	335.042	*Sclerocypris c.f. Jenkinae*	0.43	3.29	2.09	4.20	0.10	0.10	1.78

Table 3. Listed in alphabetical order by taxa, this table gives from left to right, the lab analysis number, the depth at which the sample occurs, the taxa, the raw measurements of $\delta^{13}C$ and $\delta^{18}O$ (VPDB) on shell carbonate. The next column lists the $\delta^{18}O$ values corrected for ostracode vital effects which are then used to calculate water $\delta^{18}O$ values (in red). Calculated water $\delta^{18}O$ is based on the inorganic calcite fractionation of Friedman and O'Neil (1977) and a temperature of 25 °C . Mollusc aragonite $\delta^{18}O$ is used to calculate lake water using the fractionation of Grossman and Ku (1986) at 25 °C, as modified by Dettman et al. (1999). The next column lists the standard errors for both carbon and oxygen (1-sigma), and lastly the voltage. All samples with voltages of less than 0.9 were corrected for low voltage, increasing the error in the measurement, and decreasing the precision of their measured values. Low voltage samples were not used to estimate lake water $\delta^{18}O$.

Eigenvalues			
DCA1	DCA2	DCA3	DCA4
0.5	0.5	0.34	0.34

% Variance Explained			
DCA1	DCA2	DCA3	DCA4
14.39	14.38	9.75	9.73

DCA ID	Taxa	DCA1	DCA2
Cyprid.B	*Cypridopsine n.gen. sp.B*	0.44	0.06
Cyprid.1	*Cypridopsine n.gen. sp. 1n.sp.*	2.53	-0.1
Cyprid.2	*Cypridopsine n.gen. sp.2 n.sp.*	-0.27	1.87
Zonocypris	*Zonocypris costata*	1.5	1.52
Limno.1	*Limnocythere sp.1*	0.54	1.27
Limno.4	*Limnocythere sp.4*	-1.5	1.38
Candon	*Candonopsis sp.*	-0.34	0.17
Ilyo.alta	*Ilyocypris alta*	0.23	-1.5
Ilyo.prop	*Ilyocypris propinqua*	-1.39	-1.31
Sclero.sp.	*Sclerocypris c.f. jenkinae*	-1.2	-0.42
Gompho.huwi	*Gomphocythere huwi*	1.86	-0.1

Table 4. Detrended Correspondence Analysis (DCA) results. The eigenvalues and percent variance explained by each axis are listed on the left, with the first and second axis values for each species on the right. The "DCA ID" matches the short names used in Figure C-3c, to the full names of each species.

Minerogenic Facies	Description	Zone
1	Co-dominant quartz, mica, pyrite and siderite, +/- ooids	1a, 1c
2	Rapidly alternating siderite to pyrite dominance of sand fraction mineralogy, +/- minimal mica	1b, 2a, 2b, 2c, 3a, 4a, 4b
3	Rapidly alternating pyrite and ooid dominance, minimal mica	3a, 4c
4	Basinal siderite dominance, low mica abundance, +/- minimal quartz and/or pyrite	4c, 6a, 7a, 7b, 8b
5	Devoid of any significant sand-sized minerals	5a, 6b, 7b, 8a, 8b
Biofacies	**Description**	**Zone**
1	Abundant *Botryococcus,* charred particles, +/- *Pediastrum, Polypodiaceae* sori; coincident with abundant fish fossils and chaoborids; ostracodes rare	3a, 4a, 4c
2	Abundant *Botryococcus,* charred particles, +/- *Pediastrum, Polypodiaceae* sori; coincident with decreased fish fossils and chaoborids; ostracodes rare	6a, 7a, 7b, 8a, 8b
3	*Botryococcus, Pediastrum, Polypodiaceae* sori rare to absent; Dominant *Ilyocypris, Sclerocypris, +/- Candonopsis* and/or *Limnocythere*	1a, 1c, 2a
4	*Botryococcus, Pediastrum, Polypodiaceae* sori rare to absent; Dominant *Ilyocypris*, *Sclerocypris*, +/- Cypridopsines	1a, 2c, 3a, 4a, 4b, 4c
5	*Botryococcus* abundant; *Pediastrum*, *Polypodiaceae* sori rare to absent; Dominant *Candonopsis,* abundant *Ilyocypris, +/- Sclerocypris, Limnocythere,* Cypridopsines, mollusc fragments	2b
6	*Botryococcus, Pediastrum, Polypodiaceae* sori rare to absent; Co-dominant *Cypridopsines, Limnocythere, Candonopsis* +/- mollusc fragments	6a, 6b, 7b, 8a, 8b
7	*Botryococcus* abundant; *Pediastrum, Polypodiaceae* sori rare to absent; Dominant *Cypridopsines, +/- Candonopsis, Limnocythere, Ilyocypris*	5a

Table 5. A description of the abundant and rare indicators that define each minerogenic and biologic facies, and the stratigraphic zones in which they occur.

Axis	Eigenvalue	% Variance Explained	PCA ID	Indicator	PC1	PC2
PC1	3.28	14.27	cyprid	Cypridopsines	1.58	-1.64
PC2	2.03	8.83	limno	*Limnocythere*	1.5	-1.59
PC3	1.69	7.36	candon	*Candonopsis*	1.95	-2.33
PC4	1.34	5.81	ilyo	*Ilyocypris*	2.29	0.73
PC5	1.27	5.51	sclero	*Sclerocypris*	1.84	0.15
PC6	1.16	5.05	cods	Total ostracodes	3.7	-1.51
PC7	1.1	4.78	broken	Broken valves	3.43	-1.11
PC8	1.04	4.5	whole	Whole carapaces	1.11	-1.1
PC9	0.96	4.16	adult	Adult valves	2.67	-1.28
PC10	0.91	3.94	carbcoat	Carbonate coated valves	1.82	-1.25
PC11	0.89	3.87	fish	Fish fossils	-0.36	-2.32
PC12	0.86	3.72	char	Charred Particles	-1.97	-2.75
PC13	0.82	3.59	ped	*Pediastrum*	-1.54	-1.59
PC14	0.79	3.44	poly	*Polypodiaceae* sori	-1.52	-0.88
PC15	0.77	3.36	chaob	Chaoborid Fragments	-1.02	-2.94
PC16	0.72	3.13	botryo	*Botryococcus*	-2.9	-1.78
PC17	0.65	2.83	pyrite	Pyrite	1.16	1.36
PC18	0.62	2.69	qtz	Quartz	0.82	1.94
PC19	0.57	2.48	mica	Mica	0.48	2.11
PC20	0.54	2.35	OM-Sid	OM-rich siderite	0.5	1.94
PC21	0.39	1.71	BasinSid	Basinal siderite	-1.46	-0.1
PC22	0.37	1.63	ooid	Ooids	1.11	1.05
PC23	0.23	1	molluscFrag	Mollusc Fragments	1.13	-0.71

Table 6. Principal Components Analysis (PCA) results. The eigenvalues and percent variance explained by each axis are listed on the left. The first and second axis values for each indicator is on the right. The "PCA ID" matches the short names used in Figure C-6 and Figure C-S1, to the full names of each indicator.

APPENDIX D: PERMISSIONS

APPENDIX A: THE ENVIRONMENTAL CONTEXT FOR THE ORIGINS OF MODERN HUMAN DIVERSITY: A SYNTHESIS OF REGIONAL VARIABILITY IN AFRICAN CLIMATE 150,000-30,000 YEARS AGO, is reproduced with permission from Elsevier.

Blome, M.W., Cohen, A.S., Tryon, C.A., Brooks, A.S., Russell, J., 2012. The environmental context for the origins of modern human diversity: a synthesis of regional variability in African climate 150,000-30,000 years ago. Journal of Human Evolution 62, 563-592.